ESTIMATION OF EMISSION STRENGTH AND AIR POLLUTANT CONCENTRATIONS BY LAGRANGIAN PARTICLE MODELING

A Thesis
Presented to
The Academic Faculty

by

Kasemsan Manomaiphiboon

In Partial Fulfillment
of the Requirements for the Degree
Doctor of Philosophy in Environmental Engineering
School of Civil and Environmental Engineering

Georgia Institute of Technology
February 2004

ESTIMATION OF EMISSION STRENGTH AND AIR POLLUTANT CONCENTRATIONS BY LAGRANGIAN PARTICLE MODELING

Approved by:

Dr. Armistead G. Russell, Chairman

Dr. Michael H. Bergin

Dr. Philip J. W. Roberts

Dr. Donald R. Webster

Dr. P. K. Yeung

February 10. 2004

To my parents,
Banyong and Aree Manomaiphiboon

ACKNOWLEDGEMENTS

I wish to express my gratitude to Dr. Armistead Russell for his support and guidance during my entire study at Georgia Tech. It has been a privilege to work under his supervision. I thank Drs. Michael Bergin, Philip Roberts, Donald Webster, and P.K. Yeung for their kind being in my thesis committee. My learning in fluid mechanics and turbulence started from the last two.

I thank Dr. David Roberts of the Georgia Tech Research Institute and his team for their leadership in the Rubbertown field study conducted in Kentucky. I thank Dr. Kelvin Doty (University of Alabama, Huntsville) and Dr. Jim St. John (Georgia Institute of Technology) for their discussion on uncertainty work, Dr. Monique Leclerc (University of Georgia) for her assistance in analyzing air samples collected in the Rubbertown field study, and Dr. Paolo Monti (Università degli Studi di Roma "La Sapienza", Italy), Howard Rodean, Drs. Brian Sawford and Michael Borgas (CSIRO, Australia) and Dr. P. K. Yeung (Georgia Institute of Technology) for their inputs and comments on some parts of the thesis. Several simulation parts in the uncertainty work were implemented on a UNIX cluster of the Office of Information Technology (Georgia Institute of Technology). I acknowledge the financial support from the U.S. Environmental Protection Agency under Contract No. CR827327-01 and the Georgia Power Company. My postgraduate study has been made possible by an award from the governments of Japan and Thailand, administered by the National Development Educational Center (NADEC), Ministry of University Affairs (Thailand). In addition, I thank my school, the Georgia Institute of Technology, for my graduate research assistantship and many good experiences.

My thanks are extended to all people at the Air Quality Group for their friendship and assistance in my work, the Thai Student Association for having offered me an opportunity to hold friendship among Thais in Atlanta, Kasemchart Sriwalai for his many helpful suggestions about computers, and others whom I have come across and collaborated with both directly and indirectly. I am indebted to my parents, Banyong and Aree, and family back in Thailand for their love and everything. I thank my wife, Supinda, for her love, support, and sacrifices given to me in this endeavor.

ABSTRACT

Air quality modeling integrates the knowledge of how physical and chemical processes affect pollutants in the atmosphere. One category of air quality modeling is Lagrangian particle modeling that has been widely applied to pollutant dispersion in the atmospheric boundary layer (ABL). It treats the migration of a pollutant as a random process and accounts for extensive details of atmospheric turbulence and meteorology. The motivation of this thesis is the importance of applying this modeling technique as a tool to estimating emission strength and pollutant concentrations using data from direct measurement.

The main theme of the thesis deals with the development and application of a Lagrangian particle model (LPM) to estimating emission strength and air pollutant concentrations specifically for the short-range dispersion of an air pollutant in the ABL. The model performance was evaluated with two experimental data sets: one obtained from the Rubbertown field study and the other from the Project Prairie Grass (PPG) experiments. Satisfactory agreement was found between model predictions and PPG data, and the LPM was used as the platform of parametric uncertainty analysis. Uncertainty in model formulation, resolution, and parameters typically exist and are of importance because such uncertainty can considerably affect model results. In this thesis, effects of uncertainties in five parameters (Monin-Obukhov length, friction velocity, roughness height, mixing height, and the universal constant of the random component) of the LPM on mean ground-level concentrations were examined under slightly and moderately stable conditions. The analysis was performed under a probabilistic

framework using Monte Carlo simulations with Latin hypercube sampling and linear regression modeling. It has been shown that, among the meteorological parameters, friction velocity is typically the most important input. The universal constant is another influential input because its uncertainty contribution often dominates those from most other inputs. Additional analysis of the half width of mean ground-level concentration contours has been conducted.

Further, the thesis includes four additional studies related to the Lagrangian particle modeling as follows:

- An alternative technique of formulating joint probability density functions (pdfs) of velocity for atmospheric turbulence based on the Koehler-Symanowski technique has been presented, with emphasis on the ABL under convective conditions. A number of joint pdfs have been illustrated and discussed.
- Several aspects of local increments in a multidimensional single-particle LPM have been analyzed and discussed. The main tools used for the analysis are the algebra of Ito integrals and the Wagner-Platen formula. By doing so, additional understanding of the model validity of the model and the accuracy of the solution to the model in numerical simulation can be gained.
- Analogy between the diffusion limit of LPMs and the classical theory of turbulent diffusion has been discussed. The diffusion limit refers to the asymptotic condition where the local decorrelation time scale of turbulence becomes zero. The method used in performing the asymptotic reduction was the projection formalism.
- Some proposed forms of the Lagrangian velocity autocorrelation of turbulence has been briefly discussed using a set of mathematical and physical requirements.

TABLE OF CONTENTS

LIST OF TABLES

LIST OF FIGURES

NOMENCLATURE

Chapter 2:

Δ	Differential or local increment
δ_{ij}	Kronecker delta function's component (i, j)
ε	Mean energy dissipation rate
ϕ_i	Function, see Eq. (2.4)
π	3.141592654 …
η	Kolmogorov length scale
ν	Kinematic viscosity
τ, τ_{ij}	Covariance matrix of velocity and its component (i, j)
τ^{-1}, $(\tau^{-1})_{ij}$	Inverse of τ and its component (i, j)
τ_η	Kolmogorov time scale
a_i	Drift coefficient's component i
b_{ij}	Diffusion coefficient's component (i, j)
C	Concentration
C_o	Universal constant
D	Molecular diffusivity
I	Indicator function
L	Characteristic length scale of a turbulent flow
l	Turbulent motions of scale l
N	Number of simulated particles
$O(.)$	Quantity of big order (.)
p_E	Probability density function of (Eulerian) velocity
Q	Emission strength of a continuous source
R	Reaction term
S	Emission strength of an instantaneous source
S	External source or sink of a pollutant's mass
T_p	Interparticle time of particles released from a continuous source
T_r	Residence time of a particle within a grid cell
t	Time
U_i	Mean of u_i
$\boldsymbol{u}$, u_i	Velocity vector and its component i
u'	Characteristic velocity scale of a turbulent flow
u_η	Kolmogorov velocity scale
V	Volume of a grid cell
W_i	Standard Brownian motion's component i
$\boldsymbol{x}$, x_i	Position (or displacement) vector and its component i
$\langle\ \rangle$	Expectation (or mean) of a random variable

Chapter 3:

α	Constant, see Eq. (3.16)

χ	Function, see Eq. (3.3)
δ_{ij}	Kronecker delta function's component (i, j)
ε	Mean energy dissipation rate
ϕ_i	Function, see Eq. (3.7)
π	3.141592654 …
θ	Mean wind direction
σ_u^2, σ_v^2, σ_w^2	Variances of along-wind, crosswind, and vertical velocities, respectively
σ_y, σ_z	Lateral and vertical dispersion parameters
τ, τ_{ij}	Covariance matrix of velocity and its component (i, j)
τ^{-1}, $(\tau^{-1})_{ij}$	Inverse of τ and its component (i, j)
τ_{uw}	Covariance between along-wind and crosswind velocities
ψ_M	Businger stability function (or its modification)
a_i	Drift coefficient's component i
b_{ij}	Diffusion coefficient's component (i, j)
C	Mean ground-level concentration
CIC	Crosswind-integrated mean ground-level concentration
CIC^*	CIC scaled by Q
C_o	Universal constant
c_u, c_v, c_w	Constants, see Eq. (3.16)
E	Summation term, see Eq. (3.13)
g	Gravity constant
h	Mixing height or inversion depth
h_s	Source height
k	von Karman constant
L	Monin-Obukhov length
p_E	Probability density function of (Eulerian) velocity
Q	Emission strength of a continuous source
q	Parameter, see Eq. (3.11)
R^2	Coefficient of determination
s	Distance along an arc
T'	Fluctuating component of temperature
T	Mean near-surface absolute temperature
U	Mean horizontal or along-wind velocity
U_i	Mean of u_i
u_*	Friction velocity
u_i	Velocity's component i
w_*	Convective velocity scale
w'	Fluctuation component of vertical velocity
x	Along-wind distance
x_i	Position (or displacement) 's component i
y	Lateral or crosswind distance
z	Elevation or height
z_o	Surface roughness height
$\langle\ \rangle$	Ensemble average or expectation of a random variable

Chapter 4:

α	Constant, see Eq. (4A.3)
β	Regression coefficient
β_0	Regression intercept
Δ	Differential or local increment
Δ_{cell}	Size of a grid cell
δ_{ij}	Kronecker delta function's component (i, j)
ε	Mean energy dissipation rate
ϕ_i	Function, see Eq. (4.4)
γ	Concentration ratio, see Section 4.4.1
κ_1, κ_2	Regression coefficients, see Eq. (4.11)
π	3.141592654 …
σ_u^2, σ_v^2, σ_w^2	Variances of along-wind, crosswind, and vertical velocities, respectively
τ, τ_{ij}	Covariance matrix of velocity and its component (i, j)
τ^{-1}, $(\tau^{-1})_{ij}$	Inverse of τ and its component (i, j)
τ_l	Local decorrelation time scale
τ_{uw}	Covariance between along-wind and crosswind velocities
ψ_M	(Modified) Businger stability function
a_i	Drift coefficient's component i
b_{ij}	Diffusion coefficient's component (i, j)
C	Mean ground-level concentration
C^*	C scaled by Q
C^*_{Base}	C^* calculated for a base case
CIC	Crosswind-integrated mean ground-level concentration
CIC^*	CIC scaled by Q
C_o	Universal constant
CV	Coefficient of variation
c_s	Constant in Zilitinkevich's expression
c_u, c_v, c_w	Constants, see Eq. (4A.3)
GS	Global sensitivity
g	Gravity constant
H	Mean surface heat flux
HW	Half width of a profile of C^*
h	Mixing height or inversion depth
k	von Karman constant
L	Monin-Obukhov length
M	Mean or sample mean
M_{Base}	Mean defined at a base case
N	Number of data point
N_{LHS}	Sample size in Latin hypercube sampling
p_E	Probability density function of (Eulerian) velocity
Q	Emission strength of a continuous source
Q_m	Emission strength predicted by a model
Q_o	Reference emission strength

R(x, y)	Ground-level receptor at coordinate (x, y)
R^2	Coefficient of determination
SD	Standard deviation or sample standard deviation
SK	Skewness parameter or sample skewness parameter
s	Distance along an arc
T	Mean near-surface absolute temperature
t	Time
U	Mean horizontal or along-wind velocity
UC	Uncertainty contribution
U_i	Mean of u_i
$\boldsymbol{u}$, u_i	Velocity vector and its component i
u_*	Friction velocity
u_{10}	Mean wind speed at $z = 10$ m
W_i	Standard Brownian motion's component i
X_q	Input q in linear regression modeling
x	Along-wind distance
$\boldsymbol{x}$, x_i	Position (or displacement) vector and its component i
y	Lateral or crosswind distance
z	Elevation or height
z_o	Surface roughness height

Chapter 5:

α_{i+}, α_{j+}	Parameters, see Eq. (5.2)
α_{ij}	Non-negative parameter's component (i, j), see Section 5.2
δ_{ij}	Kronecker delta function's component (i, j)
ρ_{XY}	Correlation coefficient of random variables X and Y
σ_A, σ_B	Parameters, see Eq. (5.10)
σ_U, σ_W	Standard deviations of U and W
A	Parameter, see Eq. (5.10)
B	Parameter, see Eq. (5.10)
C_{ij}	Function, see Eq. (5.2)
D_i	Function, see Eq. (5.3)
F	Joint probability (or cumulative) distribution function
F_X	Probability distribution functions of random variable X
f	Joint probability density function
f_X	Probability density functions of random variable X
G	Function, see Eq. (5.1)
h	Mixing height or inversion depth
k	von Karman constant
L	Monin-Obukhov length
m	Parameter, see Eq. (5.12)
m_A, m_B	Parameters, see Eq. (5.10)
q	Parameter, see Eq. (5.15)
r	Parameter, see Eq. (5.12)
s_U, s_W (or s)	Skewness parameters of U and W

U, u	Horizontal velocity variable and its value
W, w	Vertical velocity variable and its value
w_*	Convective velocity scale
X_i, x_i	Real-valued univariate i and its value
z	Elevation or height
$\langle\ \rangle$	Ensemble average or expectation of a random variable

Chapter 6:

Δ	Timestep, differential of time, or local time increment
Δf	Differential or local increment of f
$\delta(f)$	Local numerical error of f, see Eq. (6.39)
$\delta_{i,\,j}$	Kronecker delta function's component (i, j)
$\widetilde{\delta}_{\{A\}}$	Indicator function of statement A (equal to unity if A is true, otherwise 0)
$\bar{\varepsilon}$	Mean energy dissipation rate
ϕ	Velocity-dependent scalar function
$\lambda_{i,\,j,\,k,\,l}$	Function's component (i, j, k, l), see Eq. (6.26)
σ	Standard deviation of velocity in a one-dimensional turbulent flow
τ	Local time scale of large motions or eddies
τ_η	Kolmogorov time scale
$\boldsymbol{\Omega}$	Sample space of all possible trajectories
ω	Trajectory or realization
ψ	Velocity-independent scalar function
$\mathfrak{I}$	σ-algebra on $\boldsymbol{\Omega}$
$\mathfrak{I}^o$	Equivalent to $\mathfrak{I}^{t_o}$
$\mathfrak{I}^t$	History of a stochastic process' evolution up to time t
$\boldsymbol{a}$, a_i	Drift coefficient vector and its component i
a	Drift coefficient of a one-dimensional Lagrangian particle model
$\boldsymbol{b}$, $b_{i,j}$	Diffusion coefficient matrix and its component i
b	Diffusion coefficient of a one-dimensional Lagrangian particle model
$\mathbf{C}^k$	Class of k-time differentiable scalar functions
$Cov(.)$	Covariance of two random variables
D	Parameter equal to $2d$
$\mathbf{D}_f$	Smooth domain of f
d	Number of dimensions of a turbulent flow
f	Arbitrary scalar function
$f^\dagger$	Exact numerical value of f, see Eq. (6.39)
I	Integral term equivalent to unity
$I_{\widetilde{\mu}}$	Integral term, where $\widetilde{\mu}$ is an integer sequence, see Eq. (6.12)
$I_{\widetilde{\mu}(-)}$	Integral term, where $\widetilde{\mu}(-)$ is a modified integer sequence, see Eq. (6A.3)
$\mathbf{L}_2$	Class of norm-squared integrable scalar functions
L, L_β	Linear differential operators in the Ito formula, see Eq. (6.5)
$N(a, b)$	Normally distributed with mean a and variance b

$n!$	n-factorial
$O(.)$	Quantity of big order (.)
$\mathbf{P}$	Probability measure of $\mathfrak{I}$
$\boldsymbol{Q}$, Q_α	Drift coefficient vector, see Eq. (6.2), and its component α
$\mathbf{R}$	One-dimensional set of real numbers
$R_{f,n}$	Remainder term after stochastic expansion of f up to n^{th}-tuple integrals
$\mathbf{R}^n$	n-dimensional set of real numbers
$\boldsymbol{S}$, $S_{\alpha,\beta}$	Diffusion coefficient matrix, see Eq. (6.2), and its component (α, β)
T	Integration time
T_i	Function's component i, see Eq. (6.54)
t	Time
t_o	Initial time
$\boldsymbol{u}$, u_i	Lagrangian velocity vector and its component i
$\boldsymbol{u}_E$	Eulerian velocity
$V_{i,j}$	Function's component (i, j), see Eq. (6.59)
$\boldsymbol{W}$, $W_{i\,(\text{or}\,\alpha)}$	Standard Brownian motion vector and its component i (or α)
W_0	Parameter equivalent to t
$\boldsymbol{x}$, x_i	Position (or displacement) vector and its component i
$\boldsymbol{Y}$, Y_α	State vector, see Eq. (6.2), and its component α
$\boldsymbol{Y}^o$	Initial $\boldsymbol{Y}$
Z_α	Integrated Brownian motion vector and its component α
$\langle\ \rangle$	Ensemble average or expectation of a random variable
$\langle\ \vert\ \rangle$	Conditional ensemble average or expectation of a random variable

Chapter 7:

$(\boldsymbol{1}-\boldsymbol{P})$	Complement operator of $\boldsymbol{P}$
[. , .]	Commutative property for two operators
$\boldsymbol{1}$	Identity operator
$\beta_{0\text{-}}$, β_1, β_2	Functions, see Eq. (7.75)
$\bar{\varepsilon}$	Mean energy dissipation rate
Δ	Timestep or local time increment
δ	Dirac delta function
$\delta_{\lambda,\lambda'}$	Kronecker delta function's component (λ, λ')
Φ	Function, see Eq. (7B.5)
ϕ	Function, see Eq. (7.3)
φ_0	Function equivalent to p_E
$\varphi_{n\,(\text{or}\,\lambda)}$	Eigenfunction n (or λ) of $\boldsymbol{L}_1$
θ	Variable whose dimension is time
σ	Standard deviation of velocity in a one-dimensional turbulent flow
σ_l	Local characteristic velocity scale of large motions or eddies
π_1, π_2, π_3, …	Functions, see Eqs. (7.9) and (7.16)
τ	Variable whose dimension is time
τ_l	Local characteristic time scale of energy-containing eddies
τ_{sh}	Local time scale of nonstationarity and inhomogeneity of a turbulent flow

ξ	Time lag
ψ	Turbulence variable that defines the deterministic field of a turbulent flow
a	Drift coefficient
a_λ	Coefficient in eigenfunction expansion
b	Diffusion coefficient
C_o	Universal constant
f	Arbitrary real-valued function
f_λ	Function that is a solution of Eq. (7.B1)
$\tilde{f}$	Laplace transform of f
$\mathbf{H}$	Hilbert space
H	Function, see Eq. (7.72)
H_n	Hermite polynomial n
K_D	Eddy diffusivity
$\boldsymbol{L}_1, \boldsymbol{L}_2, \boldsymbol{L}_3$	Linear differential operators, see Eqs. (7.8), (7.15), (7.76)
$\boldsymbol{L}_1^{-1}$	Inverse operator of $\boldsymbol{L}_1$
$\boldsymbol{L}_H$	Hermitian operator
$\boldsymbol{L}_p$	Laplace transform operator
$\boldsymbol{L}_p^{-1}$	Inverse Laplace transform operator
$n!$	n-factorial
$O(.)$	Quantity of big order (.)
q	Weighting function, see Eq. (7B.4)
$\boldsymbol{P}$	Projector or projection operator
p	Probability density function of (z, w) at t
$p_{1\text{-}\boldsymbol{L}_1}$	Conditional probability density function, see Eqs. (7.63) and (7.67)
$p_{2\text{-}\boldsymbol{L}_1}$	Conditional probability density function, see Eqs. (7.66) and (7.68)
p_E	Probability density function of (Eulerian) velocity w at z and t
p_s	Stationary probability density function, see Eqs. (7.20), (7.23), and (7.78)
$p_{w \mid z}$	Conditional probability density function of w at t given z at t
$p_{w \mid z, \tau}$	Conditional probability density function of w at t given (z, τ) at t
p_z	Unconditional probability density function of z at t
$p_{z, \tau}$	Unconditional probability density function of (z, τ) at t
$p_{z \mid \tau}$	Conditional probability density function of z at t given τ at t
R	Lagrangian velocity autocovariance
T_h	Local time scale of inhomogeneity of a turbulent flow
T_s	Local time scale of nonstationarity of a turbulent flow
s	Variable whose dimension is inverse of time
t	Time
t_o	Initial time
v_1, v_2	Functions, see Eqs. (7.36), (7.37), (7.50), and (7.51)
W	Standard Brownian motion
w	Lagrangian velocity
z	Position or displacement
$\langle\ \rangle$	Ensemble average or expectation of a random variable
$\langle \mid \rangle$	Conditional ensemble average or expectation of a random variable

Chapter 8:

$\bar{\varepsilon}$	Mean energy dissipation rate
π	3.141592654 …
τ	Time lag
τ_η	Kolmogorov time scale
ω	Turbulence frequency
a	Lagrangian acceleration
E_L	Lagrangian turbulent energy spectrum
k	Dimensionless universal constant
m	Loop parameter
R_L	Velocity correlation coefficient
$R_{L,a}$	Acceleration correlation coefficient
T_L	Lagrangian integral time scale
t	Time
u	Lagrangian velocity
$\langle\ \rangle$	Ensemble average or expectation of a random variable

Appendix A:

T	Mean near-surface absolute temperature
T'	Fluctuating component of temperature
u	Measured along-wind velocity
v	Measured crosswind velocity
w	Measured vertical velocity
w'	Fluctuation component of vertical velocity
z	Elevation or height
$\langle\ \rangle$	Ensemble average or expectation of a random variable

Appendix B:

θ	Mean wind direction
L	Monin-Obukhov length
Q	Emission strength of a continuous source
u_*	Friction velocity
z_o	Surface roughness height
$\langle\ \rangle$	Ensemble average or expectation of a random variable

Abbreviations:

ABL	Atmospheric boundary layer
cdf	Probability (or cumulative) distribution function
EDM	Eddy diffusion model
EL	Euler differencing scheme
FPE	Fokker-Planck equation

FTIR	Fourier-transform infrared spectrometer
GC-ECD	Gas chromatography and electron-capture technique
GPM	Gaussian plume model
KS	Koehler-Symanowski
LHS	Latin hypercube sampling
LHS	Left-hand side
LPM	Lagrangian particle model
LSM	Lagrangian stochastic model
LSW	Laser wind sensor
MC	Monte Carlo
MS	Milstein differencing scheme
MS	Uncertainty case study associated with a moderately stable condition
MS_{Base}	Base case of MS
PPG	Project Prairie Grass
pdf	Probability density function
RDM	Random displacement model
RHS	Right-hand side
S	Uncertainty case study associated with an intermediately stable condition
S_{Base}	Base case of S
SDE	Stochastic differential equation
SRS	Simple random sampling
ST	Order-1.5 strong Taylor differencing scheme
UA	Ultrasonic anemometer
WS	Uncertainty case study associated with a weakly stable condition
WS_{Base}	Base case of WS

CHAPTER 1

INTRODUCTION

1.1. Overview

Air quality models present the integrated knowledge and understanding of how physical and chemical processes affect pollutants in the atmosphere. They are important tools for both scientific and regulatory communities. One major category of air quality models deals with air pollutant dispersion (shortly, air dispersion) in the atmospheric boundary layer (ABL). A large number of air dispersion models have been developed for different purposes and applications. The most well known are Gaussian plume models in which the distribution of pollutant concentrations at downwind locations is postulated as a Gaussian function or its variants (Turner, 1970). Gaussian plume modeling is the basis for several regulatory models of the U. S. Environmental Protection Agency, such as the Industrial Source Complex (ISC) model and, recently, the AERMOD model (U.S. EPA, 2004). Examples of other air dispersion models are the similarity-based approximations (van Ulden, 1978; Briggs, 1982), the hybrid plume dispersion model (Hanna and Paine, 1989), the second-order closure integrated model plume (Sykes et al., 1984), and the Lagrangian particle model (Thomson, 1987; Wilson and Sawford, 1996). Lagrangian particle modeling is also called the Lagrangian stochastic modeling. In this thesis, both name are used interchangeably in this thesis. Due to increasing advances in understanding the physics of the ABL, recent air dispersion models incorporate more

details of atmospheric turbulence and meteorology, leading to better soundness and validity in their formulations and applications.

The ABL is defined as the layer of the atmosphere that is significantly affected by the presence of the ground surface. Flows in this region are primarily controlled by the characteristics of the ground surface and thermal-mechanical interactions between the surface and the air adjacent to the ground surface. The lowest part (≈ 10%) of the ABL is customarily called the surface boundary layer (SBL). Although there is no precise definition of this layer, it is generally referred to as the region above the ground where vertical fluxes vary only slightly or are approximately constant. For this reason, it is also called the constant flux layer. Influences from larger atmospheric scales also play a role in complicating a flow in a local scale. Usually, flows in the ABL are turbulent and associated with high Reynolds numbers, especially during the day, because the surface-air interaction causes hydrodynamic instability, giving rise to chaotic fluid (air) motions with different scales called “eddies”. For example, suppose the depth of the ABL is 1 km, the characteristic turbulent velocity scale is 1 m s^{-1}, and the kinematic viscosity of air is of the order of 10^{-5} m^2 s^{-1}. Based on these values, the corresponding Reynolds number is of the order of 10^7. Accordingly, pollutant dispersion in the ABL is dominantly controlled by turbulence. The degree of turbulence also varies temporally. In the nighttime, the ABL becomes stably stratified and less turbulent because the ground surface is cooling and a stable temperature gradient is induced extending from the ground. The stable temperature gradient suppresses turbulence generated by the wind shear, and turbulence can exist only in the presence of moderate or strong winds. Besides turbulence, the dispersion of a pollutant may become more complicated by the physical

properties of a pollutant (such as heavy or light gases) and chemical reactions between the pollutant and the ambient air.

Lagrangian particle modeling is a type of turbulence modeling in which the migration of a pollutant is treated as a random process in a Lagrangian coordinate reference frame and a pollutant particle is assumed to be equivalent to a fluid particle that moves along well with a flow streamline. This type of modeling has gained considerable interest from scientific community and has been widely and successfully applied to turbulent dispersion problems, especially in the ABL (e.g. Luhar and Britter, 1989; Flesch et al. 1995; Rotach et al., 1996). Development of this type of modeling dates back to the solution of a Brownian motion and to the classic work of Taylor (1921) and has been advanced along with increased insight into the physics of turbulence (Rodean, 1996, Chapters 1 and 2). It has been known that the Lagrangian particle modeling gives accurate results, compared to several other modeling types, primarily because it can account for the great number of details that govern dispersion mechanisms in a turbulent flow. Moreover, effects from both spatial inhomogeneity and temporal non-stationarity of a turbulent flow can be incorporated into the modeling directly. Nevertheless, in practice, such flow details may not be comprehensively available, leading to some level of difficulty and uncertainty in implementation. Lagrangian particle modeling usually requires a relatively large computational time in implementation because a large number of particle trajectories need to be simulated in order to have high statistical reliability and confidence in inferring pollutant concentrations.

A Lagrangian particle model (LPM) (or a Lagrangian stochastic model (LSM)) typically consists of several physical and mathematical components in its formulation and

implementation. Its major assumption is that the joint evolution of the position and velocity of a fluid particle proceeds over time in a Markov manner, which is described as a set of stochastic differential equations (SDEs) (or Langevin equations). In the SDEs, there are two coefficients involved: drift and diffusion. The drift coefficient represents the local acceleration of the fluid particle associated with a number of turbulence statistics whereas the diffusion coefficient represents the acceleration due to random forcing. The form of the former is determined by the well-mixed condition (Thomson, 1987), and that of the latter is determined by the inertial subrange theory (Kolmogorov, 1941). Figure 1-1 shows a schematic of the main components in a typical LPM. The numerical implementation of LPMs is straightforward and natural in concept. That is, a set of particles is released from a source, and their simulated trajectories are tracked. By doing so, the concentration at a particular location or receptor downwind from the source is statistically estimated as a linear function of the number of particles present in the neighborhood of that location.

For dispersion problems in the ABL, turbulence statistics need to be obtained for characterizing the drift and diffusion coefficients. Although direct measurement is desirable, it is often impossible to be conducted comprehensively for the entire spatial or temporal domain of interest. An alternative is resorting to modeling or interpolating such statistics. One of widely used techniques is interpolating turbulence statistics by similarity-based formulas that are scaled by a group of meteorological parameters as a function of elevation above the ground. For the ABL under unstable conditions, the key scaling parameters are convective velocity scale, Monin-Obukhov length, and mixing

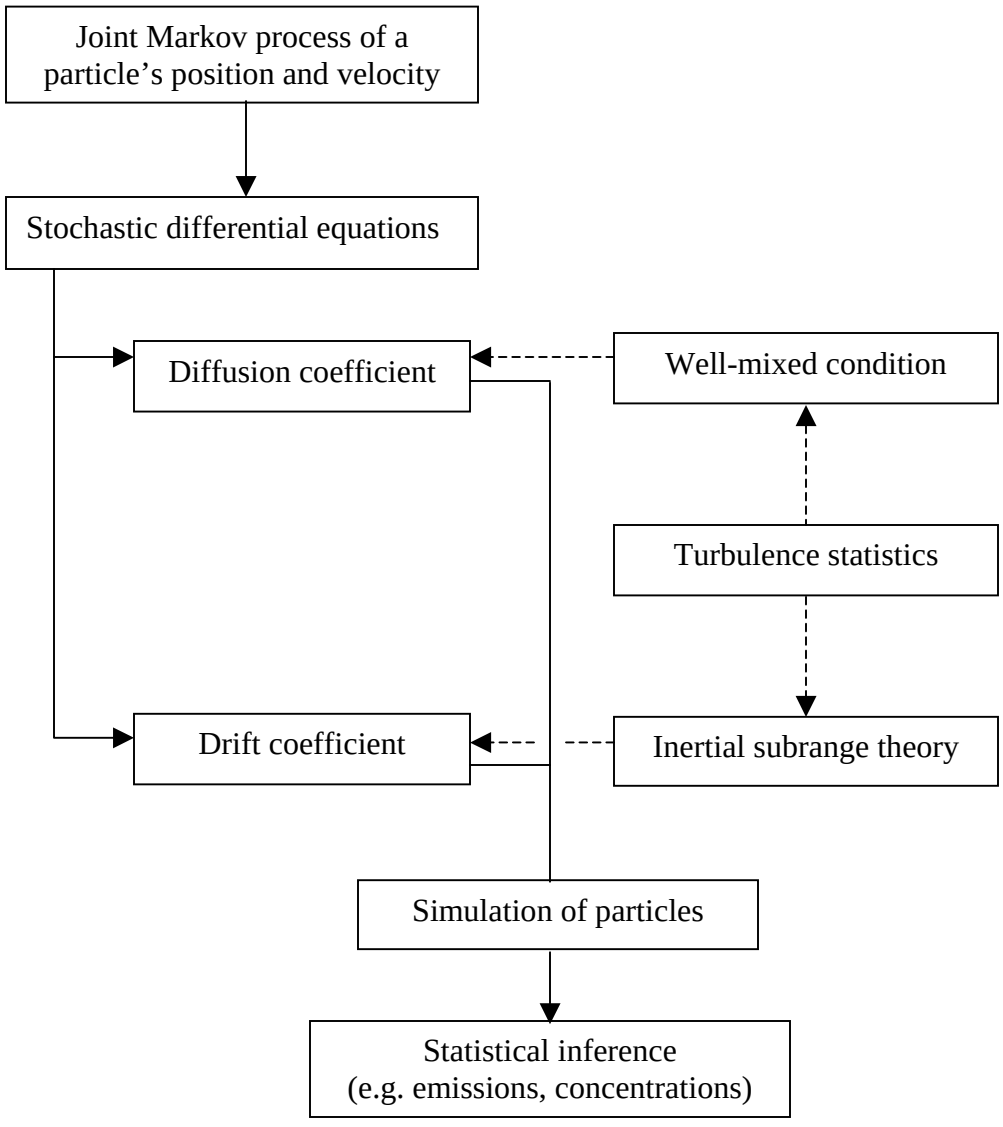

Figure 1-1. Schematic of main components in an LPM

height while, under stable conditions, they are friction velocity, Monin-Obukhov length, and mixing height. In practice, using similarity-based interpolations can sometimes lead to a certain level of errors or uncertainties in model predictions or results. The reason is that the values of meteorological parameters may not be precisely estimated or measured. So, determining how the uncertainty in a model output is induced due to the uncertainties in model inputs is important in that it helps to establish the uncertainty level of model outputs and also helps to specify model inputs that are influential to the model outputs (i.e. inputs of importance). In the area of air dispersion, this information is useful for model users and decision makers in model evaluation, risk assessment, air quality management, and particularly generic to this thesis, the estimation of emission strength and air pollutant concentrations.

Motivated by the development and applicability of the Lagrangian particle modeling and the increased knowledge of the ABL, this thesis is to develop an LPM and apply it to estimating emission strength and pollutant concentrations downwind for short-range dispersion. Due to the importance of considering effects of uncertainty in a computer model on its results, it is also of interest of this thesis to perform the uncertainty analysis of the LPM for some particular aspects of such uncertainty. To examine the model performance, predictions by the model were compared to measurement data obtained from the Rubbertown field study and from Project Prairie Grass (PPG) experiments. The Rubbertown field study is a project initiated and organized by the Georgia Tech Research Institute (GTRI) with the collaboration of the Air Quality Group of the department of Civil and Environmental and the U.S. Army Soldier and Biological Chemical Command (SBCCOM), under the sponsorship of the U.S. Environmental

Protection Agency (U. S. EPA). The field study was conducted in summer 2000 at the Dupont Dow Facility in the Rubbertown industrial complex, Louisville, Kentucky. In the project, an innovative non-Doppler laser wind sensor was developed by the GTRI, and its performance was tested in the field. In addition, a dispersion experiment was carried out using several measurement instruments to collect concentration and meteorological data for use in the modeling. The PPG experiments (Barad, 1958) are considered the most comprehensive dispersion field experiments ever conducted in North America and have been extensively used in testing various dispersion models. Along with the development and application of the LPM, four additional studies related the Lagrangian particle modeling were conducted. They are described as follows:

A first study concerns the analytical formulation of joint probability density functions (pdfs) of velocity in the ABL. This subject is motivated by the fact that the pdf of velocity is an important component in turbulence modeling, especially Lagragian particle modeling, because it provides the information for one-point statistics of velocity that can be used to characterize the drift coefficient of an LPM. Moreover, the pdf formulation for one velocity component (i.e. for one-dimensional turbulence) has been considerably investigated and developed while that for more than one velocity component is far less advanced. Here, an alternative technique called the Koehler-Symanowski formulation (Koehler and Symanowski, 1995) is presented, by which a joint pdf is constructed by taking advantage of the available information of its associated marginal pdfs.

A second study deals with local increments involved in LPMs. The rationale is that the validity of an LPM essentially relies on a number of assumptions, one of which is

the magnitude of a time scale within which the models proceed properly theoretically and numerically. For example, Pope (2002) found that although the form of the diffusion coefficient of a typical LPM takes an isotropic form (see Chapter 2), a large departure from isotropy could take place during numerical simulations. Monti and Leuzzi (1996) expressed concern of the possibility of highly sensitive or overflow behavior of an LPM during simulations and necessarily reduced time step sizes to be very small. Thomson (1987), Rotach et al. (1996), and Schwere et al. (2002) restricted time step sizes by some *ad hoc* strategies for the simple and widely used Euler differencing scheme. Thus, it is of interest to investigate the roles that local increments play. The tool used in doing so is the algebra of multiple stochastic integrals, enabling the local increment of a variable (or a function) and its statistics to be expressed as a series expansion. Here, several aspects of such local increments are analyzed, including those related to the form of the diffusion coefficient, those arising from the truncation of higher-order terms of certain numerical differencing schemes, and the roles of the restriction strategies of time step sizes for the Euler scheme.

A third study presents a theoretical analogy between the diffusion limit of LPMs and the classical theory of turbulent diffusion of Taylor (1921). The diffusion limit refers to the asymptotic condition where the local decorrelation time scale of turbulence becomes zero, causing an LPM to reduce to a random displacement model (RDM). Note that an RDM is a stochastic model in which the position of a particle is explicitly modeled as a Markov process and are considered equivalent to an eddy diffusion model. Some workers have applied them to the problems of turbulent diffusion (Rodean, 1996, p.

41-42, and references therein). The method used in performing the asymptotic analysis is the formalism of projection method (Gardiner, 1997, Chapter 6).

A fourth study briefly discusses some proposed forms of Lagrangian velocity autocorrelation for turbulent diffusion using simple mathematical and physical requirements.

1.2. Scope and Objectives

This thesis revolves around the technique of Lagrangian particle modeling applies it as a tool to air dispersion problems. The framework of this thesis is the short-range dispersion of a non-reactive neutrally-buoyant pollutant in the ABL, and the thesis is divided into the following parts:

Part 1: Estimation of emission strength and pollutant concentrations by an LPM

Objectives:

- Develop a three-dimensional source-receptor LPM for estimating emission strength and pollutant concentrations downwind.
- Evaluate the performance of the developed LPM using the data collected and processed from the Rubbertown field study and the PPG experiments.

Part 2: Uncertainty analysis of an LPM under weakly and moderately stable conditions

Objectives:

- Evaluate how uncertainties in a number of parameters of the LSM developed in Part 1 affect mean ground-level concentrations and the half-width of mean ground-level concentration contours at a distance from a continuous point source using Monte Carlo simulations with Latin hypercube sampling and linear regression modeling.
- Specify parameters (or inputs) of importance of the model.

Part 3: An alternative approach in formulating joint pdfs of velocity in the ABL

Objectives:

- Apply the Koehler-Symanowski technique to formulating joint pdfs of velocity in the ABL, with emphasis on the ABL under convection conditions.
- Illustrate and discuss a number of pdfs formulated by this technique.

Part 4: Local increments of first-order LPMs and their roles in numerical implementation

Objectives:

- Apply the algebra of multiple stochastic integrals to analyzing a number of local increments and their statistics involved in multidimensional LPMs.
- Examine local increments and their statistics related to the form of the diffusion coefficient.
- Examine the hierarchy of local numerical errors arising from the truncation of higher-order terms from three numerical differencing schemes: the Euler, Milstein, and order-1.5 strong Taylor schemes, with emphasis on the first scheme.
- Discuss the roles of a number of restriction strategies of time step sizes for the Euler scheme.

Part 4: Analogy between the diffusion limit of LPMs and the classical theory of turbulent diffusion

Objectives:

- Qualitatively relate the concept of the correlation function of velocity defining the eddy diffusivity at large times for stationary isotropic turbulence in Taylor (1921) to the case of nonstationary inhomogeneous turbulence.

Part 5: Evaluation of some proposed forms of Lagrangian velocity autocorrelation for turbulent diffusion

Objectives:

- Discuss some proposed forms of Lagrangian velocity autocorrelation for stationary isotropic turbulence using a number of mathematical and physical requirements.

1.3. Thesis Organization

The contents of the remaining eight chapters of the thesis are as follows: Chapter 2 describes the relevant physical and mathematical components of the Lagrangian particle modeling. Chapter 3 provides the details of the Rubbertown field measurements and the PPG experiments and those of the LPM developed and used in the study as well as the model evaluation. Chapter 4 presents the formal evaluation of effects of uncertainties in a number of parameters in the developed LPM on mean ground-level concentrations under weakly and moderately stable conditions. As seen, Chapters 2-4

constitute the main focus of the thesis. For Chapters 5-8, they correspond to the four additional studies related to the Lagrangian particle modeling. Chapter 5 presents an alternative technique in analytically formulating of joint probability density functions of velocity for turbulent flows in the ABL. In Chapter 6, the analysis of local increments involved in LPMs is conducted, and the results from the analysis are discussed in detail. Chapter 7 presents a theoretical analogy between the diffusion limit of LPMs and the classical theory of turbulent diffusion. In Chapter 8, some proposed forms of Lagrangian velocity autocorrelation are examined using some simple mathematical and physical requirements. Finally, Chapter 9 gives the relevant conclusions and comments of the thesis and suggests future work.

References

Barad, M. L. (Editor) (1958) Project Prairie Grass, A Field Program in Diffusion. Vol. 1. Geographical Research Paper No. 59, Air Force Cambridge Research Center, Belford, Massachusetts.

Briggs, G. A. (1982) Similarity forms for ground-source surface-layer diffusion. Boundary-Layer Meteor. 23, 489-502.

Flesch, T. K., Wilson, J. D., Yee, E. (1995) Backward-time Lagrangian stochastic dispersion models and their application to estimate gaseous emissions. J. Appl. Meteor. 34, 1320-1332.

Gardiner, C. W. (1997) Handbook of Stochastic Methods. Springer, New York.

Hanna, S. R., Paine, R. J. (1989) Hybrid plume dispersion model (HPDM) development and evaluation. J. Appl. Meteor. 21, 206-224.

Koehler, K. J. and Symanowski, J. T. (1995) Constructing multivariate distributions with specific marginal distributions. J. Multivariate Anal. 55, 261-282.

Kolmogorov, A. N. (1941) The Local Structure of turbulence in incompressible viscous fluid for very large Reynolds numbers. Dokl. Akad. Nauk. 30, 301-305.

Luhar, A. K., Britter, R. E. (1989) A random walk model for dispersion in inhomogeneous turbulence in a convective boundary layer. Atmos. Environ. 23, 1911-1924.

Monti, P., Leuzzi, G. (1996) A closure to derive a three-dimensional well-mixed trajectory-model for non-Gaussian, inhomogeneous turbulence. Boundary-Layer Meteor. 80, 311-331.

Pope, S. B. (2002) Stochastic Lagrangian models for velocity in homogeneous turbulent shear flow. Phys. Fluids 14, 1696-1702.

Rodean, H. C. (1996) Stochastic Lagrangian Models of Turbulent Diffusion. Monograph No. 48, American Meteorological Society, Boston, Massachusetts.

Rotach, M. W., Gryning, S. E., Tassone, C. (1996) A two-dimensional Lagrangian stochastic dispersion model for daytime conditions. Q. J. R. Meteorol. Soc. 122, 367-389.

Schwere, S., Stohl, A., Rotach, M. W. (2002) Practical considerations to speed up Lagrangian stochastic particle models. Comput. Geosci. 28, 143-154.

Sykes, R. I., Lewellen, W. S., Parker, S. F. (1984) A turbulent transport model for concentration fluctuations and fluxes, J. Fluid Mech. 139, 193-218.

Taylor, G. I. (1921) Diffusion by continuous movements. Proc. Lond. Math. Soc. 20, 196-211.

Thomson, D. J. (1987) Criteria for the selection of stochastic models of particle trajectories in turbulent flows. J. Fluid Mech. 180, 529-556.

Turner, D. B. (1970) Workbook of Atmospheric Dispersion Estimates. U. S. EPA, Office of Air Programs, Research Triangle Park, North Carolina.

van Ulden, A. P. (1978) Simple estimates for vertical diffusion from sources near the ground. Atmos. Environ. 12, 2125-2129.

Wilson, J. D., Sawford, B. L. (1996) Review of Lagrangian stochastic models for trajectories in the turbulent atmosphere. Boundary-Layer Meteor. 78, 191-210.

U. S. EPA (2004) Support center for regulatory air models (SCRAM). http://www.epa.gov/ttn/scram.

CHAPTER 2

DESCRIPTION OF LAGRANGIAN PARTICLE MODELING

In this chapter, a brief historical review of Lagrangian particle model is given while more details can be seen in Rodean (1996, Chapter 2). The mathematical and physical fundamentals of Lagrangian particle modelin are described for an incompressible turbulent flow, which include fluid and marked particles, model formulation, Kolmogorov's hypotheses, Markov assumption, and statistical inference of emission strength and mean concentrations.

2.1. Historical Background

The foundation of Lagrangian particle modeling dates back to botanist Robert Brown's observation of the irregular motion of small pollen grains suspended on a water surface in early 19th century. This behavior became known later as Brownian motion and was successfully explained in a probabilistic framework by Einstein (1905). Following Einstein's work, Smoluchowski (1906) and Langevin (1908) developed two complementary theories for the motion of particles in fluids. Langevin presented a stochastic differential equation (which was later named after him, i.e. Langevin equation) for the random movement of a particle while Smoluchowski described it as an evolving probability distribution by a partial differential equation. Both approaches have become standard techniques for describing a variety of random (or stochastic) phenomena,

especially Markov processes. Since then, the theory of Markov processes and stochastic differential equations had been advanced by many workers such as A. D. Fokker, K. Ito, A. N. Kolmogorov, L. S. Ornstein, R. L. Stratonovich, G. E. Uhlenbeck, and N. Weiner.

Parallel to the theory of random processes is ever-increased understanding of physics of turbulence and turbulent flows. Taylor (1921) introduced a classical concept of how to relate mass diffusion in a turbulent flow to velocity autocorrelation function, which was extended further by Richardson (1926). Kolmogorov (1941) developed an influential theory, customarily called inertial-subrange or K41 theory, including a number of hypotheses characterizing small-scale motions in a turbulent flow. Obukhov's (1959) is the first to suggest that a Markov process be used to model a turbulent diffusion, which is currently known as Lagrangian particle (or stochastic) modeling of turbulent diffusion. This idea has been adopted and extended considerably. The theoretical rigor of this modeling technique is due to several works during past twenty-five years, e.g. Durbin (1983), Pope (1985, 1987), Sawford (1985), and Thomson (1987, 1990). Importantly, Thomson (1987) introduced a fundamental concept called the well-mixed condition that helps characterize Lagragian particle models (LPMs) in an appropriate and systematic manner. Recent developments have dealt with specification and treatment of boundary conditions for a model, characterization and verification of the drift coefficient of a model, application to various turbulent flows, and model development for concentration fluctuations due to turbulent diffusion (Sawford, 1992; Wilson and Sawford, 1996; Pope, 2000, Chapter 12). One major factor that has led to the wide application of the modeling technique in practice is the availability of high-speed computational resources.

2.2. Fluid and Marked Particles

In an LPM, a fluid element is considered both "a fluid particle" and "a marked particle". The term "a fluid particle" is used to designate the part of a flow being followed. A fluid particle presumably represents a fluid element whose size is much larger than the molecular length scale but at least smaller than the smallest scale to be resolved in a problem. In the context of turbulence, the upper bound of its size is approximately the Kolmogorov scale. When existing in a flow, the fluid particle moves kinematically along a streamline or holds its own entity without disturbing the flow.

Conservation of mass for a marked particle in a Lagrangian coordinate reference is written as

$$\frac{\mathrm{d}C}{\mathrm{d}t} = D\frac{\partial^2 C}{\partial x_i^2} + S + R, \tag{2.1}$$

where $C \equiv C(\boldsymbol{x},t)$ is the concentration at location $\boldsymbol{x}$ and time t, D is the molecular diffusivity, S is the external source or sink, and R is the gain or loss by reactions. When the dispersion of a pollutant is dominated or controlled by turbulence, the molecular diffusivity D may be neglected. As a consequence, since a Lagrangian coordinate reference frame is attached onto a fluid particle along its entire migration, the source term S automatically becomes zero. Then, Eq. (2.1) is reduced to $\mathrm{d}C/\mathrm{d}t = R$, where $C \equiv C(t)$ is now the concentration (or mass load) associated with the particle. If there is no

reaction involved in the dispersion, the reaction term R disappears (i.e. $\mathrm{d}C/\mathrm{d}t = 0$). This corollary suggests that the entire mass of a fluid particle is always held constant.

2.3. Model Formulation

An LPM is based essentially on the assumption that a joint process of a fluid (and marked) particle's position and velocity ($\boldsymbol{x}$, $\boldsymbol{u}$) in a turbulent flow evolves continuously with time in a Markov manner. In three dimensions, the joint process can be expressed by the following set of stochastic differential equations (SDEs)

$$\begin{aligned} \mathrm{d}x_i &= u_i \, \mathrm{d}t, \quad \text{and} \\ \mathrm{d}u_i &= a_i \, \mathrm{d}t + b_{ij} \, \mathrm{d}W_j , \end{aligned} \tag{2.2}$$

where i and j (= 1, 2, and 3) are the Cartesian directional indices, $a_i \equiv a_i(\boldsymbol{x}, \boldsymbol{u}, t)$ is the drift coefficient in direction i, $b_{ij} \equiv b_{ij}(\boldsymbol{x}, t)$ is the component (i, j) of the velocity-independent diffusion coefficient, and $\mathrm{d}W_j$ is the differential of a Weiner process in direction j. Eq. (2.2) is also called the Langevin equation of the process. All variables in the above equation are defined at time t. The Weiner process is the uncorrelated Gaussian forcing with mean zero and variance $\mathrm{d}t$, and its differential represents an external random acceleration (acting on a fluid particle) with properties $\left\langle \mathrm{d}W_i(s)\,\mathrm{d}W_i(t) \right\rangle = 0$ for $s \neq t$ and $\left\langle \mathrm{d}W_i(t)\,\mathrm{d}W_j(t) \right\rangle = 0$ for $i \neq j$. Note that all equations in this chapter are written in a tensor form where the summation over indices applies. The Markov assumption is considered acceptable for the reason that the acceleration of fluid particles is typically

autocorrelated only over times of order of τ_η that is small for a turbulent flow with a large Reynolds number. The above model is subject to two necessary conditions: the inertial subrange theory (Kolmogorov, 1941) and the well-mixed condition (Thomson, 1987). According to the former condition, b_{ij} takes the universal form

$$b_{ij} = \delta_{ij} \, (C_o \, \varepsilon)^{1/2} \, , \tag{2.3}$$

where δ_{ij} is the Kronecker delta function, C_o is the dimensionless universal constant, and ε is the mean dissipation rate of turbulent kinetic energy. The well-mixed condition states that if the particles of a pollutant are initially well mixed (in both position and velocity spaces) in a flow, they will remain so. According to this condition, Thomson showed that the expression of a_i can be written as follows:

$$a_i = \frac{1}{p_E} \frac{\partial}{\partial u_j} \left(\frac{1}{2} b_{ik} \, b_{jk} \, p_E \right) + \frac{\phi_i}{p_E} \, , \tag{2.4}$$

where $p_E \equiv p_E(\boldsymbol{x}, \boldsymbol{u}, t)$ is the probability density function of (Eulerian) velocity and the function $\phi_i \equiv \phi_i(\boldsymbol{x}, \boldsymbol{u}, t)$ satisfies the relation

$$\frac{\partial \phi_i}{\partial u_i} = -\frac{\partial p_E}{\partial t} - \frac{\partial (u_i \, p_E)}{\partial x_i} \, , \tag{2.5}$$

subject to the boundary condition

$$\phi_i \to 0 \quad \text{as} \quad |\boldsymbol{u}| \to \infty . \tag{2.6}$$

For two and three dimensions, there generally exist a large (or infinite) number of solutions to Eq. (2.5), causing the non-uniqueness problem for the form of a_i. If p_E is given to be Gaussian (or normally distributed), i.e.

$$p_E = \frac{1}{(2\pi)^{3/2}(\text{Det } \tau)^{1/2}} \exp\left[-\frac{1}{2}(u_i - U_i)(\tau^{-1})_{ij}(u_j - U_j) \right], \tag{2.7}$$

the simplest form of ϕ_i is (Thomson, 1987)

$$\begin{aligned} \frac{\phi_i}{p_E} = {} & \frac{\partial U_i}{\partial t} + U_j \frac{\partial U_i}{\partial x_j} + \frac{1}{2}\frac{\partial \tau_{ij}}{\partial x_j} + \left[\frac{\partial U_i}{\partial x_j} + \frac{1}{2}(\tau^{-1})_{mj}\left(\frac{\partial \tau_{im}}{\partial t} + U_k \frac{\partial \tau_{im}}{\partial x_k} \right) \right](u_j - U_j) \\ & + \frac{1}{2}(\tau^{-1})_{mj} \frac{\partial \tau_{im}}{\partial x_k}(u_j - U_j)(u_k - U_k) . \end{aligned} \tag{2.8}$$

where π = 3.141592654 … , τ is the covariance matrix of velocity, τ^{-1} is the inverse matrix of τ, and U_i is the mean (Eulerian) velocity in direction i,

2.4. Kolmogorov's Hypotheses

According to Kolmogorov (1941), for any turbulent flow with a large Reynolds number, the turbulent energy of the flow is transferred from larger scales of motion to

smaller scales of motion through a mechanism called the "energy cascade". The cascade eventually goes to the end of turbulence scale where most of the transferred energy dissipates quickly into thermal energy by viscosity. The mean dissipation rate of turbulent energy (denoted by ε) can be approximated by $\varepsilon = u'^3 / L$, where u' is the characteristic velocity scale of a turbulent flow, L is the characteristic length scale of the flow (whose magnitude is of the order of the flow geometry), and ν is the kinematic viscosity of a fluid. At the end of scale, the smallest length scale (η), velocity scale (u_η), and time scale (τ_η) have a universal form that is uniquely determined by ν and the mean energy dissipation rate ε are estimated by $\eta = (\nu^3 / \varepsilon)^{1/4}$, $u_\eta = (\varepsilon\nu)^{1/4}$, and $\tau_\eta = (\nu / \varepsilon)^{1/2}$, respectively. These smallest scales are typically referred to as the Kolmogorov scales. The region below the Komogorov scales is conventionally called the dissipation subrange. For the turbulent motions of scale l in the range $\eta << l << L$, their statistics are locally isotropic (i.e. invariant to the rotation and reflection of the coordinate axes) and have a universal form that is uniquely determined by ε and independent of ν. The region corresponding to this range is called the inertial subrange.

By applying some stochastic properties of the Weiner process to Eq. (2.1) (see its details in Section 6.4 of Chapter 6), it can be shown that, at time t,

$$\left\langle (u_i(t+\Delta t) - u_i(t)) \cdot (u_j(t+\Delta t) - u_j(t)) \right\rangle = b_{ik} b_{jk} \cdot \Delta t + O((\Delta t)^2), \tag{2.9}$$

where Δt is a timestep size at time t. In the inertial subrange, the right-hand-side (RHS) term of the above equation is equal to $\delta_{ij} C_o \varepsilon \cdot \Delta t$ (Monin and Yaglom, 1975, p. 358),

simply yielding Eq. (2.2) (strictly speaking, for small Δt). For the universal constant C_o, there has been an inconsistency in its reported values, ranging widely from 2 to 10 (for review, see Du et al. (1995) and Degrazia and Anfossi (1998)). This work uses the value of 3.0, according to the estimate $C_o = 3.0 \pm 0.5$ by Du et al. (1995).

2.5. Statistical Inference of Emission Strength and Mean Concentrations

To implement an LPM, a large number of particles are required to be simulated in order to obtain high confidence and reliability in statistical inference. Generally, tens of thousands of particles are used in practice. Following the concept of a marked particle, dispersion process is conservative, i.e. there is no gain or loss of the mass of a pollutant after release from an emission source. Hence, it is straightforward that the pollutant concentration at any location is linearly proportional to the emission strength of the source. For an instantaneous source, suppose that a mass strength of S is released and that a total of N particles are generated at the same initial time and carries an equal amount of load S while migrating. It is straightforward to express the mean concentration at location $\boldsymbol{x}$ and time t (denoted by $\langle C(\boldsymbol{x},t)\rangle$) as the linear proportionality to the relationship between the emission strength and the number of particles present at time t within a grid cell placed at location $\boldsymbol{x}$. That is,

$$\langle C(\boldsymbol{x},t)\rangle = \frac{S}{NV}\sum_{i=1}^{N} I(i^{\text{th}}\text{particle in } V) \tag{2.10}$$

where V is the volume of the grid cell placed at location $\boldsymbol{x}$, $I(i^{\text{th}}\text{particle in } V)$ is the indicator function that equals unity for the i^{th} particle present in the grid cell at time t and, otherwise, zero.

For a continuous source with an emission rate of Q, one method in implementing the model is releasing one particle at a time from the source successively with an equal interparticle time (T_p). With this, an amount of mass load QT_p is assigned to each particle. Suppose that the source has released a pollutant for a long period of time such that the concentration field downwind from the source becomes steady (i.e. independent of time). Then, the mean concentration can be computed by

$$\langle C(\boldsymbol{x})\rangle = \frac{QT_p}{V}\sum_{i=1}^{N} I(i^{\text{th}}\text{particle in } V)\,. \tag{2.11}$$

An alternative method for a continuous source is based on the concept of total residence time, by which (i) each particle is generated at the same initial time, (ii) the residence time that each particle spends inside a grid cell is recorded and summed up with those from the other particles, and (iii) the concentration is linearly proportional to the total residence time. In other words,

$$\langle C(\boldsymbol{x})\rangle = \frac{Q}{NV}\sum_{i=1}^{N} T_r(i^{\text{th}}\text{particle in } V)\,, \tag{2.12}$$

where $T_r(i^{\text{th}}\text{particle in } V)$ is the residence time for which the i^{th} particle spends within the grid cell at location $\boldsymbol{x}$ and the other variables are the same as previously. One major advantage of this method is that the spatial-temporal variation of each particle's trajectory is better captured.

2.6. Parameterization of Turbulence Statistics for an LPM

For simulation of particles in an LPM, this thesis assumes an idealized condition where atmospheric turbulence is stationary and horizontally homogeneous and the turning of the wind aloft is neglected and Monin-Obukhov similarity theory and its extension apply. The stationary assumption is generally considered acceptable for short-range dispersion because the travel time average of a cloud of particles is not so large that atmospheric conditions change significantly. Accordingly, any derivative terms of turbulence statistics with respect to time, required by the model, become zero, and any derivative terms with respect to the horizontal coordinates also become zero. All turbulence statistics required by the model can be estimated by similarity-based interpolation formulas proposed in the literature as a function of elevation. Specifically, a logarithmic wind profile is used to interpolate the mean wind in the horizontal plane. It is noted that, in such interpolation formulas, turbulence statistics are scaled by a number of scaling metrological parameters such as Monin-Obukhov length, friction velocity (or convective velocity scale), mixing height or inversion depth, and surface roughness height. Figure 2-1 shows a schematic of the parameterization of turbulence statistics for an LPM in the thesis.

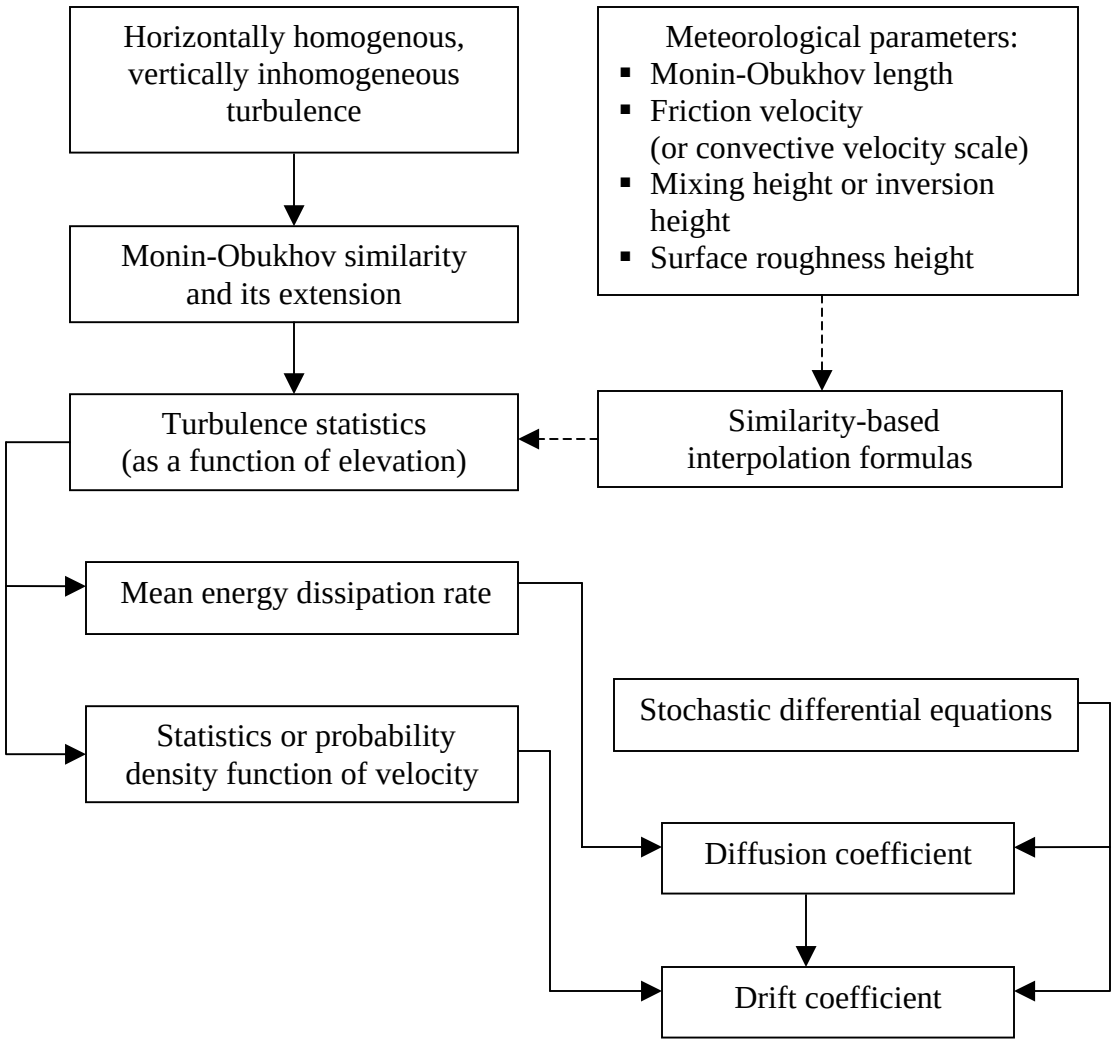

Figure 2-1. Parameterization of turbulence statistics for an LPM

References

Degrazia, G., Anfossi, D. (1998) Estimation of the Kolmogorov constant C_o from classical statistical diffusion theory. Atmos. Environ. 32, 3611-3614.

Du, S., Sawford, B. L., Wilson, J. D., Wilson, D. J. (1995) Estimation of the Kolmogorov constant (C_o) for the Lagrangian structure function, using a second-order Lagrangian model of grid turbulence. Phys. Fluids 7, 3083-3090.

Durbin, P. A. (1983) Stochastic Differential Equations and Turbulent Dispersion. NASA Ref. Pub.1103.

Einstein, A. (1905) Uber die von der molekularkinetischen Theorie der Warme geforderte Bewegung von in ruhenden Flussigkeiten suspendierten Teilchen. Ann. der Physik, 17, 549-560.

Kolmogorov, A. N. (1941) The local structure of turbulence in incompressible viscous fluid for very large Reynolds numbers. Dokl. Akad. Nauk. 30, 301-305.

Langevin, P. (1908) Sur la th'eorie du mouvement brownien. Comptes. Rendues, 146, 530-533.

Monin, A. S., Yaglom, A. M. (1975) Statistical Fluid Mechanics. Vol. 2, MIT Press, Cambridge, Massachusetts.

Obukhov, A. M. (1959) Description of turbulence in terms of Lagrangian variables. Adv. Geophys., 6, 113-116.

Pope, S. B. (1985) PDF methods of turbulent reactive flows. Prog. Energy Combust. Sci., 11, 119-192.

Pope, S. B. (1987) Consistency conditions for random-walk models of turbulent dispersion. Phys. Fluids, 30, 2374-2379.

Pope, S. B. (2000) Turbulent Flows. Cambridge University Press, Cambridge.

Richardson, L. F. (1926) Atmospheric diffusion shown on a distance-neighbor graph. Proc. Roy. Soc. Lond. A, 110, 709-737.

Rodean, H. C. (1996) Stochastic Lagrangian Models of Turbulent Diffusion. Monograph No. 48, American Meteorological Society, Boston, Massachusetts.

Sawford, B. L. (1985) Lagrangian statistical simulation of concentration mean and fluctuation fields. J. Appl. Meteor., 24, 1152-1166.

Sawford, B. L. (1991) Reynolds number effects in Lagrangian stochastic models of turbulent dispersion. Phys. Fluids. 3, 1577-1586.

Sawford, B. L. (1993) Recent developments in the Lagrangian stochastic theory of turbulent dispersion. Boundary-Layer Meteor., 62, 197-215.

Smoluchowski, M. von (1906) Zur kinetischen Theorie der Brownschen Molekularbewegung und der Suspensionen. Ann. Phys., 21, 756-780.

Taylor, G. I. (1921) Diffusion by continuous movements. Proc. Lond. Math. Soc., 20, 196-211.

Thomson, D. J. (1987) Criteria for the selection of stochastic models of particle trajectories in turbulent flows. J. Fluid Mech. 180, 529-556.

Thomson, D. J. (1990) A Stochastic model for the motion of particle pairs in isotropic high-Reynolds-number turbulence, and its application to the problem of concentration variance. J. Fluid Mech., 210, 113-153.

Wilson, J. D., and Sawford, B. L. (1996) Review of Lagrangian stochastic models for trajectories in the turbulent atmosphere. Boundary-Layer Meteor., 78, 191-210.

CHAPTER 3

FIELD MEASUREMENTS AND ESTIMATION OF EMISSION STRENGTH AND POLLUTANT CONCENTRATIONS BY LAGRANGIAN PARTICLE MODELING

Lagrangian particle modeling typically requires detailed information of a turbulent flow by which the simulated trajectory of a particle can be properly characterized, resulting in accurate model predictions. In its applications to dispersion problems in the atmospheric boundary layer (ABL), such information can be derived through similarity theory for the ABL by which a turbulence quantity or statistic is expressed as a function of elevation and a set of scaling parameters. Advances in theories and measurements help increase our knowledge and understanding of the physics of the ABL and continuously improve the soundness of the similarity-based formulation for various turbulence statistics. In this chapter, a Lagrangian particle model (LPM) is constructed, and all turbulence statistics required by the model are quantified by similarity-based interpolation formulas that have been proposed for the ABL. The LPM implemented here will be used as a platform for further analysis (specifically, uncertainty analysis) in the next chapter. Model predictions are to be compared to field measurement data to examine the capability of the model. Two field studies chosen for comparison are the Rubbertown field study and the Project Prairie Grass (PPG) experiments, as discussed in Chapter 1. The details of each field study and the comparison between model results and field data for each study are given here.

3.1. Rubbertown Field Study

The Rubbertown field study was conducted at the Dupont Dow Facility in the Rubbertown industrial complex, Louisville, Kentucky on June 20-23, 2000. The objectives of the study were to test the performance of a non-Doppler laser wind sensor (LWS) developed by the Georgia Tech Reasearch Institute (GTRI) and to conduct a short-range dispersion experiment (GTRI, 2001). Results from the dispersion experiment were to be compared to predictions given by the LPM and using such data to assess the ability of the LPM. Figure 3-1a displays the aerial view of the Rubbertown area and its surroundings, and Figure 3-1b shows the enlarged view of the Dupont Dow Facility. The overall area within a radius of 5 km of the Dupont Dow Facility is industrial and residential, and its terrain is generally flat but highly non-uniform. There was no dispersion experiment during the first three days in the field due to weather constraints and the preparation, calibrations, and tests of all instruments. The dispersion experiment was performed in the afternoon of the final day of the study (June, 23) when weather condition was mildly humid (≈ 50-60% relative humidity), and partly cloudy (≈ 1/4 sky).

In the experiment, sulfur hexafluoride (SF_6) was released from a laboratory-grade SF_6 gas cylinder (>99% pure, molecular weight = 146.0) in the backyard area of the Dupont Dow Facility at a height of 1.5 m above the ground. SF_6 was chosen as a tracer gas because of its chemical inertness to reactions and absorption. Furthermore, it can be detected at low levels by various measurement techniques. Another reason is that SF_6 is non-toxic and non-flammable, which is of safety concern for the area. A continuous

a)

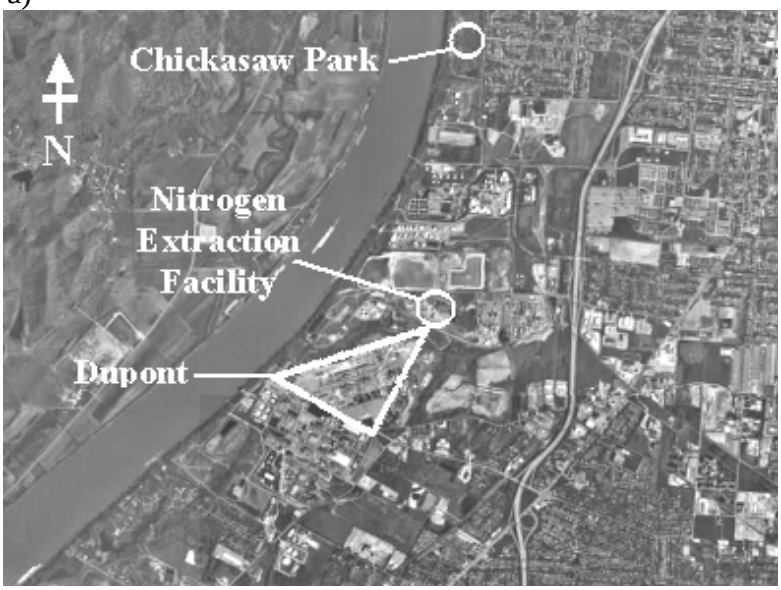

b)

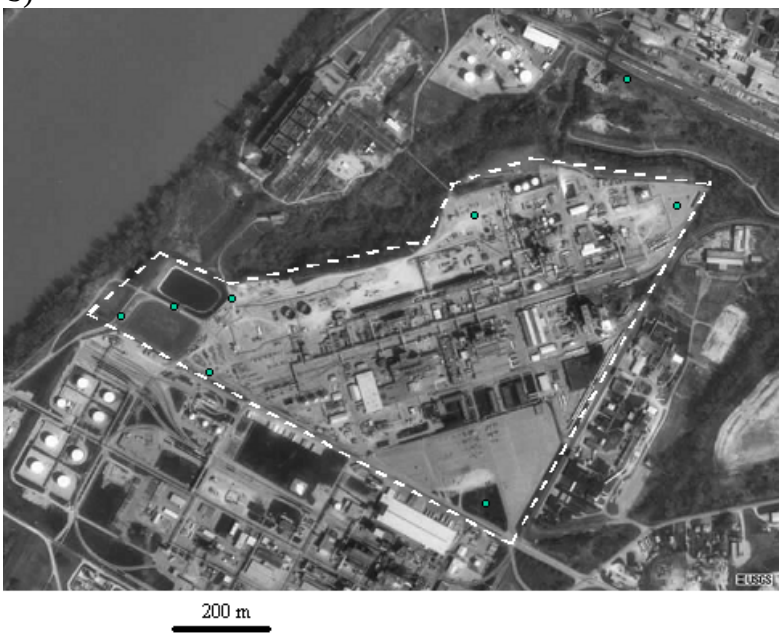

Figure 3-1. Aerial views of: a) Rubbertown area and b) Dupont Dow Facility

release of 40 lpm (equivalent to 3.9 kg s^{-1} at the field condition) of SF_6 began at 14:00 and ended at 16:30. Figure 3-2 shows the SF_6 release unit used in the field study. A number of different instruments were employed to collect concentration and meteorological data, and they were set up at two chosen sites. The first site was an open area adjacent to the Nitrogen Extracting Facility located approximately 400 m from the release location in the northeast direction (≈ 30° from the north). There was a long tree line 3 to 4 m high above the ground and 40 m away in front of the setup. Also, a small building stood 30 m aside of the setup. The team experienced difficulty finding an ideal measurement site that was close to the release point. A Fourier transform infrared spectrometer (FTIR) and a compact meteorological station were stationed at this site. The second site was a large grass area of the Chickasaw Park, approximately 2.3 km away from the release pointing the northeastern direction (≈ 20° from the north). At this site, an FTIR, two ultrasonic anemometers (UAs), a bag-sampling unit, the LWS, and a scintillometer were installed. The open paths of the FTIRs, LWS, and scintillometer were 100-150 m long and oriented approximately perpendicular to the wind direction at 1.5 m above the ground. The local wind direction prior to setup was roughly determined using a wind vane and a smoke candle. The FTIRs were set to collect SF_6 data at 1-min intervals. Wind data from the scintillometer were used for calibrating and testing the LWS and not for calculating meteorological parameters here. The first UA was 2-axis with an output frequency of 1.99 s and installed onto a fixed mast at 4 m above the ground and recorded simultaneously two horizontal wind components (perpendicular to one another). The second UA was 2-axis with an output frequency of 0.99 s, equipped

Figure 3-2. SF_6 release unit

Figure 3-3. Bag-sampling unit

With a temperature sensor, installed onto the same mast at approximately the same height as the first UA. Its output frequency is 0.99 s. It recorded vertical wind velocity. An additional data set of horizontal wind velocity was obtained from the LWS. Thirteen 1-liter Tedlar-PVF bags were used for continuously sampling the ambient air and hung on a pole at a height of 2.0 m from the ground, as shown in Figure 3-3. An air pump filled each bag for 15 min. The bag sampling started at 13:45 and ended at 17:00. Figure 3-4 shows the instrument setup at the Chickasaw Park, and Figure 3-5 shows the graphic representation of the two measurement sites and the release location.

Wind and temperature data obtained at the second site (i.e. the Chickasaw Park) were used to estimate several meteorological parameters, including the Monin-Obukhov length (L), friction velocity (u_*), surface roughness height (z_o), and mean wind direction (θ) clockwise from the direction of the release location and the Chickasaw Park. L represents the height above the ground surface at which the mechanical turbulence production balances the thermal production. This provides a measure of stability of the ABL. By definition,

$$L = \frac{-u_*^3 T}{g\, k\, \langle w'T' \rangle}, \tag{3.1}$$

where g is the gravitational acceleration (= 9.81 m s^{-2}), k is the von Karman constant (≈ 0.4), T is the near-surface temperature (K), T' is the fluctuation component of T, w' is the fluctuating component of vertical velocity, , $\langle w'T' \rangle$ is the vertical turbulent heat flux,

a)

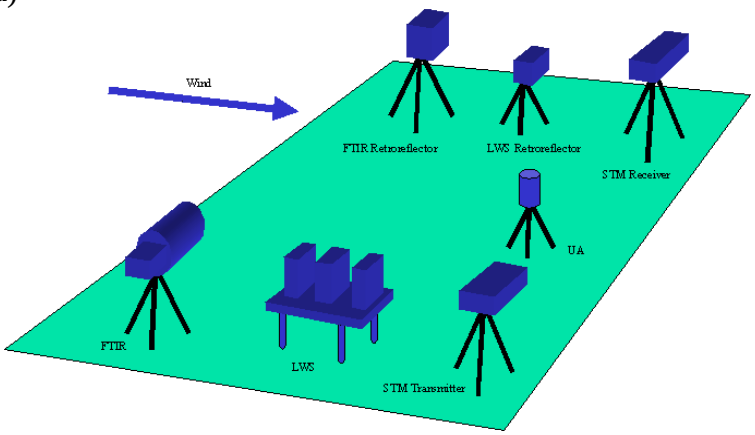

b)

Figure 3-4. Instrument setup at the Chickasaw Park

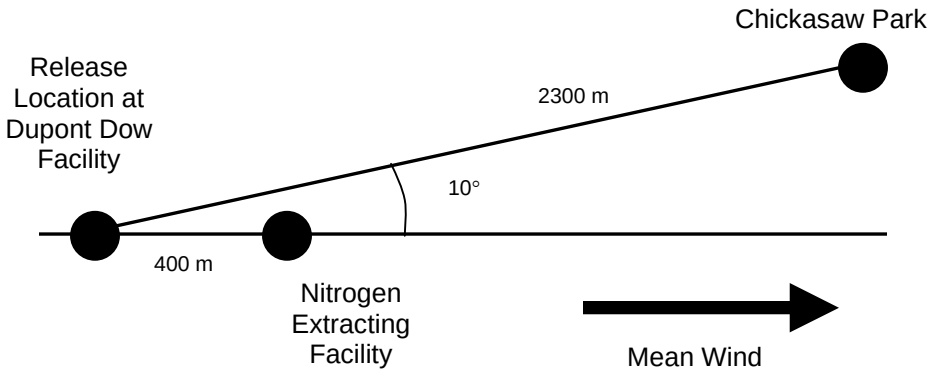

Figure 3-5. Distances and directions between the release location and the two measurement sites

and $\langle\ \rangle$ is the ensemble average (equivalent to the time average in this case) of a variable. u_* represents the surface shear stress or momentum transfer onto the ground by the adjacent air. From the surface-flux profile relationship in the surface boundary layer, the mean horizontal velocity (U) is governed by a logarithmic law and expressed by (van Ulden and Holtslag, 1985):

$$U = \frac{u_*}{k}\left[\ln\left(\frac{z}{z_o}\right) - \psi_M\left(\frac{z}{L}\right) + \psi_M\left(\frac{z_o}{L}\right)\right]. \tag{3.2}$$

The function ψ_M is the Businger stability function that is defined by

$$\psi_M = 2\ln\left(\frac{1+\chi}{2}\right) + \ln\left(\frac{1+\chi^2}{2}\right) - 2\arctan(\chi) + \frac{\pi}{2} \quad (\text{for } L < 0)\text{, and} \tag{3.3}$$

$$\psi_M = -4.7\ (\text{or} -5)\frac{z}{L} \quad (\text{for } L > 0)\text{,} \tag{3.4}$$

where $\pi = 3.14159265\ldots$, $\chi = (1-16\,z/L)^{1/4}$, and z is the height or elevation above the ground. In unstable conditions, another important scaling parameter is convective velocity scale (w_*) that is related to u_* by the relation

$$w_* = u_*\left(\frac{-h}{k\,L}\right)^{1/3}, \tag{3.5}$$

where h is the mixing height of the ABL and its value is typically large, up to 1-2 km under strongly convective conditions. The value of h was not available in the PPG report but assumed to be large in this work (here, 1 km or 1000 m). van Ulden and Holtslag (1985) emphasized that the forms of ψ_M given in Eqs. (3.3) and (3.4) are valid only for $z < L$ but, in unstable conditions, Eq. (3.3) can be used for $z >> L$ (maybe even up to $z = h$) and that, for stable conditions, an alternative form is recommended for $z > L$:

$$\psi_M = -17 \left[1 - \exp\left(-0.29\frac{z}{L}\right)\right]. \tag{3.6}$$

For more details of the measurement instruments and their setup, refer to GTRI (2001)

Table 3-1 gives a summary of meteorological parameters measured or derived in the field study. Note that the results in the table were processed only from time-series data (given in Appendix A of the thesis) measured during 14:30-15:30 because of the presence of non-stationarity for a longer time window. Obtained from solving Eqs. (3.1) and (3.2) for z = 1.6 and 4 m, the values of L, u_*, and z_o equal –5.3 m, 0.19 m s^{-1}, and 0.35 m, respectively. The small negative L suggests a highly unstable or strongly convective condition. For comparison with model predictions, SF_6 concentrations from the FTIR at the Nitrogen Extracting Facility and the bag sampling at the Chickasaw Park were used because concentrations were extremely low at the Chickasaw Park and could not be detected by the FTIR. In other words, its minimum detectable level is not low (or sensitive) enough to measure such low concentrations. Figures 3-6 and 3-7 show the

Table 3-1. Meteorological parameters in the Rubbertown field study

Variable	Unit	Value	Measurement Height (m)
$U(4)$	$m\,s^{-1}$	0.75	4.0
$U(1.6)$	m s-1	0.50	1.6
$\langle w'T' \rangle$	$K\,m\,s^{-1}$	0.09	1.6
T	K	306.0	1.6
θ	degree	9.9	4.0
L	m	-5.3	
u_*	$m\,s^{-1}$	0.19	
z_o	m	0.35	
h	m	1000[a]	
w_*	$m\,s^{-1}$	1.43	

[a]: Assumed to be large for a strongly convective condition

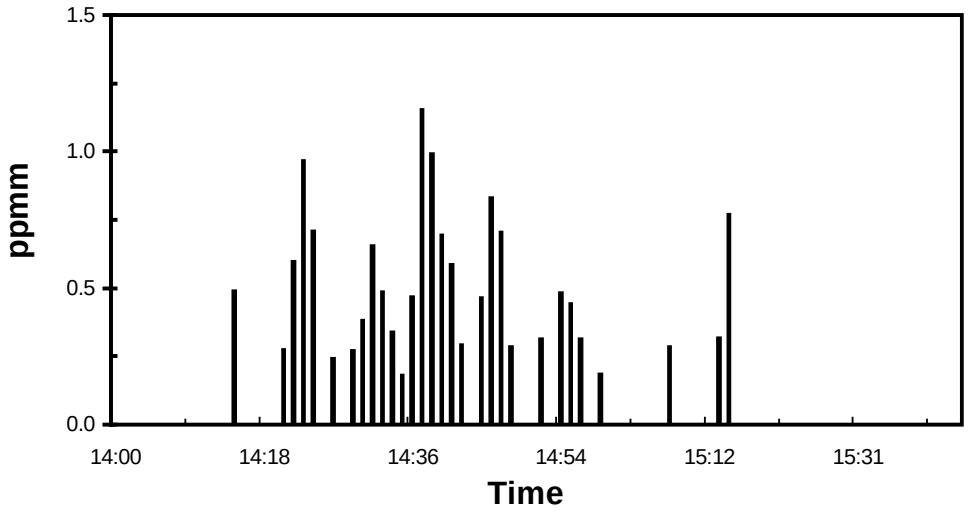

Figure 3-6. SF_6 concentrations at the Nitrogen Extracting Facility by the FTIR

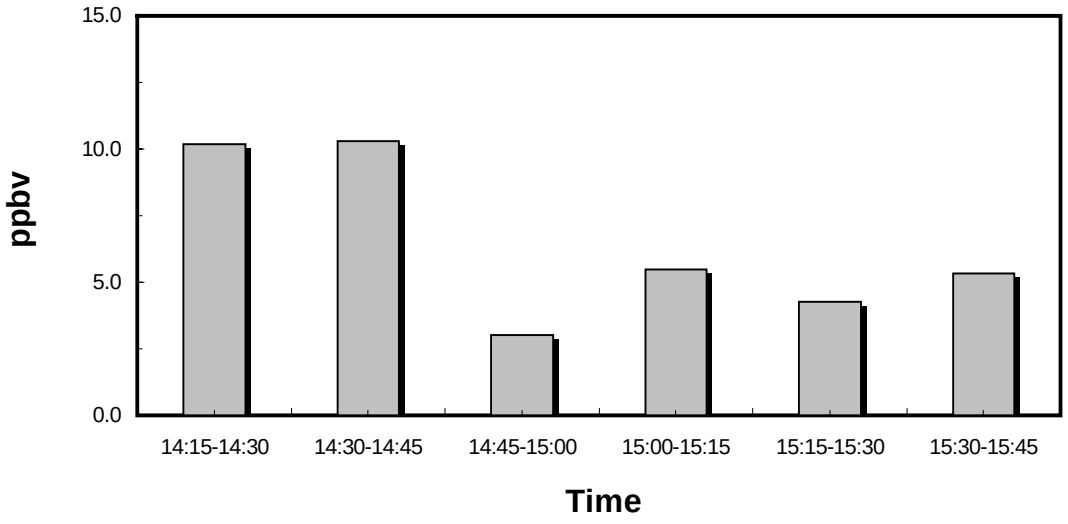

Figure 3-7. SF_6 concentrations at the Chickasaw Park by bag sampling and GC-ECD

time series of SF_6 from the two measurement sites. The former is from the FTIR whereas the latter is from the bag samples later analyzed by gas chromatography using electron-capture device (GC-ECD) with the assistance of Dr. Monique Leclerc of the University of Georgia. The time series in Figure 3-6 is somewhat intermittent, being zero (specifically, below the minimum detectable level of the GC-ECD) for some periods. Like the wind data, the mean concentration of SF_6 at each location is a time average over the period of 14:30-15:30. The background SF_6 concentration was found to approximately equal 1.9 ppbv based on the bag sampling conducted in the early period of measurement, which is much higher than the typical values found in the literature (≈ 3-5 pptv). Some possible reasons for this large difference are that, due to a limited number of air samples collected from the field, calibrating the GC-ECD could not be performed comprehensively or that there were unknown sources of SF_6 in the area and its vicinity. The time-series data presented in Figure 3-6 are of the measured concentrations less the background concentration. The mean concentrations that are averaged over the chosen time window at the Nitrogen Extracting Facility and the Chickasaw Park were found to eqaul 0.23 ppmm (parts per million by mass) (equivalent to 260 $\mu g\ m^{-3}$ at the field condition) and 6.4 ppbv (parts per billion by volume) (equivalent to 37 $\mu g\ m^{-3}$ at the field condition), respectively.

3.2. Comparison of Concentrations from the Rubbertown Field Study and the LPM

The LPM developed in the previous chapter was implemented to calculate the SF_6 concentrations at both measurement locations, based on the field conditions described

above. The drift coefficient of the model is given to take the simplest form based on a Gaussian probability density function (pdf) of velocity, i.e.

$$a_i = -\left(\frac{C_o \varepsilon}{2}\right)(\tau_{ik})^{-1}(u_k - U_k) + \frac{\phi_i}{p_E}, \tag{3.7}$$

where

$$\begin{aligned}\frac{\phi_i}{p_E} = {} & \frac{\partial U_i}{\partial t} + U_j \frac{\partial U_i}{\partial x_j} + \frac{1}{2}\frac{\partial \tau_{ij}}{\partial x_j} + \left[\frac{\partial U_i}{\partial x_j} + \frac{1}{2}(\tau^{-1})_{mj}\left(\frac{\partial \tau_{im}}{\partial t} + U_k \frac{\partial \tau_{im}}{\partial x_k}\right)\right](u_j - U_j) \\ & + \frac{1}{2}(\tau^{-1})_{mj}\frac{\partial \tau_{im}}{\partial x_k}(u_j - U_j)(u_k - U_k).\end{aligned} \tag{3.8}$$

All variables in Eqs. (3.7) and (3.8) are defined in the previous chapter. It has been shown that velocity pdfs in unstable conditions are typically characterized by a significant degree of positive skewness (Baerentsen and Berkowicz, 1984; Luhar et al., 1996; Anfossi et al., 1997). However, incorporating higher-than-second-order moments of velocity with an appropriate closure for a multidimensional LPM is known to be very difficult and not adequately advanced. Therefore, the above-specified drift coefficient is regarded as an *ad hoc* approach to the problem. Flesch and Wilson (1992), as well as Leuzzi and Monti (1998), examined prediction performance between their complex LPMs and an LPM with the simplest diffusion coefficient and surprisingly found that the latter was capable of yielding satisfactory results (or even superior results).

An idealized condition was assumed, in which atmospheric turbulence is stationary and horizontally homogeneous and the turning of the wind aloft is neglected. The stationary assumption is generally considered acceptable for short-range dispersion. Accordingly, any derivative terms with respect to t in Eq. (3.8) become zero. x_3 denotes the vertical distance (or elevation) above the ground, and U_3 is set to zero. The mean wind in the horizontal plane is aligned parallel to the x_1 axis and denoted by U as previously. It follows that U_2, U_3, τ_{12} (= τ_{21}), and τ_{23} (= τ_{32}), and any derivative terms with respect to x_1 or x_2 equal zero, simplifying the calculation of Eq. (3.8). For convenience, x_1, x_2, and x_3 will be replaced by x, y, and z, respectively, and τ_{11}, τ_{22}, τ_{33}, and τ_{13} (= τ_{31}) will be rewritten as σ_u^2, σ_v^2, σ_w^2, and τ_{uw}, respectively. Eqs (3.2) and (3.3) are used to compute U. The rest of the turbulence statistics were determined by the following similarity-based interpolation formulas for $L < 0$ as a function of elevation.

- Variances and covariance: From Rodean (1996, Chapter 12),

$$\frac{\sigma_u^2}{w_*^2} = \frac{\sigma_v^2}{w_*^2} = \left(\frac{k}{|h/L|} \right)^{2/3} \left[4.5\left(1-\frac{z}{h}\right)^{3/2} + 0.6|h/L|^{2/3} \right], \tag{3.9}$$

$$\frac{\sigma_w^2}{w_*^2} = 1.8\left(\frac{z}{h}\right)^{2/3}\left(1-0.8\frac{z}{h}\right)^2, \quad \text{and} \tag{3.10}$$

$$\frac{\tau_{uw}}{u_*^2} = -\left(1-\frac{z}{h}\right)^{3/2-q} \text{ with } q = -\frac{1}{2}\frac{h}{L}\left(1-\frac{h}{L}\right)^{-1}. \tag{3.11}$$

- Mean energy dissipation: From Rodean (1996, Chapter 12),

$$\varepsilon = \frac{u_*^3}{k\,z}\left(1-0.75\frac{z}{L}\right)\left(1-0.85\frac{z}{h}\right)^{3/2} - 0.3\frac{z}{L}. \qquad (3.12)$$

The relations in Eqs. (3.9)-(3.11) satisfy the statistical inequality $\tau_{uw}^2 \le \sigma_u^2\,\sigma_w^2$ for $z_o \le z \le h$. In simulation, perfect reflection of a particle when encountering the ABL top (i.e. $z = h$) and the horizontal plane at $z = z_o$ was carried out. Following Flesch et al. (1995), the fluctuating velocity components in both along-wind and vertical directions are reversed to their opposite signs after reflection.

It is also of practical interest to compare the results from the LPM to those given by a traditional Gaussian plume model (GPM). In the GPM, the mean concentration at receptor location (x, y, z) is calculated as follows (Schnelle and Dey, 2000, p. 11-2):

$$C(x,y,z) = \frac{Q}{2\pi\,\sigma_y\,\sigma_z\,U}\exp\left[-\frac{1}{2}\left(\frac{y}{\sigma_y}\right)^2\right]\left\{\begin{array}{l}\exp\left[-\frac{1}{2}\left(\frac{z-h_s}{\sigma_z}\right)^2\right] \\ +\exp\left[-\frac{1}{2}\left(\frac{z+h_s}{\sigma_z}\right)^2\right]+E\end{array}\right\}, \qquad (3.13)$$

where Q is the emission strength, U is the mean wind speed that is aligned with the x-axis, σ_y is the lateral dispersion parameter along the y-axis, σ_z is the vertical dispersion parameter along the z-axis, and h_s is the source height. The expression of E is given by

$$E = \sum_{n=1}^{k} \left\{ \begin{array}{l} \exp\left[-\frac{1}{2}\left(\frac{z - h_s - 2nh}{\sigma_z} \right)^2 \right] + \exp\left[-\frac{1}{2}\left(\frac{z + h_s - 2nh}{\sigma_z} \right)^2 \right] \\ + \exp\left[-\frac{1}{2}\left(\frac{z - h_s + 2nh}{\sigma_z} \right)^2 \right] + \exp\left[-\frac{1}{2}\left(\frac{z + h_s + 2nh}{\sigma_z} \right)^2 \right] \end{array} \right\}. \qquad (3.14)$$

Eqs. (3.13) and (3.14) account for complete reflection of the pollutant mass from the ground and the ABL top. In practice, k in Eq. (3.14) should be a sufficiently large integer (here, $k = 5$). The corresponding dimensions of Q and σ_y (or σ_z) are Mass Time^{-1} and Length, respectively. Unlike the LPM, the dispersion parameterization for the above GPM is not explicitly based on a number of basic meteorological parameters but the Pasquill stability classification. Since the dispersion in question is under very unstable condition, it can be approximated as Pasquill stability class A in which the lateral and vertical dispersion parameters are expressed as a function of x. From Briggs (1972), these parameters are also dependent on topography that is categorized into open-country (or rural) and urban conditions. For stability class A with $100 < x < 10000$ m (Schnelle and Dey, 2000, p. 7-4),

$$\begin{aligned} \sigma_{y,\text{rural}} &= 0.22\, x (1 + 0.001 x)^{-1/2}, \\ \sigma_{z,\text{rural}} &= 0.20\, x, \\ \sigma_{y,\text{urban}} &= 0.32\, x (1 + 0.004 x)^{-1/2}, \quad \text{and} \\ \sigma_{z,\text{urban}} &= 0.24\, x (1 + 0.001 x)^{1/2}. \end{aligned} \qquad (3.15)$$

Figure 3-8 shows the mean ground-level concentrations (shortly, concentrations along the mean wind direction aligned with both the source and the Nitrogen Extracting

Facility (i.e. along the plume centerline) while Figure 3-9 shows those in the crosswind or lateral direction at the Chickasaw Park. In both figures, five different sets of concentration are given, corresponding to the LPM and the GPM parameterized for rural and urban background. Two different values of the mean wind speed in Eq. (3.13) were representatively used: U at $z = 1.5$ m that is the source height and U at $z = 10$ m that is the height normally used for dispersion from a near-ground source. They are denoted by $U(1.5)$ and $U(10)$, respectively. A plus (+) sign corresponds to the concentration measured at each location in the field study. As seen, the GPMs mostly give lower estimates of concentration than the LPM models, for the spatial domain in question. Furthermore, concentrations from the GPM for the rural background are lower that the urban background and sensitive to the magnitude of mean wind speed used in calculation. It is straightforward from Eq. (3.13) that using $U(1.5)$ in the calculations yields higher concentrations than $U(10)$ for the GPM. Along the plume centerline, concentrations fall off rapidly for the GPM, approximately with an exponent of –2 with respect to the distance from the source while the falloff for the LPM is relatively low. Differences between predictions given by the LPM and by the GPM increase with distance. At the Nitrogen Extracting Facility, the difference is approximately an order of magnitude and becomes two orders of magnitude at a distance of 2000 m., and the measured concentration agrees most with the prediction by the GPM for urban background using $U(1.5)$. In the crosswind direction, concentration decreases with distance from the plume centerline. The rates of such decreases in the GPMs are however small compared to that in the LPM, indicating that the width of the corresponding crosswind

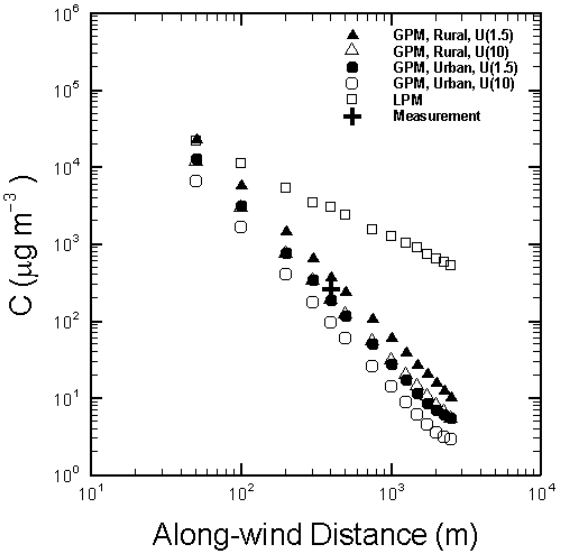

Figure 3-8. Concentrations along the plume centerline by the LPM and the GPM at the Nitrogen Extracting Facility

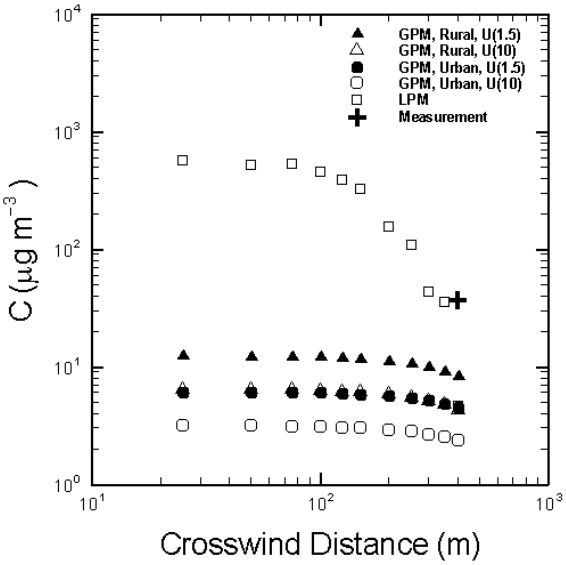

Figure 3-9. Concentrations in the crosswind direction (through the Chickasaw Park) by the LPM and the GPM at the Chickasaw Park

concentration profile by the LPM is smaller than those by the GPM. There is a large difference of approximately two orders of magnitude between predictions given by the LPM and by the GPM, especially close to the plume centerline. At the Chickasaw Park, the measured concentration appears to stay close to the fall-off trend given by the LPM. Nevertheless, the difference is relatively small but the measured concentration overshoots the predictions by both models by about one order of magnitude.

It is fair to say that both LPM and GPM applied to the Rubbertown field study do not show good agreement with the measured concentrations. Although the GPM for an urban background performed well at the Nitrogen Extracting Facility, all models give underestimates at the Chickasaw Park. One major deficiency of the above comparison is lack of a sufficiently large number of measured concentrations (here, only two data points were used), leading to statistical inconclusiveness in model evaluation. Moreover, the parameterization of turbulence and dispersion parameters for the models used in this application is essentially limited only to the idealized condition where the degree of non-uniformity of a terrain should be minimal, which is in fact not the case here. Characterizing the turbulence field of a highly non-uniform terrain is important for the dispersion over a short-range scale but such information is not available for the study. Therefore, it is important to use a more appropriate data set for comparison. Large differences between model predictions and measurements in the comparison could also result from inaccuracy in estimating meteorological parameters, some of which may be influential to a model output and the errors of their estimates considerably affect the model output. The structural formulation of the LPM in question is also important. In the field study, the dispersion took place under a strongly convective condition. Under

convective conditions, the pdf of vertical velocity tends to be positively skewed due to the asymmetry of updraft and downdraft (Baerentsen and Berkowicz, 1984; Luhar et al., 1996). Thus, the assumption of a Gaussian velocity pdf may not be well represented. However, incorporating higher-order moments of velocity into the Lagrangian particle modeling has been known to be difficult and has not been sufficiently advanced.

3.3. Project Prairie Grass (PPG) Experiments

Given the experimental issues encountered when using the data of the Rubbertown field study, it became important to find an appropriate data set to assess model capabilities. In doing so, a data set from the PPG experiments (Barad, 1958) was adopted. The PPG experiments are considered the most comprehensive field study of short-range dispersion conducted in the past 50 years in North America. There were a total of 70 runs conducted under both stable and unstable conditions. The field terrain was smooth and grass-covered. Sulfur dioxide (SO_2) was released from a continuous point source. Constant release rates ranged from 39 to 104 g s^{-1}. Various types of instruments were employed to collect meteorological data simultaneously. There was no report of material deposition in the experiments, and it should be small over the distances studied. Ground-level concentrations associated with the release were measured at a height of 1.5 m along crosswind arcs at intervals of 2° at 50, 100, 200, and 400 m and at intervals of 1° at 800 m.

3.4. Comparison of Concentrations from the PPG Experiments and the LPM

Ground-level concentrations from 25 runs under stable conditions (Run Nos. 17, 18, 21, 22, 23, 24, 28, 29, 32, 35, 36, 37, 38, 39, 40, 41, 42, 46, 53, 54, 55, 56, 58, 59, and 60) were chosen for comparison with those simulated by the model, and their reported values are given in Appendix B of the thesis. In these runs, the source was set at 0.46 m above the ground. A set of meteorological and terrain data (i.e. L, u_*, and z_o) corresponding to the chosen runs, processed by van Ulden (1978), were adopted as inputs for the model. The previous LPM was used but its turbulence statistics were parameterized by a different set of similarity-based interpolation formulas (for $L > 0$). Similar to before, the assumption of a stationary and horizontally homogeneous turbulent flow is assumed. The mean horizontal wind speed (U) was determined by Eqs. (3.2) and (3.6). The last term in the brackets of Eq. (3.2) was neglected because the value of z_o in the PPG experiments is very small (0.008 m), according to van Ulden (1978). The rest of statistics were computed using the following formulas:

- Variances and covariance: A number of studies express the second-order moments of velocity as follows:

$$\frac{\sigma_u^2}{u_*^2} = c_u\left(1-\frac{z}{h}\right)^{\alpha}, \qquad \frac{\sigma_v^2}{u_*^2} = c_v\left(1-\frac{z}{h}\right)^{\alpha},$$

$$\frac{\sigma_w^2}{u_*^2} = c_w\left(1-\frac{z}{h}\right)^{\alpha}, \text{ and } \frac{\tau_{uw}}{u_*^2} = -\left(1-\frac{z}{h}\right)^{\alpha}. \tag{3.16}$$

A large variation in the reported values of α, c_u, c_v, and c_w is found in the literature. For instance, Hanna (1982) uses: $\alpha = 2$, $c_u = 4.0$, and $c_v = c_w = 1.7$; Arya (1984): $\alpha = 2$, $c_u = 5.8 \geq c_v \geq c_w = 2.6$; Nieuwstadt (1984): $\alpha = 1.5$, $c_w = 1.96$; Sorbjan (1986), $\alpha = 2$, $c_w = 2.5$; and Lenschow et al. (1988): $\alpha = 1.75$, $c_u = c_v = 4.5$, and $c_w = 3.1$. From the Monin-Obukhov theory, the turbulence statistics in Eq. (3.16) are approximately constant for small heights. A literature survey by Panofsky and Dutton (1984, p. 160) suggests c_u = 4.8-6.3, c_v = 3.0-4.8, and c_w = 1.2-2.0. A review by Dias et al. (1995) gives c_w = 1.3-2.3. It is seen that the above values of α, c_u, c_v, and c_w are 1.5-2, 4.0-6.3, 1.7-5.8, and 1.2-3.1, respectively. For the modeling here, $\alpha = 2$, $c_u = 4.0$, $c_v = 3.0$, and $c_w = 1.5$ were chosen, and these values meet the inequality $\tau_{uw}^2 \leq \sigma_u^2 \sigma_w^2$ for all $z \leq h$.

- Mean energy dissipation rate: Following Sorbjan (1986) with α in Eq. (3.16) equal to 2,

$$\varepsilon = \frac{u_*^3}{k\,z}\left(1+3.7\frac{z}{L}\right)\left(1-\frac{z}{h}\right)^3 . \tag{3.17}$$

Note that since the PPG dispersion took place for a short scale of < 1 km, it was assumed that the dispersion occurred within in the surface boundary layer. As such, the reduced forms of the formulas in Eqs. (3.16) and (3.17) by taking the limit $z/h \to 0$ were used.

The results from comparisons between measurement data and model predictions are shown in Figures 3-10 and 3-11. In the figures, *CIC* denotes the crosswind-integrated

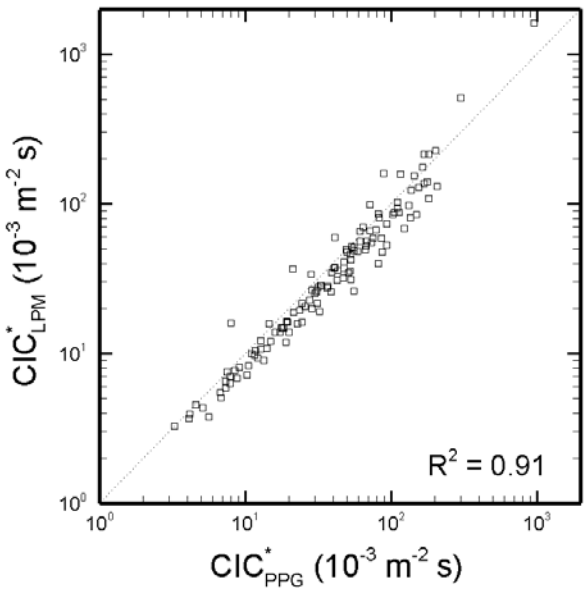

Figure 3-10. Comparison of CIC^* values from the PPG data and the LPM

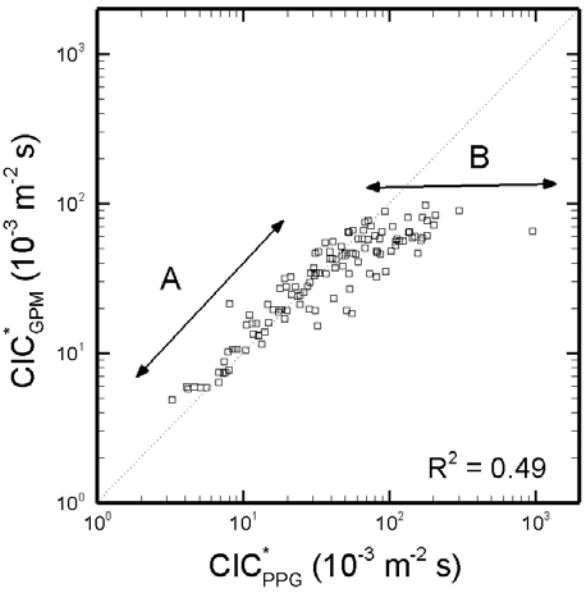

Figure 3-11. Comparison of CIC^* values from the PPG data and the GPM

concentration (defined as $CIC = \int_{s \in \text{arc}} C \, \mathrm{d}s$, where C is the (mean ground-level) concentration at a particular location and s is the distance along an arc) while $CIC^* = CIC / Q$, where Q is the release rate. The corresponding dimensions of Q, C, CIC, and CIC^* are Mass Time^{-1}, Mass Length^{-3}, Mass Length^{-2}, and Length^{-2} Time, respectively. In Figure 3-10, the CIC^* values from 25 runs under stable conditions (Run Nos. 17, 18, 21, 22, 23, 24, 28, 29, 32, 35, 36, 37, 38, 39, 40, 41, 42, 46, 53, 54, 55, 56, 58, 59, and 60) and those from the LPM are compared. In these runs, the source was set at 0.46 m above the ground. It is seen that a good fit with a high coefficient of determination (R^2) of 0.91 are achieved, though a majority of model values are slightly lower than the PPG data. In Figure 3-11, the CIC^* values from the same 25 runs and those from the GPM are shown. Note that Brigg's parameterization of the dispersion parameters for Gaussian plume modeling is not based on basic meteorological parameters but Pasquill stabilities instead. For the purpose of comparison, it is assumed here that, for any PPG run with $L \leq 50$, the dispersion is classified as Pasquill stability class E (i.e. weakly stable) and, for that with $L > 50$, it corresponds to class F (i.e. moderately stable). The expressions of the lateral and vertical dispersion parameters for these classes given by Briggs for open-country (or rural) with $100 < x < 10000$ m (Schnelle and Dey, 2000, p. 7-4) are as follows: For class E,

$$\begin{aligned} \sigma_{y,\text{rural}} &= 0.06x(1+0.0001x)^{-1/2}, \quad \text{and} \\ \sigma_{z,\text{rural}} &= 0.03x(1+0.0003x)^{-1}. \end{aligned} \tag{3.18}$$

For class F,

$$\sigma_{y,\text{rural}} = 0.04\,x\,(1+0.0001x)^{-1/2}, \quad \text{and}$$
$$\sigma_{z,\text{rural}} = 0.016x\,(1+0.0003\,x)^{-1}. \tag{3.19}$$

From the figure, the GPM performs well for region A where most data points are associated with weakly stable conditions, clearly, tends to give underestimates for region B where most data points are associated with near-source receptors and moderately stable conditions. The overall fit by the GPM has a much lower R^2 value (0.49) than that by the LPM.

To extend the above results, it is possible to convert predicted concentration data to emission strength data simply using their linear relationship in Section 2.4, Chapter 2). The results from doing so are shown in Figures 3.12 and 3.13. Since most of Q values used in the PPG experiments fall in a narrow range of 35-45 g s^{-1}, the plots in the figures become fairly scattered. Thus, it is appropriate to use a common measure in evaluating the performance of both models, which is normalized gross error (μ) that is defined by (Russell and Dennis, 2000)

$$\mu = \frac{1}{N}\sum_{i=1}^{N}\frac{\left|Q_m - Q_o\right|}{Q_o}, \tag{3.20}$$

where N is the number of data point, Q_o is the reference emission strength , and Q_m is the emission strength by a model. Table 3.2 gives a summary of normalized gross errors of

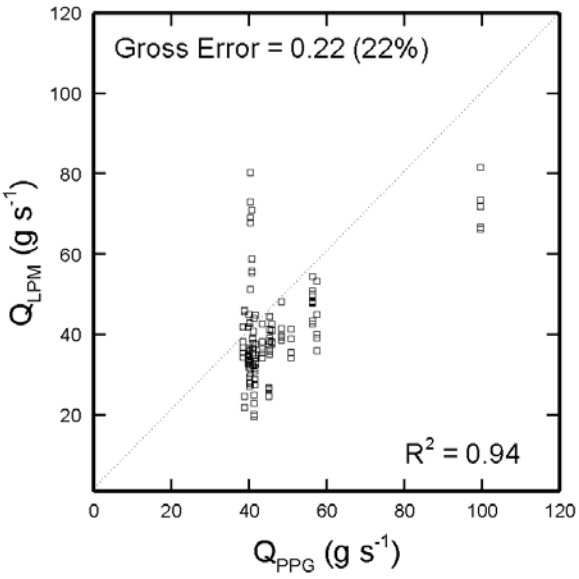

Figure 3-12. Comparison of *Q* values from the PPG data and the LPM

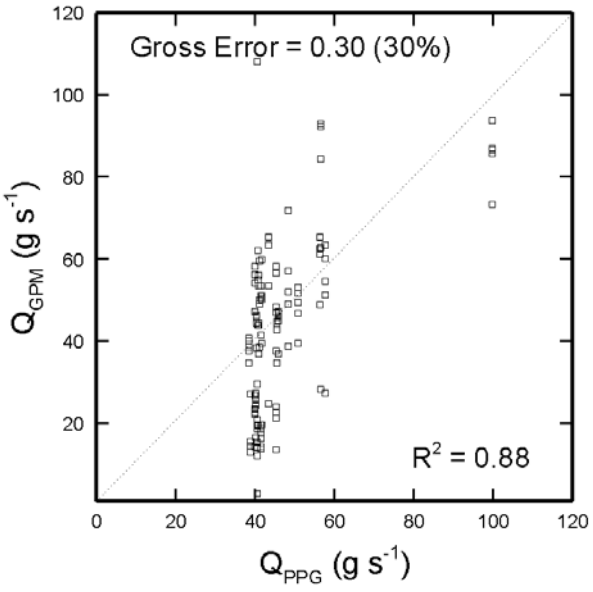

Figure 3-13. Comparison of *Q* values from the PPG data and the GPM

Table 3-2. Normalized gross errors of emission strength by the LPM and the GPM based on the PPG data

	Gross error (μ)	
	LPM	GPM
Overall (all data points)	22%	30%
Near-source receptors	19%	31%
Distant receptors	25%	30%
Weakly stable conditions	15%	13%
Moderately stable conditions	28%	45%

emission strength estimated by the LPM and the GPM. From the table, the normalized gross errors by the LPM are less than those by the GLP in almost every case (including the overall comparison based on all data points shown in Figures 3-12 and 3-13), except for dispersion under weakly stable conditions where both models performs comparably. It is apparent that the LPM yields more accurate estimates especially for receptors located near the source and dispersion under moderately stable conditions. Note that, in the table, near-source receptors correspond to those on the 50-m and 100-m arcs.

According to the above evaluation that the performance of the LPM is satisfactory based on the comprehensive PPG data. Furthermore, to examine its prediction for lateral dispersion, concentration data in the PPG report were reconsidered. Since the mean wind direction does not align with the measurement locations where maximum concentrations occur in many PPG runs. However, those locations appear not to stay far from the mean wind direction for a certain runs. Here, 10 PPG runs (Run Nos. 23, 24, 28, 37, 38, 39, 42, 55, 56, and 59) are representatively chosen for comparison of point-wise concentrations (using reported data from sampling stations on each arc) and the results from doing so are shown in Figure 3-14. It is seen that good agreement with a high R^2 value (0.86) is obtained, though the data points associated with very low concentrations appear somewhat scattered, as seen in Figure 3-14b where a log-log scale is used.

3.5. Summary

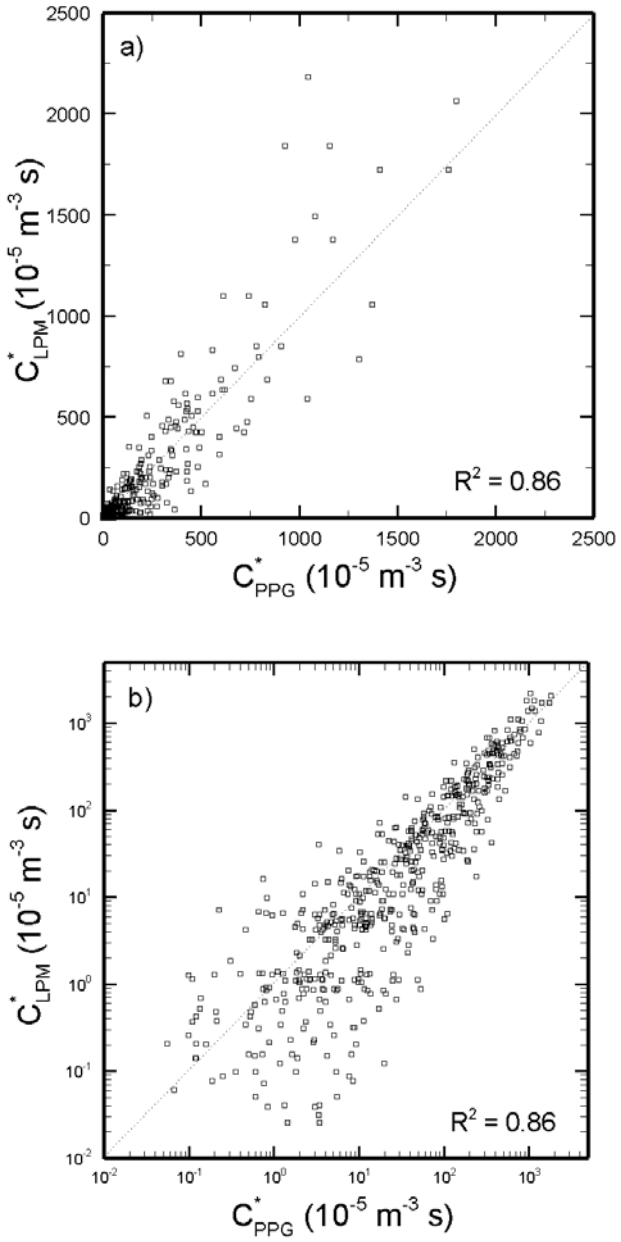

Figure 3-14. Comparison of C^* values from the PPG data and the LPM: a) linear-linear scale and b) log-log scale

Comparison of mean ground-level concentrations predicted by the LPM with the two different data sets from the Rubbertown field study and the PPG experiments has been shown. The basic meteorological parameters were quantified in both field studies, and the turbulence parameters required by the LPM were estimated using their similarity-based interpolation formulas proposed in the literature. Predictions by the traditional GPM were also given for comparison. It has been shown that, for the Rubbertown field study, no satisfactory agreement was found for both models. However, the GPM gave results that compared well at the Nitrogen Extracting Facility but not further downwind. Due to lack of a sufficiently large number of measured concentrations in the field study, model evaluation could not be properly concluded. In addition, a limitation from using the parameterization of turbulence and dispersion parameters intended for a uniform terrain may have also caused uncertainty in model predictions since the background terrain of the field study is highly non-uniform. Inaccuracy in estimating some meteorological parameters and the model formulation based on the assumption of a Gaussian velocity pdf under convective conditions could also affect model outputs as well. The model evaluation using the PPG data was statistically well conducted due to the availability of a large data set and more appropriate field conditions. That is, the PPG experiments were implemented over a smooth uniform terrain that is suitable for the applicability of the LPM here. Overall agreement between model predictions by the LPM and field data chosen for stable conditions was achieved, though some large deviations exist at very low concentrations. Since the LPM parameterized for stable conditions has performed well, it is then adopted as the platform for parametric uncertainty analysis in the following chapter.

References

Anfossi, D., Ferrero, E., Sacchetti, D., Trini Castelli, S. (1997) Comparison among empirical probability density functions of the vertical velocity in the surface layer based on higher order correlations. Boundary-Layer Meteor. 82, 193-218.

Arya, S. P. S. (1984) Parametric relations for the atmospheric boundary layer. Boundary-Layer Meteor. 30, 57-73.

Baerentsen J. H., Berkowicz, R. (1984) Monte Carlo simulation of plume dispersion in the convective boundary layer. Atmos. Environ. 18, 701-712.

Barad, M. L. (Ed.) (1958) Project Prairie Grass, A Field Program in Diffusion. Vol. 1. Geographical Research Paper No. 59, Air Force Cambridge Research Center, Belford, Massachusetts.

Briggs, G. A. (1972) Diffusion Estimation for Small Emissions. In ERL, ARL USAEC Report ATDL-106, U.S. Atomic Energy Commission, Oak Ridge, Tennessee.

Dias, N. L., Brutsaert, W., Wesely, M. L. (1995) Z-less stratification under stable conditions. Boundary-Layer Meteor. 75, 175-187.

Du, S., Sawford, B. L., Wilson, J. D., Wilson, D. J. (1995) Estimation of the Kolmogorov constant (C_o) for the Lagrangian structure function, using a second-order Lagrangian model of grid turbulence. Phys. Fluids 7, 3083-3090.

Flesch, T. K., Wilson, J. D. (1992) A two-dimensional trajectory-simulation model for non-Gaussian, inhomogeneous turbulence within plant canopies. Boundary-Layer Meteor. 61, 349-374.

Flesch, T. K., Wilson, J. D., Yee, E. (1995) Backward-time Lagrangian stochastic dispersion models and their application to estimate gaseous emissions. J. Appl. Meteor. 34, 1320-1332.

GTRI (2001) Remote Sensing Technology to Support the Toxics Release Inventory. Technical Report, Georgia Tech Research Institute, Atlanta.

Hanna, S. R. (1982) Applications in air pollution modeling. in Atmospheric Turbulence and Air Pollution Modelling, edited by Nieuwstadt, F. T. M. and van Dop, H., D. Reidel Publishing, 37-68.

Hanna, S. R. (1982) Applications in air pollution modeling. in Atmospheric Turbulence and Air Pollution Modelling, edited by Nieuwstadt, F. T. M. and van Dop, H., D. Reidel Publishing, 37-68.

Holtslag, A. A. M., Nieuwstadt, F. T. M. (1986) Scaling the atmospheric boundary layer. Boundary-Layer Meteor. 36, 201-209.

Law, A. M., Kelton, W. D. (2000) Simulation Modeling and Analysis. McGraw-Hill, Boston, Massachusetts.

Lenschow, D. H., Li, X. S., Zhu, C. J., Stankov, B. B. (1988) The stably stratified boundary layer over the Great Plains. I. Mean and turbulence structure. Boundary-Layer Meteor. 42, 95-121.

Leuzzi, G., Monti, P. (1998) Particle trajectory simulation of dispersion around a building, Atmos. Environ. 32. 203-214.

Luhar, A. K., Hibberd, M. F., Hurley, P. J. (1996) Comparison of closure schemes used to specify the velocity PDF in Lagrangian stochastic dispersion models for convective conditions. Atmos. Environ. 30, 1407-1418.

Nieuwstadt, F. T. M. (1984) The turbulent structure of the stable, nocturnal boundary layer. J. Atmos. Sci. 41, 2202-2216.

Panofsky, H. A., Dutton, J. A. (1984) Atmospheric Turbulence: Models and Methods for Engineering Applications. Wiley, New York.

Press, W. H., Teukolsky, S. A., Vetterling, W. T., Flannery, B. P. (1992) Numerical Recipes in FORTRAN. Cambridge University Press, Cambridge.

Rodean, H. C. (1996) Stochastic Lagrangian Models of Turbulent Diffusion. Monograph No. 48, American Meteorological Society, Boston.

Russell, A. G., Dennis, R. L. (2000) NARSTO critical review of photochemical models and modeling. Atmos. Environ. 34, 2283-2324.

Schnelle, K. B., Dey, P. R. (2000) Atmospheric Dispersion Modeling Compliance Guide. McGraw-Hill, New York.

Sorbjan, Z. (1986) On similarity in the atmospheric boundary layer. Boundary-Layer Meteor. 34, 377-397.

van Ulden, A. P. (1978) Simple estimates for vertical diffusion from sources near the ground. Atmos. Environ. 12, 2125-2129.

van Ulden, A., Holtslag, A. (1985) Estimation of atmospheric boundary layer parameters for diffusion applications. J. Climate Appl. Meteor. 24, 1196-1207.

CHAPTER 4

EFFECTS OF UNCERTAINTIES IN PARAMETERS OF A LAGRANGIAN PARTICLE MODEL ON MEAN GROUND-LEVEL CONCENTRATIONS UNDER STABLE CONDITIONS

(Coauthor: A. G. Russell)

(This chapter is an extended version of the preliminary work: Manomaiphiboon, K., Russell, A. G. (2003) Uncertainty study of a Lagrangian particle model for short-range dispersion under stable and neutral conditions. Proceedings of the 96th annual conference of the Air and Waste Management Association, San Diego)

Abstract

This work evaluates the effects of uncertainties in five parameters or inputs of a source-receptor Lagrangian particle model on mean ground-level concentrations. The scope of work is short-range dispersion in the atmospheric boundary layer under slightly and moderately stable conditions over smooth flat terrain within 3 km downwind from a continuous point source located near the ground. Model inputs include four meteorological parameters (Monin-Obukhov length, friction velocity, roughness height, and mixing height) and the universal constant in the random component of the model. Model outputs of interest are ground-level mean concentrations at a number of receptors downwind from the source. The analysis was performed for the atmospheric conditions

corresponding to stability indices (defined as the ratio of mixing height to Monin-Obukhov length) of 1.3, 2.5, and 4.2. Input uncertainties were propagated through the model using Monte Carlo simulations with Latin hypercube sampling. Linear regression modeling was used to statistically partition an output uncertainty and determine the relative importance of an input to an output. Additional analysis of the half width of ground-level mean concentration contours at a distance from the source was performed but in a limited manner. It is shown that, among the meteorological parameters, friction velocity is an important input whose uncertainties contribute significantly to the concentration uncertainties. The uncertainty contributions from Monin-Obukhov length and mixing height are generally not important for most receptors but both tend to increase in importance when the degree of stability decreases. Another influential input is the universal constant whose uncertainty contribution often dominates those from most other inputs. However, it has little or no influence for some distances in the lateral direction. The overall contribution from roughness height was found to be slight. For the half width of concentration contours, the two largest contributors to uncertainty are the universal constant and Monin-Obukhov length whereas the contributions from the other inputs are not significant.

4.1. Introduction

Air quality modeling integrates our knowledge of how physical and chemical processes affect pollutants in the atmosphere. One major category of air quality modeling deals with the dispersion of pollutants in the atmospheric boundary layer

(ABL). A large number of air dispersion models have been developed for different purposes and applications. The most well known are Gaussian plume models in which pollutant concentrations at downwind locations are postulated to be distributed in a Gaussian form or its variants (Turner, 1970). Gaussian plume modeling is the basis for several regulatory models of the U. S. Environmental Protection Agency, such as the Industrial Source Complex (ISC) model and, recently, the AERMOD model (U.S. EPA, 2004). Examples of other dispersion models are the similarity-based approximations (van Ulden, 1978; Briggs, 1982), the hybrid plume dispersion model (Hanna and Paine, 1989), the second-order closure integrated model plume (Sykes et al., 1984), and the Lagrangian particle (or stochastic) model (Thomson, 1987; Wilson and Sawford, 1996). Lagrangian particle modeling has been widely applied to turbulent dispersion problems, both in the ABL (e.g. Luhar and Britter, 1989; Flesch et al., 1995; Rotach et al., 1996; Venkatram and Du, 1997; Rao, 1999) and in the built environment (e.g. Naslund et al., 1994; Leuzzi and Monti, 1998). In the modeling, the migration of a pollutant is treated as a stochastic process in a Lagrangian coordinate reference. This type of modeling has proven to give relatively accurate results because it accounts for extensive details of a turbulent flow governing dispersion mechanisms. However, it generally requires a large computational time in implementation due to a large number of particle trajectories simulated.

Recent air dispersion models have taken advantage of advances in understanding the physics of the ABL and incorporated more details of atmospheric turbulence and meteorology, leading to greater soundness and validity in their formulations and applications. Nevertheless, such information may not be precisely known, routinely

measured, or completely available for preprocessing as model parameters or inputs, which gives rise to some level of uncertainty in the modeling process. Uncertainty in a computer model can generally be categorized as parametric uncertainty and structural uncertainty (Tatang et al., 1997). The former is associated with incomplete knowledge of the exact values of model parameters while the latter is from the inaccuracy of treatment or formulation of physical and chemical processes, inexact numerical scheme, and inadequate model resolution. Determining how model outputs are affected by such uncertainty is important in that it not only helps to establish the confidence and reliability of the model outputs but also helps to specify influential model components or parameters. In air quality modeling, this information is useful for model users and decision makers in model evaluation, risk assessment and air quality management.

In this work, parametric uncertainty is addressed. Several approaches to deal with parametric uncertainty have been developed and applied to environmental and geophysical problems. The simplest method is the Taylor series approximation where the uncertainty in a model output (i.e. an output uncertainty) is approximately expressed as the summation of first-order (and, possibly, second-order) terms associated with the uncertainties in model inputs (i.e. input uncertainties). One limitation of the method is that it is a local approach, considering the behavior of a model output only in the vicinity of its base (i.e. best-estimate or nominal) case (Morgan and Henrion, 1990, p. 176). It may not be applicable for a nonlinear model with large perturbations or uncertainties in inputs. Monte Carlo (MC) methods are the most straightforward in propagating parametric uncertainty through a computer model. They are implemented under a probabilistic framework in which input uncertainties are characterized by probability

distributions and sampled by the simple random sampling (SRS) method. The cost of implementing MC simulations is high because a large set of samples is required in order to achieve a high confidence level in the statistical inference of results. To reduce computational time, the Latin hypercube sampling (LHS) method (Iman and Shortencarier, 1984) may be used as an alternative to the SRS. The LHS ensures adequate coverage of a distribution during sampling. However, it is known that constructing tolerance intervals for statistical quantities are not suitable for results from the LHS or, if so, they can only be approximate. Besides those methods, other numerical techniques developed for parametric uncertainty are the Fourier amplitude sensitivity test method (McRae et al., 1982), the probability collocation method (Tatang et al., 1997), and the stochastic response surface modeling (Isukapalli et al., 1998).

Many workers have examined parametric uncertainty using MC methods. For short-range air dispersion models, Freeman et al. (1986) and Yegnan et al. (2002) studied the ISC model using the Taylor series approximation and compared results to those from MC simulations. Irwin et al. (1987) determined the error bounds of area coverage of maximum ground-level concentrations predicted by a Gaussian plume model with a plume rise calculation. Examples of other applications using MC methods are long-range transport of sulfur in atmosphere (Alcomo and Bartnicki, 1987), atmospheric nitrogen chemistry modeling (Derwent, 1987), reactivities of volatile organic compounds and emissions from fuels based on a photochemical mechanism model (Yang and Milford, 1996), the urban airshed model (Hanna et al., 1998), a Lagrangian photochemical air parcel model (Bergin et al., 1999), and mesoscale sulfuric acid dispersion (Dabberdt and

Miller, 2000). Russell and Dennis (2000) reviewed several aspects of uncertainties in regional air quality models.

In this work, we present results from the uncertainty analysis of a Lagrangian particle model (LPM) for short-range dispersion in the ABL whose turbulence statistics are parameterized by similarity-based interpolation formulas. The model inputs included in the analysis are four basic meteorological parameters (Monin-Obukhov length (L), friction velocity (u_*), roughness height (z_o), and mixing height (h)) and the universal constant in the random component of the model (C_o). The model outputs of interest are mean ground-level concentrations (shortly, concentrations) at a number of receptors downwind from a continuous point source located near the ground. Here, the dispersion under stable conditions ($L > 0$) over smooth flat terrain is considered. Six cases are studied and associated with three stable conditions corresponding to stability indices (defined by h / L) of 1.3, 2.5, and 4.2. All input uncertainties are propagated through the model using MC simulations with the LHS. Linear regression modeling is employed to statistically partition an output uncertainty and determine the relative importance of each input in terms of uncertainty contribution. Additional analysis for the half width of concentration contours (estimated as the lateral distance equivalent to twice the standard deviation of a fitted Gaussian concentration profile) at a distance from the source is performed but in a limited manner.

4.2. LPM description

In this section, the LPM used in this work is concisely described. Following Thomson (1987) and Wilson and Sawford (1996), a joint process of a fluid particle's position and velocity (***x***, ***u***) in a turbulent flow evolves continuously with time in a Markov manner. A pollutant particle is equivalently represented by a fluid particle that moves along a flow streamline. In three dimensions, the joint process is expressed by the following set of stochastic differential equations

$$\begin{aligned} \mathrm{d}x_i &= u_i \, \mathrm{d}t, \quad \text{and} \\ \mathrm{d}u_i &= a_i \, \mathrm{d}t + b_{ij} \, \mathrm{d}W_j \, , \end{aligned} \tag{4.1}$$

where i and j (= 1, 2, and 3) are the Cartesian directional indices, $a_i \equiv a_i(\boldsymbol{x}, \boldsymbol{u}, t)$ is the drift coefficient in direction i, $b_{ij} \equiv b_{ij}(\boldsymbol{x}, t)$ is the component (i, j) of the velocity-independent diffusion coefficient, and $\mathrm{d}W_j$ is the component j of uncorrelated Gaussian forcing with mean zero and variance dt. The above variables are defined at time t. The model is subject to two necessary conditions: the inertial subrange theory (Kolmogorov, 1941) and the well-mixed condition (Thomson, 1987). According to the former condition, b_{ij} takes the universal form

$$b_{ij} = \delta_{ij} \, (C_o \, \varepsilon)^{1/2} \, , \tag{4.2}$$

where δ_{ij} is the Kronecker delta function, C_o is the dimensionless universal constant, and ε is the mean dissipation rate of turbulent kinetic energy. The latter condition determines

the form of a_i , which depends on the probability density function of (Eulerian) velocity (denoted by p_E). Here, p_E is assumed to be Gaussian (i.e. normally distributed), i.e.

$$p_E = \frac{1}{(2\pi)^{3/2}(\text{Det }\tau)^{1/2}} \exp\left[-\frac{1}{2}(u_i - U_i)(\tau^{-1})_{ij}(u_j - U_j) \right], \tag{4.3}$$

where π = 3.141592654 …, τ is the covariance matrix of velocity, τ^{-1} is the inverse matrix of τ, and U_i is the mean (Eulerian) velocity in direction *i*. The Gaussian character is used only as an approximation (i.e. not precise, as emphasized in Anfossi et al. (1997)). The simplest form of a_i is used (Thomson, 1987):

$$a_i = -\left(\frac{C_o \varepsilon}{2} \right)(\tau^{-1})_{ik}(u_k - U_k) + \frac{\phi_i}{p_E}, \tag{4.4}$$

where

$$\begin{aligned} \frac{\phi_i}{p_E} = \frac{\partial U_i}{\partial t} + U_j \frac{\partial U_i}{\partial x_j} + \frac{1}{2}\frac{\partial \tau_{ij}}{\partial x_j} + \left[\frac{\partial U_i}{\partial x_j} + \frac{1}{2}(\tau^{-1})_{mj}\left(\frac{\partial \tau_{im}}{\partial t} + U_k \frac{\partial \tau_{im}}{\partial x_k} \right) \right](u_j - U_j) \\ + \frac{1}{2}(\tau^{-1})_{mj} \frac{\partial \tau_{im}}{\partial x_k}(u_j - U_j)(u_k - U_k). \end{aligned} \tag{4.5}$$

Eqs. (4.1)-(4.5) are written in a tensor form where the summation over indices applies. The idealized condition was assumed in which atmospheric turbulence is stationary and horizontally homogeneous and the turning of the wind aloft is neglected. The stationary

assumption is typically considered acceptable for short-range dispersion when the average travel time of pollutant particles is of order one hour or less (which is the case here). Accordingly, any derivative terms with respect to t in Eq. (4.5) become zero. Here, x_3 denotes the vertical distance (or elevation) above the ground, and U_3 is set to zero. The mean wind in the horizontal plane is aligned parallel to the x_1 axis. It follows that U_2, U_3, τ_{12} (= τ_{21}), and τ_{23} (= τ_{32}), and any derivative terms with respect to x_1 or x_2 equal zero, simplifying the calculation of Eq. (4.5). The rest of statistics required by the model were determined from similarity-based interpolation formulas as a function of elevation, and these are given in Appendix. For convenience, x_1, x_2, and x_3 will be replaced by x, y, and z, respectively, and U_1, τ_{11}, τ_{22}, τ_{33}, and τ_{13} (= τ_{31}) will be rewritten as U, σ_u^2, σ_v^2, σ_w^2, and τ_{uw}, respectively.

To examine the performance of the current LPM, dispersion data from the Project Prairie Grass (PPG) short-range dispersion experiments (Barad, 1958) were compared to model predictions. In the PPG experiments, there were a total of 70 runs conducted under both stable and unstable conditions. The field terrain was smooth and grass-covered. Sulfur dioxide (SO_2) was released from a continuous point source. Constant release rates ranged from 39 to 104 g s^{-1}. Various types of instruments were employed to collect meteorological data simultaneously. There was no report of material deposition in the experiments. Ground-level concentrations associated with the release were measured at a height of 1.5 m along crosswind arcs at intervals of 2° at 50, 100, 200, and 400 m and at intervals of 1° at 800 m. A set of meteorological and terrain data from the PPG experiments processed by van Ulden (1978) were adopted as inputs for the model. The results from comparisons between measurement data and model predictions are shown in

Figure 4-1. In the figure, *CIC* denotes the crosswind-integrated (mean gound-level) concentration (defined as $CIC = \int_{s \in \text{arc}} C \, \mathrm{d}s$, where C is the concentration at a particular location and s is the distance along an arc) while $CIC^* = CIC / Q$, where Q is the release rate. The corresponding dimensions of Q, C, CIC, and CIC^* are Mass Time^{-1}, Mass Length^{-3}, Mass Length^{-2}, and Length^{-2} Time, respectively. In Figure 4-1a, the CIC^* values from 25 runs under stable conditions (Run Nos. 17, 18, 21, 22, 23, 24, 28, 29, 32, 35, 36, 37, 38, 39, 40, 41, 42, 46, 53, 54, 55, 56, 58, 59, and 60) and those from the model are compared. In these runs, the source was set at 0.46 m above the ground. It is seen that a good fit with a high coefficient of determination (R^2) of 0.91 are achieved, though the majority of model values is slightly lower than the PPG data. To account for lateral dispersion, we reconsidered the concentration data in the PPG report and found that, in many runs, the mean wind direction does not align with the measurement locations where maximum concentrations occur. However, those locations appear not to stay far from the mean wind direction for most runs. To simplify the comparison, each measurement arc was divided into two intervals: inner (±5°) and outer. The crosswind-integrated concentrations corresponding to these intervals were calculated for 17 PPG runs (out of 25) (indicated by underlines). The results are shown in Figure 4-1b. The good agreement is seen for the concentrations corresponding to the inner intervals whereas those corresponding to the outer intervals are somewhat scattered particularly for very low concentrations. A high R^2 value of 0.97 is obtained for the overall fit.

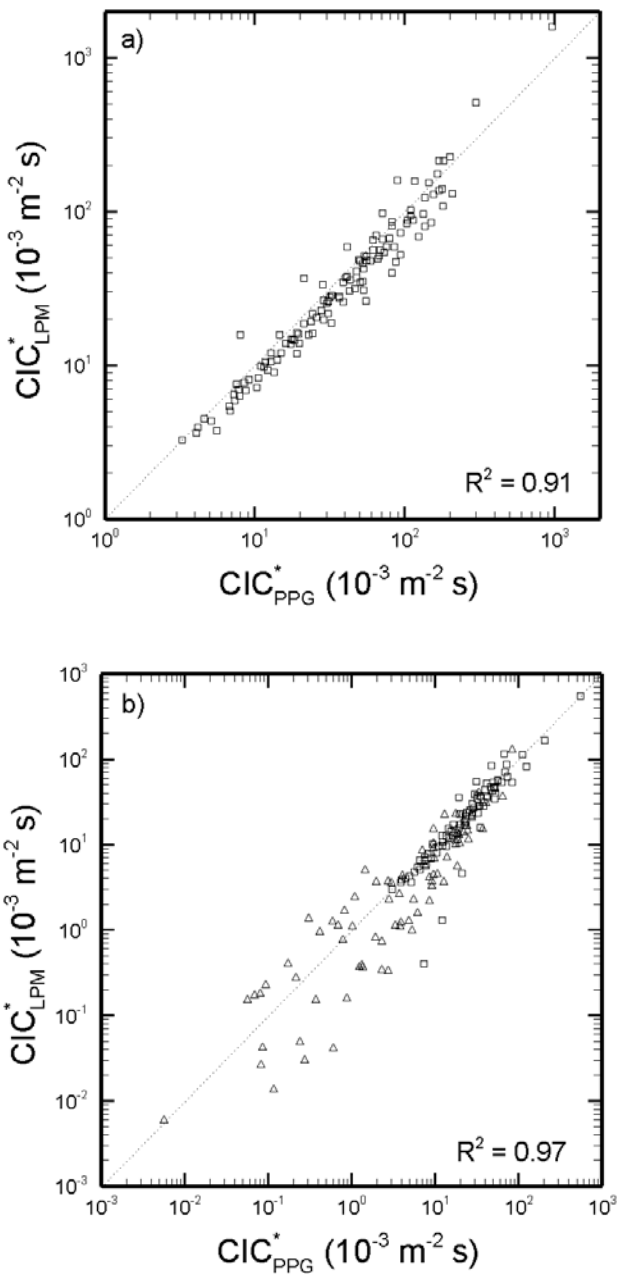

Figure 4-1. Comparison of CIC^* values from the PPG data and the LPM: a) entire arcs and b) divided arcs (square: inner, triangle: outer)

4.3. Case Studies and Numerical Details

4.3.1. Case descriptions

The stable ABL typically occurs during the nighttime when the ground surface is cooling down and a stable temperature gradient is induced extending from the ground. The stable temperature gradient suppresses turbulence generated by the wind shear, and turbulence exists only in the presence of moderate or strong winds. From the scaling schematic of Holtslag and Nieuwstadt (1986), the stable ABL is empirically divided into different regions depending on elevation and degree of stability, including surface boundary layer, local scaling layer, *z*-less scaling layer, near-neutral upper layer, and intermittency layer. The intermittent layer usually exists in the uppermost part of the ABL and can extend downward throughout the ABL depth when stability is very strong. Turbulence in the intermittent layer is known to be sporadic and difficult to characterize. This work is limited to weakly and moderately stable conditions where turbulence is characterizable and plays an important role.

As noted above, six cases are studied and associated with three stable conditions with h/L = 1.3, 2.5, and 4.2 (based on their means, see Table 4-1). The uncertain inputs include Monin-Obukhov length (L), friction velocity (u_*), roughness height (z_o), and mixing height (h) and the universal constant (C_o). The parameters L, u_*, and h are three key variables in scaling turbulence quantities in the stable ABL. Three cases correspond to h/L = 2.5 and three levels of uncertainties (in terms of standard deviation) in meteorological parameters that are assumed to be low (10% of their mean values), medium (20%), and high (30%). For conciseness, these three cases will be referred to as S[10], S[20], and S[30], respectively. For h/L = 1.3 (weakly stable) and 4.2

(moderately stable), due to computational-cost constraint, only the medium level (i.e. 20%) is considered, and the cases corresponding to these values will be referred to as WS[20] and MS[20], respectively. In each case, the mean of z_o is set to 1 cm (0.01 m), and a neutrally-buoyant non-reactive pollutant is released from a continuous point source located near the ground with a height of 1.0 m.

In practice, uncertainties in meteorological parameters can come from various sources, depending on measurement accuracy, instruments, and methods as well as the assumptions and relations of empirical formulas used for their estimation. Fast-response instruments have been available for measuring some basic variables (e.g. velocity and temperature), which enables various turbulence quantities to be derived directly. van Ulden and Holtslag (1985) outlined the details of estimating and preprocessing several meteorological parameters for the ABL. For example, u_* can be estimated by either profile or energy budget methods. The value of z_o can be computed using either a wind profile or its approximate relations to the normalized standard wind speed or maximum wind gust. Wilczak and Phillips (1984) conducted field measurements of a number of meteorological quantities (e.g. wind speed, velocity variances, temperature, and mixing height) under daytime convective conditions, compared them with the estimates from surface layer flux-profile relationships and an inversion rise model, and found that most of those meteorological quantities have a mean difference of 10-30%. Lena and Desiato (1999) evaluated the performance of ten empirical formulas proposed for estimating mixing heights during nighttime with the measurement data from sound detection and ranging (SODAR) system and radio acoustic sounding system (RASS), showing that large differences in estimates exists among the formulas themselves and measurements.

In terms of normalized mean standard error, the differences range from 0.25 to as high as 8.96. They found that the formulas given by Benkley and Schulman (1979) and Nieuwstadt (1984) give fair results. The former takes the form $h \propto u_{10}^{3/2}$, where u_{10} is the mean wind speed at 10 m above the ground, while the latter takes Zilitinkevich's (1972) expression: $h = c_s (u_* L / f)^{1/2}$, where $c_s \approx 0.4$ and f is the Coriolis parameter. L is defined by $L = -u_*^3 T / k g H$, where T is the mean near-surface absolute temperature, k is the von Karman constant (≈ 0.4), g is the gravity constant, and H is the mean surface heat flux. Then, the uncertainty in L can be associated with the uncertainties in the values of u_*, H, and T. Like u_*, H can also be estimated from the profile or energy budget methods. The importance of meteorological fields and their uncertainties for air quality models was noted in Lewellen and Sykes (1989). However, such uncertainties have not been extensively reported and sufficiently archived, leading to difficulty in their characterization.

There has been an inconsistency in the reported values of the universal constant C_o, ranging widely from 1.6 to 10 (for review, see Rodean (1996), Du et al. (1995) and Degrazia and Anfossi (1998)). So, it is of practical interest to include this constant in the analysis. Here, the values of 3.0 and 0.5 are used as its mean and standard deviation, respectively, according to the estimate $C_o = 3.0 \pm 0.5$ by Du et al. (1995). The input uncertainties are assumed to be independent and log-normally distributed. Lognormal distributions are commonly applied to parameters whose values are nonnegative (Bergin et al., 1999). They are usually suitable for environmental variables that are widely distributed and tend to have a few large values whereas normal distributions are more suitable for some particular parameters such as mean wind direction and temperature

(Hanna et al., 1998). Other distribution types (e.g. triangular, log-uniform, and log-triangular) have also been used (NCRP, 1996). Some workers (Freeman et al., 1986; Yegnan et al., 2002) have treated all input uncertainties as independent normally distributed variables. Thus, it is of interest to include an additional case using the same information as S[20] but assuming each input uncertainty to be normally distributed in order to see how results change due to different distribution types. This supplementary case will be referred to as S[20N]. Clipped distributions are often preferred in order to exclude unrealistic or extreme values of inputs during random sampling (Derwent, 1987; Hanna et al., 1998). Here, 98%-probability clipped lognormal and normal distributions (i.e. 1% of probability clipped at each of the upper and lower ends of a distribution) were implemented. It is important to note that the independence among input uncertainties may be viewed as only approximate because the correlations are not known or quantified. As mentioned earlier, the uncertainty in one input may be directly or indirectly associated with those of others and propagated through their physical, chemical, or mathematical relations. Incorporating such associations into analysis is often difficult due to lack of complete knowledge of uncertainties but can improve results.

Table 4-1 summarizes the means and standard deviations of uncertain inputs in each case. The means of meteorological parameters in S[.] and MS[.] are guided by the values used in the numerical work of Brost and Wyngaard (1978) and that the values of h/L in the last column are based on their means. A base case is referred to as the condition for which the mean of each input is used in calculation. The base cases of WS[.], S[.], MS[.] are denoted by WS_{Base}, S_{Base}, and MS_{Base}, respectively. The heat fluxes

Table 4-1. Inputs and their uncertainties in the six chosen cases

No.	Case	Input					Distribution [c]	h/L [d]
		L (m) M[a] ± SD[b]	u_* (m s^{-1}) M ± SD	z_o (cm) M ± SD	h (m) M ± SD	C_o M ± SD		
1	WS[20]	400 ± 20%[e]	0.41 ± 20%	1.0 ± 20%	500 ± 20%	3.0 ± 0.5	Lognormal	1.3
2	S[10]	60 ± 10%	0.23 ± 10%	1.0 ± 10%	150 ± 10%	3.0 ± 0.5	Lognormal	2.5
3	S[20]	60 ± 20%	0.23 ± 20%	1.0 ± 20%	150 ± 20%	3.0 ± 0.5	Lognormal	2.5
4	S[30]	60 ± 30%	0.23 ± 30%	1.0 ± 30%	150 ± 30%	3.0 ± 0.5	Lognormal	2.5
5	S[20N]	60 ± 20%	0.23 ± 20%	1.0 ± 20%	150 ± 20%	3.0 ± 0.5	Normal	2.5
6	MS[20]	12 ± 20%	0.15 ± 20%	1.0 ± 20%	50 ± 20%	3.0 ± 0.5	Lognormal	4.2

[a] Mean of distribution
[b] Standard deviation of distribution
[c] 98%-clipped distributions
[d] Based on their means
[e] Percentage of the mean

corresponding to these base cases are approximately –0.013, –0.015, and –0.021 K m s^{-1} (at a mean surface temperature of 293 K), respectively. Since the dispersion process in question is conservative (i.e. no loss and gain of the pollutant's mass after release), it is proper to use the concentration form $C^* = C/Q$, where C and Q are as defined previously. The corresponding dimension of C^* is Length^{-3} Time. The spatial domain of the dispersion considered here is within 3 km downwind from the source, extending from that of the PPG experiments (~ 1 km). For conciseness, R(x, y) is used to denote the receptor at coordinates (x, y). There are six receptors representatively chosen along the plume centerline, which are R(100,0), R(200,0), R(500,0), R(1000,0), R(2000,0), and R(3000, 0), and eight receptors in the lateral direction (i.e. crosswind) at distance x = 2000 m, which are R(2000, ±25), R(2000, ±50), R(2000, ±75), and R(2000, ±100). As seen, these receptors are within the range of ±100 m in the lateral direction where the maximum and large concentrations take place and are generally of most practical concern. Another reason for limiting consideration only to those receptors is that concentrations at locations beyond that range become quite noisy and can considerably affect results during linear regression modeling. Since the dispersion is symmetrical around the plume centerline (or y = 0), the concentrations at R(x, y) and R(x,–y) are equivalent. Thus, $\mathrm{R}(x, \pm y)$ will be shortened to R(x, | y|).

4.3.2. Numerical details

4.3.2.1. LPM

The explicit Euler differencing scheme was used for numerical integration, by which Eq. (4.1) is rewritten into the following discrete form

$$\Delta x_i^n = x_i^{n+1} - x_i^n = u_i^n \, \Delta t^n \,, \quad \text{and}$$
$$\Delta u_i^n = u_i^{n+1} - u_i^n = a_i^n \, \Delta t^n + b_{ij}^n \, \Delta W_j^n \,, \tag{4.6}$$

where n is the timestep, Δt^n is the size of timestep n, ΔW_j^n is normally distributed with mean zero and variance Δt^n. The Marsaglia-Bray algorithm (Press et al., 1992, p. 280) was used to generate random numbers for a normal univariate. To initialize the velocity of a particle, the Scheuer-Stoller algorithm (Law and Kelton, 2000, p. 480) for a normal multivariate with a nonzero covariance matrix was employed. Perfect reflection of a particle when encountering the ABL top (at $z = h$) and the ground (assumed at $z = z_o$) was carried out. Following Flesch et al. (1995), the fluctuating velocity components in both along-wind and vertical directions are reversed to their opposite signs after reflection.

To calculate the concentration at a particular receptor, a grid cell (3D) was placed aligned with the center of the receptor. The method of a total residence time was employed, by which (i) each particle is generated at the same initial time, (ii) the residence time that each particle spends inside the grid cell is recorded and summed up with those from the other particles, and (iii) the concentration is linearly proportional to the total residence time. We examined different grid cell sizes and different numbers of particles per simulation for the three base cases (i.e. WS_{Base}, S_{Base}, and MS_{Base}). Square (in x-y) grid cells were used for simplicity, and the cell height was set to 2.0 m for each receptor. Δ_{cell} denotes the width of a grid cell. When Δ_{cell} at a receptor is too large, the local resolution of concentration is lost. On the contrary, if Δ_{cell} is small, the local resolution can be maintained but the rate of convergence becomes slow, requiring more

particles per simulation (otherwise the result would still be unstable and tend to be noisy). Final values of Δ_{cell} were approximately set as follows: In WS[.] and S[.], Δ_{cell} equals 2.5 m for $0 < x \leq 500$ m and is linearly adjusted to 22.5 m for 2500 m $< x \leq 3000$ m while, in MS[.], Δ_{cell} is linearly adjusted to 17.5 m for 2500 m $< x \leq 3000$ m instead. Further sensitivity tests were performed for Δ_{cell} in the three base cases by varying its specified values by ±10%. The results before and after doing so were slightly different and not very sensitive to such changes. For cell height, values of 1.0, 2.0, 3.0, and 4.0 m were tested. It was found that strongly negative sensitivity of concentration exists for receptors near the source but there is little sensitivity for distant receptors. Since the value of 2.0 m yielded satisfactory results from comparison to the PPG data, it was chosen for use. Figure 4-2 shows a graphic representation of concentration contours computed by the model for each base case. It is seen that the contours are spread out in WS_{Base} and S_{Base} and become relatively narrow for MS_{Base}. In the figure, systematic contours of very small concentrations are captured but somewhat irregular, suggesting $C^* \sim 0.1 \times 10^{-5}$ m^{-3} s as the resolution limit of the model in this application. The cross marks in Figure 4-2b indicate the receptors selected for the analysis. As many as 6×10^4 particles per simulation were needed for the convergence at the receptors within 1000 m (in the along-wind direction) from the source whereas more particles were still needed for more distant receptors. For such receptors, 8×10^4 particles were sufficient, and this particle number was adopted. Figure 4-3 shows an example of the results from convergence tests on number of particles per simulation at receptors R(200,0) and R(2000,50) for the three base cases. Concentrations are not stable for small particle numbers but slowly change

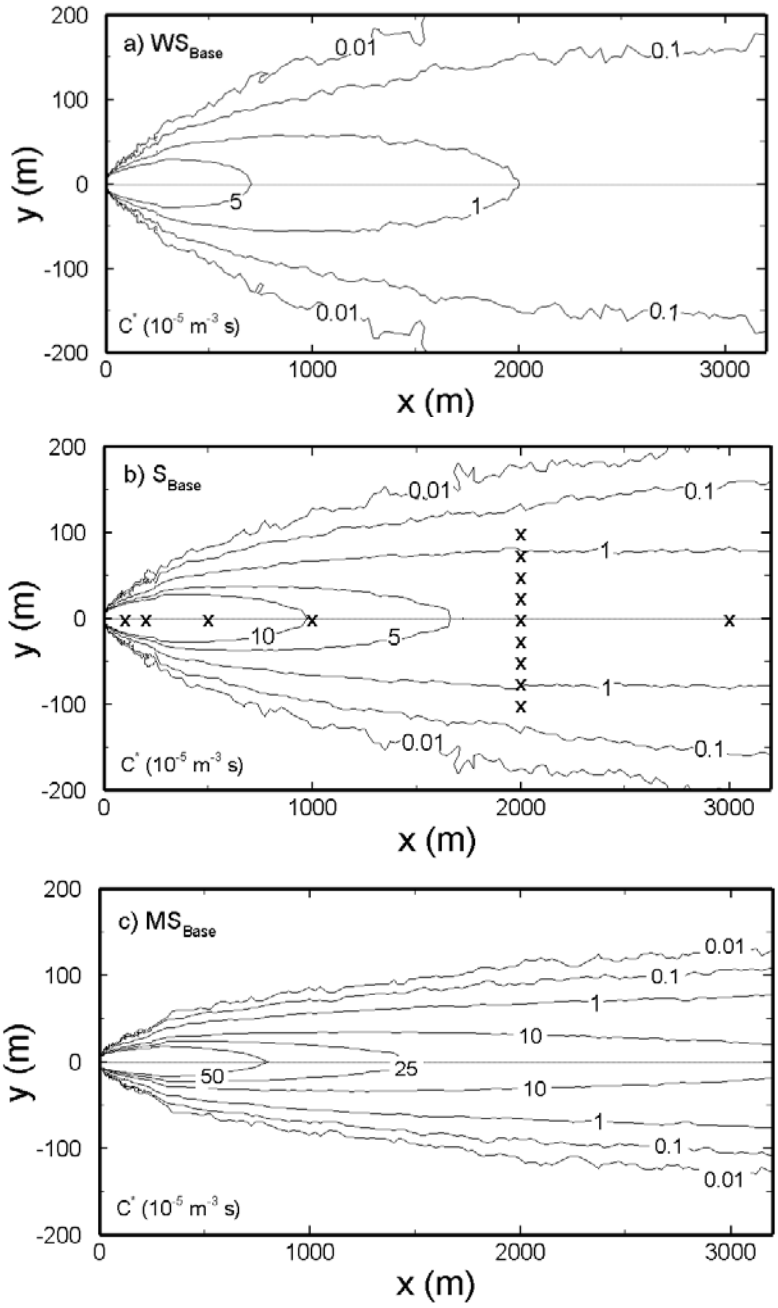

Figure 4-2. Example of concentration contours calculated by the LPM: a) WS_{Base}, b) S_{Base}, and c) WS_{Base}

(i.e. converge) for large particle numbers.

It is also necessary to control the timestep size Δt^n to be small for each step in order to obtain accurate trajectories. We conducted a test similar to that of Flesch and Wilson (1992) for each base case, by which Δt^n was set to equal $0.1\tau_l$, $0.05\tau_l$, $0.02\tau_l$, $0.01\tau_l$, and $0.005\tau_l$, where τ_l is called the local decorrelation time and estimated as $\tau_l = 2\sigma_w^2 / C_o\varepsilon$. When a particle stays in the neighborhood of or within a grid cell of interest, Δt^n is additionally constrained to be less than the residence time for the particle. The results showed only slight changes for $\Delta t^n = 0.02\tau_l$ and lower. Hence, $\Delta t^n = 0.02\tau_l$ was used. As for computational times required in running the model, they were approximately 3, 4, and 6 hr for WS_{Base}, S_{Base}, and MS_{Base}, respectively, on a 500-MHz processor. The average travel time of the cloud of particles migrating from the source to the end of the spatial domain in question was found to be less than 0.5 hr for each base case which is well within the time frame of short-range dispersion.

4.3.2.2. LHS, MC simulations, and linear regression modeling

The LHS method, developed by Mckay et al. (1979), is a stratified random sampling by which the sample space for an input is divided up into a number of layers and input values are obtained by sampling separately from within each layer. Its procedure is concisely described as follows: Suppose that a number of observations (N_{LHS}) for an output are planned. A set of N_{LHS} values of each input (i.e. a sample of size N_{LHS} of each input) must then be generated. To do so, first divide each input distribution

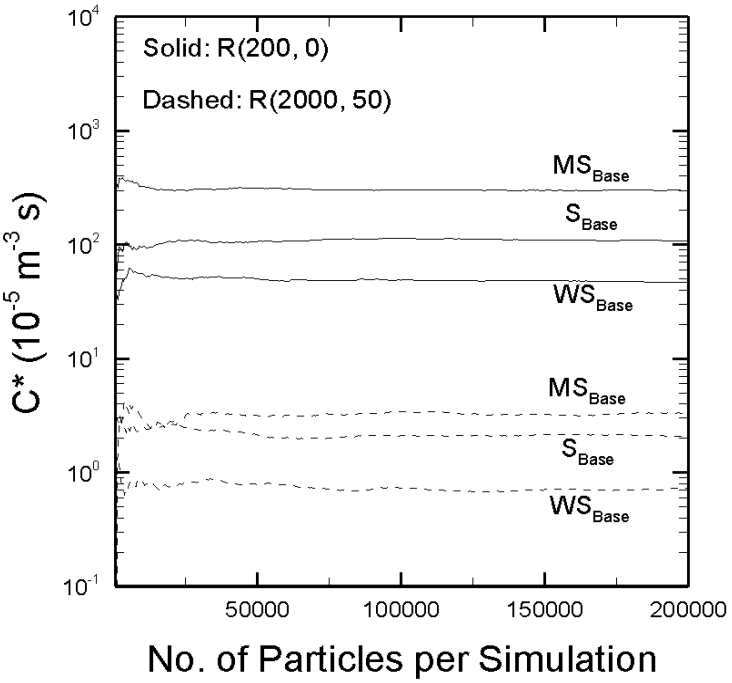

Figure 4-3. Convergence of C^* on No. of particles per simulation for WS_{Base}, S_{Base}, and WS_{Base} at: a) R(200, 0) and b) R(2000, 50)

into N_{LHS} equiprobable intervals. A single input value is selected either at random from within or at the midpoint of each interval. The N_{LHS} values of one input are randomly paired without replacement with the N_{LHS} values of another input to form N_{LHS} pairs of input values. These pairs are randomly combined without replacement with the N_{LHS} values of the next input to form N_{LHS} triplets of input values. The process is continued for the other inputs. Finally, N_{LHS} sets of input values are obtained for MC simulations.

To economize the computational cost of the entire analysis, it is important to determine a manageable sample size for MC simulations. In doing so, S[20] was chosen as a reference, and different values of N_{LHS} (here, 50, 75, 100, and 200) were tested. N_{LHS} = 100 was selected because the observed changes in the first three moments of C^* were small. As an example, the convergence results at R(200, 0) and R(2000, 50) are shown in Figure 4-4. In the figure, *M*, *SD*, and *SK* denote the sample mean, the sample standard deviation, the sample skewness parameter, respectively, and $SK^{1/3}$ is the cube root of *SK*. *M* appears stable for each N_{LHS} at both receptors while *SD* still varies much for N_{LHS} = 50 and 75 at R(200,0). For $SK^{1/3}$, the relative differences are still considerable for N_{LHS} = 50 but become bounded within ±10% from N_{LHS} = 75. One caution of using the LHS is spurious correlations among inputs that always take place during random pairing. In this work, all off-diagonal terms in the Spearman rank correlation matrix of inputs after random pairing in each case in the analysis were low (< 0.1).

Additional useful results can be drawn from partitioning an output uncertainty to specify inputs of greatest importance. A widely used technique is linear regression modeling in which results from MC simulations are used in constructing an empirical

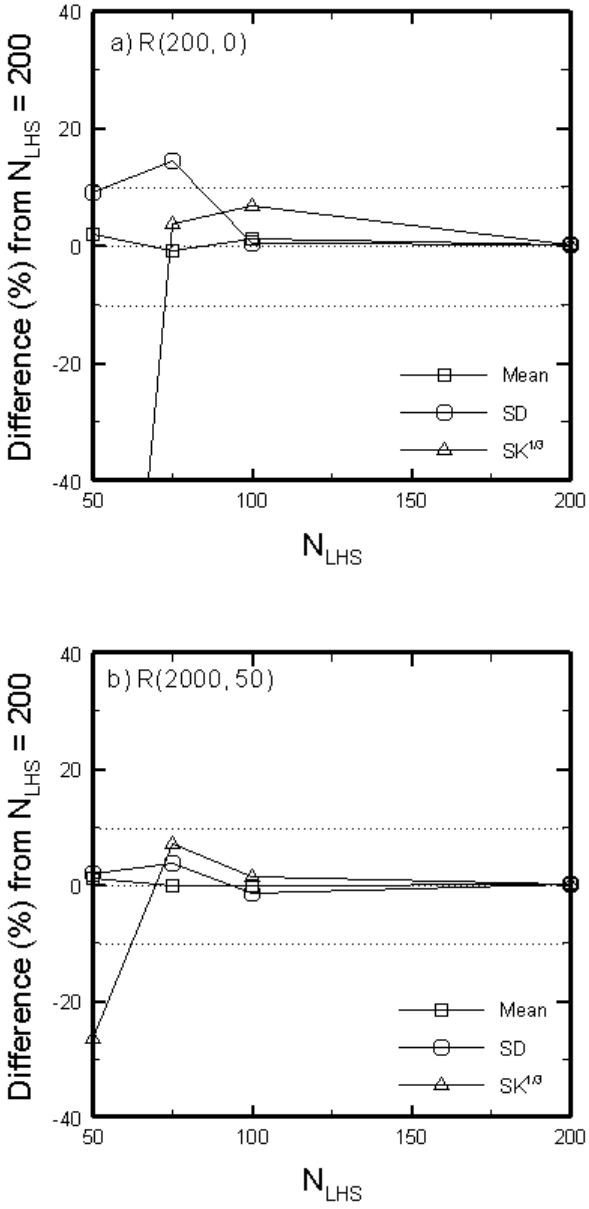

Figure 4-4. Convergence of the first three moments of C^* on N_{LHS} for S[20] at: a) R(200, 0) and b) R(2000, 50)

relationship between output and inputs (NCRP, 1996 and references therein; Yang and Milford, 1996; Bergin et al., 1999; Helton and Davis. 2002). The regression technique is simple in both concept and implementation and enables the global sensitivity of an output with respect to an input to be readily estimated. In this work, the linear regression equation is given by

$$C^* = \beta_0 + \sum_q \beta(X_q)\, X_q \,, \tag{4.7}$$

where X_q is input q (= 1, 2, … , N = 5), β_0 is the regression intercept, $\beta(X_q)$ is the regression coefficient for input q, and C^* is the output (concentration). Regression coefficients are determined by the method of least squares (Neter et al., 1996, p. 217-228). The significance of $\beta(X_q)$ can be viewed as an aggregate first-order measure of the change of C^* due to a unit change in X_q, and it represents the global sensitivity of C^* to X_q or the influence of X_q on C^*. To reduce the effect of different scales of inputs, a standardized version of Eq. (4.7) was used, where X_q and C^* were normalized to zero mean by their respective sample means and to unit variance by their respective sample standard deviations. As a result, β_0 becomes zero, and $\beta(X_q)$ is dimensionless. The uncertainty contribution from X_q to the uncertainty (in terms of variance) in C^*, denoted by $UC(X_q)$, is

$$UC(X_q)\,(\%) = \beta^2(X_q) \times 100\,. \tag{4.8}$$

The global sensitivity of C^* with respect to X_q, denoted by $GS(X_q)$, is computed as

$$GS(X_q) = \beta(X_q)\frac{SD(C^*)}{SD(X_q)}, \tag{4.9}$$

where $SD(X_q)$ is the sample standard deviation of X_q, and $SD(C^*)$ is the sample standard deviation of C^*. Eq. (4.9) results from taking the first-order derivative of C^* with respect to X_q. Note that $\beta(X_q)$ in Eqs. (4.8) and (4.9) is from the standardized regression.

To verify the adequacy of a regression model, the residual plot of each input and the normal plot of output residuals were checked. The proper character of a residual plot should exhibit a scattered (i.e. not grouped) pattern around zero, and that of the normal plot should not display a large departure from a straight line. The value of R^2 of a regression model was also compared with the sum of all uncertainty contributions, i.e. $\sum_q UC(X_q)$, to inspect the degree of spurious correlations arising during the LHS. Since input uncertainties are assumed to be independent, both quantities are equal (Helton and Davis, 2002). However, they normally differ in practice because of the presence of such spurious correlations. In this work, the magnitude of their difference was checked and found to be less than 10%, i.e. $|\sum_q UC(X_q) - R^2| / R^2 < 0.1$, for all regression models in the analysis.

4.4. Results and Discussion

4.4.1. Comparison of concentration uncertainties

Concentration results and their first three moments obtained from MC simulations with the LHS for the six cases chosen in the study are presented in Table 4-2. In the table, γ is the ratio of the concentration from a particular base case (C^*_{Base}) to the concentration mean (M) from MC simulations, CV ($=SD/M$) is the coefficient of variation (defined as the ratio of the sample standard deviation, SD, to the sample mean, M) of concentration, $SK^{1/3}$ is the cube root of the sample skewness parameter of concentration. (Results for R(2000, 100) in MS[20] are not given because most concentrations from MC simulations at this receptor fell below the resolution limit of the model and are not appropriate for use.) It is seen that M decreases away from the source and from the plume centerline. The values of γ are not far from unity (0.95-1.20), and the level of input uncertainties plays an important role in the value of γ. That is, γ increases from S[10] to S[30], except for R(2000, 75) and R(2000, 100) where γ is only slightly changed. A large departure from unity may not be explicitly explained but indicates the presence of a nonlinear relation between inputs and output. When the relation between inputs and an output is linear, γ will be close to unity regardless of input uncertainties. It is evident from S[10] to S[30] that the larger the input uncertainties, the larger the CV values. The CV trends do not vary much along the plume centerline. However, in the lateral direction, CV decreases and then increases, especially in MS[20] where the largest CV (= 0.67) occurs. All concentrations are shown to be positively skewed, even in

Table 4-2. Concentration results from MC simulations for each case

Case		Distance (m) along plume centerline						Lateral distance (m) from plume centerline at x = 2000 m				
		100	200	500	1000	2000	3000	0	25	50	75	100
WS[20]	M[a]	165.62	52.07	10.68	3.27	1.04	0.55	1.04	0.93	0.76	0.49	0.29
	γ[b]	1.05	1.08	1.07	1.11	1.15	1.09	1.15	1.12	0.98	1.11	1.03
	CV[c]	0.27	0.29	0.32	0.31	0.34	0.35	0.34	0.32	0.31	0.28	0.35
	$SK^{1/3}$[d]	0.96	1.19	0.95	1.02	1.06	1.36	1.06	1.11	0.96	0.95	0.69
S[10]	M	328.27	111.17	27.30	10.14	4.02	2.46	4.02	3.51	2.24	1.11	0.43
	γ	1.01	1.03	1.01	1.05	1.02	1.05	1.02	0.99	1.02	0.95	1.03
	CV	0.19	0.22	0.23	0.23	0.22	0.22	0.22	0.20	0.15	0.14	0.27
	$SK^{1/3}$	0.78	0.79	0.80	0.80	0.80	0.80	0.80	0.64	0.64	0.69	0.56
S[20]	M	336.82	114.71	28.23	10.52	4.22	2.55	4.22	3.67	2.33	1.13	0.45
	γ	1.03	1.06	1.04	1.09	1.07	1.09	1.07	1.04	1.06	0.96	1.07
	CV	0.25	0.28	0.28	0.29	0.30	0.30	0.30	0.27	0.23	0.23	0.35
	$SK^{1/3}$	0.85	0.91	0.93	0.97	0.99	0.94	0.99	0.88	0.95	0.92	0.75
S[30]	M	357.44	121.85	30.45	11.23	4.59	2.80	4.59	3.89	2.44	1.15	0.45
	γ	1.10	1.13	1.12	1.16	1.17	1.20	1.17	1.10	1.11	0.98	1.07
	CV	0.34	0.36	0.38	0.38	0.38	0.39	0.38	0.38	0.31	0.33	0.44
	$SK^{1/3}$	0.84	0.87	0.90	0.90	0.90	0.97	0.90	0.90	0.90	0.99	1.01
S[20N]	M	336.15	114.05	28.07	10.49	4.18	2.53	4.18	3.57	2.36	1.13	0.43
	γ	1.03	1.05	1.04	1.08	1.06	1.08	1.06	1.01	1.08	0.97	1.03
	CV	0.29	0.32	0.29	0.33	0.33	0.34	0.33	0.31	0.27	0.31	0.46
	$SK^{1/3}$	1.14	1.14	1.04	1.14	1.10	1.15	1.10	1.08	1.05	0.99	0.84
MS[20]	M	755.21	310.05	98.38	43.85	20.47	13.69	20.47	12.75	3.41	0.40	-
	γ	1.07	1.03	1.05	1.06	1.06	1.09	1.06	1.05	1.02	0.98	-
	CV	0.26	0.28	0.29	0.29	0.28	0.28	0.28	0.24	0.30	0.67	-
	$SK^{1/3}$	0.95	0.90	0.97	0.94	0.86	0.92	0.86	0.98	0.89	0.97	-

[a] Sample mean of concentration (10^{-5} m^{-3} s)

[b] $\gamma = M / C^{*}_{Base}$, where C^{*}_{Base} is the concentration from its correponding base case

[c] Coefficient of variation ($= SD/M$) where SD is the sample standard deviation of concentration

[d] Cube root of the sample skewness parameter

S[20N] where all input uncertainties are normally distributed. Furthermore, the results in S[20] and S[20N] are comparable but those in former have smaller skewness. That is, the concentration distributions in S[20N] have heavier tails than those in S[20]. Relatively small skewness is found in S[10]. The degree of stability also has a strong influence on skewness, as seen in WS[20] where skewness appears to be larger for the receptors along and close to the plume centerline than in S[20] and MS[20]. Figure 4-5 shows an example of the cumulative probability plots of concentrations at R(200, 0) and R(2000, 50) in WS[20], S[20], and MS[20].

4.4.2. Uncertainty contributions and inputs of importance

Uncertainty contributions from the inputs and the global sensitivities of concentrations were obtained from incorporating results from MC simulations into linear regression modeling. Results for the receptors along the plume centerline and those for the receptors in the lateral direction are shown in Tables 4-3 and 4-4, respectively. All final regression models (of C^*) did not use u_* as an input but u_*^{-1} instead. The reason is that regression models with u_*, when used, were found to have serious inadequacies as follows: The residual plots of u_* deviated considerably from the desired character for most receptors, exhibiting a common pattern of positive and negative (concave-like) residuals of u_* grouped together. Moreover, their normal plots were not close to a straight line. Thus, the original regression model in Sec. 3.2 required modification. In doing so, some alternative polynomial forms of u_* (here, $u_*^{m/2}$ for $m = \pm 1, \pm 2, \ldots$) were examined. It was found that u_*^{-1} was a simple and practical choice, giving satisfactory

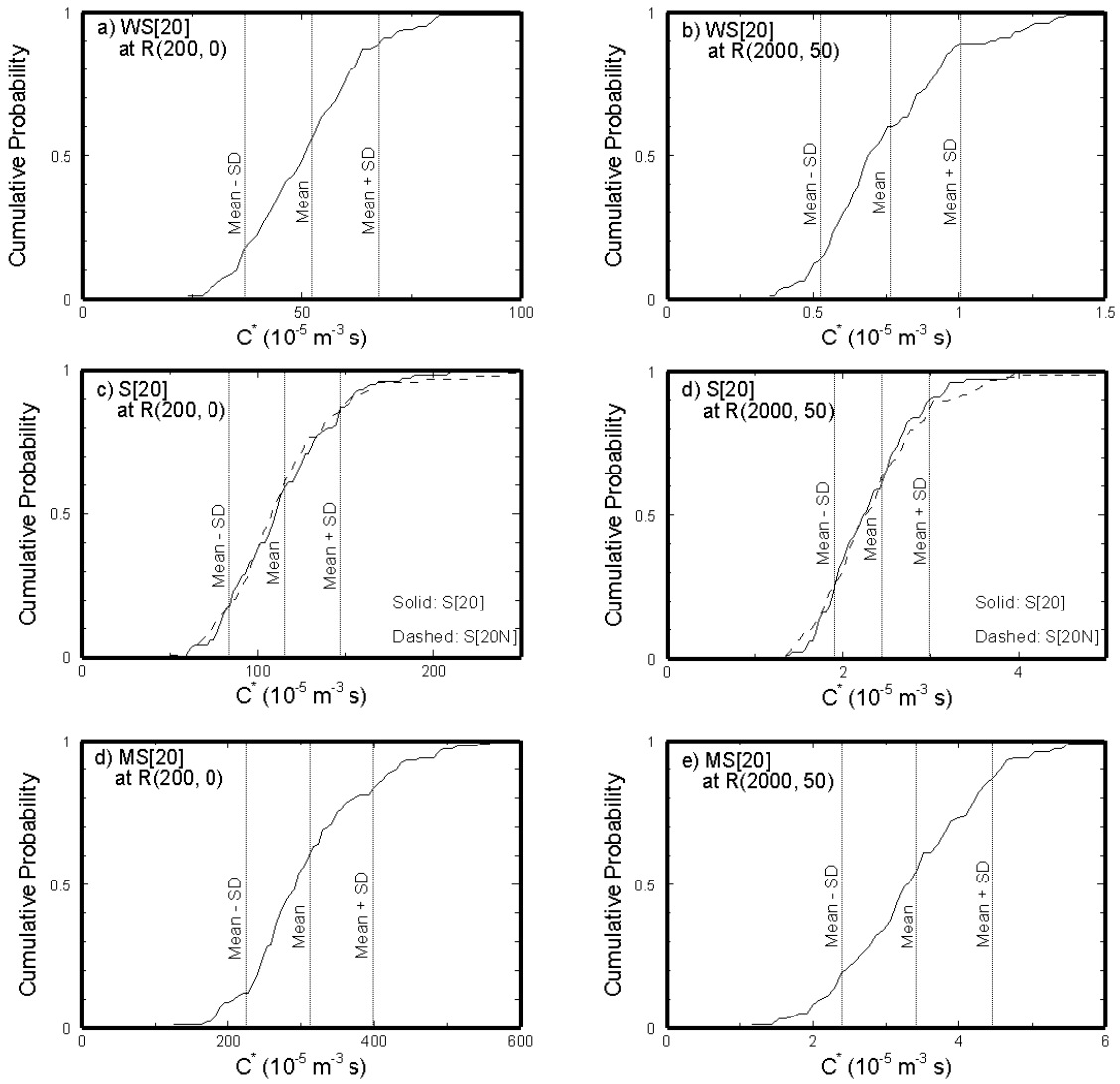

Figure 4-5. Cumulative probability plots from MC simulations: a) WS[20] at R(200, 0), b) WS[20] at R(2000, 50), c) S[20] and S[20N] at R(200, 0), d) S[20] and S[20N] at R(2000, 50), e) MS[20] at R(200, 0), and f) MS[20] at R(2000, 50)

Table 4-3.Uncertainty contributions and global sensitivities of concentrations at the receptors along the mean plume centerline

Case	Input	Distance (m) along plume centerline											
		100		200		500		1000		2000		3000	
		GS[a]	*UC*[b]	*GS*	*UC*	*GS*	*UC*	*GS*	*UC*	*GS*	*UC*	*GS*	*UC*
		(R^2 = 0.95)		(R^2 = 0.91)		(R^2 = 0.91)		(R^2 = 0.84)		(R^2 = 0.81)		(R^2 = 0.74)	
WS[20]	L	0.0	0.0	0.0	0.5	0.0	0.3	0.0	1.6	0.0	1.5	0.0	3.0
	u_*	-404.7	55.6	-127.1	45.6	-28.0	44.6	-7.5	36.1	-2.7	37.9	-1.3	31.9
	z_o	-22.1	0.9	-11.8	2.2	-1.3	0.5	-0.7	1.7	-0.2	0.7	-0.1	1.0
	h	0.0	0.0	0.0	0.1	0.0	0.0	0.0	0.3	0.0	0.4	0.0	0.7
	C_o	56.5	37.7	20.7	41.8	4.8	45.2	1.4	44.3	0.5	40.6	0.2	37.1
		(R^2 = 0.98)		(R^2 = 0.98)		(R^2 = 0.95)		(R^2 = 0.94)		(R^2 = 0.93)		(R^2 = 0.92)	
S[10]	L	-0.5	0.2	-0.4	0.8	-0.2	2.4	-0.1	2.3	0.0	3.6	0.0	5.2
	u_*	-1404.0	24.1	-467.1	17.9	-109.3	15.4	-46.1	19.8	-17.4	18.6	-10.1	16.7
	z_o	-44.4	0.4	-21.4	0.7	-4.9	0.6	-1.2	0.2	-0.1	0.0	-0.2	0.2
	h	0.0	0.0	0.0	0.0	0.0	0.1	0.0	0.1	0.0	0.7	0.0	0.5
	C_o	112.2	71.1	44.8	75.9	11.2	74.1	4.0	68.8	1.5	66.0	0.9	65.4
		(R^2 = 0.97)		(R^2 = 0.97)		(R^2 = 0.96)		(R^2 = 0.95)		(R^2 = 0.93)		(R^2 = 0.94)	
S[20]	L	-0.6	0.7	-0.3	1.6	-0.2	4.8	-0.1	7.9	0.0	9.8	0.0	12.6
	u_*	-1380.8	54.8	-476.3	47.7	-115.1	43.8	-44.8	44.6	-18.4	45.0	-11.4	45.6
	z_o	-44.1	1.0	-18.7	1.3	-3.1	0.5	-0.4	0.1	-0.2	0.1	-0.2	0.2
	h	-0.1	0.0	0.0	0.1	0.0	0.1	0.0	0.4	0.0	1.7	0.0	2.1
	C_o	118.7	44.7	46.9	51.1	11.9	51.5	4.4	46.4	1.7	40.2	1.0	37.1
		(R^2 = 0.97)		(R^2 = 0.96)		(R^2 = 0.95)		(R^2 = 0.94)		(R^2 = 0.94)		(R^2 = 0.92)	
S[30]	L	-0.6	0.8	-0.3	1.7	-0.1	4.2	-0.1	9.7	0.0	12.9	0.0	14.9
	u_*	-1399.9	66.9	-480.9	61.2	-120.4	54.1	-43.3	53.1	-18.0	53.4	-11.1	50.7
	z_o	-53.9	1.6	-16.3	1.1	-2.8	0.5	-0.8	0.3	-0.2	0.1	0.0	0.0
	h	0.0	0.0	0.0	0.0	0.0	0.1	0.0	0.4	0.0	0.9	0.0	1.7
	C_o	130.7	26.6	50.7	31.1	14.3	34.6	4.8	30.2	1.9	26.1	1.1	23.6
		(R^2 = 0.94)		(R^2 = 0.93)		(R^2 = 0.92)		(R^2 = 0.89)		(R^2 = 0.89)		(R^2 = 0.86)	
S[20N]	L	-0.7	0.7	-0.4	2.0	-0.1	3.2	-0.1	7.2	0.0	8.4	0.0	9.8
	u_*	-1454.1	59.4	-480.5	46.9	-108.3	44.9	-43.5	41.8	-18.0	45.1	-11.5	47.4
	z_o	-43.6	0.8	-10.4	0.3	-0.4	0.0	-0.2	0.0	0.1	0.0	0.2	0.1
	h	-0.1	0.1	0.0	0.1	0.0	0.1	0.0	0.7	0.0	2.1	0.0	1.9
	C_o	112.3	31.4	48.1	41.7	11.1	42.0	4.4	37.4	1.6	30.6	0.9	24.7
		(R^2 = 0.96)		(R^2 = 0.96)		(R^2 = 0.94)		(R^2 = 0.94)		(R^2 = 0.94)		(R^2 = 0.94)	
MS[20]	L	-18.7	4.9	-10.8	8.3	-4.4	12.8	-2.0	13.1	-0.9	13.7	-0.7	15.4
	u_*	-4839.4	55.0	-1958.5	45.3	-618.4	41.7	-289.0	45.2	-133.1	46.8	-89.3	47.5
	z_o	-65.2	0.4	-33.9	0.6	-8.8	0.3	-2.1	0.1	0.3	0.0	-0.1	0.0
	h	-0.5	0.1	-0.3	0.1	-0.2	0.3	-0.2	1.9	-0.1	3.0	-0.1	3.6
	C_o	228.5	31.8	112.5	38.8	35.9	36.5	15.0	31.4	6.4	28.1	4.0	25.2

[a] Global sensitivity with units of (10^{-5} m^{-4} s) for L, (10^{-5} m^{-4} s^2) for u_*, (10^{-3} m^{-4} s) for z_o, (10^{-5} m^{-4} s) for h, and (10^{-5} m^{-3} s) for C_o

[b] Uncertainty contribution (%) calculated from linear regression in which u_*^{-1} is used as an input

Table 4-4. Uncertainty contributions and global sensitivities of concentrations at the receptors in the lateral direction at a distance of 2000 m

Case	Input	Lateral distance (m) from plume centerline at x = 2000 m									
		0		25		50		75		100	
		GS[a]	UC[b]	GS	UC	GS	UC	GS	UC	GS	UC
		(R^2 = 0.81)		(R^2 = 0.77)		(R^2 = 0.76)		(R^2 = 0.52)		(R^2 = 0.47)	
WS[20]	L	0.0	1.5	0.0	3.0	0.0	0.3	0.0	1.2	0.0	2.6
	u_*	-2.7	37.9	-2.1	32.0	-2.1	51.1	-1.1	42.6	-0.8	43.5
	z_o	-0.2	0.7	0.0	0.0	-0.1	0.7	0.0	0.1	0.1	1.7
	h	0.0	0.4	0.0	0.5	0.0	0.2	0.0	2.4	0.0	0.0
	C_o	0.5	40.6	0.4	41.3	0.2	24.0	0.1	6.2	0.0	0.4
		(R^2 = 0.93)		(R^2 = 0.91)		(R^2 = 0.77)		(R^2 = 0.52)		(R^2 = 0.57)	
S[10]	L	0.0	3.6	0.0	4.6	0.0	0.3	0.0	0.1	0.0	1.8
	u_*	-17.4	18.6	-14.7	21.7	-9.8	40.5	-4.7	46.3	-1.8	12.4
	z_o	-0.1	0.0	-0.2	0.1	0.5	1.7	0.3	2.9	0.1	0.6
	h	0.0	0.7	0.0	0.2	0.0	1.0	0.0	1.0	0.0	2.6
	C_o	1.5	66.0	1.1	59.9	0.4	30.8	-0.1	3.2	-0.2	40.4
		(R^2 = 0.93)		(R^2 = 0.94)		(R^2 = 0.89)		(R^2 = 0.75)		(R^2 = 0.73)	
S[20]	L	0.0	9.8	0.0	10.5	0.0	4.4	0.0	0.1	0.0	10.6
	u_*	-18.4	45.0	-15.7	52.3	-9.4	63.3	-4.9	70.9	-1.9	30.9
	z_o	-0.2	0.1	-0.4	0.6	0.2	0.5	0.2	2.0	0.1	0.7
	h	0.0	1.7	0.0	0.6	0.0	1.0	0.0	0.1	0.0	0.3
	C_o	1.7	40.2	1.2	34.5	0.5	20.3	0.0	0.1	-0.2	32.6
		(R^2 = 0.94)		(R^2 = 0.94)		(R^2 = 0.93)		(R^2 = 0.93)		(R^2 = 0.75)	
S[30]	L	0.0	12.9	0.0	8.8	0.0	2.4	0.0	0.4	0.0	14.4
	u_*	-18.0	53.4	-16.3	62.4	-9.4	78.6	-5.0	88.0	-1.8	43.0
	z_o	-0.2	0.1	-0.2	0.1	0.2	0.6	0.2	1.5	0.1	2.2
	h	0.0	0.9	0.0	0.5	0.0	1.0	0.0	0.3	0.0	0.1
	C_o	1.9	26.1	1.4	21.4	0.5	8.8	-0.1	0.9	-0.2	18.8
		(R^2 = 0.89)		(R^2 = 0.85)		(R^2 = 0.77)		(R^2 = 0.64)		(R^2 = 0.59)	
S[20N]	L	0.0	8.4	0.0	5.9	0.0	2.3	0.0	0.2	0.0	9.2
	u_*	-18.0	45.1	-15.0	48.2	-9.7	58.7	-5.5	62.7	-2.2	31.3
	z_o	0.1	0.0	0.1	0.0	0.2	0.3	-0.1	0.1	-0.1	0.3
	h	0.0	2.1	0.0	1.0	0.0	0.3	0.0	0.0	0.0	4.1
	C_o	1.6	30.6	1.2	28.3	0.5	13.5	0.1	0.6	-0.2	18.4
		(R^2 = 0.94)		(R^2 = 0.89)		(R^2 = 0.72)		(R^2 = 0.69)			
MS[20]	L	-0.9	13.7	-0.3	6.2	0.2	12.0	0.1	34.2		-
	u_*	-133.1	46.8	-80.2	62.3	-24.4	50.0	-2.3	6.6		-
	z_o	0.3	0.0	-0.2	0.0	0.7	1.7	0.1	0.2		-
	h	-0.1	3.0	-0.1	3.0	0.0	0.0	0.0	0.5		-
	C_o	6.4	28.1	2.5	15.4	-0.8	13.0	-0.3	31.1		-

[a, b] Same as in Table 4-3

behavior for the residual plots of the inputs and the normal plots at all receptors in every case with few minor deviations. An example of improvement in the residual plots using u_* and then using u_*^{-1} is shown in Figure 4-6. Due to the modification, the global sensitivity of C^* to u_* is computed as

$$GS(u_*) = -\beta(u_*^{-1}) \frac{SD(C^*)}{SD(u_*^{-1})\, M^2(u_*)_{\text{Base}}}, \tag{4.10}$$

where $\beta(u_*^{-1})$ is the regression coefficient for u_*^{-1} (from the standardized regression), $M(u_*)_{\text{Base}}$ is the base value (or mean) of u_*, and the rest are the same as in Eq. (4.9).

From Table 4-3, it is clear that friction velocity and the universal constant are the most influential inputs. When the uncertainties in meteorological parameters are at the medium (20%) and high (30%) levels, the uncertainty contribution from friction velocity dominates those of the other inputs. At the low (10%) level, the contribution from the universal constant dominates. In general, the contributions from Monin-Obukhov length and mixing height are not large. However, they begin to increase for distant receptors, particularly in MS[20], which is reasonable because, in MS[20], Monin-Obukhov length and mixing height are relatively small and can significantly affect the values of turbulence statistics in the model. Also, when mixing height is small, more particles are likely to reach the ABL top at longer distances and then reflect back to low elevations. The overall contribution from roughness height is found to be only slight (< 3%). Comparing S[20] and S[20N], their results differ slightly but are comparable. The R^2

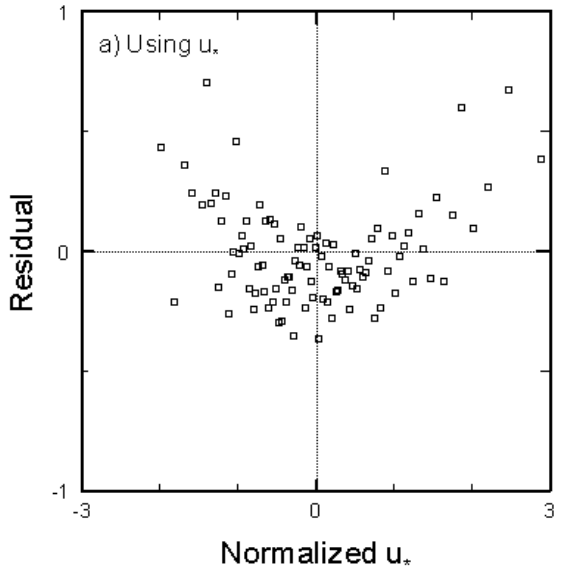

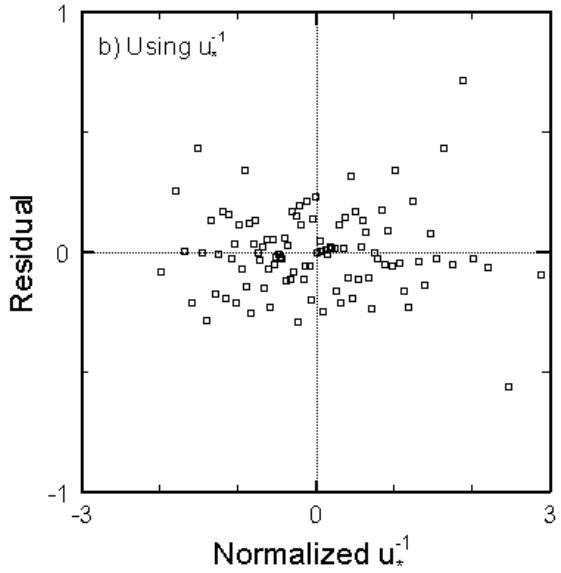

Figure 4-6. Residual plots of u_* and u_*^{-1} from standardized regression for S[20] at R(200, 0): a) using u_* and b) using u_*^{-1}

values in the table are fairly high (0.74-0.98), indicating that the regression models are capable of accounting for most of total uncertainty. For the global sensitivities, their trends are generally similar to those of uncertainty contributions since both quantities are derived from the same information (which are the regression coefficients). Most inputs are associated with negative sensitivity (i.e. an output tends to decrease with an increase in an input) while the universal constant is associated with positive sensitivity. The *GS* values appear not to be significantly affected by the level of input uncertainties, as seen in S[10]-S[30].

In Table 4-4, the largest uncertainty contributors for most receptors are friction velocity and the universal constant. Similar to the previous table, the uncertainty contribution from the universal constant dominates when the levels of uncertainties in meteorological inputs are small. Nevertheless, it tends to decline for the receptors near the plume centerline and then increase afterwards, corresponding to the change in the *GS* sign from positive to negative with the minimum of *UC* values present at some distance in between. Therefore, the uncertainty in the universal constant has little or no influence for locations in the neighborhood of the *UC* minimum. Similarly, the contribution from Monin-Obukhov length decreases for the receptors near the plume centerline and increases later, and it becomes fairly large in MS[20]. In addition, the *GS* values in S[10]-S[30] are not very sensitive to the level of input uncertainties. The contributions from roughness height and mixing height are not important. In S[20] and S[20N], the results are comparable and share similar trends. The R^2 values are high for most receptors but relatively low (0.47-0.59) for some receptors far from the plume centerline. The adequacy of the regression models with low R^2 was checked and found to be

satisfactory, suggesting that large variations in the values of both inputs and outputs exist in the regression models.

As noted in Sec. 1, additional analysis is performed for the half width of concentration contours. The half-width results at a distance of 2000 m for WS[20], S[20], and MS[20] are presented below. To determine the half width (denoted by *HW*), the profile of the concentration contours in the lateral direction in question is approximated by the Gaussian form

$$C^* = \kappa_1 \exp(-\kappa_2 y^2), \tag{4.11}$$

where κ_1 and κ_2 are the regression coefficients with dimensions of Length^{-3} Time and Length^{-2}, respectively, and determined by the method of least squares for a nonlinear regression model (Neter et al., 1996, p. 536-547). Here, *HW* is estimated as $\sqrt{2/\kappa_2}$ (equivalent to the lateral distance from the plume centerline covering twice the standard deviation of a fitted Gaussian concentration profile). As an example, the calculated and fitted concentration profiles for the three bases cases, together with their corresponding values of κ_1, κ_2, and *HW*, are given in Figure 4-7. It is seen that the calculated profiles in the figure are well fit by the above Gaussian form. To partition the uncertainty in the half width and to compute the global sensitivity of the half width to an input, the same procedures were followed with C^* in Eqs. (4.7) and (4.9) replaced by *HW*. Table 4-5 presents the results from the half-width analysis. Note that all linear regression models use u_* as an input. Their adequacy was checked and found to be satisfactory. The

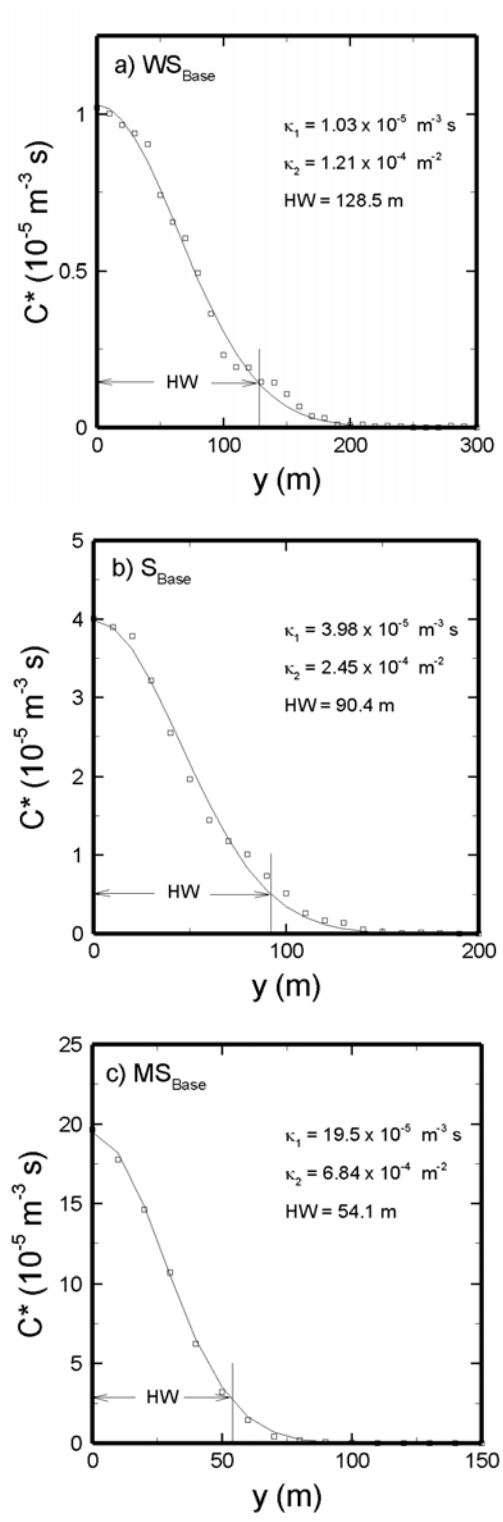

Figure 4-7. Comparison between calculated and fitted Gaussian concentration profiles at a distance of 2000 m from the source: a) WS_{Base}, b) S_{Base}, and c) WS_{Base}

Table 4-5. Uncertainty contributions and global sensitivities of the half widths of concentration contours at a distance of 2000 m

WS[20]			S[20]			MS[20]		
M[a]	129.4 m		M	94.5 m		M	53.3 m	
γ[b]	1.01		γ	1.05		γ	0.99	
CV[c]	0.13		CV	0.09		CV	0.11	
Input	GS[d]	UC[e]	Input	GS	UC	Input	GS	UC
	(R^2 = 0.56)			(R^2 = 0.82)			(R^2 = 0.75)	
C_o	-24.7	53.5	C_o	-14.9	65.7	C_o	-7.7	38.9
			L	0.3	18.2	L	1.5	34.2
			z_o	9.0	3.9	h	0.1	2.4

[a, b, c] Same as in Table 2 but for the half width of ground-level concentration contour
[d] Global sensitivity with units of (m) for C_o, (-) for L, (m cm^{-1}) or (10^2) for z_o, and (-) for h
[e] Uncertainty contribution (%) calculated from linear regression in which u_* was used as an input

regression model in S[20] is capable of accounting for most of the total uncertainty (R^2 = 0.82). When the degree of stability increases, M decreases. In each case, γ is close to unity, and CV is around 10%. For the uncertainty contributions, only inputs with an uncertainty contribution of more than 1% are given in the table. The most influential input in every case is the universal constant and has a negative sensitivity. Among the meteorological inputs, Monin-Obukhov length is now most important and has a positive sensitivity, as seen in S[20] and MS[20]. Contributions from the other inputs are relatively small.

4.5. Summary

This work has evaluated the effects of uncertainties in five inputs of a Lagrangian particle model for short-range dispersion over smooth flat terrain under weakly and moderately stable conditions. The magnitude of a concentration uncertainty increases with those of input uncertainties. Concentration uncertainties were found to show positive skewness. Results obtained from using lognormal and normal distributions for input uncertainties are comparable. Among the meteorological parameters considered here, friction velocity is most influential to the uncertainty in concentration. Uncertainties in Monin-Obukhov length and mixing height do not play an important role for most receptors when the degree of stability is low. The influence of Monin-Obukhov length in the lateral direction tends to decrease for locations near the plume centerline and then increase later. The overall contribution from roughness height is small. Besides friction velocity, another input of importance is the universal constant. Its contribution

often dominates when the uncertainties in meteorological inputs are low. Nevertheless, for some distances in the lateral direction, it becomes relatively small. The significant contributions from friction velocity and the universal constant suggest the importance of using accurate values in the modeling. For global sensitivities, they share similar trends with uncertainty contributions and are not much affected by the level of input uncertainties. Although the sensitivity of concentration to each input may be either positive or negative (depending on receptor and case considered), friction velocity is associated with strongly negative sensitivity. The universal constant is associated with positive sensitivity for most receptors but with negative sensitivity for faraway receptors in the lateral direction. For the half width of concentration contours, only the universal constant and Monin-Obukhov length contribute significantly to uncertainty and have a negative and positive sensitivity, respectively.

Acknowledgements

The authors thank Dr. Kevin Doty of the Earth Science Laboratory, University of Alabama (Huntsville) for his discussion. Several parts of simulation work were implemented on a UNIX cluster of the Office of Information Technology, Georgia Institute of Technology. This work was supported by the U.S. EPA under Contract No. CR827327-01 and the Georgia Power Company.

Appendix. Turbulence statistics for the model

In this work, we adopted the formulas that could be applied for weakly and moderately stable conditions, and their expressions are summarized below:

- Mean wind velocity (van Ulden and Holtslag, 1985):

$$U = \frac{u_*}{k}\left[\ln\left(\frac{z}{z_o}\right) - \Psi_M(z/L) + \Psi_M(z_o/L) \right], \qquad (4A.1)$$

where k is the von Karman constant ($\approx$ 0.4) and $\Psi_M(z/L)$ is the stability function modified from the original linear Businger stability function. The linear Businger stability function takes the form $\Psi_M = -4.7\,(\text{or} -5)\, z/L$ for $L > 0$ while the stability function for Eq. (4A.1) takes the form

$$\Psi_M = -17\left[1 - \exp\left(-0.29\frac{z}{L}\right)\right]. \qquad (4A.2)$$

Since z_o in this work is small (i.e. $z_o/L \sim 10^{-4}$ to 10^{-3}), the last term in the brackets in Eq. (4A.1) may be neglected. This modified stability function has the same performance as the linear Businger stability function for $z/L < 1$ but has a much better performance for $z/L > 1$ (van Ulden and Holtslag, 1985).

- Variances and covariance: A number of studies express the second-order moments of velocity as follows:

$$\frac{\sigma_u^2}{u_*^2} = c_u\left(1-\frac{z}{h}\right)^{\alpha}, \qquad \frac{\sigma_v^2}{u_*^2} = c_v\left(1-\frac{z}{h}\right)^{\alpha},$$

$$\frac{\sigma_w^2}{u_*^2} = c_w\left(1-\frac{z}{h}\right)^{\alpha}, \text{ and} \qquad \frac{\tau_{uw}}{u_*^2} = -\left(1-\frac{z}{h}\right)^{\alpha}. \tag{4A.3}$$

A large variation in the reported values of α, c_u, c_v, and c_w is found in the literature. For instance, Hanna (1982) uses: $\alpha = 2$, $c_u = 4.0$, and $c_v = c_w = 1.7$; Arya (1984): $\alpha = 2$, $c_u = 5.8 \geq c_v \geq c_w = 2.6$; Nieuwstadt (1984): $\alpha = 1.5$, $c_w = 1.96$; Sorbjan (1986), $\alpha = 2$, $c_w = 2.5$; and Lenschow et al. (1988): $\alpha = 1.75$, $c_u = c_v = 4.5$, and $c_w = 3.1$.

From the Monin-Obukhov theory, the turbulence statistics in Eq. (4A.3) are approximately constant for low elevations. A literature survey by Panofsky and Dutton (1984, p. 160) suggests $c_u = 4.8$-6.3, $c_v = 3.0$-4.8, and $c_w = 1.2$-2.0. A review by Dias et al. (1995) gives $c_w = 1.3$-2.3. It is seen that the above values of α, c_u, c_v, and c_w are 1.5-2, 4.0-6.3, 1.7-5.8, and 1.2-3.1, respectively. For the modeling in this work, we chose $\alpha = 2$, $c_u = 4.0$, $c_v = 3.0$, and $c_w = 1.5$.

- Mean energy dissipation rate: Following Sorbjan (1986) with α in Eq. (4A.3) equal to 2,

$$\varepsilon = \frac{u_*^3}{k\,z}\left(1+3.7\frac{z}{L}\right)\left(1-\frac{z}{h}\right)^3 . \qquad (4A.4)$$

Note that, when comparing between the model predictions and the PPG data, the dispersion was assumed to take place in the surface boundary layer, and the reduced forms of the formulas in Eqs. (4A.3) and (4A.4) by taking the limit $z/h \to 0$ were used.

References

Alcomo, J., Bartnicki, J. (1987) A framework for error analysis of a long-range transport model with emphasis on parameter uncertainty. Atmos. Environ. 21, 2121-2131.

Anfossi, D., Ferrero, E., Sacchetti, D., Trini Castelli, S. (1997) Comparison among empirical probability density functions of the vertical velocity in the surface layer based on higher order correlations. Boundary-Layer Meteor. 82, 193-218.

Arya, S. P. S. (1984) Parametric relations for the atmospheric boundary layer. Boundary-Layer Meteor. 30, 57-73.

Barad, M. L. (Ed.) (1958) Project Prairie Grass, A Field Program in Diffusion. Vol. 1. Geographical Research Paper No. 59, Air Force Cambridge Research Center, Belford, Massachusetts.

Benkley, C. W., Schulman, L. L. (1979) Estimation hourly mixing depth from historical meteorological data. J. Appl. Meteor. 18, 772-780.

Bergin, M. S., Noblet,, G. S., Petrini, K., Dhieux, J. R. , Milford, J. B., Harley, R. A. (1999) Formal uncertainty analysis of a Lagrangian photochemical air pollution model. Environ. Sci. Tech. 33, 1116-1126.

Briggs, G. A. (1982) Similarity forms for ground-source surface-layer diffusion. Boundary-Layer Meteor. 23, 489-502.

Brost, R. A., Wyngaard, J. C. (1978) A model study of the stably stratified planetary boundary layer. J. Atmos. Sci. 35, 1427-1440.

Dabberdt, W. F., Miller, E. (2000) Uncertainty, ensembles and air quality dispersion modeling: Applications and challenges. Atmos. Environ. 34, 4667-4673.

Degrazia, G., Anfossi, D. (1998) Estimation of the Kolmogorov constant C_o from classical statistical diffusion theory. Atmos. Environ. 32, 3611-3614.

Derwent, R. G. (1987) Treating uncertainty in models of the atmospheric chemistry of nitrogen compounds. Atmos. Environ. 21, 1445-1454.

Dias, N. L., Brutsaert, W., Wesely, M. L. (1995) Z-less stratification under stable conditions. Boundary-Layer Meteor. 75, 175-187.

Du, S., Sawford, B. L., Wilson, J. D., Wilson, D. J. (1995) Estimation of the Kolmogorov constant (C_o) for the Lagrangian structure function, using a second-order Lagrangian model of grid turbulence. Phys. Fluids 7, 3083-3090.

Flesch, T. K., Wilson, J. D. (1992) A two-dimensional trajectory-simulation model for non-Gaussian, inhomogeneous turbulence within plant canopies. Boundary-Layer Meteor. 61, 349-374.

Flesch, T. K., Wilson, J. D., Yee, E. (1995) Backward-time Lagrangian stochastic dispersion models and their application to estimate gaseous emissions. J. Appl. Meteor. 34, 1320-1332.

Freeman, D. L., Egami, R. T., Robinson, N. F., Watson, J. G. (1986) A method for propagating measurement uncertainties through dispersion models. JAPCA 36, 246-253.

Hanna, S. R. (1982) Applications in air pollution modeling. in Atmospheric Turbulence and Air Pollution Modelling, edited by Nieuwstadt, F. T. M. and van Dop, H., D. Reidel Publishing, 37-68.

Hanna, S. R., Chang, J. C., Fernau, M. E. (1998) Monte Carlo estimates of uncertainties in predictions by a photochemical grid model (UAM-IV) due to uncertainties in input variables. Atmos. Environ. 32, 3619-3628.

Hanna, S. R., Paine, R. J. (1989) Hybrid plume dispersion model (HPDM) development and evaluation. J. Appl. Meteor. 21, 206-224.

Helton, J. C. and Davis, F. J. (2002) Illustration of sampling-based methods for uncertainty and sensitivity analysis. Risk Analysis 22, 591-622.

Holtslag, A. A. M., Nieuwstadt, F. T. M. (1986) Scaling the atmospheric boundary layer. Boundary-Layer Meteor. 36, 201-209.

Iman, R. L., Shortencarier, M. J. (1984) A FORTRAN 77 Program and User's Guide for the Generation of Llatin Hypercube and Random Samples for Use with Computer

Models. NUREG/CR-3624 (SAND83-2365), Sandia National Laboratories, Albuquerque, New Mexico.

Irwin, J. S., Rao, S. T., Petersen, W. B., Turner, D. B. (1987) Relating error bounds for maximum concentration estimates to diffusion meteorology uncertainty. Atmos. Environ. 21, 1927-1937.

Isukapalli S. S., Roy, A., Georgopoulos, P. G. (1998) Stochastic response surface methods (SRSMs) for uncertainty characterization and propagation: application to environmental and biological systems. Risk Analysis 18, 351-363.

Kolmogorov, A. N. (1941) The local structure of turbulence in incompressible viscous fluid for very large Reynolds numbers. Dokl. Akad. Nauk. 30, 301-305.

Law, A. M., Kelton, W. D. (2000) Simulation Modeling and Analysis. McGraw-Hill, Boston, Massachusetts.

Lena, F., Desiato, F. (1999) Intercomparison of nocturnal mixing height estimate methods for urban air pollution modeling. Atmos. Environ. 33, 2385-2393.

Lenschow, D. H., Li, X. S., Zhu, C. J., Stankov, B. B. (1988) The stably stratified boundary layer over the Great Plains. I. Mean and turbulence structure. Boundary-Layer Meteor. 42, 95-121.

Leuzzi, G., Monti, P. (1998) Particle trajectory simulation of dispersion around a building, Atmos. Environ. 32. 203-214.

Lewellen, W. S., Sykes, R. I. (1989) Meteorological data needs for modeling air quality uncertainties. J. Atmos. Ocean. Tech. 6, 759-768.

Luhar, A. K., Britter, R. E. (1989) A random walk model for dispersion in inhomogeneous turbulence in a convective boundary layer. Atmos. Environ. 23, 1911-1924.

McKay, M. D., Beckman, R. J., Conover, W. J. (1979) A comparison of three methods for selecting values of input variables in the analysis of output from a computer code. Technometrics 21, 239-245.

McRae, G. J., Tilden, J. W., Seinfeld, J. H. (1981) Global sensitivity analysis - A computational implementation of the Fourier amplitude sensitivity test (FAST). Comput. Chem. Eng. 6, 15-25.

Morgan, M., Henrion M. (1990) Uncertainty: A Guide to Dealing with Uncertainty in Quantitative Risk and Policy Analysis. Cambridge University Press, Cambridge.

Naslund, E., Rodean, H. C., Nasstrom, J. S. (1994) A comparison between two stochastic diffusion models. Boundary-Layer Meteor. 67, 369-384.

NCRP (1996) A Guide for Uncertainty Analysis in Dose and Risk Assessments Related to Environmental Contamination. NCRP Commentary No. 14, Edited by Hoffman, E. A., National Council on Radiation Protection and Measurements, Bethesda, Maryland.

Neter, J., Wasserman, W.. Kutner, M. H., Nachtschiem, C. J. (1996) Applied Linear Statistical Models. McGraw-Hill, Boston, Massachusetts

Nieuwstadt, F. T. M. (1984) The turbulent structure of the stable, nocturnal boundary layer. J. Atmos. Sci. 41, 2202-2216.

Panofsky, H. A., Dutton, J. A. (1984) Atmospheric Turbulence: Models and Methods for Engineering Applications. Wiley, New York.

Press, W. H., Teukolsky, S. A., Vetterling, W. T., Flannery, B. P. (1992) Numerical Recipes in FORTRAN. Cambridge University Press, Cambridge.

Rao, K. S. (1999) Lagrangian stochastic modeling of dispersion in the stable boundary layer. Boundary-Layer Meteor. 90, 541-549.

Rodean, H. C. (1991) The universal constant for the Lagrangian structure function. Phys. Fluids. 3, 1479-14780.

Rotach, M. W., Gryning, S. E., Tassone, C. (1996) A two-dimensional Lagrangian stochastic dispersion model for daytime conditions. Q. J. R. Meteorol. Soc. 122, 367-389.

Russell, A. G., Dennis, R. L. (2000) NARSTO critical review of photochemical models and modeling. Atmos. Environ. 34, 2283-2324.

Sorbjan, Z. (1986) On similarity in the atmospheric boundary layer. Boundary-Layer Meteor. 34, 377-397.

Sykes, R. I., Lewellen, W. S., Parker, S. F. (1984) A turbulent transport model for concentration fluctuations and fluxes, J. Fluid Mech. 139, 193-218.

Tatang, M. A., Pan, W., Prinn, R. G., McRae, G. J. (1997) An efficient method for parametric uncertainty analysis of numerical geophysical models. J. Geophysic. Res. 102, 21,925-21,932.

Thomson, D. J. (1987) Criteria for the selection of stochastic models of particle trajectories in turbulent flows. J. Fluid Mech. 180, 529-556.

Turner, D. B. (1970) Workbook of Atmospheric Dispersion Estimates. U. S. EPA, Office of Air Programs, Research Triangle Park, North Carolina.

U. S. EPA (2004) Support center for regulatory air models (SCRAM). http://www.epa.gov/ttn/scram.

van Ulden, A. P. (1978) Simple estimates for vertical diffusion from sources near the ground. Atmos. Environ. 12, 2125-2129.

van Ulden, A., Holtslag, A. (1985) Estimation of atmospheric boundary layer parameters for diffusion applications. J. Climate Appl. Meteor. 24, 1196-1207.

Venkatram, A., Du, S. (1997) An analysis of the asymptotic behavior of cross-wind-integrated ground-level concentrations using Lagrangian stochastic simulation. Atmos. Environ. 31, 1467-1476.

Wilczak, J. M., Phillips, M. S. (1984) An indirect estimation of convective boundary layer structure for use in routine dispersion models. EPA-600/3-84-091, U.S. EPA, Research Triangle Park, North Carolina.

Wilson, J. D., Sawford, B. L. (1996) Review of Lagrangian stochastic models for trajectories in the turbulent atmosphere. Boundary-Layer Meteor. 78, 191-210.

Yang, Y.-J., Milford, J. B. (1996) Quantification of uncertainty in reactivity adjustment factors from reformulated gasolines and methanol fuels. Environ. Sci. Technol. 30, 196-203.

Yegnan, A., Williamson, D. G. and Graettinger, A. J. (2002) Uncertainty analysis in air dispersion modeling. Env. Model. Software 17, 639-649.

Zilitinkevich, S. S. (1972) On the determination of the height of the Ekman boundary layer. Boundary-Layer Meteor. 3, 141-145.

CHAPTER 5

FORMULATION OF JOINT PROBABILITY DENSITY FUNCTIONS OF VELOCITY FOR TURBULENT FLOWS: AN ALTERNATIVE APPROACH

(K. Manomaiphiboon and A. G. Russell, Atmos. Environ. 37 (2003), 4917-4925)

Abstract

This work presents an alternative technique in formulating an analytical form of the joint probability density function (pdf) of velocity for turbulent flows. The technique was rigorously developed by Koehler and Symanowski (1995) [J. Multivariate Anal. 55, 261-282], by which a joint pdf is constructed based on the prescribed or given knowledge of marginal distributions and strictly conserves the original shape of each marginal density. The technique also provides flexibility in estimating parameters required in the pdf to fit a specified correlation. The scope of work is limited to the formulation for two velocity components due to less difficulty in examining their correlation structure. Illustrated and discussed are a number of pdfs, with emphasis on atmospheric turbulence where the vertical velocity is assumed to be positively skew and negatively correlated with the horizontal velocity.

5.1. Introduction

Probability density functions (pdfs) of velocity are fundamental in studying and modeling statistical characteristics of a turbulent flow. They form an essential basis

required for some classes of turbulence modeling, such as Lagrangian stochastic modeling of turbulent diffusion (Thomson, 1987; Wilson and Sawford, 1996). Two general ways to obtain such pdfs are of direct measurement and analytical (or empirical) approximation. Although the former is straightforward and desirable, the latter is of importance in that, from a practical viewpoint, it offers an alternative when the information obtained from direct measurement is not comprehensive or sufficient and, from a modeling viewpoint, it enables mathematics to be handled directly.

For turbulence in the atmospheric boundary layer (ABL), a Gaussian pdf is typically assumed as an approximation when the degree of thermal convection from the ground is slight or insignificant. It has however been acknowledged that the Gaussian character is not precise even in neutral conditions, as emphasized in Anfossi et al. (1997). Deviation from the Gaussianity is quite more evident for convective conditions where the transport asymmetry due to different contributions from the updraft and downdraft causes the pdf of vertical velocity to be positively skew (Luhar et al., 1996, and references therein). There has been an intensive advance in formulating non-Gaussian pdfs of one velocity component. Several pdf forms have been proposed in the literature, including bi-Gaussian (Baerentsen and Berkowicz, 1984; Weil, 1990; Luhar et al., 1996), Chi-type with a skewness parameter (Thomson, 1987), Gram-Charlier series expansion (Anfossi et al., 1997; Maurizi and Tampieri, 1999), and maximum missing information (mmi) (Du et al., 1994). An mmi pdf is generally considered preferable because its entropy (i.e. a measure associated with incomplete or missing information) is maximized, giving the least biased result. For pdfs of more than one velocity component in non-Gaussian turbulence, relatively few studies have been conducted, and most of them are based on an

assumed pdf form and a number of known velocity moments with some additional closures to a set of nonlinear equations associated with the velocity moments. Flesch and Wilson (1992) constructed a joint pdf of two velocity components in studying turbulent diffusion within plant canopies by assuming it as a linear combination of Gaussian pdfs. Monti and Leuzzi (1996) applied a similar technique for three velocity components. Rotach et al. (1996) formulated a joint pdf based on a mixture of two limiting pdfs (Gaussian and bi-Gaussian). The mmi principle can also be extended to the case of more than one velocity, and its applicability may depend on the extent of given information (e.g. how many velocity moments to be used for an mmi pdf) and the complexity of nonlinear equations involved in the formulation.

For this work, the focus is a case when the marginal density function (shortly, marginal density) of each velocity component is given and well characterized and a joint pdf (shortly, pdf) is formulated based on this information. The work is primarily motivated by the fact that the pdf formulation for one velocity component has, to date, been advanced and relatively comprehensive. Adopted here is a technique proposed by Koehler and Symanowski (1995) (to be referred hereafter to as KS). The essence of this technique is that a pdf is deduced from its probability distribution function (i.e. cumulative distribution function or cdf) that assumes a specific functional form and also strictly conserves the original shape of each marginal distribution or density. The technique can also be applied to any specific set of marginal densities and provides flexibility of fitting a desired correlation between a pair of random variables, especially in a bivariate system. Although the technique was developed for a multidimensional framework, the scope of work here is limited to a bivariate case due to less difficulty in

examining the effect of association parameters (next section) on correlation. A concise description of the KS formulation is provided below. Details can be found in the original work. For illustration, an idealized framework is assumed for the ABL, where the distributions of the horizontal and vertical velocities are assumed to be Gaussian and positively-skew bi-Gaussian, respectively, with the presence of negative correlation between them. A number of pdfs are given and discussed.

5.2. KS Formulation

Here, let $X_1, X_2, \ldots, X_p$ denote real-valued univariates (i.e. non-joint scalar-valued random variables) for $p \geq 1$ and ρ_{XY} denote the usual product moment (or Pearson's) correlation coefficient (shortly, correlation) of random variables X and Y. Let $F \equiv F(x_1, x_2, \ldots, x_p)$ be the joint cdf of $X_1, X_2, \ldots, X_p$ and $F_{X_1} \equiv F_{X_1}(x_1)$, $F_{X_2} \equiv F_{X_2}(x_2)$, $\ldots$, $F_{X_p} \equiv F_{X_p}(x_p)$ be their respective marginal distributions. Similarly, $f \equiv f(x_1, x_2, \ldots, x_p)$ is the joint pdf of $X_1, X_2, \ldots, X_p$, and $f_{X_1} \equiv f_{X_1}(x_1)$, $f_{X_2} \equiv f_{X_2}(x_2)$, $\ldots$, $f_{X_p} \equiv f_{X_p}(x_p)$ are their respective marginal densities. According to KS, F takes the form

$$F = \prod_{i=1}^{p} F_{X_i} \times G\,, \tag{5.1}$$

where $G \equiv G(x_1, x_2, \ldots, x_p)$ is a dimensionless function that reflects the level of association (in a sense, correlation or dependence) of random variables. Its expression is

specifically given by $G = \prod_{i<}^{p} \prod_{j}^{p} C_{ij}^{-\alpha_{ij}}$, where $\alpha_{ij} = \alpha_{ji} \geq 0$ is the association parameter (shortly, parameter) for all $i, j = 1, 2, \ldots, p$ and

$$C_{ij} = C_{ji} = F_{X_i}^{1/\alpha_{i+}} + F_{X_j}^{1/\alpha_{j+}} - F_{X_i}^{1/\alpha_{i+}} F_{X_j}^{1/\alpha_{j+}}, \tag{5.2}$$

with $\alpha_{i+} = \alpha_{i1} + \alpha_{i2} + \ldots + \alpha_{ip} > 0$ and $\alpha_{j+} = \alpha_{j1} + \alpha_{j2} + \ldots + \alpha_{jp} > 0$ for all $i, j = 1, 2, \ldots, p$. The form of F in Eq. (5.1) is similar to the famous Farlie-Gumbel-Morgenstern cdf (Johnson, 1987, Section 10.1) though G is defined differently. Moreover, it may be viewed as a generalization of the generalized Burr-Pareto-logistic distributions (Caputo, 1998). It is clear from Eq. (5.2) that C_{ij} is bounded between zero and unity for all i, j because the value of $F_{X_i}^{1/\alpha_{i+}}$ ranges only from zero to unity. It is here assumed that F and f are smooth over the entire domain of these univariates. A familiar relation between F and f can be given by $f = \partial^p F / \partial x_1 \partial x_2 \ldots \partial x_p$. Following Eqs. (5.1) and (5.2), f can be written by

$$f = \prod_{i=1}^{p} \left(f_{X_i} D_i \prod_{j=i+1}^{p} C_{ij}^{-\alpha_{ij}} \right) \times \left[1 + \sum_{i=1}^{p} \sum_{j=i+1}^{p} \left(\alpha_{ij}\, \alpha_{i+}^{-1}\, \alpha_{j+}^{-1}\, D_i^{-1}\, D_j^{-1}\, C_{ij}^{-2}\, F_{X_i}^{1/\alpha_{i+}} F_{X_j}^{1/\alpha_{j+}} \right) \right], \tag{5.3}$$

where

$$D_i = \alpha_{i+}^{-1} \left[\alpha_{ii} + \sum_{k \neq i}^{p} \left(\alpha_{ik}\, F_{X_k}^{1/\alpha_{k+}}\, C_{ik}^{-1} \right) \right]. \tag{5.4}$$

With G defined above, F_{X_i} and f_{X_i} are conserved for all i. As stated by KS, the above formulation always yields positive association between any pair of X_i and X_j for $i \neq j$, which is a corollary deduced from the treatise of Marshall and Olkin (1988). When X_1, X_2, … , X_p are positively associated, nonnegative correlation between any pair of X_i and X_j for $i \neq j$ is implied (i.e. $\rho_{X_i X_j} \geq 0$). For details of the association of a pair of random variables and its properties, see Barlow and Proschan (1975, p. 29-31). Nevertheless, it is noted that negative correlation for a pair of random variables in the KS formulation can also be achieved using the concept of symmetry when one of their marginal densities is symmetrical around zero (see Section 5.3.1) or using the concept of a survival function (see Section 5.3.2). Now, specifically consider a bivariate system (X_1, X_2) (i.e. $p = 2$). Eqs. (5.1), (5.3) and (5.4) can then be written as follows:

$$F = F_{X_1} F_{X_2} C_{12}^{-\alpha_{12}}, \tag{5.5}$$

$$f = f_{X_1} f_{X_2} D_1 D_2 C_{12}^{-\alpha_{12}} \left(1 + \alpha_{12}\, \alpha_{1+}^{-1} \alpha_{2+}^{-1} D_1^{-1} D_2^{-1} C_{12}^{-2} F_{X_1}^{1/\alpha_{1+}} F_{X_2}^{1/\alpha_{2+}}\right), \tag{5.6}$$

$$D_1 = \alpha_{1+}^{-1}\left[\, \alpha_{11} + (\alpha_{12}\, F_{X_2}^{1/\alpha_{2+}} C_{12}^{-1}) \,\right], \quad \text{and} \quad D_2 = \alpha_{2+}^{-1}\left[\, \alpha_{22} + (\alpha_{12}\, F_{X_1}^{1/\alpha_{2+}} C_{12}^{-1}) \,\right]. \tag{5.7}$$

To the authors' knowledge, there have so far been no general relations established for the association (or correlation) structure and the association parameter α_{ij}. Notwithstanding, the essential conditions of two limiting cases for the bivariate marginal distribution of any pair (X_i, X_j), pairwise independence and upper Fréchet bound, were given by KS. That is, for the above bivariate system in Eq. (5.5), X_1 and X_2 become

independent (i.e. $F = F_{X_1} F_{X_2}$) when either 1) $\alpha_{12} \to 0$ and both α_{1+} and α_{2+} are finitely nonzero or 2) both $\alpha_{1+} \to \infty$ and $\alpha_{2+} \to \infty$. Furthermore, F in Eq. (5.5) approaches the upper Fréchet bound as $\alpha_{12} \to 0$ when both $\alpha_{11} / \alpha_{1+} \to 0$ and $\alpha_{22} / \alpha_{2+} \to 0$. The only situation enabling this is that both α_{11} and α_{22} decrease to zero faster than α_{12}. These conditions can be verified through considering Eq. (5.5). Note that the upper Fréchet bound is defined as the minimum of all marginal distributions. For a system of p univariates, the upper Fréchet bound is $\min\left[F_{X_1}, F_{X_2}, ..., F_{X_p} \right]$. According to a classical result by Fréchet (1951), the joint cdf F will not be larger than the upper Fréchet bound, i.e. $F \leq \min\left[F_{X_1}, F_{X_2}, ..., F_{X_p} \right]$ for all (x_1, x_2, … , x_p). In addition, the upper Fréchet bound itself is a cdf that conserves its marginal distributions or densities (Kemp, 1963), and all correlations of the upper Fréchet bound are maximal (Dall'Aglio, 1972; Kotz et al., 2000, 44-47). For more details of the Fréchet bounds (both upper and lower) and their properties, see Dall'Aglio (1972). Some additional properties related to the KS formulation can be found in Caputo (1998).

5.3. Illustrations and Discussion

In the following, a bivariate system (X_1, X_2) ≡ (U, W) is considered, where U and W specifically denote the horizontal and vertical velocity components in the ABL, respectively. The domain of (U, W) is given to be the entire real plane. As said in Section 5.1, U is assumed to be Gaussian while W is bi-Gaussian with positive skewness. Without loss of generality, $\langle U \rangle$ and $\langle W \rangle$ are set to zero, where $\langle\ \rangle$ is the ensemble

average of a random variable. The Gaussian pdf of U and the bi-Gaussian pdf of W are denoted by $f_U \equiv f_U(u)$, and $f_W \equiv f_W(w)$, respectively, and the cdfs of U and W are denoted by $F_U \equiv F_U(u)$ and $F_W \equiv F_W(w)$, respectively. Their expressions are summarized below:

Gaussian:

$$f_U = \frac{1}{\sqrt{2\pi}\ \sigma_U} \exp\left(-\frac{1}{2}\frac{u^2}{\sigma_U^2}\right), \tag{5.8}$$

$$F_U = \frac{1}{2}\ \mathrm{erf}\left(\frac{1}{\sqrt{2}}\frac{u}{\sigma_U}\right)+\frac{1}{2}, \tag{5.9}$$

Bi-Gaussian:

$$f_W = \frac{A}{\sqrt{2\pi}\,\sigma_A}\exp\left[-\frac{(w-m_A)^2}{2\sigma_A^2}\right]+\frac{B}{\sqrt{2\pi}\,\sigma_B}\exp\left[-\frac{(w+m_B)^2}{2\sigma_B^2}\right], \quad \text{and} \tag{5.10}$$

$$F_W = \frac{A}{2}\ \mathrm{erf}\left(\frac{1}{\sqrt{2}}\frac{w}{\sigma_A}-\frac{1}{\sqrt{2}}\frac{m_A}{\sigma_A}\right)+\frac{B}{2}\ \mathrm{erf}\left(\frac{1}{\sqrt{2}}\frac{w}{\sigma_B}+\frac{1}{\sqrt{2}}\frac{m_B}{\sigma_B}\right)+\frac{1}{2}(A+B), \tag{5.11}$$

where, according to the closure scheme proposed by Luhar et al. (1996),

$$m = \frac{2}{3}s_W^{1/3}, \quad r = \frac{(1+m^2)^3\, s_W^2}{(3+m^2)^2\, m^2}, \quad A = \frac{1}{2}\left[1-\left(\frac{r}{4+r}\right)^{1/2}\right], \quad B = 1-A,$$

$$\sigma_A = \sigma_W\left[\frac{B}{A(1+m^2)}\right]^{1/2},\ \sigma_B = \sigma_W\left[\frac{A}{B(1+m^2)}\right]^{1/2},\ m_A = m\sigma_A,\ \text{and}\ m_B = m\sigma_B. \tag{5.12}$$

By definition, σ_U and σ_W are the standard deviations of U and W, respectively (i.e. $\sigma_U = \left\langle U^2 \right\rangle^{1/2}$ and $\sigma_W = \left\langle W^2 \right\rangle^{1/2}$). Let s_U and s_W denote the skewness parameters of U and W, respectively (i.e. $s_U = \left\langle U^3 \right\rangle / \sigma_U^3$ and $s_W = \left\langle W^3 \right\rangle / \sigma_W^3 > 0$). Since $s_U = 0$, s_W will be shortened as just s for convenience. When s approaches zero, the bi-Gaussian form is asymptotically reduced to the Gaussian form. Plots of f_U and f_W are not shown here but can be seen in Luhar et al. (1996).

5.3.1. Investigation

Before proceeding, it is important to first investigate some general characteristics of a pdf based on the KS formulation and the chosen marginal densities. Using the relations described in Section 5.2, the pdf of (U, W) can be formulated in a straightforward manner. Figure 5-1 shows the contour plots of pdfs with four different sets of (α_{11}, α_{12}, α_{22}) with $s = 0.4$. All plots have $\rho_{UW} \geq 0$, except for Figure 5-1d where $\rho_{UW} < 0$. Figure 5-1c presents the case of pairwise independence of U and W by setting $\alpha_{11} \neq 0$, $\alpha_{12} = 0$, and $\alpha_{22} \neq 0$. Notice that the plot in Figure 5-1d is nothing but the mirror image (on zero plane: $u = 0$) of Figure 5-1a, having the same correlation with an opposite sign. Algebraically, the mirror image is obtained by replacing u with $-u$ in the right-hand-side term of Eq. (5.6) (due to the symmetry of f_U). One caution to note is that replacing w with $-w$ also produces negative correlation but does not conserve f_W.

Next, it is also of practical interest to examine some aspects of the effect of association parameters α_{11}, α_{12}, and α_{22} on the correlation structure (specifically speaking, what range of correlation can be found?) for the current bivariate system. To do so, recall the fact that the upper Fréchet bound of a multivariate system itself is a cdf with the maximal correlation. So, it is appropriate to first fix α_{11} and α_{22} at zero and then determine the trend of ρ_{UW} by varying the value of α_{12} alone. The results from doing so are shown by Line 1 in Figure 5-2.

All results given in Figure 5-2 are of negative correlation. The values of ρ_{UW} (and also other velocity statistics) were calculated by numerical integration over the entire real plane of (U, W) using logarithmic transformation (Press et al., 1992, p. 139-140) with extension to two variables. In performing the integration for some sets of (α_{11}, α_{22}), computational difficulty was encountered when α_{12} is small. According to our investigation, this is directly associated to the tail surface of a pdf (whose values are extremely small), causing overflows in evaluating a number of terms required in the KS formulation (e.g. the right-hand-side term in Eq. (5.6)). To avoid this problem, such tails were truncated. To maintain computational accuracy, the numerical values of the first three moments of U and W were checked, and the absolute differences from their specified values were controlled to be 1) < 0.01 for $\langle U \rangle$, $\langle W \rangle$, and $s_U^{1/3}$ and 2) < 1% for $\sigma_U^{1/2}$, $\sigma_W^{1/2}$, and $s^{1/3}$. It is seen from Line 1 that the larger the magnitude of ρ_{UW} is, the smaller α_{12} becomes (i.e. the closer to the upper Fréchet bound F approaches). The magnitude of ρ_{UW} is high (> 0.9) at the upper end of the line. Note that it should not be

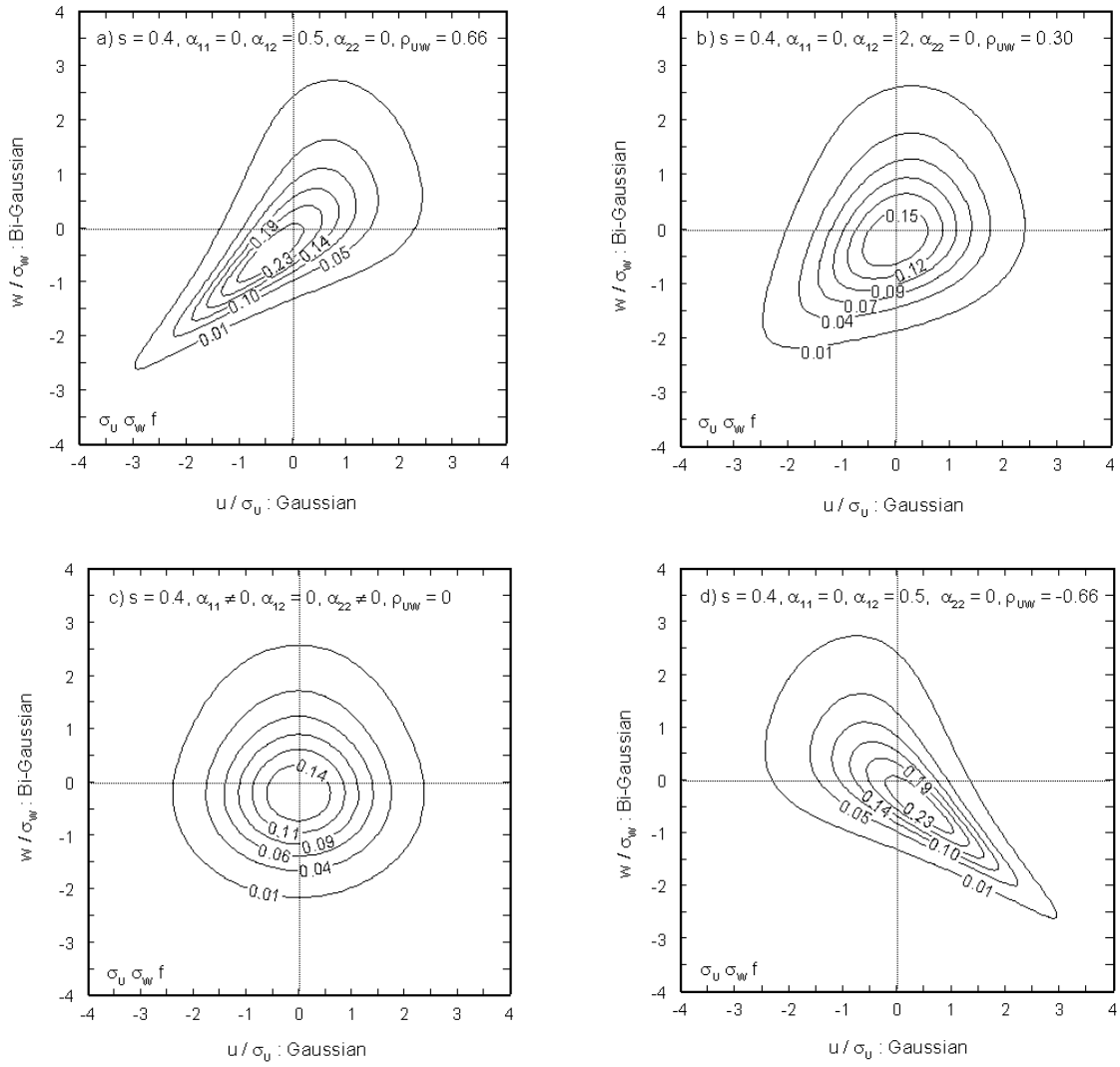

Figure 5-1. Contour plots of the pdfs of (U, W) for $s = 0.4$ and four different sets of (α_{11}, α_{12}, α_{22}) for the chosen bivariate system: a) $\alpha_{11} = 0$, $\alpha_{12} = 0.5$, $\alpha_{22} = 0$, b) $\alpha_{11} = 0$, $\alpha_{12} = 2$, $\alpha_{22} = 0$, c) $\alpha_{11} \neq 0$, $\alpha_{12} = 0$, $\alpha_{22} \neq 0$, and d) $\alpha_{11} = 0$, $\alpha_{12} = 0.5$, $\alpha_{22} = 0$ (with u replaced by $-u$)

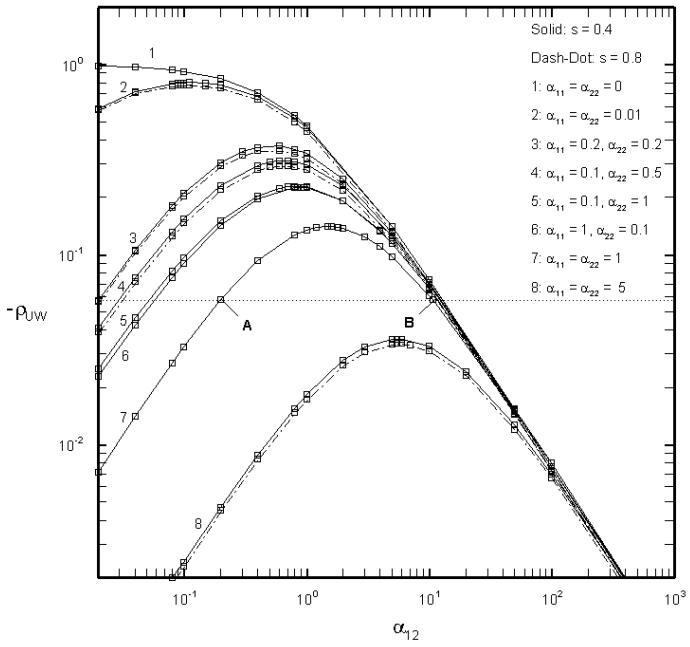

Figure 5-2. Effect of α_{12} on correlation for different sets of (α_{11}, α_{22}) for the chosen bivariate system

anticipated that $\rho_{UW} \to -1$ as $\alpha_{12} \to 0$ since there is no requirement that is the case. For the lower end, the trend decreases to zero, equivalent to the second condition of pairwise independence (see Section 5.2). Lines 2-8 show the results for different nonzero values of α_{11} and α_{22}, where pairwise independence can be approached when $\alpha_{12} \to 0$ or ∞. It is thus expected that there must be at least one maximum in the correlation in between. It is found that there is only one maximum present in each line. The majority of results in Figure 5-2 use $s = 0.4$, with some given for $s = 0.8$ for comparison. However, they share similar trends, with the magnitude of ρ_{UW} slightly lower for $s = 0.8$ as seen in Lines 2, 3-4, and 8. Also notice that many different sets of (α_{11}, α_{12}, α_{22}) can be found to fit a correlation. However, they do not necessarily have the same higher cross product moments. For example, in Line 7 (i.e. $\alpha_{11} = \alpha_{22} = 1$), Pt. A corresponding to $\rho_{UW} \approx -0.058$ with $\alpha_{12} = 0.2$ has $\left\langle UW^2 \right\rangle / \sigma_U \sigma_W^2 \approx 0.005$ and $\left\langle U^2 W \right\rangle / \sigma_U^2 \sigma_W \approx -0.016$ whereas Pt. B corresponding to the same ρ_{UW} with $\alpha_{12} \approx 10.7$ has $\left\langle UW^2 \right\rangle / \sigma_U \sigma_W^2 \approx 0.025$ and $\left\langle U^2 W \right\rangle / \sigma_U^2 \sigma_W \approx -0.039$.

5.3.2. Application to the ABL

To formulate a pdf by the KS formulation for the idealized ABL, all statistics of U and W are given to be independent of time and interpolated as a function of elevation z. Interpolation formulas for convective conditions are used, where key scaling parameters are convective velocity scale w_*, mixing height (or inversion depth) h, and Monin-Obukhov length L (< 0). Several formulas have been proposed in the literature. For the sole purpose of illustration, this work adopts:

$$\frac{\langle U^2 \rangle}{w_*^2} \text{ or } \frac{\sigma_U^2}{w_*^2} = \left(\frac{k}{|h/L|} \right)^{2/3} \left[4.5\left(1-\frac{z}{h}\right)^{3/2} + 0.6|h/L|^{2/3} \right], \qquad (5.13)$$

$$\frac{\langle W^2 \rangle}{w_*^2} \text{ or } \frac{\sigma_W^2}{w_*^2} = 1.8\left(\frac{z}{h}\right)^{2/3}\left(1-0.8\frac{z}{h}\right)^2, \quad \text{and} \qquad (5.14)$$

$$\frac{-\langle UW \rangle}{w_*^2} = \left(\frac{k}{|h/L|} \right)^{2/3} \left(1-\frac{z}{h}\right)^{3/2-q} \text{ with } q = \frac{1}{2}\frac{|h/L|}{(1+|h/L|)}, \qquad (5.15)$$

where k is the von Karman constant (≈ 0.4). In addition, s is assumed to equal 0.8 for simplicity. The above formulas are from Eqs. (12.26), (12.15 or 12.16), and (12.31) in Rodean (1996), respectively. Significant convection is assumed with h/L set to –100.

Two solution sets of (α_{11}, α_{12}, α_{22}) for the velocity pdfs according to the statistics specified above are given in Figure 5-3: one with α_{11} and α_{22} being fixed at 0.2 and the other with α_{11} and α_{22} being fixed at 0.1 and 0.5, respectively. They correspond to Lines 3 and 4 in Figure 5-2, respectively, where there typically exist two different values of α_{12} yielding the same correlation: one on the upward side of a maximum (where ρ_{UW} increases with α_{12}) and the other on the downward side. In Figure 5-3, α_{12} is calculated for z/h = 0.001, 0.01, 0.05, 0.1, 0.2, … , 0.9, 0.99, and 0.999, based on the upward side for the reason that α_{12} will not grow very large when ρ_{UW} is small. Note that all formulas in Eqs. (5.13)-(5.15) meet the inequality $\langle UW \rangle^2 \le \langle U^2 \rangle \langle W^2 \rangle$ for $z/h \le 1$, except for very small z/h. Since ρ_{UW} decreases with height, α_{12} is large near the ABL bottom and

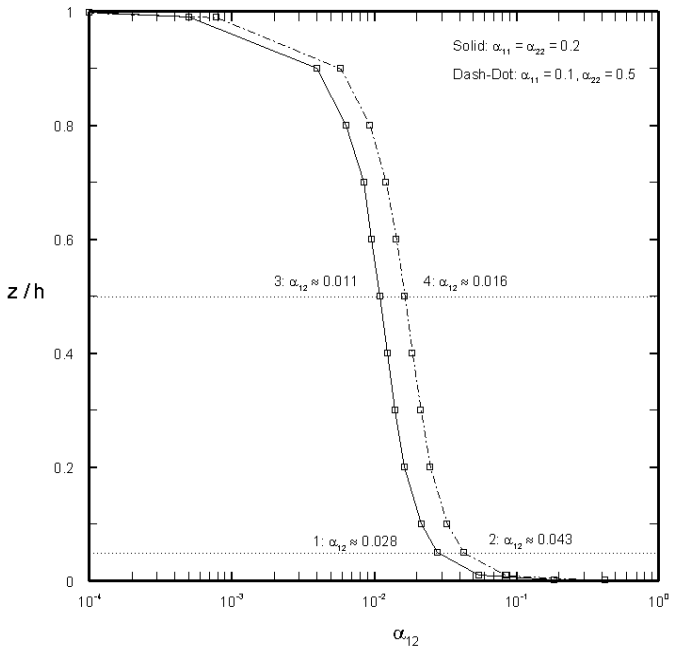

Figure 5-3. Values of α_{12} calculated to fit the correlation based on the interpolation formulas in Eqs. (5.13)-(5.15) with $h / L = -100$

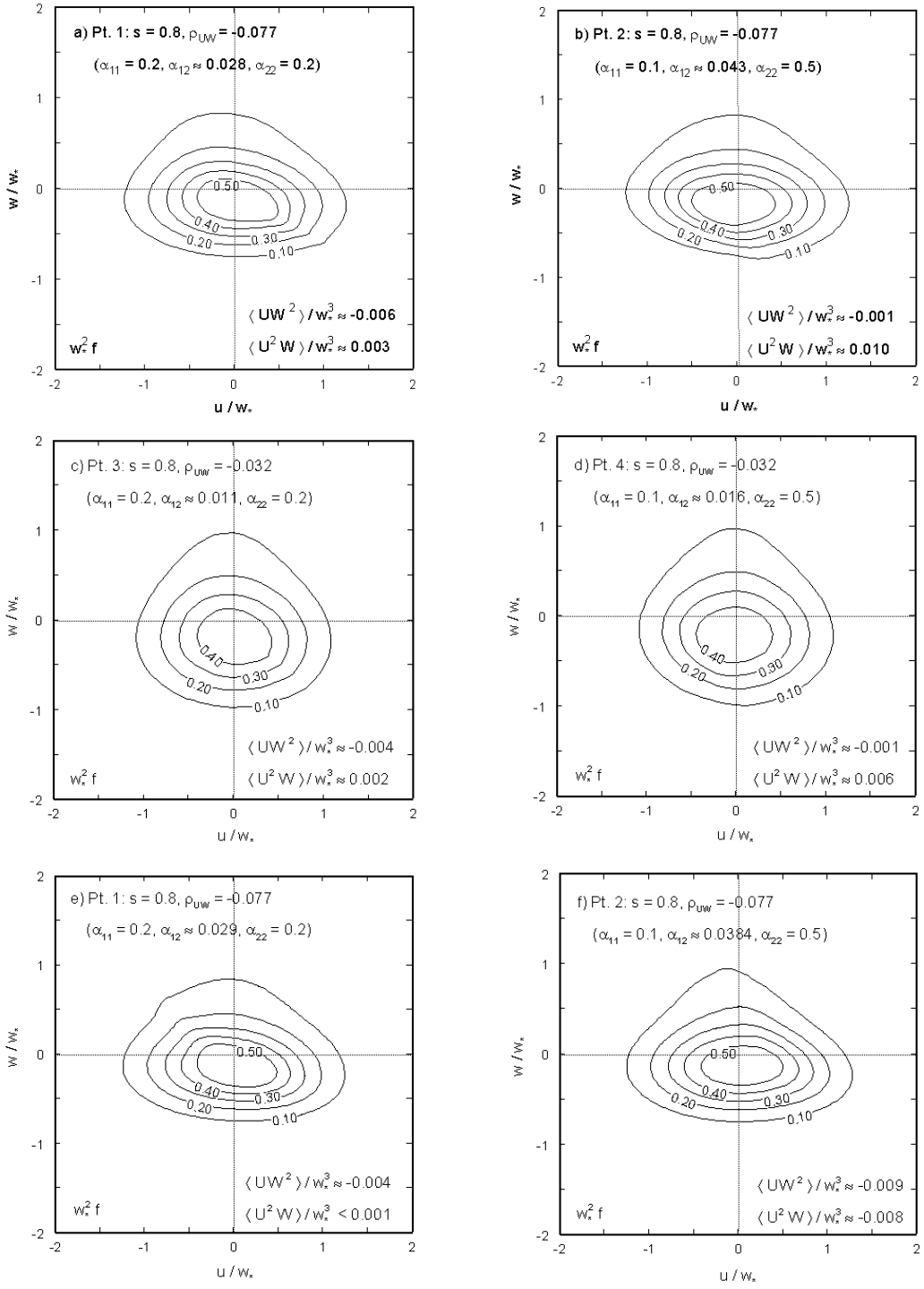

Figure 5-4. Contour plots of the pdfs corresponding to the four chosen points in Figure 5-3

small near the ABL top. Four points (Pts. 1-4) in the figure are chosen for contour plots in Figure 5-4. The first two are at $z/h = 0.05$, and the other two are at $z/h = 0.5$. The scaling parameter used to transform U and W into a non-dimensional form in Figure 5-4 is w_* (not σ_U and σ_W as previously). Comparing Figures 5-4a and 5-4b (corresponding to Pts. 1 and 2, respectively), while similar, the former appears to develop a small sharp diagonal ridge in the fourth quadrant. Another difference is in their higher cross product moments such as $\left\langle UW^2 \right\rangle$ and $\left\langle U^2W \right\rangle$ (see the lower right corner of each contour plot). For Figures 5-4c and 5-4d (corresponding to Pts. 3 and 4, respectively), similar findings are drawn.

So far, negative correlation has been considered through taking advantage of the symmetry of f_U. A more general method suggested by KS can be carried out, which is the concept of a survival function. For a system of p univariates, pairwise negative correlation between X_i and each of the other variables can be achieved (with all marginal densities still conserved) by directly substituting $1-F_{X_i}$ for F_{X_i} in Eqs. (5.1)-(5.3). Customarily, $1-F_{X_i}$ is called the survival function of X_i. The principle behind the method is quite natural. To help clarify this, an arbitrary bivariate system (X, Y) is considered here without loss of generality, where X and Y are univariates. Let R be another univariate with $R = -X$. It then follows that

$$f_R(-r) = f_X(r) \quad \text{and} \quad F_R(-r) = 1 - F_X(r). \tag{5.16}$$

Also, $\rho_{RY} = -\rho_{XY}$. With these, the first step is formulating F_{RY} and f_{RY} using the KS technique as usual, having $\rho_{RY} \geq 0$. The next steps are: replace r with $-r$ in the expressions of F_{RY} and f_{RY}, apply Eq. (16), and rearrange all terms. As a result, $F_{XY} \equiv F(x, y)$ and $f_{XY} \equiv f(x, y)$ with $\rho_{XY} \leq 0$ are finally obtained. Similarly, another solution can be obtained by setting $R = -Y$ and following those steps in a similar manner. However, it should be emphasized that the results from using $1-F_X$ and $1-F_Y$ are not necessarily equivalent. Return to the bivariate system (U, W) where negative correlation has been achieved by replacing u with $-u$. In fact, doing so is exactly equivalent to using $1-F_U$ due to the symmetry of f_U. For pdfs using $1-F_W$, two examples are illustrated in Figures 5-4e and 5-4f, showing the contour plots of the pdfs corresponding to Pts. 1 and 2, respectively (with α_{12} recalculated to fit the desired correlations). By comparison, Figures 5-4a and 5-4e are of the same correlation and also look similar. However, a ridge develops diagonally and appears to be abruptly sharp in the fourth quadrant of the former but in the second quadrant of the latter. Furthermore, their triple product moments are shown to be different. For Figures 5-4b and 5-4f, both are clearly different and do not have a sharp ridge appearing on the surface.

In conclusion, the KS formulation offers an alternative way to analytically formulate a pdf using the knowledge of marginal densities and provides a large class of pdfs that fit a given correlation. It may be used in practice when marginal densities are well characterized or specified and a joint pdf is required to conserve its marginal distributions or densities. Since more than one solution is possible, selecting a better or more practical choice requires consideration of higher product cross moments. Examination should be conducted to check if the desired range of each higher product

cross moment is found for a chosen set of the association parameters in a pdf. However, the information of such moments is often unavailable. An alternative way is considering the entropy of a pdf given its marginal densities and correlation, by which one with higher entropy may be favored over one with lower entropy. Although the inherent nature of the KS formulation is of positive association, the concept of a survival function can be used to obtain negative correlation. As seen, the illustration and discussion were limited to the formulation for two velocity components. Nevertheless, the KS formulation can be extended to three velocity components in a straightforward manner.

Acknowledgements

The authors thank Dr. Paolo Monti, Università degli Studi di Roma "La Sapienza" (Italy) for his suggestions and discussion. The useful comments of anonymous reviewers were appreciated. This work was supported by the U.S. EPA under Contract No. CR827327-01.

References

Anfossi, D., Ferrero, E., Sacchetti, D., Trini Castelli, S. (1997) Comparison among empirical probability density functions of the vertical velocity in the surface layer based on higher order correlations. Boundary-Layer Meteor. 82, 193-218.

Baerentsen J. H., Berkowicz, R. (1984) Monte Carlo simulation of plume dispersion in the convective boundary layer. Atmos. Environ. 18, 701-712.

Barlow, R. E., Proschan, F. (1975) Statistical Theory of Reliability and Life Testing. Holt, Rinehart and Winston, New York.

Caputo, A. (1998) Some properties of the family of Koehler-Symanowski distributions. The Collaborative Research Center (SFB) 386, Discussion Paper No. 103, University of Munich.

Dall'Aglio, G. (1972) Fréchet classes and compatibility of distribution functions. Symp. Math. 9, 131-150.

Du, S., Wilson, J. D., Yee, E. (1994) Probability density functions for velocity in the convective boundary layer and implied trajectory models. Atmos. Environ. 28, 1211-1217.

Flesch, T. K., Wilson, J. D. (1992) A two-dimensional trajectory-simulation model for non-Gaussian, inhomogeneous, turbulence within plant canopies. Boundary-Layer Meteor. 61, 349-374.

Fréchet, M. (1951) Sur les tableaux de corrélation dont les marges sont données. Ann. Univ. Lyon., Sci. 14, 53-77.

Johnson, M. E. (1987) Multivariate Statistical Simulation. Wiley, New York.

Kemp, J. F. (1963) Advanced problem No. 5894. Am. Math. Mon. 80, 73. (Solution by Blyth. C. R., Am. Math. Mon. 80, 413).

Koehler, K. J., Symanowski, J. T. (1995) Constructing multivariate distributions with specific marginal distributions. J. Multivariate Anal., 55, 261-282.

Kotz, S., Balakrishnan, N., Johnson, N. L. (2000) Continuous Multivariate Distributions. Vol. 1: Models and Applications. Wiley, New York.

Luhar, A. K., Hibberd, M. F., Hurley, P. J. (1996) Comparison of closure schemes used to specify the velocity PDF in Lagrangian stochastic dispersion models for convective conditions. Atmos. Environ. 30, 1407-1418.

Marshall, A. W., Olkin, I. (1988) Families of multivariate distributions. J. Amer. Statist. Assoc. 83, 834-841.

Maurizi, A., Tampieri, F (1999) Velocity probability density functions in Lagrangian dispersion models for inhomogeneous turbulence. Atmos. Environ. 33, 281-289.

Monti, P., Leuzzi, G. (1996) A closure to derive a three-dimensional well-mixed trajectory-model for non-Gaussian, inhomogeneous turbulence. Boundary-Layer Meteor. 80, 311-331.

Press, W. H., Teukolsky, S. A., Vetterling, W. T., Flannery, B. P. (1992) Numerical Recipes in FORTRAN. Cambridge University Press, Cambridge.

Rotach, M. W., Gryning, S. E., Tassone, C. (1996) A two-dimensional Lagrangian stochastic dispersion model for daytime conditions. Q. J. R. Meteorol. Soc. 122, 367-389.

Rodean, H. C. (1996) Stochastic Lagrangian Models of Turbulent Diffusion. Monograph No. 48, American Meteorological Society, Boston.

Thomson, D. J. (1987) Criteria for the selection of stochastic models of particle trajectories in turbulent flows. J. Fluid Mech. 180, 529-556.

Weil, J. C. (1990), A diagnosis of the asymmetry in top-down bottom-up diffusion using a Lagrangian stochastic model, J. Atmos. Sci., 47, 501-515.

Wilson, J. D., Sawford, B. L. (1996) Review of Lagrangian stochastic models for trajectories in the turbulent atmosphere. Boundary-Layer Meteor. 78, 191-210.

CHAPTER 6

LOCAL INCREMENTS IN LAGRANGIAN STOCHASTIC MODELS OF TURBULENT DIFFUSION

(Coauthor: A. G. Russell)

Abstract

This work considers a number of mathematical aspects of local increments in a first-order single-fluid Lagrangian stochastic model of turbulent diffusion. The algebra of Ito stochastic integrals and the concept of stochastic expansion are used in analyzing local increments and their statistics in multidimensional turbulence. First, the statistics of the local increment of a function associated with the model and those related to the diffusion coefficient of the model are discussed. It is addressed that the high-order terms in the expansion of the velocity structure function intrinsically exhibit strong anisotropic and velocity-dependent behavior, which may affect the underlying assumption of the isotropic form of the diffusion coefficient of the model. Second, local numerical errors arising from the truncation of higher-order terms in the Euler, Milstein, and order-1.5 strong Taylor schemes are concisely given. The accuracy of numerical solutions by those schemes is examined analytically. Lastly, a number of restriction strategies of time step sizes that have been used in the literature for the Euler scheme and their roles in numerical implementation are investigated in detail.

6.1. Introduction

Lagrangian stochastic modeling is a type of turbulence modeling, which has been considerably advanced from the seminal work of Taylor (1921) and widely used for studying the transport of a scalar in a turbulent flow (Thomson, 1987; Pope, 1994; Wilson and Sawford, 1996). Its formulation assumes the kinematics of a fluid particle moving in the Lagrangian coordinate reference as a stochastic process. Some major advantages of this type of modeling are that it is capable of directly incorporating the nonstationarity and inhomogeneity of turbulence and its numerical implementation is conceptually natural and straightforward. In the class of first-order single-fluid Lagrangian stochastic models (LSMs), the joint process of a particle's displacement and velocity ($\boldsymbol{x}$, $\boldsymbol{u}$) is assumed to evolve continuously with time in a Markov fashion, which is the framework of this study. It is also well known that a large number of increments in the evolution of an LSM involve from one point of time to the next. From a physical viewpoint, turbulence contains a broad range of scales of motion from the smallest (or Kolmogorov) scale to the large scale determined by flow geometry. From a mathematical viewpoint, the model formulation is presented in a differential form (i.e. defined over an infinitesimal time dt). As the model propagates itself over a small time increment Δ, the model is integrated to obtain its new state, which can be expressed as a stochastic expansion series. However, it is impossible to include all expansion terms in consideration, necessarily leading to the truncation of high-order terms. As a consequence, fine structures associated with the truncated terms are lost, giving rise to two additional quantities: local *numerical* increments and local *numerical* errors (see their definitions in Section 6.5). The adjective "local" is used to emphasize that Δ is

being small at any particular points of time. The particle's velocity (i.e. Lagrangian velocity) will be referred to as the velocity for conciseness.

Motivated by the above facts, this work applies the algebra of Ito stochastic integrals and the concept of stochastic expansion to analyzing local increments and their statistics in detail during the propagation of the model over a time increment. The objective of doing so is to gain some additional understanding toward the validity and accuracy of the model during a time increment. For the sake of generality, the analysis is done for multidimensional turbulence. First, the definition of stochastic differential equations (SDEs) of the model in a vector-matrix form is described and followed with some essentials of Ito calculus (mainly, Ito formula, Wagner-Platen formula, and a standard convention for Ito integrals). These not only are useful in stochastically expanding the local increment of a function associated with (or evolving with) the model but also facilitate determining the statistics of a local increment, particularly in the multidimensional framework. Then, the general forms of the first three order statistics of the local increment of a function associated with the model are given. Some statistics related to the diffusion coefficient of the model are discussed in detail. Furthermore, local numerical errors arising from the truncation of higher-order terms in numerical differencing schemes are included. Although there are numerous schemes available for numerical stochastic integration (Kloeden and Platen, 1989), only the Euler, Milstein, and order-1.5 strong Taylor schemes are considered here, with emphasis on the first due to its simplicity and widespread use. To help qualitatively compare and discuss the accuracy of the results predicted by the implementation of those schemes, the classical model for one-dimensional stationary homogeneous turbulence is adopted. Two major advantages

of using this model are that its analytical solutions are available and the model itself is linear enabling the numerical solutions to be directly deduced through some recurrent relations of the local increments of the state variables (i.e. $\boldsymbol{x}$ and $\boldsymbol{u}$). Lastly, a number of restriction strategies of time step sizes for the Euler scheme for one-dimensional turbulence, which have been used in many workers (e.g. Thomson, 1987; Rotach et al., 1996; Schwere et al., 2002), are considered. It is of interest here to examine the roles that those strategies play in numerical simulation within a multidimensional framework.

The analysis does not include the presence of a spatial boundary where a viscous-dominated region exists. Some techniques have been proposed to specially treat such problems. For instance, Dreeben and Pope (1998) use a wall function in the model so that Reynolds stresses in a near-wall region can be characterized. Another approach is to separate the turbulence-dominated (or away-from-wall) region from the viscosity-dominated (or near-wall) region, assuming the error arising from excluding the viscosity-dominated region to be insignificant. With this, only the turbulence-dominated region remains in consideration. For details of this approach, see Wilson and Flesh (1993), Thomson and Montgomery (1994), and references therein.

6.2. Mathematical Descriptions

6.2.1. Notations

Before proceeding, some notations and symbols that will be used in the future are given here. A bold letter usually denotes a nonscalar quantity. A dot (.) represents proper variables in a function or an expression. The letter **R** is the entire set of real

numbers, $\mathbf{C}^k(\mathbf{R}^n, \mathbf{R})$ is the class of k-time differentiable scalar functions: $\mathbf{R}^n \rightarrow \mathbf{R}$, where n is a positive integer, and $\mathbf{L}_2$ is the class of norm-squared (L_2-type) integrable scalar functions. When a function is said to be velocity-dependent, it means that the value of the function at any time depends on the value of $\boldsymbol{u}$ at that time. Likewise, a velocity-independent function is a function whose value at any time does not depend on $\boldsymbol{u}$ at that time. The symbol $O(.)$ denotes a scalar quantity of the order (.). A lower-case Roman subscript (e.g. i, i_1, i_2, j, j_1, j_2, k, etc.) denotes a directional index and takes on the value of 1, 2, … , d (where d is the number of dimensions of turbulence). Similarly, a lower-case Greek subscript (e.g. α, α_1, α_2, β, β_1, β_2, η, etc.) denotes an integer index and takes on the values of 1, 2, … D (where $D = 2d$, as will be seen later). These subscripts are also allowed to be zero when they are members of an integer sequence of an Ito integral variable (see Section 6.3.2). The letter ω represents a trajectory or realization of the model. $N(a,b)$ denotes a normal distribution with mean a and variance b, and $Cov(.)$ denotes the covariance of two random variables. Only Cartesian coordinates are used, and tensor algebra always strictly applies unless indicated otherwise. The n^{th}-order statistic of the component(s) of Eulerian velocity $\boldsymbol{u}_E$ at location $\boldsymbol{x}$ and at time t is denoted by $\left\langle u_{i_1} u_{i_2} \ldots u_{i_n} \right\rangle \equiv \left\langle u_{i_1} u_{i_2} \ldots u_{i_n} \right\rangle (\boldsymbol{x}, t)$, where $\langle\ \rangle$ is the ensemble average. Since the Eulerian velocity equals the Lagrangian velocity at $\boldsymbol{x}$ and at t, $\boldsymbol{u}_E$ is written as just $\boldsymbol{u}$.

6.2.2. Stochastic differential equations

Given a trajectory ω, the joint process $\{(\boldsymbol{x}^t, \boldsymbol{u}^t)\}$ in d-dimensional turbulence is expressed by the following system of SDEs

$$\begin{aligned} \mathrm{d}\boldsymbol{x}^t(\omega) &= \boldsymbol{u}^t(\omega)\,\mathrm{d}t\,, \\ \mathrm{d}\boldsymbol{u}^t(\omega) &= \boldsymbol{a}^t(\omega)\,\mathrm{d}t + \boldsymbol{b}^t(\omega)\,\mathrm{d}\boldsymbol{W}^t(\omega)\,, \end{aligned} \tag{6.1}$$

where $\boldsymbol{a}^t(\omega) \equiv \boldsymbol{a}(\boldsymbol{x}^t(\omega), \boldsymbol{u}^t(\omega), t)$ is the d-dimensional drift coefficient vector related to $\mathrm{d}\boldsymbol{u}^t(\omega)$, $\boldsymbol{b}^t(\omega) \equiv \boldsymbol{b}(\boldsymbol{x}^t(\omega), \boldsymbol{u}^t(\omega), t)$ is the $d \times d$ diffusion coefficient matrix for $\mathrm{d}\boldsymbol{u}^t(\omega)$, and $\boldsymbol{W}^t(\omega)$ is the d-dimensional vector-valued uncorrelated standard Weiner processes. The superscript t is used to specify the time at which a variable (or a function) is evaluated or defined. All differentials and variables above are defined at time $t \in [t_o, T]$, where t_o and T are the initial time and the integration time, respectively. To convert the above system into a vector-matrix form in a formal manner, let $\{\boldsymbol{Y}^t\} \equiv \{(\boldsymbol{x}^t, \boldsymbol{u}^t)\}$ and the triplet ($\boldsymbol{\Omega}$, $\boldsymbol{\mathfrak{I}}$, $\mathbf{P}$) be its corresponding probability space, where $\boldsymbol{\Omega}$, $\boldsymbol{\mathfrak{I}}$, and $\mathbf{P}$ are the sample space of all possible trajectories (i.e. $\forall\, \omega \in \boldsymbol{\Omega}$), the σ-algebra on $\boldsymbol{\Omega}$, and the probability measure for $\boldsymbol{\mathfrak{I}}$, respectively. Then, Eq. (6.1) can be rewritten by

$$\mathrm{d}\boldsymbol{Y}^t(\omega) = \boldsymbol{Q}^t(\omega)\,\mathrm{d}t + \boldsymbol{S}^t(\omega)\,\mathrm{d}\boldsymbol{W}^t(\omega)\,, \tag{6.2}$$

where $\boldsymbol{Y}^t(\omega)$ is the D-dimensional solution vector, $\boldsymbol{Q}^t(\omega) \equiv \boldsymbol{Q}(\boldsymbol{Y}^t(\omega), t)$ is the D-dimensional drift coefficient vector, $\boldsymbol{S}^t(\omega) \equiv \boldsymbol{S}(\boldsymbol{Y}^t(\omega), t)$ is the $D \times D$ symmetric diffusion coefficient matrix, and $\boldsymbol{W}^t(\omega)$ is now D-dimensional. Comparison of Eq. (6.1) and Eq. (6.2) gives

$$\boldsymbol{Y}^t(\omega)=\begin{bmatrix}\boldsymbol{x}^t(\omega)\\ \boldsymbol{u}^t(\omega)\end{bmatrix},\quad \boldsymbol{Q}^t(\omega)=\begin{bmatrix}\boldsymbol{u}^t(\omega)\\ \boldsymbol{a}^t(\omega)\end{bmatrix},\quad \text{and}\quad \boldsymbol{S}^t(\omega)=\begin{bmatrix}0 & 0\\ 0 & \boldsymbol{b}^t(\omega)\end{bmatrix}, \tag{6.3}$$

So, it follows that $D = 2d$. It is seen that only the second half of the noise components in $\boldsymbol{W}^t(\omega)$ in Eq. (6.2) plays a role in the evolution while the first half is trivial (i.e. dummy) due to zero-valued components in $\boldsymbol{S}^t(\omega)$. Given the initial condition $\boldsymbol{Y}^o(\omega)\equiv\boldsymbol{Y}^{t_o}(\omega)$, the integration of Eq. (6.2) from t_o to t is

$$\boldsymbol{Y}^t(\omega)-\boldsymbol{Y}^o(\omega)=\int_{t_o}^{t}\boldsymbol{Q}(\boldsymbol{Y}^{t'}(\omega),t')\,\mathrm{d}t'+\int_{t_o}^{t}\boldsymbol{S}(\boldsymbol{Y}^{t''}(\omega),t'')\,\mathrm{d}\boldsymbol{W}^{t''}(\omega), \tag{6.4}$$

for $t_o \le t' \le t \le T$. The last term on the right-hand side (RHS) above is an Ito stochastic integral (i.e. its integrand being nonanticipative). It is important to note that the SDE in Eq. (6.2) needs to satisfy the Lipschitz and growth restriction conditions so that the pathwise uniqueness and existence of a solution trajectory $\boldsymbol{Y}^t(\omega)$ are ensured (Gardiner, 1997, p. 94; Øksendal, 2000, p. 66-70), as assumed here. Then, it can be said that $\boldsymbol{Y}^t(\omega)$, $\boldsymbol{Q}^t(\omega)$, and $\boldsymbol{S}^t(\omega)$ belong to $\mathbf{L}_2(T)$ for all $t \in [t_o, T]$. For conciseness, given a fixed trajectory ω, the notations $\boldsymbol{x}^t(\omega)$, $\boldsymbol{u}^t(\omega)$, $\boldsymbol{Y}^t(\omega)$, $\boldsymbol{Q}^t(\omega)$, $\boldsymbol{S}^t(\omega)$, and $\boldsymbol{W}^t(\omega)$ will be shortened as $\boldsymbol{x}^t$, $\boldsymbol{u}^t$, $\boldsymbol{Y}^t$, $\boldsymbol{Q}^t$, $\boldsymbol{S}^t$, and $\boldsymbol{W}^t$, respectively.

It has been acknowledged that the model is not rigorously justified because the particle's acceleration is still correlated over the order of the Kolmogorov time scale τ_η (Monin and Yaglom, 1975, p. 370, Wilson and Sawford, 1996). When the model

propagates itself over $\Delta \sim \tau_\eta$ (or smaller), the Markovian assumption is violated. However, the Fourier analysis by Wilson and Zhuang (1989) for stationary isotropic turbulence suggests that an unlimited decrease in a time step does not produce any significant effect in dispersion because, first, the low frequency end of the velocity spectrum is most effective in dispersion and, second, there is small variation in the low frequency end of spectrum as the constant time increment takes on different values. Unfortunately, difficulties and complexities arise and appear hard to resolve in the case of nonstationary inhomogeneous turbulence (Pasquill and Smith, 1983, p. 29). To make the analysis possible, it is necessary to assume that the velocity fluctuations attributed to the nonstationarity and inhomogeniety contribute to the energy spectrum mostly in low frequencies such that an unlimited decrease in a time step size does not deteriorate the results.

One consistency condition of the model in question is the inertial subrange theory (Kolmogorov, 1941), which allows the form of $\boldsymbol{b}$ in Eq. (6.1) to be determined based on the velocity structure function for a time increment within the inertial subrange (i.e. for $\tau_\eta << \Delta << \tau$, where τ is the local time scale of large motions or eddies). Also, τ is sometimes called the local decorrelation time scale of the velocity. In this range, turbulence is locally isotropic, and turbulence statistics have a universal form as a function of the mean dissipation rate of turbulent kinetic energy ($\overline{\varepsilon}$) and independent of viscosity. Through some mathematical relationship, the form of $\boldsymbol{b}$ can be found. For $\boldsymbol{a}$ in Eq. (6.1), it is a function of velocity, local pressure gradient, velocity moments and their gradients, mean dissipation rate, etc. Two conventional approaches used in determining the form of $\boldsymbol{a}$ are: direct closures (Pope, 1994) and the well-mixed condition (Thomson,

1987). The former applies a certain level of modeling some turbulence statistics to give a closed form of $\boldsymbol{a}$. The latter imposes a mathematical constraint that the distribution of particles initially well mixed (with respect to both position and velocity) will always remain so, by which $\boldsymbol{a}$ can be solved through the Fokker-Planck equation corresponding to the model.

6.3. Ito and Wagner-Platen Formulas

6.3.1. Ito Formula

Let an arbitrary $\mathfrak{I}$-measurable scalar function $f \equiv f(\boldsymbol{Y}^t, t)$ associated with the model in question belong to the classes $\mathbf{L}_2(T)$ and $\mathbf{C}^{k\geq 2}(\mathbf{D}_f \times [t_o, T], \mathbf{R})$, where $\mathbf{D}_f \subset \mathbf{R}^D$ is the smooth domain of f. The Ito formula expresses the differential form of f by (Gardiner, 1997, p. 95-96; Øksendal, 2000, p. 48-49)

$$\mathrm{d}f(\boldsymbol{Y}^t, t) = L\, f(\boldsymbol{Y}^t, t)\,\mathrm{d}t + L_\beta f(\boldsymbol{Y}^t, t)\,\mathrm{d}W_\beta^t\,, \tag{6.5}$$

where L and L_β are the linear differential operators defined by

$$\begin{aligned} L &= \frac{\partial}{\partial t} + Q_\alpha \frac{\partial}{\partial Y_\alpha} + \left(\frac{1}{2} S_{\alpha,\eta} S_{\beta,\eta}\right) \frac{\partial^2}{\partial Y_\alpha Y_\beta}, \quad \text{and} \\ L_\beta &= S_{\alpha,\beta} \frac{\partial}{\partial Y_\alpha}\,. \end{aligned} \tag{6.6}$$

From Eq. (6.5), it is seen that any function f associated with the model also evolves stochastically with time.

6.3.2. Wagner-Platen Formula

The Wagner-Platen (or Ito-Taylor) formula (Wagner and Platen, 1978; Platen and Wagner, 1982) expresses the increment of a function associated with an SDE by integral terms. For example, the integration of Eq. (6.5) over $[t, t + \Delta] \subset [t_o, T]$ gives

$$\begin{aligned}\Delta f(\boldsymbol{Y}^t, t) &\equiv f(\boldsymbol{Y}^{t+\Delta}, t+\Delta) - f(\boldsymbol{Y}^t, t) \\ &= \int_t^{t+\Delta} L\, f(\boldsymbol{Y}^{t'}, t')\,\mathrm{d}t' + \int_t^{t+\Delta} L_\beta\, f(\boldsymbol{Y}^{t'}, t')\,\mathrm{d}W_\beta^{t'} \\ &= L\, f(\boldsymbol{Y}^t, t) \int_t^{t+\Delta} \mathrm{d}t' + L_\beta\, f(\boldsymbol{Y}^t, t) \int_t^{t+\Delta} \mathrm{d}W_\beta^{t'} + R_{f,1}\,,\end{aligned} \tag{6.7}$$

where $R_{f,n}$ is the remainder term after expansion up to n^{th}-tuple integrals for n being a positive integer (for Eq. (6.7), $n = 1$). Because each integral on the last line of Eq. (6.7) is of Ito type, the term in front of it is then called an Ito coefficient. If f belongs to $\mathbf{C}^{k\geq 4}(\mathbf{D}_f \times [t_o, T], \mathbf{R})$, it is straightforward to write $R_{f,1}$ as follows:

$$\begin{aligned}R_{f,1} = &\int_t^{t+\Delta}\int_t^{t'} L\,L\, f(\boldsymbol{Y}^{t''}, t'')\,\mathrm{d}t''\,\mathrm{d}t' + \int_t^{t+\Delta}\int_t^{t'} L\,L_\beta\, f(\boldsymbol{Y}^{t''}, t'')\,\mathrm{d}t''\,\mathrm{d}W_\beta^{t'} \\ &+ \int_t^{t+\Delta}\int_t^{t'} L_\beta L\, f(\boldsymbol{Y}^{t''}, t'')\,\mathrm{d}W_\beta^{t''}\mathrm{d}t' + \int_t^{t+\Delta}\int_t^{t'} L_{\beta_1} L_{\beta_2}\, f(\boldsymbol{Y}^{t''}, t'')\,\mathrm{d}W_{\beta_1}^{t''}\mathrm{d}W_{\beta_2}^{t'}\,.\end{aligned} \tag{6.8}$$

Note that the results in Eqs. (6.7) and (6.8) are obtained using

$$
\begin{aligned}
\int_t^{t'} \mathrm{d}\, Lf(\boldsymbol{Y}^{t''}, t'') &= L\, f(\boldsymbol{Y}^{t'}, t') - L\, f(\boldsymbol{Y}^{t}, t) \\
&= \int_t^{t'} L\, L\, f(\boldsymbol{Y}^{t''}, t'')\, \mathrm{d}t'' + \int_t^{t'} L\, L_\beta\, f(\boldsymbol{Y}^{t''}, t'')\, \mathrm{d}W_\beta^{t''}, \quad \text{and} \\
\int_t^{t'} \mathrm{d}\, L_\beta f(\boldsymbol{Y}^{t''}, t'') &= L_\beta f(\boldsymbol{Y}^{t'}, t') - L_\beta f(\boldsymbol{Y}^{t}, t) \\
&= \int_t^{t'} L\, L_\beta\, f(\boldsymbol{Y}^{t''}, t'')\, \mathrm{d}t'' + \int_t^{t'} L_{\beta_1}\, L_\beta\, f(\boldsymbol{Y}^{t''}, t'')\, \mathrm{d}W_{\beta_1}^{t''}.
\end{aligned}
\tag{6.9}
$$

It is also possible to continue expanding Δf by applying the same procedures to each integrand in Eq. (6.8) as long as the higher-order derivatives of f exist. For example, for $f \in \mathbf{C}^{k \geq 6}(\mathbf{D}_f \times [t_o, T], \mathbf{R})$,

$$
\begin{aligned}
\Delta f(\boldsymbol{Y}^t, t) = {} & L\, f(\boldsymbol{Y}^t, t) \int_t^{t+\Delta} \mathrm{d}t' + L_\beta f(\boldsymbol{Y}^t, t) \int_t^{t+\Delta} \mathrm{d}W_\beta^{t'} \\
& + L\, L\, f(\boldsymbol{Y}^t, t) \int_t^{t+\Delta} \int_t^{t'} \mathrm{d}t''\, \mathrm{d}t' + L\, L_\beta\, f(\boldsymbol{Y}^t, t) \int_t^{t+\Delta} \int_t^{t'} \mathrm{d}t''\, \mathrm{d}W_\beta^{t'} \\
& + L_\beta L\, f(\boldsymbol{Y}^t, t) \int_t^{t+\Delta} \int_t^{t'} \mathrm{d}W_\beta^{t''}\, \mathrm{d}t' + L_{\beta_1} L_{\beta_2}\, f(\boldsymbol{Y}^t, t) \int_t^{t+\Delta} \int_t^{t'} \mathrm{d}W_{\beta_1}^{t''}\, \mathrm{d}W_{\beta_2}^{t'} + R_{f,2},
\end{aligned}
\tag{6.10}
$$

where

$$
\begin{aligned}
R_{f,2} = & \int_t^{t+\Delta}\int_t^{t'}\int_t^{t''} L\,L\,L\,f(\boldsymbol{Y}^{t'''},t''')\,\mathrm{d}t'''\,\mathrm{d}t''\,\mathrm{d}t' \\
& + \int_t^{t+\Delta}\int_t^{t'}\int_t^{t''} L\,L\,L_\beta\,f(\boldsymbol{Y}^{t'''},t''')\,\mathrm{d}t'''\,\mathrm{d}t''\,\mathrm{d}W_\beta^{t'} \\
& + \int_t^{t+\Delta}\int_t^{t'}\int_t^{t''} L\,L_\beta\,L\,f(\boldsymbol{Y}^{t'''},t''')\,\mathrm{d}t'''\,\mathrm{d}W_\beta^{t''}\,\mathrm{d}t' \\
& + \int_t^{t+\Delta}\int_t^{t'}\int_t^{t''} L_\beta\,L\,L\,f(\boldsymbol{Y}^{t'''},t''')\,\mathrm{d}W_\beta^{t'''}\,\mathrm{d}t''\,\mathrm{d}t' \\
& + \int_t^{t+\Delta}\int_t^{t'}\int_t^{t''} L\,L_{\beta_1}L_{\beta_2}\,f(\boldsymbol{Y}^{t'''},t''')\,\mathrm{d}t'''\,\mathrm{d}W_{\beta_1}^{t''}\mathrm{d}W_{\beta_2}^{t'} + \ldots \\
& + \int_t^{t+\Delta}\int_t^{t'}\int_t^{t''} L_{\beta_1}\,L_{\beta_2}L_{\beta_3}\,f(\boldsymbol{Y}^{t'''},t''')\,\mathrm{d}W_{\beta_1}^{t'''}\,\mathrm{d}W_{\beta_2}^{t''}\mathrm{d}W_{\beta_3}^{t'}\,.
\end{aligned}
\tag{6.11}
$$

The first three integral terms on the RHS of Eq. (6.10) can be evaluated readily. The next two turn more difficult, and the last term becomes extremely difficult. The evaluation and expressions of these integrals are given and concisely discussed in the Appendix. A standard convention is adopted for Ito integrals (Wagner and Platen, 1978; Platen and Wagner, 1982; Kloeden and Platen, 1991; Li and Liu, 1997) to ease the algebraic manipulation. That is, the variable $I_{\tilde{\mu}}$ is used to denote such integrals according to the following definition:

Definition: Let $\tilde{\mu}$ be an integer sequence $\mu_1, \mu_2, \ldots, \mu_g \in \{0, 1, 2, 3, \ldots\}$ and $g \geq 0$. The definition of $I_{\tilde{\mu}}$ is given by

$$
I_{\tilde{\mu}} = \int_t^{t+\Delta} \ldots \int_t^{t_3}\int_t^{t_2} \mathrm{d}W_{\mu_1}^{t_1}\,\mathrm{d}W_{\mu_2}^{t_2} \ldots \mathrm{d}W_{\mu_g}^{t_g}\,, \tag{6.12}
$$

where $I_{\tilde{\mu}}$ is evaluated at t, and $W_0^t \equiv t$. In case of $\tilde{\alpha}$ being null (i.e. $g = 0$), $I_{\tilde{\mu}} = I$ is given equal to unity (i.e. $I = 1$). As said previously, each parenthesized subscript of a variable denotes the time at which that variable is defined. Some examples of using Eq. (6.12) are given below:

$$
\begin{aligned}
&I_0 = \int_t^{t+\Delta} \mathrm{d}t', \quad I_1 = \int_t^{t+\Delta} \mathrm{d}W_1^{t'}, \\
&I_{0,0} = \int_t^{t+\Delta} \int_t^{t'} \mathrm{d}t'' \, \mathrm{d}t', \quad I_{0,1} = \int_t^{t+\Delta} \int_t^{t'} \mathrm{d}t'' \, \mathrm{d}W_1^{t'}, \\
&I_{1,3,0} = \int_t^{t+\Delta} \int_t^{t'} \int_t^{t''} \mathrm{d}W_1^{t'''} \, \mathrm{d}W_3^{t''} \, \mathrm{d}t', \quad \text{and} \quad I_{1,4,2} = \int_t^{t+\Delta} \int_t^{t'} \int_t^{t''} \mathrm{d}W_3^{t'''} \, \mathrm{d}W_4^{t''} \, \mathrm{d}W_2^{t'}.
\end{aligned}
\tag{6.13}
$$

When a multiplication product of two Ito integrals is desired, the formula in Eq. (6A.3) (see Appendix) is helpful and can be used for its calculation. Following the above definition, the RHS terms of Eqs. (6.10) and (6.11) can be rewritten by

$$
\begin{aligned}
\Delta f = {} & L f \cdot I_0 + L_j f \cdot I_j \\
& + L L f \cdot I_{0,0} + L L_j f \cdot I_{0,j} \\
& + L_j L f \cdot I_{j,0} + L_{j_1} L_{j_2} f \cdot I_{j_1,j_2} + R_{f,2}, \quad \text{and}
\end{aligned}
\tag{6.14}
$$

$$
\begin{aligned}
R_{f,2} = {} & L L L f \cdot I_{0,0,0} + L L L_j f \cdot I_{0,0,j} + L L_j L f \cdot I_{0,j,0} \\
& + L L_{j_1} L_{j_2} f \cdot I_{0,j_1,j_2} + L_j L L f \cdot I_{j,0,0} + L_{j_1} L L_{j_2} f \cdot I_{j_1,0,j_2} \\
& + L_{j_1} L_{j_2} L f \cdot I_{j_1,j_2,0} + L_{j_1} L_{j_2} L_{j_3} f \cdot I_{j_1,j_2,j_3} + R_{f,3},
\end{aligned}
\tag{6.15}
$$

respectively. For a special case of $f \in \mathbf{C}^{\infty}(\mathbf{D}_f \times [t_o, T], \mathbf{R})$, it can also be shown that

$$\Delta f(\boldsymbol{Y}^t, t) = \sum_{n=1}^{\infty} \frac{1}{n!} \left[\Delta \cdot \frac{\partial}{\partial t} + \Delta Y_\alpha \cdot \frac{\partial}{\partial Y_\alpha} + \Delta \cdot \left(\frac{1}{2} S_{\alpha,\eta} S_{\beta,\eta} \right) \frac{\partial^2}{\partial Y_\alpha \partial Y_\beta} \right]^n f, \qquad (6.16)$$

where $n!$ is the n-factorial, the bracketed term $[\,]^n$ is expanded in a binomial manner, and the resulting expansion operating on f is evaluated at $(\boldsymbol{Y}^t, t)$. Notice that the relation in Eq. (6.16) is similar to a traditional Taylor series except for the appearance of the last term in the brackets $[\,]^n$. The RHS of Eq. (6.16) is directly obtained from rearranging Eq. (6.3) and then integrating both sides over Δ (6.i.e. from t to $t + \Delta$). The importance of the above formula is that the expansion of Δf can be expressed in terms of both Δ and $\Delta \boldsymbol{Y}^t$, which helps indicate the leading order of the local numerical error of Δf once the local numerical error of $\Delta \boldsymbol{Y}^t$ is known.

Since the statistical behavior of local increments is central to this study, it is appropriate to briefly address another mathematical notation representing a conditional expectation before proceeding. As a convention, the expectation of a function $f \equiv f(\boldsymbol{Y}^t, t)$ associated with the process $\{\boldsymbol{Y}^t\}$ at the future time $t + \Delta$ given $\Im^t$ is written as $\left\langle f(\boldsymbol{Y}^{t+\Delta}, t + \Delta) \,|\, \Im^t \right\rangle$, where $\Im^t$ represents the history of the evolution of the process from beginning until the present time (i.e. from t_o to t). (Customarily, $\Im^t$ is a member of the increasing family of sub σ-algebras of $\mathfrak{I}$ in the triplet up to time t, and $\{\Im^t\}$ is called the filtration to which the process is adapted.) Because the process in question is Markovian,

only the knowledge of the process at the present time matters. Then, it immediately follows that (Øksendal, 2000, p. 31-33)

$$
\begin{aligned}
&\text{(a)}\ \left\langle f(\boldsymbol{Y}^{t+\Delta}, t+\Delta) \,|\, \Im^t \right\rangle = \left\langle f(\boldsymbol{Y}^{t+\Delta}, t+\Delta) \,|\, \boldsymbol{Y}^t \right\rangle, \\
&\text{(b)}\ \left\langle f(\boldsymbol{Y}^{t}, t) \,|\, \Im^o \right\rangle = \left\langle f(\boldsymbol{Y}^{t}, t) \,|\, \boldsymbol{Y}^o \right\rangle, \\
&\text{(c)}\ \left\langle \Delta f \,|\, \Im^t \right\rangle = \left\langle f(\boldsymbol{Y}^{t+\Delta}, t+\Delta) \,|\, \boldsymbol{Y}^t \right\rangle - f(\boldsymbol{Y}^t, t), \quad \text{and} \\
&\text{(d)}\ \left\langle \Delta f \,|\, \Im^o \right\rangle = \left\langle f(\boldsymbol{Y}^{t+\Delta}, t+\Delta) \,|\, \boldsymbol{Y}^o \right\rangle - f(\boldsymbol{Y}^o, t_o).
\end{aligned}
\tag{6.17}
$$

where $\Im^o \equiv \Im^{t_o}$. As seen in Eq. (6.17), the notation $\Im^t$ makes convenient conditioning the process in question to be defined at present time *t*, and then it will be used for the rest of the work.

6.4. Statistics of Local Increments

In the following, the subscript *t* will be dropped off from variables or functions defined or evaluated at time *t* for convenience (e.g. $\boldsymbol{Y}^t, \boldsymbol{x}^t, \boldsymbol{u}^t \rightarrow \boldsymbol{Y}, \boldsymbol{x}, \boldsymbol{u}$). As stated in Section 6.2, the inertial subrange theory is required as a consistency condition of the model. According to the theory, for $\tau_\eta << \Delta << \tau$, the diffusion coefficient of the model (or $\boldsymbol{b}$) can take a universal form that is independent of $\boldsymbol{u}$ but depends only on $\bar{\varepsilon}$ and Δ only. It is thus appropriate to write $\boldsymbol{b} \equiv \boldsymbol{b}(\boldsymbol{x}, t)$ instead. Here, it is of interest to examine the general form of the statistics (up to third order) of the local increment of a function associated with the model in question (which will be helpful for future analysis) and to discuss those related to $\boldsymbol{b}$ in detail. Before proceeding, it is useful for future work to

explicitly write here the expansion forms of the local increments of some basic functions (here, Δx_i and Δu_i). To do so, using the Wagner-Platen formula in Eq. (6.14) for $f \equiv x_i$ gives

$$\begin{aligned}\Delta x_i = {} & u_i\, I_0 + a_i\, I_{0,0} + b_{i,j}\, I_{j,0} \\ & + \left(\frac{\partial a_i}{\partial t} + a_k \frac{\partial a_i}{\partial u_k} + u_k \frac{\partial a_i}{\partial x_k} + \frac{1}{2} b_{k,m} b_{l,m} \frac{\partial^2 a_i}{\partial u_k \partial u_l} \right) I_{0,0,0} \\ & + \left(\frac{\partial b_{i,j}}{\partial t} + a_k \frac{\partial b_{i,j}}{\partial u_k} + u_k \frac{\partial b_{i,j}}{\partial x_k} \right) I_{0,j,0} + b_{k,j} \frac{\partial a_i}{\partial u_k} I_{j,0,0} + R_{x_i,2} \,.\end{aligned} \tag{6.18}$$

where

$$\begin{aligned}R_{x_i,2} = {} & \left(\frac{\partial a_i}{\partial t} + a_k \frac{\partial a_i}{\partial u_k} + u_k \frac{\partial a_i}{\partial x_k} + \frac{1}{2} b_{k,m} b_{l,m} \frac{\partial^2 a_i}{\partial u_k \partial u_l} \right) I_{0,0,0} \\ & + \left(\frac{\partial a_i}{\partial t} + a_k \frac{\partial a_i}{\partial u_k} + u_k \frac{\partial a_i}{\partial x_k} + \frac{1}{2} b_{k,m} b_{l,m} \frac{\partial^2 a_i}{\partial u_k \partial u_l} \right) I_{0,0,0} \\ & + \left(\frac{\partial b_{i,j}}{\partial t} + a_k \frac{\partial b_{i,j}}{\partial u_k} + u_k \frac{\partial b_{i,j}}{\partial x_k} \right) I_{0,j,0} + b_{k,j} \frac{\partial a_i}{\partial u_k} I_{j,0,0} + R_{x_i,3} \,.\end{aligned} \tag{6.19}$$

The Ito coefficients $L L_j x_i$, $L_{j_1} L_{j_2} x_i$, $L L L_j x_i$, $L L_{j_1} L_{j_2} x_i$, $L_{j_1} L L_{j_2} x_i$, and $L_{j_1} L_{j_2} L_{j_3} x_i$ are zero and thus do not appear in Eqs. (6.18) and (6.19). Likewise, for Δu_i,

$$\begin{aligned}\Delta u_i = {} & a_i \cdot I_0 + b_{i,j} \cdot I_j + \\ & + \left(\frac{\partial a_i}{\partial t} + a_k \frac{\partial a_i}{\partial u_k} + u_k \frac{\partial a_i}{\partial x_k} + \frac{1}{2} b_{k,m} b_{l,m} \frac{\partial^2 a_i}{\partial u_k \partial u_l} \right) \cdot I_{0,0} \\ & + \left(\frac{\partial b_{i,j}}{\partial t} + u_k \frac{\partial b_{i,j}}{\partial x_k} \right) \cdot I_{0,j} + b_{k,j} \frac{\partial a_i}{\partial u_k} \cdot I_{j,0} + R_{u_i,2} \, .\end{aligned} \tag{6.20}$$

Note that the term $L_{j_1} L_{j_2} u_i$ does not appear in Eq. (6.20) due to its zero value. For the full expression of $R_{u_i,2}$, it cannot be given here due to its lengthiness. In addition to Δx_i and Δu_i, consider the local increment of a velocity-independent function $\psi \equiv \psi(\boldsymbol{x}, t)$. Given $\psi \in \mathbf{C}^k(\mathbf{D}_\psi \times [t_o, T], \mathbf{R})$ (where $\mathbf{D}_\psi \subset \mathbf{R}^d$ represents the corresponding smooth domain, and k is large), its local increment can be expressed by

$$\begin{aligned}\Delta\psi(\boldsymbol{x},t) = {} & \left(\frac{\partial \psi}{\partial t} + u_k \frac{\partial \psi}{\partial x_k} \right) I_0 \\ & + \left(\frac{\partial^2 \psi}{\partial t^2} + 2 u_k \frac{\partial^2 \psi}{\partial t \, \partial x_k} + a_k \frac{\partial \psi}{\partial x_k} + u_k u_l \frac{\partial^2 \psi}{\partial x_k \partial x_l} \right) I_{0,0} + b_{k,j} \frac{\partial \psi}{\partial x_k} I_{j,0} + R_{\psi,2} \, .\end{aligned} \tag{6.21}$$

Note that $L L_j \psi$ and $L_{j_1} L_{j_2} \psi$ are zero.

6.4.1. General forms of the statistics of the local increments of a function

For simplicity, any scalar function associated with the model can be categorized into two categories: velocity-dependent and -independent, which are denoted by $\phi^{(.)} \equiv \phi^{(.)}(\boldsymbol{x}, \boldsymbol{u}, t)$ and $\psi^{(.)} \equiv \psi^{(.)}(\boldsymbol{x}, t)$, respectively. Examples of the former type are u_i, a_i, etc., and those of the latter type are x_i, $\langle u_i \rangle$, $\langle u_i u_j \rangle$, $b_{i,j}$, $\bar{\varepsilon}$, etc. To facilitate the

analysis, those functions are assumed to be fairly smooth such that all derivatives required in the following expressions exist. For velocity-dependent functions, it can be shown using Eqs. (6.14), (6.18), (6A.1), and (6A.3) that

$$\left\langle \Delta\phi^{(1)} \mid \Im_t \right\rangle = L\phi^{(1)} \cdot \Delta + \frac{1}{2} L L \phi^{(1)} \cdot \Delta^2 + O(\Delta^3), \tag{6.22}$$

$$\begin{aligned} &\left\langle \Delta\phi^{(1)} \cdot \Delta\phi^{(2)} \mid \Im_t \right\rangle \\ &\quad = \delta_{j_1,j_2} L_{j_1} \phi^{(1)}{}_1 \cdot L_{j_2} \phi^{(2)} \cdot \Delta \\ &\qquad + \begin{pmatrix} L\phi^{(1)} \cdot L\phi^{(2)} + \frac{1}{2} \delta_{j_1,j_2} \delta_{j_3,j_4} L_{j_1} L_{j_2} \phi^{(1)} \cdot L_{j_3} L_{j_4} \phi^{(2)} \\ + \frac{1}{2} \delta_{j_1,j_2} L_{j_1} \phi^{(1)} \cdot L L_{j_2} \phi^{(2)} + \frac{1}{2} \delta_{j_1,j_2} L_{j_1} \phi^{(1)} \cdot L_{j_2} L \phi^{(2)} \\ + \frac{1}{2} \delta_{j_1,j_2} L L_{j_1} \phi^{(1)} \cdot L_{j_2} \phi^{(2)} + \frac{1}{2} \delta_{j_1,j_2} L_{j_1} L \phi^{(1)} \cdot L_{j_2} \phi^{(2)} \end{pmatrix} \cdot \Delta^2 + O(\Delta^3), \quad \text{and} \end{aligned} \tag{6.23}$$

$$\begin{aligned} &\left\langle \Delta\phi^{(1)} \cdot \Delta\phi^{(2)} \cdot \Delta\phi^{(3)} \mid \Im_t \right\rangle \\ &\quad = \begin{pmatrix} \delta_{j_1,j_2} L\phi^{(1)} \cdot L_{j_1} \phi^{(2)} \cdot L_{j_2} \phi^{(3)} \\ + \delta_{j_1,j_2} L_{j_1} \phi^{(1)} \cdot L\phi^{(2)} \cdot L_{j_2} \phi^{(3)} \\ + \delta_{j_1,j_2} L_{j_1} \phi^{(1)} \cdot L_{j_2} \phi^{(2)} \cdot L\phi^{(3)} \\ + \lambda_{j_1,j_2,j_3,j_4} L_{j_1} \phi^{(1)} \cdot L_{j_2} \phi^{(2)} \cdot L_{j_3} L_{j_4} \phi^{(3)} \\ + \lambda_{j_1,j_3,j_2,j_4} L_{j_1} \phi^{(1)} \cdot L_{j_3} \phi^{(3)} L_{j_2} L_{j_4} \phi^{(2)} \\ + \lambda_{j_2,j_3,j_1,j_4} L_{j_2} \phi^{(2)} \cdot L_{j_3} \phi^{(3)} \cdot L_{j_1} L_{j_4} \phi^{(1)} \end{pmatrix} \cdot \Delta^2 + O(\Delta^3), \end{aligned} \tag{6.24}$$

where δ_{j_1,j_2} is the Kronecker delta function, and $\lambda_{j_1,j_2,j_3,j_4}$ satisfies $\left\langle I_{j_1} I_{j_2} I_{j_3,j_4} \mid \Im_t \right\rangle = \lambda_{j_1,j_2,j_3,j_4} \cdot \Delta^2$. According to Eq. (6A.3),

$$\begin{aligned}\left\langle I_{j_1} I_{j_2} I_{j_3,j_4} \mid \Im_t \right\rangle &= \left\langle \left(I_{j_1,j_2} + I_{j_2,j_1} + I_0\right) I_{j_3,j_4} \mid \Im_t \right\rangle \\ &= \left\langle I_{j_1,j_2} I_{j_3,j_4} \mid \Im_t \right\rangle + \left\langle I_{j_2,j_1} I_{j_3,j_4} \mid \Im_t \right\rangle + \left\langle I_0 I_{j_3,j_4} \mid \Im_t \right\rangle \\ &= \left(\frac{1}{2}\delta_{j_1,j_3}\delta_{j_2,j_4} + \frac{1}{2}\delta_{j_2,j_3}\delta_{j_1,j_4} \right)\cdot\Delta^2 \ .\end{aligned} \tag{6.25}$$

Note that the last term in the second line equals zero according to the mean value theorem (Gardiner, 1997, p. 90). As a result,

$$\lambda_{j_1,j_2,j_3,j_4} = \frac{1}{2}\delta_{j_1,j_3}\delta_{j_2,j_4} + \frac{1}{2}\delta_{j_2,j_3}\delta_{j_1,j_4} \ , \tag{6.26}$$

Similarly, for velocity-independent functions,

$$\begin{aligned}&\left\langle \Delta\psi^{(1)} \mid \Im_t \right\rangle \\ &\quad = \left(\frac{\partial\psi^{(1)}}{\partial t} + u_k \frac{\partial\psi^{(1)}}{\partial x_k} \right)\cdot\Delta \\ &\qquad + \frac{1}{2}\left(\frac{\partial^2\psi^{(1)}}{\partial t^2} + 2u_k \frac{\partial^2\psi^{(1)}}{\partial t\,\partial x_k} + a_k \frac{\partial\psi^{(1)}}{\partial x_k} + 2u_k u_l \frac{\partial^2\psi^{(1)}}{\partial x_k \partial x_l} \right)\cdot\Delta^2 + O(\Delta^3) \ ,\end{aligned} \tag{6.27}$$

$$\begin{aligned}&\left\langle \Delta\psi^{(1)} \cdot \Delta\psi^{(2)} \mid \Im_t \right\rangle \\ &\quad = \prod_{n=1}^{2}\left(\frac{\partial\psi^{(n)}}{\partial t} + u_{k_n} \frac{\partial\psi^{(n)}}{\partial x_{k_n}} \right)\cdot\Delta^2 \\ &\qquad + \frac{1}{3}\delta_{j_1,j_2}\prod_{n=1}^{2}\left(b_{k_n,j_n} \frac{\partial\psi^{(n)}}{\partial x_{k_n}} \right)\cdot\Delta^3 + O(\Delta^4) \ , \quad \text{and}\end{aligned} \tag{6.28}$$

$$
\begin{aligned}
&\left\langle \Delta\psi^{(1)} \cdot \Delta\psi^{(2)} \cdot \Delta\psi^{(3)} \mid \Im_t \right\rangle \\
&\quad = \prod_{n=1}^{3} \left(\frac{\partial \psi^{(n)}}{\partial t} + u_{k_n} \frac{\partial \psi^{(n)}}{\partial x_{k_n}} \right) \cdot \Delta^3 \\
&\quad + \left(\begin{array}{l}
\dfrac{1}{3} \delta_{j_2, j_3} \left(\dfrac{\partial \psi^{(1)}}{\partial t} + u_k \dfrac{\partial \psi^{(1)}}{\partial x_k} \right) \cdot \prod_{n=2}^{3} \left(b_{k_n, j_n} \dfrac{\partial \psi^{(n)}}{\partial x_{k_n}} \right) \\
+ \dfrac{1}{3} \delta_{j_1, j_3} \left(\dfrac{\partial \psi^{(2)}}{\partial t} + u_k \dfrac{\partial \psi^{(2)}}{\partial x_k} \right) \cdot \prod_{n=1 \& 3} \left(b_{k_n, j_n} \dfrac{\partial \psi^{(n)}}{\partial x_{k_n}} \right) \\
+ \dfrac{1}{3} \delta_{j_1, j_2} \left(\dfrac{\partial \psi^{(3)}}{\partial t} + u_k \dfrac{\partial \psi^{(3)}}{\partial x_k} \right) \cdot \prod_{n=1}^{2} \left(b_{k_n, j_n} \dfrac{\partial \psi^{(n)}}{\partial x_{k_n}} \right)
\end{array} \right) \cdot \Delta^4 + O(\Delta^5) \; .
\end{aligned}
\tag{6.29}
$$

Notice that although Eqs. (6.27)-(6.29) are the reduced forms of Eqs. (6.22)-(6.24).

6.4.2. Statistics of local increments related to the form of the diffusion coefficient

As noted previously, the form of $\boldsymbol{b}$ is based on using the velocity structure function for for $\tau_\eta << \Delta << \tau$. That is,

$$
b_{i,m} b_{j,m} = \left\langle \Delta u_i \cdot \Delta u_j \mid \Im_t \right\rangle , \tag{6.30}
$$

which takes the isotropic universal form (Monin and Yaglom, 1975, p. 358)

$$
\left\langle \Delta u_i \cdot \Delta u_j \mid \Im_t \right\rangle = \delta_{i,j} \, C_o \, \bar{\varepsilon} \, , \tag{6.31}
$$

where C_o is the universal Kolmogorov constant. It is of interest here to discuss the validity of Eq. (6.30) to some extent. To do so, it is necessary to express the velocity

structure function as an expansion of Δ. Using Eq. (6.23), the velocity structure function in Eq. (6.30) can be expressed by

$$\left\langle \Delta u_i \cdot \Delta u_j \mid \Im_t \right\rangle = \underbrace{b_{i,m} b_{j,m}}_{\text{(I)}} \cdot \Delta + \underbrace{\left\{ a_i a_j + \left[b_{i,m} \left(\frac{\partial b_{j,m}}{\partial t} + u_k \frac{\partial b_{j,m}}{\partial x_k} \right) + b_{i,m} b_{k,m} \frac{\partial a_j}{\partial u_k} \right] \right\}}_{\text{(II)}} \cdot \Delta^2 + O(\Delta^3) . \quad (6.32)$$

The above result clearly shows that the expansion of the velocity structure function may not permit $\boldsymbol{b}$ to be truly both isotropic and velocity-independent as posed in its definition. This can directly be seen from the high-order terms on the RHS of Eq. (6.32) (specifically, Term (II) in which both $\boldsymbol{u}$ and $\boldsymbol{a}$ appear). Although the form of $\boldsymbol{a}$ is not yet specified, it is known to be an explicit function of $\boldsymbol{u}$ (i.e. velocity-dependent). Moreover, the high-order terms are not necessary to have an isotropic form. To reduce the effect of anisotropy and velocity dependence for the relations in Eqs. (6.30)-(6.31), it is important to maintain the magnitudes of Terms (II) and high-order terms to be much smaller than that of Term (I). In this spirit, it seems appropriate to impose the following constraint

$$\left| \text{(I)} \right| >> \left| \text{(II)} \right| \cdot \Delta . \quad (6.33)$$

for all *i*, *j*, so that the validity of the definition of $\boldsymbol{b}$ is ensured to good approximation of $O(\Delta)$. Implementing the above constraint may result in Δ being smaller than the time scales in the inertial subrange, but this may be permitted due to the assumption of the

unlimited decrease in Δ (see the end of Section 6.1). The anisotropic behavior of $\boldsymbol{b}$ found in numerical simulation is also reported in Pope (2002) where the results from a first-order LSM and direct numerical simulation (DNS) for multi-dimensional stationary homogeneous turbulence are compared. It was found that $\boldsymbol{b}$ can possess significant anisotropy.

As discussed above, there is an inconsistency between the form of $\boldsymbol{b}$ given by the inertial subrange theory and the mathematics associated with the model. To further discussion, consider $\left\langle (\Delta u_i - \left\langle \Delta u_i \mid \Im_t \right\rangle) \cdot (\Delta u_j - \left\langle \Delta u_j \mid \Im_t \right\rangle) \mid \Im_t \right\rangle$, the velocity structure function in a central sense, where

$$\left\langle \Delta u_i \mid \Im_t \right\rangle \equiv \left\langle u_{i(t+\Delta)} \mid \Im_t \right\rangle - \left\langle u_i \mid \Im_t \right\rangle = \left\langle u_{i(t+\Delta)} \mid \Im_t \right\rangle - u \,. \tag{6.34}$$

In light of the local isotropy in the inertial subrange, Δu_i has an isotropic probability function that is independent of x_i and u_i (Monin and Yaglom, 1975, p. 358-359), resulting in the odd moments of Δu_i being zero. Accordingly,

$$\left\langle (\Delta u_i - \left\langle \Delta u_i \mid \Im_t \right\rangle) \cdot (\Delta u_j - \left\langle \Delta u_j \mid \Im_t \right\rangle) \mid \Im_t \right\rangle = \left\langle \Delta u_i \cdot \Delta u_j \mid \Im_t \right\rangle = C_o \, \bar{\varepsilon} \, \Delta \,, \tag{6.35}$$

for $\tau_\eta << \Delta << \tau$. Using Eq. (6.24), its corresponding expansion is

$$
\begin{aligned}
&\left\langle (\Delta u_i - \left\langle \Delta u_i \mid \Im_t \right\rangle) \cdot (\Delta u_j - \left\langle \Delta u_j \mid \Im_t \right\rangle) \mid \Im_t \right\rangle \\
&\quad = \left\langle (u_{i_{(t+\Delta)}} - \left\langle u_{i_{(t+\Delta)}} \mid \Im_t \right\rangle) \cdot (u_{j_{(t+\Delta)}} - \left\langle u_{j_{(t+\Delta)}} \mid \Im_t \right\rangle) \mid \Im_t \right\rangle \\
&\quad = \left\langle \Delta u_i \cdot \Delta u_j \mid \Im_t \right\rangle - a_i a_j \cdot \Delta^2 + O(\Delta^3) \\
&\quad = \underline{b_{i,m} b_{j,m}} \cdot \Delta + \underline{\left[b_{i,m} \left(\frac{\partial b_{j,m}}{\partial t} + u_k \frac{\partial b_{j,m}}{\partial x_k} \right) + b_{i,m} b_{k,m} \frac{\partial a_j}{\partial u_k} \right]} \cdot \Delta^2 + O(\Delta^3) .
\end{aligned}
\tag{6.36}
$$

(III) (IV)

It is understood that the relations given by Eqs. (6.32) and (6.36) should be equivalent from Eq. (6.35) but are in fact different. The reason is that the model does not perfectly account for the physical behavior of a fluid particle (strictly speaking, in view of local isotropy). Notice that the only difference between Terms (II) and (IV) are the presence of $a_i a_j$. Notwithstanding, it cannot be said that Eq. (6.36) is more appealing because the form of $\boldsymbol{a}$ is not specified.

In addition, there is another possible choice besides the above statistics, as given in Eq. (6.27) of Thomson. It is the structure function of displacement in a central sense, i.e. $\left\langle (\Delta x_i - \left\langle \Delta x_i \mid \Im_t \right\rangle) \cdot (\Delta x_j - \left\langle \Delta x_j \mid \Im_t \right\rangle) \mid \Im_t \right\rangle$ that can be expanded as follows:

$$
\begin{aligned}
&\left\langle (\Delta x_i - \left\langle \Delta x_i \mid \Im_t \right\rangle) \cdot (\Delta x_j - \left\langle \Delta x_j \mid \Im_t \right\rangle) \mid \Im_t \right\rangle \\
&\quad = \left\langle (x_{i_{(t+\Delta)}} - \left\langle x_{i_{(t+\Delta)}} \mid \Im_t \right\rangle) \cdot (x_{j_{(t+\Delta)}} - \left\langle x_{j_{(t+\Delta)}} \mid \Im_t \right\rangle) \mid \Im_t \right\rangle \\
&\quad = \underline{\frac{1}{3} b_{i,m} b_{j,m}} \cdot \Delta^3 + \underline{\left[\frac{1}{3} b_{i,m} \left(\frac{\partial b_{j,m}}{\partial t} + u_k \frac{\partial b_{j,m}}{\partial x_k} \right) + \frac{1}{4} b_{i,m} b_{k,m} \frac{\partial a_j}{\partial u_k} \right]} \cdot \Delta^4 + O(\Delta^5) .
\end{aligned}
\tag{6.37}
$$

(III) (IV)

The LHS terms share a similarity to those of Eqs. (6.33) and (6.36) in that the first term on the RHS is the tensor product $b_{i,m}b_{j,m}$. However, the displacement structure function does not have a universal form in the inertial subrange and is of no use from a practical standpoint.

It should be noted that even though $\boldsymbol{b}$ is given to be velocity-independent, the statistics of its local increment are usually not so. For example, let $b_{i,j} \equiv b(\boldsymbol{x}, t)$ for $i = j$. It is not difficult to show that

$$\left\langle \left(\Delta b(\boldsymbol{x},t)\right)^n \mid \Im_t \right\rangle = \left(\frac{\partial b}{\partial t} + u_k \frac{\partial b}{\partial x_k} \right)^n \cdot \Delta^n + O(\Delta^{n+1}) , \tag{6.38}$$

for n is a positive integer. The bracketed term on the RHS above contains $\boldsymbol{u}$, indicating that the LHS term is dependent on the velocity.

6.5. Some Aspects of Local Numerical Increments and Errors

To obtain the solution to an SDE, the integration of the equation has to be carried out either analytically or numerically. Nevertheless, the analytical solutions may be available only for an SDE that is linear (and nonlinear but reducible to linear). For many, their solutions have to be obtained through numerical integration using a numerical scheme. As mentioned in Section 6.1, only a few number of expansion terms remain after the truncation of high-order terms for a scheme, causing local numerical errors to take place and then be propagated along the path of integration. Briefly discussed here

are the local numerical errors arising from the truncation in the Euler, Milstein, and order-1.5 strong Taylor schemes (to be referred hereafter to as EL, MS, and ST, respectively). To numerically integrate the model in question, the time domain [t_o, T] is discretized into N intervals (not necessarily equal for every interval), where N is a large positive integer. Let t_k be the integration time at step k (for $k = 0, 1, 2, \ldots, N-1, N$), and let $\Delta^{(k)}$ be the time step size at time t_k (i.e. $\Delta^{(k)} \equiv t_{k+1} - t_k$, with $t_{k=0} \equiv t_o$ and $t_N \equiv T$). For a given trajectory, define $\delta(f)^{(k)}$ as the local numerical error of a scalar function $f \equiv f(\boldsymbol{x}, \boldsymbol{u}, t)$ at step k (i.e. at t_k), i.e.

$$\delta(f)^{(k)} \equiv f^{\dagger(k+1)} - f^{(k+1)}, \tag{6.39}$$

where $f^{\dagger(k+1)}$ and $f^{(k+1)}$ are the exact and numerical values of f at t_{k+1}, respectively, *assuming* $(\boldsymbol{x}^{(k)}, \boldsymbol{u}^{(k)})$ *to be exact at step k*. Thus, it is straightforward to write

$$\Delta f^{\dagger(k)} = \Delta f^{(k)} + \delta(f)^{(k)}, \tag{6.40}$$

where $\Delta f^{\dagger(k)} \equiv f^{\dagger(k+1)} - f^{(k)}$ and $\Delta f^{(k)} \equiv f^{(k+1)} - f^{(k)}$ are the exact (without truncation) and numerical (with truncation) increments of f, respectively, given high-precision calculation (which is assumed to be the case here). For conciseness, $\Delta^{(k)}$ and $I_{\tilde{\alpha}}^{(k)}$ will be hereafter written as just Δ and $I_{\tilde{\alpha}}$, respectively.

The differencing description of the EL, MS, and ST schemes and local numerical errors related to them are given below:

EL: By definition, the scheme is written by

$$\Delta Y_\alpha^{(k)} = L Y_\alpha^{(k)} \cdot I_0 + L_\beta Y_\alpha^{(k)} \cdot I_\beta \,, \tag{6.41}$$

where Y_α is the α th component of the solution vector $\boldsymbol{Y}$. Using Eqs. (6.19) and (6.21), (6.41) can be alternatively written by

$$\begin{aligned} \Delta x_i^{(k)} &= u_i^{(k)} \cdot \Delta, \quad \text{and} \\ \Delta u_i^{(k)} &= a_i{}^{(k)} \cdot \Delta + b_{i,j}{}^{(k)} \cdot \Delta W_j \,, \end{aligned} \tag{6.42}$$

with

$$\begin{aligned} \delta(x_i)^{(k)} &= b_{i,j}^{(k)} I_{j,0} + O(\Delta^2) \,, \quad \text{and} \\ \delta(u_i)^{(k)} &= \left[\left(\frac{\partial b_{i,j}}{\partial t} \right)^{(k)} + u_m^{(k)} \left(\frac{\partial b_{i,j}}{\partial x_m} \right)^{(k)} \right] I_{0,j} + b_{m,j}^{(k)} \left(\frac{\partial a_i}{\partial u_m} \right)^{(k)} I_{j,0} + O(\Delta^2) \,. \end{aligned} \tag{6.43}$$

Note that all derivative terms above are evaluated at $(\boldsymbol{x}^{(k)}, \boldsymbol{u}^{(k)}, t_k)$. It is seen that the leading orders of $\delta(x_i)^{(k)}$ and $\delta(u_i)^{(k)}$ are generally of $O(\Delta^{3/2})$ (based on the orders of the standard deviations of $I_{j,0}$ and $I_{0,j}$). As for the local numerical error of a function for this scheme, their evaluation may not be as straightforward as in Eq. (6.43) because the scheme integrates the model with respect to the state variables (not functions associated with it). Therefore, one may have to evaluate it indirectly through the relation

in Eq. (6.10) instead under the assumption that the function is fairly smooth. In that case, it can be approximately said that

$$\begin{aligned} &\delta(\phi)^{(k)} \sim O(\Delta^{3/2}), \quad \text{and} \\ &\delta(\psi)^{(k)} \sim O(\Delta^{3/2}), \end{aligned} \tag{6.44}$$

where ϕ and ψ denotes arbitrary velocity-dependent and -independent scalar functions, respectively.

MS: For this scheme,

$$\Delta Y_\alpha^{(k)} = L Y_\alpha^{(k)} \cdot I_0 + L_\beta Y_\alpha^{(k)} \cdot I_\beta + L_{\beta_1} L_{\beta_2} Y_\alpha^{(k)} \cdot I_{\beta_1,\beta_2}. \tag{6.45}$$

As seen, this scheme requires the random number generation of I_{β_1,β_2}, which is extremely difficult in practice for $\beta_1 \neq \beta_2$ (see Appendix). However, using Eqs. (6.19) and (6.21), Eq. (6.45) finally turns out to be equivalent to Eq. (6.42), which is the EL scheme. Hence, the results given by Eqs. (6.43) and (6.44) for the EL scheme automatically apply for this scheme.

ST: By definition,

$$\begin{aligned}\Delta Y_\alpha^{(k)} = & L Y_\alpha^{(k)} \cdot I_0 + L_\beta Y_\alpha^{(k)} \cdot I_\beta + \\ & L L Y_\alpha^{(k)} \cdot I_{0,0} + L L_\beta Y_\alpha^{(k)} \cdot I_{0,\beta} + L Y_\alpha^{(k)} \cdot I_{\beta,0} + \\ & L_{\beta_1} L_{\beta_2} Y_\alpha^{(k)} \cdot I_{\beta_1,\beta_2} + L_{\beta_1} L_{\beta_2} L_{\beta_3} Y_\alpha^{(k)} \cdot I_{\beta_1,\beta_2,\beta_3},\end{aligned} \tag{6.46}$$

Using Eqs. (6.19) and (6.21) again, the above equation becomes

$$\begin{aligned}\Delta x_i^{(k)} &= u_i^{(k)} \cdot \Delta + \frac{1}{2} a_i^{(k)} \cdot \Delta^2 + b_{i,j}^{(k)} \cdot \Delta Z_j, \quad \text{and} \\ \Delta u_i^{(k)} &= a_i^{(k)} \cdot \Delta + b_{i,j}^{(k)} \cdot \Delta W_j \\ &\quad + \frac{1}{2}\left[\left(\frac{\partial a_i}{\partial t}\right)^{(k)} + a_m^{(k)}\left(\frac{\partial a_i}{\partial u_m}\right)^{(k)} + u_m^{(k)}\left(\frac{\partial a_i}{\partial x_m}\right)^{(k)} + \frac{1}{2} b_{k,m}^{(k)} b_{l,m}^{(k)}\left(\frac{\partial^2 a_i}{\partial u_k \partial u_l}\right)^{(k)}\right] \cdot \Delta^2 \\ &\quad + \left[\left(\frac{\partial b_{i,j}}{\partial t}\right)^{(k)} + u_m^{(k)}\left(\frac{\partial b_{i,j}}{\partial x_m}\right)^{(k)}\right] \cdot (\Delta W_j \cdot \Delta - \Delta Z_j) + b_{m,j}^{(k)}\left(\frac{\partial a_i}{\partial u_m}\right)^{(k)} \cdot \Delta Z_j,\end{aligned} \tag{6.47}$$

with

$$\begin{aligned}\delta(x_i)^{(k)} &= \left[\left(\frac{\partial b_{i,j}}{\partial t}\right)^{(k)} + u_k^{(k)}\left(\frac{\partial b_{i,j}}{\partial x_k}\right)^{(k)}\right] I_{0,j,0} + b_{k,j}^{(k)}\left(\frac{\partial a_i}{\partial u_k}\right)^{(k)} I_{j,0,0} + O(\Delta^3), \quad \text{and} \\ \delta(u_i)^{(k)} &= (L_{j_1} L L_{j_2} u_i)^{(k)} \cdot I_{j_1,0,j_2} + (L_{j_1} L_{j_2} L u_i)^{(k)} \cdot I_{j_1,j_2,0} + O(\Delta^3).\end{aligned} \tag{6.48}$$

The random number generation of I_{β_1,β_2} and $I_{\beta_1,\beta_2,\beta_3}$ is required in the scheme. Fortunately, the Ito coefficients corresponding to these integrals are zero, causing them to drop out and enabling the scheme to be implemented. The disadvantage of the scheme is that a number of derivative terms of ***a*** are needed to be evaluated for every time step and

can be computationally burdensome, especially when the form of $\boldsymbol{a}$ is complex or not analytically available. For a function associated with the model, Eq. (6.10) suggests that

$$\begin{aligned} &\delta(\phi)^{(k)} \sim O(\Delta^2), \quad \text{and} \\ &\delta(\psi)^{(k)} \sim O(\Delta^{5/2}), \end{aligned} \tag{6.49}$$

where ϕ and ψ are the same as in Eq. (6.44).

Evidently, the ST scheme is of the highest order among all three schemes considered here

6.6. Restriction of Time Step Sizes for the Euler Scheme

In the following, considered is how small time step sizes should be in the numerical integration of the model for the EL scheme. It is true that a constant time step size can be used in integration, but it often turns out not to be practical especially when the nonstationarity and inhomogeneity exist in the problem (requiring the size to be extremely small). Thus, the use of variable time step sizes becomes necessary. The basic idea behind it is to restrict time step sizes to be small so that the trajectories of the model are well representative of the exact solutions but not too small to make the computation uneconomical. In addition, small time step sizes are important in that the loss of fine structure due to the truncation of high-order terms in the scheme is reduced. To the authors' knowledge, there have so far been no standards or well-established criteria proposed for selecting the variable time step sizes for the EL scheme. However, Thomson suggested a number of restriction strategies for one-dimensional stationary

inhomogeneous case, and others have adopted them in practice. Those strategies are: for step *k*,

$$\Delta = \min\left[\frac{0.1\sigma^{(k)2}}{b^{(k)2}}, \frac{0.1\sigma^{(k)}}{\left|a^{(k)}\right|}, \frac{0.01\sigma^{(k)}}{\left|u^{(k)}(\partial\sigma/\partial x)^{(k)}\right|}\right], \tag{6.50}$$

where $\sigma^{(k)}$ denotes $\left\langle u^{(k)2}\right\rangle^{1/2}$, and all directional indices are dropped out for one-dimensional turbulence. Although the above strategies are somewhat tentative, they are indeed useful in a sense that they are to ensure the accuracy of numerical results to a certain degree.

To discuss the roles of those strategies, it is perhaps appropriate to begin with stating that the time step size at a particular step should be sufficiently small that the magnitudes of local numerical errors with respect to $\boldsymbol{x}$ and $\boldsymbol{u}$ are small so as to achieve the high accuracy of the results. In other words, $\Delta x_i^{\dagger(k)}$ and $\Delta u_i^{\dagger(k)}$ should be well approximated by $\Delta x_i^{(k)}$ and $\Delta u_i^{(k)}$, respectively, for all $i = 1, 2, \ldots, d$. This also implies that all statistics of $\Delta x_i^{\dagger(k)}$ and $\Delta u_i^{\dagger(k)}$ should be approximated by those of $\Delta x_i^{(k)}$ and $\Delta u_i^{(k)}$, respectively. Thus, it is straightforward to impose:

$$\begin{aligned} &\text{(a)}\ \left|\Delta x_i^{(k)}\right| >> \left|\delta(x_i)^{(k)}\right|, \quad \text{and} \\ &\text{(b)}\ \left|\Delta u_i^{(k)}\right| >> \left|\delta(u_i)^{(k)}\right|, \end{aligned} \tag{6.51}$$

respectively. However, the above inequalities are not of much help since most of them are stochastic in nature, inhibiting algebraic solution. Then, it appears necessary to impose constraints in terms of statistics instead. For conciseness, the discussion is here limited only to the first two orders. In doing so, impose the following inequalities:

$$
\begin{aligned}
&\text{(a)}\ \left|\left\langle \Delta x_i^{(k)} \mid \Im^{(k)} \right\rangle\right| >> \left|\left\langle \delta(x_i)^{(k)} \mid \Im^{(k)} \right\rangle\right|, \\
&\text{(b)}\ \left|\left\langle \Delta x_i^{(k)} \cdot \Delta x_j^{(k)} \mid \Im^{(k)} \right\rangle\right| >> \left| \begin{array}{l} \left\langle \Delta x_i^{(k)} \cdot \delta(x_j)^{(k)} \mid \Im^{(k)} \right\rangle \\ +\left\langle \Delta x_j^{(k)} \cdot \delta(x_i)^{(k)} \mid \Im^{(k)} \right\rangle \\ +\left\langle \delta(x_i)^{(k)} \delta(x_j)^{(k)} \mid \Im^{(k)} \right\rangle \end{array} \right|, \\
&\text{(c)}\ \left|\left\langle \Delta u_i^{(k)} \mid \Im^{(k)} \right\rangle\right| >> \left|\left\langle \delta(u_i)^{(k)} \mid \Im^{(k)} \right\rangle\right|, \quad \text{and} \\
&\text{(d)}\ \left|\left\langle \Delta u_i^{(k)} \cdot \Delta u_j^{(k)} \mid \Im^{(k)} \right\rangle\right| >> \left| \begin{array}{l} \left\langle \Delta u_i^{(k)} \cdot \delta(u_j)^{(k)} \mid \Im^{(k)} \right\rangle \\ +\left\langle \Delta u_j^{(k)} \cdot \delta(u_i)^{(k)} \mid \Im^{(k)} \right\rangle \\ +\left\langle \delta(u_i)^{(k)} \delta(u_j)^{(k)} \mid \Im^{(k)} \right\rangle \end{array} \right|,
\end{aligned}
\tag{6.52}
$$

where $\Im^{(k)} = \Im_{(t_k)}$. The inequalities above will be referred to as the restriction strategies S1-S4, respectively. Using the algebra of Ito integral as previously, it can be shown that

$$
\begin{aligned}
&\text{(a)}\ \left\langle \Delta x_i^{(k)} \mid \Im^{(k)} \right\rangle = u_i^{(k)} \cdot \Delta, \\
&\text{(b)}\ \left\langle \Delta x_i^{(k)} \cdot \Delta x_j^{(k)} \mid \Im^{(k)} \right\rangle = u_i^{(k)} u_j^{(k)} \cdot \Delta^2, \\
&\text{(c)}\ \left\langle \Delta x_i^{(k)} \cdot \delta(x_j)^{(k)} \mid \Im^{(k)} \right\rangle = \frac{1}{2} u_i^{(k)} a_j^{(k)} \cdot \Delta^3 + O(\Delta^4). \\
&\text{(d)}\ \left\langle \delta(x_i)^{(k)} \mid \Im^{(k)} \right\rangle = \frac{1}{2} a_i^{(k)} \cdot \Delta^2 + O(\Delta^3), \quad \text{and} \\
&\text{(e)}\ \left\langle \delta(x_i)^{(k)} \delta(x_j)^{(k)} \mid \Im^{(k)} \right\rangle = \frac{1}{3} \delta_{m,n}\, b_{i,m}^{(k)}\, b_{j,n}^{(k)} \cdot \Delta^3 + O(\Delta^4).
\end{aligned}
\tag{6.53}
$$

Likewise,

(a) $\left\langle \Delta u_i^{(k)} \mid \Im^{(k)} \right\rangle = a_i^{(k)} \cdot \Delta$,

(b) $\left\langle \Delta u_i^{(k)} \cdot \Delta u_j^{(k)} \mid \Im^{(k)} \right\rangle = \delta_{m,n} b_{i,m}^{(k)} b_{j,n}^{(k)} \cdot \Delta + a_i^{(k)} a_i^{(k)} \cdot \Delta^2$,

(c) $\left\langle \Delta u_i^{(k)} \cdot \delta(u_j)^{(k)} \mid \Im^{(k)} \right\rangle$

$$= \frac{1}{2}\delta_{m,n}\left\{ b_{i,m}^{(k)}\left[\left(\frac{\partial b_{j,n}}{\partial t} \right)^{(k)} + u_k^{(k)} \left(\frac{\partial b_{j,n}}{\partial x_k} \right)^{(k)} \right] + b_{i,m}^{(k)}\left[b_{k,n}^{(k)} \left(\frac{\partial a_j}{\partial u_k} \right)^{(k)} \right] \right\} \cdot \Delta^2 + O(\Delta^3) ,$$

(d) $\left\langle \delta(u_i)^{(k)} \mid \Im^{(k)} \right\rangle$

$$= \frac{1}{2}\left[\left(\frac{\partial a_i}{\partial t} \right)^{(k)} + a_k^{(k)} \left(\frac{\partial a_i}{\partial u_k} \right)^{(k)} + u_k^{(k)} \left(\frac{\partial a_i}{\partial x_k} \right)^{(k)} + \frac{1}{2} b_{k,m}^{(k)} b_{l,m}^{(k)} \left(\frac{\partial^2 a_i}{\partial u_k \partial u_l} \right)^{(k)} \right] \cdot \Delta^2 + O(\Delta^3) ,$$

and

(e) $\left\langle \delta(u_i)^{(k)} \cdot \delta(u_j)^{(k)} \mid \Im^{(k)} \right\rangle$

$$= \frac{1}{3}\delta_{m,n} \times \left\{ \begin{array}{l} 2\left[\left(\frac{\partial b_{i,m}}{\partial t} \right)^{(k)} + u_k^{(k)} \left(\frac{\partial b_{i,m}}{\partial x_k} \right)^{(k)} \right] \cdot \left[\left(\frac{\partial b_{j,n}}{\partial t} \right)^{(k)} + u_k^{(k)} \left(\frac{\partial b_{j,n}}{\partial x_k} \right)^{(k)} \right] \\ + \left[\left(\frac{\partial b_{i,m}}{\partial t} \right)^{(k)} + u_k^{(k)} \left(\frac{\partial b_{i,m}}{\partial x_k} \right)^{(k)} \right] \cdot \left[b_{k,n}^{(k)} \left(\frac{\partial a_j}{\partial u_k} \right)^{(k)} \right] \end{array} \right\} \cdot \Delta^3 + O(\Delta^4) . \quad (6.54)$$

By Eqs. (6.53) and (6.54), the restriction strategies given by Eq. (6.52) are found:

S1: Combining (6.53a, d) in (6.52a) gives

$$\left| u_i^{(k)} \right| \cdot \Delta \; >> \; \frac{1}{2} \left| a_i^{(k)} \right| \cdot \Delta^2 + O(\Delta^3) . \quad (6.55)$$

If the last term on the RHS above is neglected (which is appropriate due to Δ being small), Eq. (6.55) then suggests

$$\Delta \ << \ \min\left[\frac{2\left| u_i^{(k)} \right|}{\left| a_i^{(k)} \right|}, \text{ for all } i = 1, 2, \ \ldots \ , d \right], \tag{6.56}$$

where the summation over *i* does not apply. When this strategy is applied, it can be said that the EL scheme approximates $\left| \left\langle \Delta x_i^{\dagger(k)} \mid \Im^{(k)} \right\rangle \right|$ to $O(\Delta^2)$. For the one-dimensional case, if $\left| u^{(k)} \right|$ is replaced by $\sigma^{(k)}$, Eq. (6.56) is simplified to just

$$\Delta \ << \ \frac{2\sigma^{(k)}}{\left| a^{(k)} \right|}, \tag{6.57}$$

which is consistent with the first strategy in Eq. (6.50).

S2: Combining Eqs. (6.53b, c, e) in Eq. (6.52b) gives

$$\left| \ u_i^{(k)} u_j^{(k)} \right| \cdot \Delta^2 \ >> \ \left| \frac{1}{2} u_i^{(k)} a_j^{(k)} + \frac{1}{2} u_j^{(k)} a_i^{(k)} + \frac{1}{3} \delta_{i,j} b_{i,m}^{(k)} b_{j.m}^{(k)} \right| \cdot \Delta^3 + O(\Delta^4), \tag{6.58}$$

Once the last term on the RHS is neglected, the above inequality suggests

$$\Delta << \min\left[\frac{\left| u_i^{(k)} u_j^{(k)} \right|}{V_{i,j}^{(k)}}, \text{ for all } i,\ j = 1, 2, \ldots, d \right], \tag{6.59}$$

where the summation over *i* and *j* does not apply, and

$$V_{i,j}^{(k)} = \frac{1}{2}\left| u_i^{(k)} a_j^{(k)} \right| + \frac{1}{2}\left| u_j^{(k)} a_i^{(k)} \right| + \frac{1}{3}\delta_{i,j} b_{i,m}^{(k)} b_{j.m}^{(k)} . \tag{6.60}$$

When the above strategy is applied, the EL scheme approximates $\left| \left\langle \Delta x_i^{\dagger(k)} \Delta x_j^{\dagger(k)} \mid \Im^{(k)} \right\rangle \right|$ to $O(\Delta^3)$. For the one-dimension case, Eq. (6.59) is just

$$\Delta << \frac{\sigma^2}{\left| u^{(k)} a^{(k)} \right| + \frac{1}{3} b^{(k)2}} . \tag{6.61}$$

Furthermore, if excluding the cross statistics and substituting $\sigma^{(k)}$ for $\left| u^{(k)} \right|$, Eq. (6.61) is simplified to

$$\Delta << \frac{3\sigma^2}{b^{(k)2}} . \tag{6.62}$$

which is consistent with the second strategy in Eq. (6.50).

S3: Combining Eqs. (6.54a, d) in Eq. (6.52c) gives

$$\left| a_i^{(k)} \right| \cdot \Delta \;>>\; \frac{1}{2} \left| \begin{array}{l} \left(\frac{\partial a_i}{\partial t} \right)^{(k)} + a_k^{(k)} \left(\frac{\partial a_i}{\partial u_k} \right)^{(k)} + u_k^{(k)} \left(\frac{\partial a_i}{\partial x_k} \right)^{(k)} \\ + \frac{1}{2} b_{k,m}^{(k)} b_{l,m}^{(k)} \left(\frac{\partial^2 a_i}{\partial u_k \partial u_l} \right)^{(k)} \end{array} \right| \cdot \Delta^2 + O(\Delta^3) . \qquad (6.63)$$

Once the last term on the RHS is neglected, Eq. (6.63) suggests

$$\Delta \;<<\; \min \left[\frac{2 \left| a_i^{(k)} \right|}{T_i^{(k)}}, \text{ for all } i = 1, 2, \ldots, d \right], \qquad (6.64)$$

where the summation over *i* does not apply, and

$$T_i^{(k)} = \left| \left(\frac{\partial a_i}{\partial t} \right)^{(k)} \right| + \left| a_k^{(k)} \left(\frac{\partial a_i}{\partial u_k} \right)^{(k)} \right| + \left| u_k^{(k)} \left(\frac{\partial a_i}{\partial x_k} \right)^{(k)} \right| + \frac{1}{2} b_{k,m}^{(k)} \; b_{l,m}^{(k)} \left| \left(\frac{\partial^2 a_i}{\partial u_k \partial u_l} \right)^{(k)} \right| . \qquad (6.65)$$

As seen, using this strategy is also straightforward and helps ensure the approximation of $\left| \left\langle \Delta u_i^{\dagger(k)} \mid \Im^{(k)} \right\rangle \right|$ to $O(\Delta^2)$. However, the derivatives of $\boldsymbol{a}$ needs to be evaluated, which can be time-consuming if the form of $\boldsymbol{a}$ is complicated or not analytically available.

For S4, it can be obtained using Eqs. (6.54b, c, e) in (6.52d) and neglecting all terms of $O(\Delta^3)$ and higher, resulting in a complicated cubic relation (with respect to Δ). Therefore, this strategy may not be suitable for use. As for the last strategy in Eq. (6.50),

it is straightforward to see that the strategy concerns the locality of a time increment for a scalar function. That is, the time step size should not be too large to change the value of the function during a time step. So, it is important to select a time step size being small compared to the time scale of the nonstationarity and inhomogeneity of turbulence that is generally defined as the characteristic time scale of the tangent of the function. Because many functions are associated with the model, it is necessary to limit only those that are essential to the model, e.g. $\langle u_i \rangle$, $\langle u_i u_j \rangle$, $\langle u_i u_j u_k \rangle$, $\bar{\varepsilon}$, etc. Such functions are typically smooth and also independent of $\boldsymbol{u}$. Now, suppose that there are n functions chosen for consideration. Also, let them be denoted by $\psi^{(i)} \equiv \psi^{(i)}(\boldsymbol{x}, t)$ for i = 1, 2, … , n. Then, the time step size at step k should be restricted to be small such that.

$$\Delta << \left[\frac{\left| (\psi^{(i)})^{(k)} \right|}{\left| \left(\frac{\partial \psi^{(i)}}{\partial t} \right)^{(k)} \right| + \left| u_m^{(k)} \left(\frac{\partial \psi^{(i)}}{\partial x_m} \right)^{(k)} \right|}, \text{ for all } i = 1, 2, \ldots, n \right], \qquad (6.66)$$

which is consistent with Eq. (6.50). It should be emphasized again that the restriction strategies described above are tentative (i.e. not based upon a rigorous treatment). Nevertheless, they are conceptually simple and can ensure the accuracy of the simulation results to some extent (at least in terms of local statistics). Extension to higher-order statistics is also possible but may not be practical.

6.7. Conclusions

Several aspects of local increments in a first-order single-particle Lagrangain stochastic model of turbulent diffusion at large Reynolds numbers have been analyzed and discussed. The framework of this study is nonstationary inhomogeneous turbulence under the assumption that an unlimited decrease in a time increment does not deteriorate the solution of the model. Another major basis of the work is the inertial subrange theory of Kolmogorov. The main tools employed in the analysis are the algebra of Ito integrals and the concept of stochastic expansion. The Wagner-Platen formula is of great importance to appropriately express the local increment of a function associated with the model to as a series of the time increment. For the statistics of a local increment, their determination is facilitated using the product formula of two Ito integrals. Using these tools enables us to determine the expanded forms of the statistics of local increments and those related to the diffusion coefficient of the model.

The analysis shows that the form of the diffusion coefficient of the model possesses an intrinsic tendency of anisotropy and velocity dependence, which can be clearly seen from high-order terms in the expansion of the velocity structure function. In order to alleviate these physical effects to good approximation, the magnitude of a time increment should be sufficiently small certain constraints are satisfied. An inconsistency arises between the local isotropy in the inertial subrange and the mathematical formulation of the model, which is seen directly from considering another structure function that is the velocity structure function in a central sense. Since turbulence is locally isotropic, this velocity structure function also has a universal form and thus can be used as an alternative in assigning the form of the diffusion coefficient. From the

standpoint of local isotropy, both velocity structure functions are comparable. However, it turns out that the expansions of these velocity structure functions are different, which is indicative of the aforementioned inconsistency.

In investigating local numerical increments and errors for the Euler (EL), Milstein (MS), and order-1.5 strong Taylor (ST) schemes, it is straightforward to say that the ST scheme is the best among all in terms of accuracy because of the higher level of truncating high-order terms in the scheme. Hence, the local numerical errors of a function in the ST scheme are in general of a higher order than those of the other two schemes. Given the isotropic (and velocity-independent) diffusion coefficient, both EL and ML schemes turn out to be equivalent for the model in question. The roles of three restriction strategies of time step sizes for the Euler scheme that have been applied by some workers have been examined. Two of them are to constrain time step sizes to be small such that the accuracy of the first- and second-order statistics of Δx_i is ensured. The other strategy corresponds to the restriction of the local time scale of nonstationarity and inhomogeneity of turbulence. Extension to the first-order statistic of Δu_i is made but its corresponding strategy may not be practical for use when the drift coefficient does not have a simple form.

Acknowledgements

The authors thank Drs. Michael Borgas (CSIRO, Australia) and P. K. Yeung of (Georgia Institute of Technology) for their helpful discussion. This work is supported by the U.S. EPA under Contract No. CR827327-01.

Appendix. Ito Integrals

Only single to triple integrals will be briefly described below, which is sufficient for this work. Following the relation given by Eq. (6.18) of Kloeden and Platen (1991) and also Section 4.2.5 of Gardiner (1997), it can be shown that

$$
\begin{aligned}
&I_0 = \Delta, \quad I_\beta = \Delta W_\beta, \quad I_{0,0} = \frac{1}{2}\Delta^2, \quad I_{\beta,0} = \Delta Z_\beta, \quad I_{0,\beta} = \Delta W_\beta \cdot \Delta - \Delta Z_\beta, \\
&I_{\beta_1,\beta_2} = \frac{1}{2}(\Delta W_\beta)^2 - \frac{1}{2}\Delta \quad (\text{only for } \beta_1 = \beta_2 = \beta), \quad I_{0,0,0} = \frac{1}{6}\Delta^3, \quad \text{and} \\
&I_{\beta_1,\beta_2,\beta_3} = \frac{1}{6}(\Delta W_\beta)^3 - \frac{1}{2}\Delta W_\beta \cdot \Delta \quad (\text{only for } \beta_1 = \beta_2 = \beta_3 = \beta),
\end{aligned}
\tag{6A.1}
$$

where ΔW_β is the Weiner increment in direction β, ΔZ_β is the increment of the integrated Brownian process in direction β, and all variables are defined at t. Note that $\Delta W_\beta \sim N(0, \Delta)$ whereas $\Delta Z_\beta \sim N(0, \frac{1}{3}\Delta^3)$ with $Cov(\Delta Z_\beta, \Delta W_\beta) = \frac{1}{2}\Delta^2$. The random number generation of ΔW_β is simply carried out by the well-known Box-Mueller algorithm or other equivalent algorithms. Once a random number of ΔW_β is generated, that of ΔZ_β can be obtained by the following algorithm (Kloeden and Platen, 1989):

$$
\begin{aligned}
&\text{(a)} \quad \Delta W_\beta = \xi_1 \cdot \Delta^{1/2}, \quad \text{and} \\
&\text{(b)} \quad \Delta Z_\beta = \frac{1}{2}(\xi_1 + \frac{1}{\sqrt{3}}\xi_2) \cdot \Delta^{3/2},
\end{aligned}
\tag{6A.2}
$$

where ξ_1 and ξ_2 are independent $N(0,1)$ random variables.

For other integrals, they unfortunately do not have simple forms. Nevertheless, it is still possible to alternatively express them in Fourier series forms (Kloeden and Platen, 1991; Kloeden et al., 1992). Moreover, the algorithms for generating random numbers of such integrals has not so far been enough developed particularly for multi-dimensional problems. Gaines and Lyons (1994) proposed an advanced algorithm for the generation of I_{β_1,β_2} for $\beta_1 \neq \beta_2$. However, the algorithm is somewhat complicated. As for the moments of Ito integrals, the following product formula of two integrals can be used in their calculation (Li and Liu, 1997, Lemma 2.2):

$$\begin{aligned} I_{\tilde{\mu}} I_{\tilde{\rho}} = & \int_t^{t+\Delta} I_{\tilde{\mu}}(t'-t)\, I_{\tilde{\rho}(-)}(t'-t)\, \mathrm{d}W_{\rho_h(t')} + \int_t^{t+\Delta} I_{\tilde{\mu}(-)}(t'-t)\, I_{\tilde{\rho}}(t'-t)\, \mathrm{d}W_{\mu_g(t')} \\ & + \int_t^{t+\Delta} I_{\tilde{\mu}(-)}(t'-t)\, I_{\tilde{\rho}(-)}(t'-t)\, \tilde{\delta}_{\{\mu_g=\rho_h\neq 0\}}\, \mathrm{d}t'. \end{aligned} \tag{6A.3}$$

where $\tilde{\delta}_{\{A\}}$ is the indicator function of statement A (equal to unity if A is true, otherwise 0), $\tilde{\mu}$ and $\tilde{\rho}$ are integer sequences of subscripts $\mu_1, \mu_2, \ldots, \mu_g \in \{0, 1, 2, 3, \ldots\}$ and $\rho_1, \rho_2, \ldots, \rho_h \in \{0, 1, 2, 3, \ldots\}$, respectively, with g and $h \geq 0$, and $\tilde{\mu}(-)$ and $\tilde{\rho}(-)$ denote the new sequences resulting from deleting the last index of the original nonnull $\tilde{\mu}$ and $\tilde{\rho}$, respectively. For instance, $I_{0(-)} = I = 1$, $I_{0,1(-)} = I_0 = \Delta$, and $I_{1,4,2(-)} = I_{1,4}$. To illustrate how (6A.3) works, two examples are given. First, consider $\left\langle I_{1,3}\, I_{3,0} \mid \Im_t \right\rangle$ (for the definition of $\Im_t$, see Section 6.4). Using Eq. (6A.3), it can be shown that

$$
\begin{aligned}
& \left\langle I_{1,3}\, I_{3,0} \mid \Im_t \right\rangle \\
[1] \quad &= \left\langle \int_t^{t+\Delta} I_{1,3}(t'-t)\; I_3(t'-t)\, \underbrace{\mathrm{d}W_{0(t')}}_{=\mathrm{d}t'} \mid \Im_t \right\rangle + \left\langle \int_t^{t+\Delta} I_1(t'-t)\; I_{3,0}(t'-t)\; \mathrm{d}W_{3(t')} \mid \Im_t \right\rangle \\
&\quad + \left\langle \int_t^{t+\Delta} I_1(t'-t)\; I_3(t'-t)\, \underbrace{\tilde{\delta}_{\{3=0\neq 0\}}}_{=0}\; \mathrm{d}t' \mid \Im_t \right\rangle \\
[2] \quad &= \left\langle \int_t^{t+\Delta} I_{1,3}(t'-t)\; I_3(t'-t)\; \mathrm{d}t' \mid \Im_t \right\rangle \\
[3] \quad &= \left\langle \int_t^{t+\Delta} \int_t^{t'} I_{1,3}(t''-t)\; \underbrace{I(t''-t)}_{=1}\; \mathrm{d}W_{3(t'')}\; \mathrm{d}t' \mid \Im_t \right\rangle + \left\langle \int_t^{t+\Delta} \int_t^{t'} I_1(t''-t)\; I_3(t''-t)\; \mathrm{d}W_{3(t'')}\; \mathrm{d}t' \mid \Im_t \right\rangle \\
&\quad + \left\langle \int_t^{t+\Delta} \int_t^{t'} I_1(t''-t) \underbrace{I(t''-t)}_{=1} \underbrace{\tilde{\delta}_{\{3=3\neq 0\}}}_{=1} \mathrm{d}t''\, \mathrm{d}t' \mid \Im_t \right\rangle \\
[4] \quad &= 0 .
\end{aligned}
\tag{6A.4}
$$

From the mean value theorem (Gardiner, 1997, p. 90), the second term in Line [1] and every term in Line [3] equal zero. Alternatively, the second term in Line [3] can be evaluated as follows:

$$
\left\langle \int_t^{t+\Delta} \int_t^{t'} I_1(t''-t)\; I_3(t''-t)\; \mathrm{d}W_{3(t'')}\; \mathrm{d}t' \mid \Im_t \right\rangle = \int_t^{t+\Delta} \int_t^{t'} \left\langle I_1(t''-t)\; I_3(t''-t) \mid \Im_t \right\rangle \mathrm{d}W_{3(t'')}\; \mathrm{d}t' .
\tag{6A.5}
$$

The inner integrand on the RHS becomes zero because of I_1 and I_3 being independent. The second example is $\left\langle I_1^4 \mid \Im_t \right\rangle$. Using Eq. (6A.3) and the mean value theorem,

$$I_1^4 = (I_1 I_1)^2 = \left[2 \int_i^{t+\Delta} I_1(t'-t)\, \mathrm{d}W_{1(t')} + I_0 \right]^2 = 4 I_{1,1}^2 + 4 I_{1,1}\, I_0 + I_0^2 \,. \qquad (6A.6)$$

Using $\left\langle I_{1,1}^2 \mid \Im_t \right\rangle = \frac{1}{2}\Delta^2$ and $\left\langle I_{1,1}\, I_0 \mid \Im_t \right\rangle = 0$, thus $\left\langle I_1^4 \mid \Im_t \right\rangle = 3\Delta^2$.

References

Borgas, M. S., Sawford, B. L. (1991) The small-scale structure of acceleration correlations and its role in the statistical theory of turbulent dispersion. J. Fluid Mech. 228, 295-320.

Dreeben, T. D., Pope, S. B. (1998) Probability density function/Monte Carlo simulation of near-wall turbulent flows. J. Fluid Mech. 357, 141-166.

Gaines, J. G., Lyons, T. J. (1994) Random generation of stochastic area integrals. SIAM J. Appl. Math. 54, 1132-1146.

Gardiner, C. W. (1997) Handbook of Stochastic Methods. Springer, New York.

Kloeden, P. E., Platen, E. (1989) A survey of numerical methods for stochastic differential equations. Stoch. Hydrol. Hydraul. 3, 155-178.

Kloeden, P. E., Platen, E. (1991) Relations between multiple Ito and Strotonovich integrals. Stochastic Anal. Appl. 9, 311-321.

Kloeden, P. E., Platen, E., Wright, I. W. (1992) The approximation of multiple stochastic integrals. Stochastic Anal. Appl. 10, 431-441.

Kolmogorov, A. N. (1941) The local structure of turbulence in incompressible viscous fluid for very large Reynolds numbers. Dokl. Akad. Nauk. 30, 301-305.

Li, C. W., Liu, X. Q. (1997) Approximation of multiple stochastic integrals and its application to stochastic differential equations. Nonlinear Anal.-Theor. 30, 697-708.

Monin, A. S., Yaglom, A. M. (1975) Statistical Fluid Mechanics. Vol. 2, MIT Press, Cambridge, Massachusetts.

Øksendal, B. (2000) Stochastic Differential Equations. Springer, New York.

Pasquill, F., Smith, F. B. (1983) Atmospheric Diffusion. John Wiley & Sons, New York.

Platen, E., Wagner, W. (1982) On a Taylor formula for a class of Ito processes. Prob. Math. Statist. 3, 37-51.

Pope, S. B. (1994) Lagrangian PDF methods for turbulent flows. Annu. Rev. Fluid Mech. 26, 23-63.

Pope, S. B. (2002) Stochastic Lagrangian models for velocity in homogeneous turbulent shear flow. Phys. Fluids 14, 1696-1702.

Rotach, M. W., Gryning, S.-E., Tassone, C. (1996) A two-dimensional Lagrangian stochastic dispersion model for daytime conditions. Q. J. R. Meteorol. Soc. 122, 367-389.

Schwere, S., Stohl, A., Rotach, M. W. (2002) Practical considerations to speed up Lagrangian stochastic particle models. Comput. Geosci. 28, 143-154.

Taylor, G. I. (1921) Diffusion by continuous movements. Proc. Lond. Math. Soc. 20, 196-211.

Thomson, D. J. (1987) Criteria for the selection of stochastic models of particle trajectories in turbulent flows. J. Fluid Mech. 180, 529-556.

Thomson, D. J., Montgomery, M. R. (1994) Reflection boundary conditions for random walk models of dispersion in non-Gaussian turbulence. Atmos. Environ. 12, 1981-1987.

Wagner, W., Platen, E. (1978) Approximation of Ito integral equations. Preprint ZIMM, Akad. Wissenschaften, DDR, Berlin.

Wilson, J. D., Flesch, T. K. (1993) Flow boundaries in random-flight dispersion models: enforcing the well-mixed condition. J. Appl. Meteor. 32, 1695-1707.

Wilson, J. D., Sawford, B. L. (1996) Review of Lagrangian stochastic models for trajectories in the turbulent atmosphere. Boundary-Layer Meteor. 78, 191-210.

Wilson, J. D., Zhuang, Y. (1989) Restriction on the timestep to be used in stochastic Lagrangian models of turbulent dispersion. Boundary-Layer Meteor. 49, 309-316.

CHAPTER 7

ANALOGY BETWEEN THE DIFFUSION LIMIT OF LAGRANGIAN STOCHASTIC MODELS OF TURBULENT DIFFUSION AND THE CLASSICAL THEORY OF TURBULENT DIFFUSION

(Coauthor: A. G. Russell)

Abstract

This work presents a theoretical analogy between the diffusion limit of a general class of first-order Lagrangian stochastic models for one-dimensional nonstationary inhomogeneous turbulence and the classical theory of Taylor [Proc. Lond. Math. Soc. 20, 196-211 (1921)]. The formalism of a projection method is adopted in performing the asymptotic analysis of such models within an equilibrium framework. It is shown that the eddy diffusivity defined at the diffusion limit can be qualitatively interpreted as the area under the correlation function of velocity and that, at this limit, the differential operator of the Fokker-Planck equation corresponding to the model is asymptotically reduced to the so-called genuine differential operator. Some caution of using the asymptotic results in practice is emphasized. Verification is done by showing that the results obtained from the analysis can be recast into the form derived by the rigorous work of Thomson [J. Fluid Mech. 180, 529-556 (1987)]. In addition a particular class of first-order models whose drift coefficients are of a quadratic polynomial of velocity is revisited and more generalized. Its asymptotic analysis is demonstrated using the

projection method and the known analytical forms of eigenfunctions of the generator in an Orstein-Uhlenbeck process.

7.1. Introduction

For many deterministic and stochastic systems, their evolution involves a large number of time scales and may be reduced asymptotically to systems of fewer degrees of freedom due to a large separation of time scales. This is known to be the case of first-order well-mixed Lagrangian stochastic models (LSMs) of passive-scalar single particles (shortly, particles) in large- Reynolds-number turbulence, in which the particle's velocity is assumed to evolve continuously with time in a Markovian fashion. As a result, the joint process of the particle's displacement (z) and velocity (w) becomes Markovian. For brevity, the particle's velocity is shortened to just the velocity unless indicated otherwise. However, the evolution of z alone is in fact non-Markovian essentially due to its dependence on the initial condition of w and its noise being colored or nonwhite, i.e. the evolution of z always maintains the memory of the past from the beginning.

Following the classical theory of diffusion in stationary homogeneous turbulence given by Taylor (1921), the eddy diffusivity at large times, denoted by K_T, can be defined as the area under the curve of the correlation function of velocity versus positive time lag. According to the generalization of Durbin (1983, 1984) and Thomson (1987) for nonstationary inhomogeneous turbulence, a first-order LSM is asymptotically reduced to a zeroth-order LSM called a random displacement model (RDM) by mathematically taking the limit the local decorrelation time scale, τ_l, to zero in an RDM (i.e. $\tau_l \to 0$). The

RDM is a model that represents the Markovian evolution of z alone, and its Fokker-Planck equation (FPE) (or the effective FPE) becomes equivalent to an eddy diffusion model (EDM) of the mean concentration of a passive scalar. With this, a definition of eddy diffusivity is obtained and here denoted by K_D. However, both RDM and EDM are valid only if $\tau_l << \tau_{sh}$, where τ_{sh} is the local time scale of nonstationarity and inhomogeneity of turbulence, and theoretically approximate the behavior of the original first-order model only for times much larger than τ_l but not larger than τ_{sh}. In other words, at any particular time t, both RDM and EDM are valid only when $\tau_l << \tau_{sh}$ and approximate the first-order model only at $t + \Delta$ for $\tau_l << \Delta < \tau_{sh}$. Since the asymptotic form corresponds to the EDM, the name "diffusion limit" is then used to refer to the limit at which the asymptotic forms of first-order models are defined, as said above. Also, the names "Markov or white noise" limits are sometimes used since the evolution of z becomes Markovian and its colored noise turns white at this limit.

In Thomson (1987), the formulation of first-order models of turbulent diffusion is rigorously established, and the asymptotic analysis of such models for multidimensional turbulence is also given in his Section 3.5 based on the method of singular perturbation. It is of main interest here to formally present a mathematical connection between the asymptotic forms of first-order models that are defined at the diffusion limit for nonstationary inhomogeneous turbulence and the classical Taylor theory through the concept of equilibrium treatment for a stochastic system. Here, the formalism of projection method pioneered by Nakajima (1958), Zwanzig (1960), and Mori (1965) is adopted as an alternative technique in performing the asymptotic analysis. This technique takes into account much of the detail of a stochastic system, making it possible to solve

the FPE corresponding to the system directly. Although its algebra seems rather complicated, its manipulation is convenient due to use of a projection operator (shortly, a projector). The analysis in this work is limited to one-dimensional incompressible nonstationary inhomogeneous turbulence. Notwithstanding, it can provide some additional insight into the concept of eddy diffusivity defined at the diffusion limit. The analysis first deals with the stationary inhomogeneous case in the absence of a mean flow (to be referred hereafter as Case I) and is later extended to the nonstationary inhomogeneous case with a mean flow (to be referred hereafter as Case II). To verify the results from the analysis, it is shown that the eddy diffusivity defined at the diffusion limit, denoted by K_D, can be recast into the form derived by Thomson. An emphasis of some limitations of the asymptotic solution of the model is also given. As a supplement, this work demonstrates how the projection method can be readily applied to a particular class of first-order models whose drift coefficients are quadratic polynomials of w by taking advantage of standard Hermite polynomials. For clarity, the RDM (or EDM), is strictly referred to as the model that is asymptotically reduced from a first-order LSM.

As for the projection method, it has been employed in a broad range of research areas, particularly statistical mechanics, as a useful tool in constructing an approximate model for a stochastic system when some information or observation of the entire system is not available or can be neglected. Examples of its applications to the subject of turbulent diffusion can be seen in Grossmann and Thomae (1982) and Heppe (1998). For its fundamental theory and other applications, refer to Chaturvedi and Shibata (1979), Akhiezer and Glazman (1993 Chapter 3), and Gardiner (1997, Chapter 6). In this study,

the formalism of projection method is to a large extent similar to Gardiner (1997) where a projector operates directly on a pdf of an FPE.

7.2. Model Description

In this section, the description of a first-order LSM is concisely given. For more details, they can be found in Thomson (1987), Rodean (1996), and Wilson and Sawford (1996). The model necessarily complies with and the well-mixed condition (Thomson, 1987) and the inertial subrange theory (Kolmogorov, 1941). In essence, the model is formulated as a joint Markov process describing the evolution of (z, w) at time t, which is governed by the following system of stochastic differential equations (SDEs) of Ito type

$$\mathrm{d}z = w\,\mathrm{d}t, \tag{7.1a}$$

$$\mathrm{d}w = a\,\mathrm{d}t + b\,\mathrm{d}W, \tag{7.1b}$$

where $a \equiv a(z,w,t)$ is the drift coefficient, $b \equiv b(z,w,t)$ is the diffusion coefficient, and W is the standard Brownian motion at t. When both a and b are independent of time, the above system is said to be autonomous. It is known that the system in Eq. (7.1) is equivalent to a diffusion process governed by the FPE

$$\frac{\partial p}{\partial t} = -\frac{\partial}{\partial z}(w\,p) - \frac{\partial}{\partial w}(a\,p) + \frac{1}{2}\frac{\partial^2}{\partial w^2}(b^2 p), \tag{7.2}$$

where $p \equiv p(z,w,t)$ is here defined as the unconditional pdf of (z, w) at t. According to the well mixed condition, a takes the form

$$a = \frac{1}{2}\frac{\partial}{\partial w}(b^2 \ln p_E) + \frac{\phi}{p_E}, \tag{7.3}$$

where $p_E \equiv p_E(w_E;z,t) \equiv p_E(w_E)_{z,t}$, is the pdf of the Eulerian velocity, w_E, evaluated at location z and time t, "ln" denotes the natural logarithm, and $\phi \equiv \phi(z,w,t)$ satisfies

$$\frac{\partial \phi}{\partial w} = -\frac{\partial p_E}{\partial t} - \frac{\partial}{\partial z}(w\, p_E). \tag{7.4}$$

Because w_E equals w at any given z and t, $p_E(w_E)_{z,t}$ can be written as $p_E(w)_{z,t}$, and all statistics of w and w_E (at both z and t being fixed) are in fact equivalent. Importantly, the integrability condition for p, p_E, and ϕ requires

$$p, p_E, \text{ and } \phi \overset{s.f.}{\rightarrow} 0 \text{ as } |w| \rightarrow \infty. \tag{7.5}$$

The abbreviation "*s. f.*" is used to indicate that each quantity on the left-hand side (LHS) of the condition in Eq. (7.5) decreases sufficiently fast to zero as $|w| \rightarrow \infty$ (i.e. at the boundary of phase space with respect to w). To be consistent with the inertial subrange theory, b takes the form (Thomson, 1987; Wilson and Sawford, 1996)

$$b = (C_o \bar{\varepsilon})^{1/2} = \left(\frac{2\sigma_l^2}{\tau_l} \right)^{1/2}, \tag{7.6}$$

where C_o is the universal constant, $\bar{\varepsilon} \equiv \bar{\varepsilon}(z,t)$ is the mean dissipation rate of turbulent kinetic energy, $\sigma_l \equiv \sigma_l(z,t)$ is (loosely) defined as the local characteristic velocity scale of large eddies, and $\tau_l \equiv \tau_l(z,t)$ is also (loosely) defined as the local characteristic time scale of energy-containing eddies (shortly, the local time scale). Both σ_l and τ_l are positively valued. Note that no strict rules apply to the value of the constant in the bracketed term of the second form in Eq. (7.6). It is however required to be of $O(1)$. Here, it is assigned to equal two, as in many works (see Degrazia and Anfossi, 1998, and references therein) where σ_l and τ_l are specified as the standard deviation of velocity and the local decorrelation time, respectively. Also notice that, from Eq. (7.6), b is independent of w, i.e. $b \equiv b(z,t)$. Now, combine a and b above in Eq. (7.1) yields

$$\mathrm{d}z = w\,\mathrm{d}t, \tag{7.7a}$$

$$\mathrm{d}w = \left(\frac{\sigma_l^2}{\tau_l} \frac{\partial \ln p_E}{\partial w} + \frac{\phi}{p_E} \right) \mathrm{d}t + \left(\frac{2\sigma_l^2}{\tau_l} \right)^{1/2} \mathrm{d}W, \tag{7.7b}$$

and the FPE in Eq. (7.2) can be rewritten into the form

$$\frac{\partial p}{\partial t} = \boldsymbol{L}_1 p + \boldsymbol{L}_2 p, \tag{7.8}$$

where $\boldsymbol{L}_1$ and $\boldsymbol{L}_2$ are the linear differential operators defined by

$$\begin{aligned}
&\boldsymbol{L}_1 = -\frac{\partial}{\partial w}\pi_1 + \frac{\partial^2}{\partial w^2}\pi_2, \quad \boldsymbol{L}_2 = -\frac{\partial}{\partial z}\pi_3 - \frac{\partial}{\partial w}\pi_4 \\
&\pi_1 = \frac{\sigma_l^2}{\tau_l}\frac{\partial \ln p_E}{\partial w}, \quad \pi_2 = \frac{\sigma_l^2}{\tau_l}, \\
&\pi_3 = w, \quad \text{and} \quad \pi_4 = \frac{\phi}{p_E}.
\end{aligned} \tag{7.9}$$

Now, consider Case I. Since turbulence is stationary for this case, the system in Eq. (7.1) automatically becomes autonomous (i.e. the drift and diffusion coefficients of the system in question being independent of t). So,

$$\begin{aligned}
&a \equiv a(z,w), \quad b \equiv b(z), \quad p_E \equiv p_E(w;z) \equiv p_E(w)_z, \\
&\left\langle w^n \right\rangle \equiv \left\langle w^n \right\rangle(z), \quad \phi \equiv \phi(z,w), \quad \sigma_l \equiv \sigma_l(z), \quad \text{and} \quad \tau_l \equiv \tau_l(z).
\end{aligned} \tag{7.10}$$

The symbol $\langle\ \rangle$ is the ensemble average of a random variable, and the notation $\left\langle w^n \right\rangle$ then denotes the n^{th} moment of w for any positive integer n, i.e. $\left\langle w^n \right\rangle = \int w^n\, p_E\, \mathrm{d}w$. Because no mean flow is in this case and the incompressibility of a turbulent flow is assumed, $\langle w \rangle$ and $\partial\langle w \rangle / \partial z$ automatically become zero, respectively.

For Case II, the system is non-autonomous with the drift and diffusion coefficients are dependent on t. To facilitate the asymptotic analysis (as will be seen later), it is advantageous to convert the system to an autonomous version, which can be

done by introducing a new state variable τ (whose dimension is time). Accordingly, Eq. (7.1) is equivalently rewritten as follows:

$$\mathrm{d}z = w\,\mathrm{d}t, \tag{7.11a}$$

$$\mathrm{d}w = a\,\mathrm{d}t + b\,\mathrm{d}W, \tag{7.11b}$$

$$\mathrm{d}\tau = \mathrm{d}t, \tag{7.11c}$$

where t is the true time variable. The above system presents the joint stationary process of (z, w, τ) instead of (z, w) and also becomes autonomous. Accordingly,

$$\begin{aligned} &a \equiv a(z,w,\tau), \quad b \equiv b(z,\tau), \quad \phi \equiv \phi(z,w,\tau), \quad p_E \equiv p_E(w;z,\tau) \equiv p_E(w)_{z,\tau}, \\ &\left\langle w^n \right\rangle \equiv \left\langle w^n \right\rangle (z,\tau), \quad \sigma_l \equiv \sigma_l(z,\tau), \quad \text{and} \quad \tau_l \equiv \tau_l(z,\tau). \end{aligned} \tag{7.12}$$

Since turbulence in this case has no mean flow and is incompressible, $\langle w \rangle$ is now nonzero while $\partial \langle w \rangle / \partial z$ is still zero. The FPE corresponding to the above system is

$$\frac{\partial p}{\partial t} = -\frac{\partial p}{\partial \tau} - \frac{\partial}{\partial w}(a\,p) - \frac{\partial}{\partial z}(w\,p) + \frac{1}{2}\frac{\partial^2}{\partial w^2}(b^2 p), \tag{7.13}$$

where $p \equiv p(w,z,\tau,t)$ is the unconditional pdf of (z, w, τ) at t. The coefficients a and b here still take the same forms as in Eqs. (7.3) and (7.6), respectively, but ϕ now satisfies

$$\frac{\partial \phi}{\partial w} = -\frac{\partial p_E}{\partial \tau} - \frac{\partial}{\partial z}(w\, p_E)\,. \tag{7.14}$$

Similar to Eq. (7.8), Eq. (7.13) can be recast into the form

$$\frac{\partial p}{\partial t} = \boldsymbol{L}_1 p + \boldsymbol{L}_2 p + \boldsymbol{L}_3 p\,, \tag{7.15}$$

where $\boldsymbol{L}_1$, $\boldsymbol{L}_2$, and $\boldsymbol{L}_3$ are defined by

$$\begin{aligned}
&\boldsymbol{L}_1 = -\frac{\partial}{\partial w}\pi_1 + \frac{\partial^2}{\partial w^2}\pi_2\,, \quad \boldsymbol{L}_2 = -\frac{\partial}{\partial z}\pi_3 - \frac{\partial}{\partial w}\pi_4\,, \quad \boldsymbol{L}_3 = -\frac{\partial}{\partial \tau}\pi_5 - \frac{\partial}{\partial z}\pi_6\,, \\
&\pi_1 = \frac{\sigma_l^2}{\tau_l}\frac{\partial \ln p_E}{\partial w}\,, \quad \pi_2 = \frac{\sigma_l^2}{\tau_l}\,, \quad \pi_3 = w - \langle w \rangle\,, \\
&\pi_4 = \frac{\phi}{p_E}\,, \quad \pi_5 = 1\,, \quad \text{and} \quad \pi_6 = \langle w \rangle.
\end{aligned} \tag{7.16}$$

For clarity, the integral sign $\int$ is used to denote the integration over the phase space with respect to w (here, from $-\infty$ to ∞) while the integral sign $\int_{symb}$ indicates that the integral is only symbolically evaluated with respect to w. For example, $\int_{symb} w\, \mathrm{d}w = w^2/2$.

7.3. Projection Method

As mentioned in Section 7.1, given there exists $\tau_l << \tau_{sh}$, the diffusion limit of the system in question can be mathematically obtained and facilitated by simply imposing τ_l

$\to 0$. As a result, a large separation between the time scales of two pdfs of w and z takes place, allowing the formalism of projection method to be applied, as will be seen later.

7.3.1. Case I

To begin, let $p_{w|z} \equiv p(w,t)_z$ denote the conditional pdf of w at t given z at the same t and $p_z \equiv p(z,t)$ denote the unconditional pdf of z at t (i.e. $p_z = \int p \, \mathrm{d}w$). According to the chain rule of probability, it is straightforward to write p in Eq. (7.8) as

$$p = p_{w|z} p_z \ . \tag{7.17}$$

With τ_l being very small, it is anticipated that $p_{w|z}$ and p_z will evolve over much different time scales. To clarify this, arrange Eq. (7.8) using Eq. (7.17) to give

$$\frac{\partial p}{\partial t} = p_z \frac{\partial p_{w|z}}{\partial t} + p_{w|z} \frac{\partial p_z}{\partial t} = p_z \boldsymbol{L}_1 p_{w|z} + \boldsymbol{L}_2 (p_z p_{w|z}) \,, \quad \text{and} \tag{7.18}$$

$$\begin{aligned} p_z \frac{\partial p_{w|z}}{\partial t} &= p_z \boldsymbol{L}_1 p_{w|z} + \boldsymbol{L}_2 (p_z p_{w|z}) - p_{w|z} \frac{\partial p_z}{\partial t} \\ \frac{\partial p_{w|z}}{\partial t} &\approx \boldsymbol{L}_1 p_{w|z} \ . \end{aligned} \tag{7.19}$$

The magnitude of the first term on the right-hand side (RHS) in the first line of Eq. (7.19) is inversely proportional to τ_l and considerably large. The other terms are thus neglected as $\tau_l \to 0$. Moreover, when τ_l becomes smaller, $p_{w|z}$ is less varying with t. The reasons for this are that all eigenvalues of the operator $\boldsymbol{L}_1$ are nonnegative, and their magnitudes

are inversely proportional to τ_l (see Appendix 7B). So, it can be said that $p_{w|z}$ approaches a stationary state as $\tau_l \to 0$. In other words, $p_{w|z} \approx p_s$, where $p_s \equiv p_s(w)_z$ is the stationary pdf of *w* at *z* being fixed. This corollary suggests that the velocity variable *w* is able to adjust rapidly to the instantaneous values of *x*. So, *z* is often called the slow variable for the system while *w* is the fast variable. Eq. (7.19) is then reduced to just

$$0 \approx \boldsymbol{L}_1 p_s . \tag{7.20}$$

The solution to the above equation can be uniquely determined given the well-mixed condition and the normalization condition of p_s (i.e. $\int p_s \, \mathrm{d}w = 1$). That is, $p_s = p_E$. Hence,

$$p \overset{\tau_l \to 0}{\approx} p_E \, p_z . \tag{7.21}$$

7.3.2. Case II

Similar to Case I, let $p_{w|z,\tau} \equiv p(w,t)_{z,\tau}$ denote the conditional pdf of *w* at *t* given (*z*, τ) at the same *t* and $p_{z,\tau} \equiv p(z,\tau,t)$ denote the unconditional pdf of (*z*, τ) at *t*, i.e. $p_{z,\tau} = \int p \, \mathrm{d}w$, where $p \equiv p(z,w,\tau,t)$. From the chain rule of probability,

$$p = p_{w|z,\tau} \, p_{z,\tau} . \tag{7.22}$$

It is anticipated again that $p_{w|z,\tau}$ and $p_{z,\tau}$ will evolve over much different time scales when τ_l is very small. With the similar arguments for Case I, it can be said that as $\tau_l \to 0$, $p_{w|z,\tau}$ approaches a stationary state. Thus, $p_{w|z,\tau} \approx p_s$, where $p_s \equiv p_s(w)_{z,\tau}$ is the stationary pdf of w at (z, τ) being fixed. Consequently,

$$0 \approx \boldsymbol{L}_1 p_s . \tag{7.23}$$

The solution to the above equation can be uniquely determined given the well-mixed condition and the normalization condition of p_s (i.e. $\int p_s \, \mathrm{d}w = 1$). That is, $p_s = p_E$. Hence,

$$p \overset{\tau_l \to 0}{\approx} p_E \, p_{z,\tau} . \tag{7.24}$$

7.3.3. Projection operator

In the projection method, the RHS terms of Eqs. (7.21) and (7.24) can be written as $\boldsymbol{P}p$, where $\boldsymbol{P}$ is the projector linearly operating on p. Similarly, for an arbitrary real-valued function $f \equiv f(w, .)$ (where the dot represents the other variables) whose behavior as $|w| \to \infty$ is assumed to be the same as that of p in Section 7.2, its projection can be defined by

$$\boldsymbol{P}f = p_E \int f \, \mathrm{d}w . \tag{7.25}$$

Formally speaking, the projector $\boldsymbol{P}$ maps f in **H** into its projection onto a subspace of **H,** where **H** is in general a Hilbert space. Furthermore, define the complement of $\boldsymbol{P}$ as

$$(\boldsymbol{1}-\boldsymbol{P})f = f - \boldsymbol{P}f, \tag{7.26}$$

where $(\boldsymbol{1}-\boldsymbol{P})$ is conventionally called the complement operator of $\boldsymbol{P}$, and $\boldsymbol{1}$ is the identity operator. Following these definitions, both $\boldsymbol{P}$ and $(\boldsymbol{1}-\boldsymbol{P})$ are linear operators and hold the properties below:

$$\begin{aligned}
&\text{(a)}\ \ \boldsymbol{P}^2 \equiv \boldsymbol{P}\boldsymbol{P} = \boldsymbol{P},\\
&\text{(b)}\ \ (\boldsymbol{1}-\boldsymbol{P})^2 \equiv (\boldsymbol{1}-\boldsymbol{P})(\boldsymbol{1}-\boldsymbol{P}) = (\boldsymbol{1}-\boldsymbol{P}),\\
&\text{(c)}\ \ \boldsymbol{P} + (\boldsymbol{1}-\boldsymbol{P}) = \boldsymbol{1}, \quad \text{and}\\
&\text{(d)}\ \ \boldsymbol{P}(\boldsymbol{1}-\boldsymbol{P}) = (\boldsymbol{1}-\boldsymbol{P})\boldsymbol{P} = 0.
\end{aligned} \tag{7.27}$$

As in Gardiner (1997, p. 199), $\boldsymbol{P}$ may be expressed in terms of $\boldsymbol{L}_1$ as follows:

$$\boldsymbol{P} = \lim_{\theta\to\infty} e^{\theta \boldsymbol{L}_1}, \tag{7.28}$$

where $e^{\theta \boldsymbol{L}_1}$ is called the exponential operator (or the propagator) with respect to $\boldsymbol{L}_1$, and θ is a variable whose dimension is time Due to the importance of Eq. (7.28), its justification is given in Appendix 7B. One property of the exponential operator is that its operational integration can be carried out in a similar manner to a typical integration. Thus,

$$\int_0^{\theta} e^{\theta' \boldsymbol{L}_1}(.)\,\mathrm{d}\theta' = -\boldsymbol{L}_1^{-1}(1 - e^{\theta \boldsymbol{L}_1})(.), \tag{7.29}$$

where $\boldsymbol{L}_1^{-1}$ is the inverse operator of $\boldsymbol{L}_1$ with the identity $\boldsymbol{L}_1\boldsymbol{L}_1^{-1} = \boldsymbol{L}_1^{-1}\boldsymbol{L}_1 = \boldsymbol{1}$. Using Eq. (7.29), it follows that

$$\int_0^{\infty} e^{\theta \boldsymbol{L}_1}(.)\,\mathrm{d}\theta = -\boldsymbol{L}_1^{-1}(\boldsymbol{1} - \boldsymbol{P})(.)\,. \tag{7.30}$$

To solve Eqs. (7.9) and (7.15), a one-sided Laplace transform $\boldsymbol{L}_p$ and its inverse transform $\boldsymbol{L}_p^{-1}$ are employed, with the identity $\boldsymbol{L}_p^{-1}\boldsymbol{L}_p = \boldsymbol{1}$. By definition, the Laplace transform of a function f, $\tilde{f}(s, .)$, is

$$\boldsymbol{L}_p f \equiv \tilde{f} = \int_0^{\infty} e^{-st} f\,\mathrm{d}t, \tag{7.31}$$

where s is a variable whose dimension is time^{-1}. It can be also seen that $\tilde{f} \overset{s.f.}{\to} 0$ as $|w| \to \infty$. Note again that "*s. f.*" is used to indicate that the LHS term decreases sufficiently fast to zero as $|w| \to \infty$ that its integral over (–∞, ∞) with respect to w is defined or bounded. Some properties related to the above operators are given below:

Case I:

$$\begin{aligned} &\text{(a)}\ \ \boldsymbol{P}\boldsymbol{L}_1 = 0\,, \\ &\text{(b)}\ \ \boldsymbol{L}_1\boldsymbol{P} = 0\,, \quad \text{and} \\ &\text{(c)}\ \ \boldsymbol{P}\boldsymbol{L}_2\boldsymbol{P} = 0\,. \end{aligned} \tag{7.32}$$

The proof of (c) above is given in Appendix 7A whereas (a) and (b) are straightforward. It is not difficult to verify that both $\boldsymbol{L}_p$ and $\boldsymbol{L}_p^{-1}$ commute with $\boldsymbol{P}$, $(\boldsymbol{1}-\boldsymbol{P})$, $\boldsymbol{L}_1$ and $\boldsymbol{L}_2$. The commutative property also holds for $\boldsymbol{L}_p^{-1}$ and $\boldsymbol{L}_1^{-1}(\boldsymbol{1}-\boldsymbol{P})$, i.e. $\boldsymbol{L}_p^{-1}\boldsymbol{L}_1^{-1}(\boldsymbol{1}-\boldsymbol{P}) = \boldsymbol{L}_1^{-1}(\boldsymbol{1}-\boldsymbol{P})\boldsymbol{L}_p^{-1}$. For conciseness, [$Op_1$, Op_2] denotes that operators Op_1 and Op_2 commute.

Case II:

$$\begin{aligned} &\text{(a)}\ \ \boldsymbol{P}\boldsymbol{L}_1 = 0\,, \\ &\text{(b)}\ \ \boldsymbol{L}_1\boldsymbol{P} = 0\,, \\ &\text{(c)}\ \ \boldsymbol{P}\boldsymbol{L}_2\boldsymbol{P} = 0\,, \\ &\text{(d)}\ \ \boldsymbol{P}\boldsymbol{L}_3\boldsymbol{P} \neq 0\,, \quad \text{and} \\ &\text{(e)}\ \ \boldsymbol{P}\boldsymbol{L}_3(\boldsymbol{1}-\boldsymbol{P})p = 0\,. \end{aligned} \tag{7.33}$$

In addition, both $\boldsymbol{L}_p$ and $\boldsymbol{L}_p^{-1}$ commute with $\boldsymbol{P}$, $(\boldsymbol{1}-\boldsymbol{P})$, $\boldsymbol{L}_1$ and $\boldsymbol{L}_2$ (but not with $\boldsymbol{L}_3$). Also, $\boldsymbol{L}_p^{-1}$ and $\boldsymbol{L}_1^{-1}(\boldsymbol{1}-\boldsymbol{P})$ commute with each other, i.e. $\boldsymbol{L}_p^{-1}\boldsymbol{L}_1^{-1}(\boldsymbol{1}-\boldsymbol{P}) = \boldsymbol{L}_1^{-1}(\boldsymbol{1}-\boldsymbol{P})\boldsymbol{L}_p^{-1}$.

7.4. Asymptotic Analysis

The asymptotic analysis is performed in this section, beginning with Case I and then Case II. In general, the analytical procedures for both cases are quite similar and consist mainly of these following steps: First, apply the projector $\boldsymbol{P}$ on the FPE relevant

to each case. Second, apply the complement operator ($\boldsymbol{1} - \boldsymbol{P}$) on the same FPE. Third, Laplace transform on both equations obtained from the first two steps. Fourth, couple the resulting equations together. Last, determine the effective FPE.

7.4.1. Case I

First, apply the projector $\boldsymbol{P}$ and its complement $(\boldsymbol{1} - \boldsymbol{P})$ to Eq. (7.8), and use properties given in Eq. (7.32). After some arrangement, obtain

$$\begin{aligned} \boldsymbol{P}\left(\frac{\partial p}{\partial t}\right) &= \boldsymbol{P}\left(\boldsymbol{L}_1 + \boldsymbol{L}_2\right)\left(\boldsymbol{P} + (\boldsymbol{1} - \boldsymbol{P})\right) p \\ &= \boldsymbol{P}\boldsymbol{L}_2(\boldsymbol{1} - \boldsymbol{P})\, p, \quad \text{and} \end{aligned} \tag{7.34}$$

$$\begin{aligned} (\boldsymbol{1} - \boldsymbol{P})\left(\frac{\partial p}{\partial t}\right) &= (\boldsymbol{1} - \boldsymbol{P})\left(\boldsymbol{L}_1 + \boldsymbol{L}_2\right)\left(\boldsymbol{P} + (\boldsymbol{1} - \boldsymbol{P})\right) p \\ &= \boldsymbol{L}_1(\boldsymbol{1} - \boldsymbol{P})p + (\boldsymbol{1} - \boldsymbol{P})\boldsymbol{L}_2(\boldsymbol{1} - \boldsymbol{P})p + \boldsymbol{L}_2\boldsymbol{P}p. \end{aligned} \tag{7.35}$$

Next, let $v_1 \equiv v_1(z, w, t)$ and $v_2 \equiv v_2(z, w, t)$ denote $\boldsymbol{P}p$ and $(\boldsymbol{1} - \boldsymbol{P})p$, respectively. So,

$$\boldsymbol{P}\left(\frac{\partial p}{\partial t}\right) = \frac{\partial}{\partial t}\boldsymbol{P}p: \quad \frac{\partial v_1}{\partial t} = \boldsymbol{P}\boldsymbol{L}_2 v_2, \quad \text{and} \tag{7.36}$$

$$(\boldsymbol{1} - \boldsymbol{P})\left(\frac{\partial p}{\partial t}\right) = \frac{\partial}{\partial t}(\boldsymbol{1} - \boldsymbol{P})p: \quad \frac{\partial v_2}{\partial t} = \boldsymbol{L}_1 v_2 + (\boldsymbol{1} - \boldsymbol{P})\boldsymbol{L}_2 v_2 + \boldsymbol{L}_2 v_1, \tag{7.37}$$

respectively. Next, Laplace transforms are applied to the above equations, yielding

$$s\tilde{v}_1 - v_1(.,0) = \boldsymbol{P}\boldsymbol{L}_2\tilde{v}_2\,, \quad \text{and} \tag{7.38}$$

$$s\tilde{v}_2 - v_2(.,0) = \boldsymbol{L}_1\tilde{v}_2 + (\boldsymbol{1}-\boldsymbol{P})\boldsymbol{L}_2\tilde{v}_2 + \boldsymbol{L}_2\tilde{v}_1\,. \tag{7.39}$$

Without of loss of generality, let $v_2(.,0)$ equal zero. Next, arrange Eq. (7.39) for the expression of $\tilde{v}_2$, and insert it into the RHS term of Eq. (7.38). By doing so,

$$s\tilde{v}_1 - v_1(.,0) = \boldsymbol{P}\boldsymbol{L}_2\left[s - \boldsymbol{L}_1 - (\boldsymbol{1}-\boldsymbol{P})\boldsymbol{L}_2\right]^{-1}\boldsymbol{L}_2\tilde{v}_1. \tag{7.40}$$

To order of τ_l (i.e. $O(\tau_l)$), only the second term in the brackets $[\ ]^{-1}$ remains. So, Eq. (7.40) is reduced to just

$$s\tilde{v}_1 - v_1(.,0) = -\boldsymbol{P}\boldsymbol{L}_2\,\boldsymbol{L}_1^{-1}\boldsymbol{L}_2\tilde{v}_1\,. \tag{7.41}$$

Using (c) in Eq. (7.32) and the commutative property of [$\boldsymbol{L}_p$, $(\boldsymbol{1}-\boldsymbol{P})$] and [$\boldsymbol{L}_p$, $\boldsymbol{L}_2$],

$$s\tilde{v}_1 - v_1(.,0) = -\boldsymbol{P}\boldsymbol{L}_2\,\boldsymbol{L}_1^{-1}(\boldsymbol{1}-\boldsymbol{P})\boldsymbol{L}_2\tilde{v}_1\,. \tag{7.42}$$

Applying inverse Laplace transforms to both sides yields

$$\frac{\partial}{\partial t}\boldsymbol{P}p = -\boldsymbol{P}\boldsymbol{L}_2\,\boldsymbol{L}_1^{-1}(\boldsymbol{1}-\boldsymbol{P})\boldsymbol{L}_2\boldsymbol{P}p. \tag{7.43}$$

One can see that the above equation presents the intermediately reduced form of Eq. (7.8). In search for the final or asymptotic form, more work needs to be done. To do so, using Eqs. (7.9) and (7.25), Eq. (7.43) becomes

$$p_E \frac{\partial p_z}{\partial t} = p_E \left[\underbrace{\int \frac{\partial}{\partial z}\left(w \boldsymbol{L}_1^{-1}(\boldsymbol{1}-\boldsymbol{P})\boldsymbol{L}_2 \boldsymbol{P} p \right) \mathrm{d}w}_{\text{(I)}} + \underbrace{\int \frac{\partial}{\partial w}\left(\frac{\phi}{p_E} \boldsymbol{L}_1^{-1}(\boldsymbol{1}-\boldsymbol{P})\boldsymbol{L}_2 \boldsymbol{P} p \right) \mathrm{d}w}_{\text{(II)}} \right]. \quad (7.44)$$

The evaluation of Terms (I) and (II) is given in Appendix 7C, showing that Term (II) is zero. So, only Term (I) remains. With p_E on each side taken out,

$$\frac{\partial p_z}{\partial t} = \frac{\partial}{\partial z}\left(\underbrace{\int_0^\infty \int w e^{\theta \mathbf{L}_1}(w p_E)\, \mathrm{d}w \mathrm{d}\theta}_{\equiv K_D} \frac{\partial p_z}{\partial z} \right). \quad (7.45)$$

The effective FPE of the system for Case I is finally obtained as shown above. Notice that the underlined term has the dimension of diffusivity (i.e. length^2 time^{-1}). Thus, define this term as the eddy diffusivity at the diffusion limit, denoted by $K_D \equiv K_D(z)$. Due to the fact that the mean concentration of a passive scalar, denoted by $C \equiv C(z,t)$, is always linearly proportional to p_z, the effective FPE in Eq. (7.45) is thus equivalent to the EDM of the mean concentration of a passive scalar

$$\frac{\partial C}{\partial t} = \frac{\partial}{\partial z}\left(K_D \frac{\partial C}{\partial z} \right). \quad (7.46)$$

For the SDE or RDM equivalent to the effective FPE in Eq. (7.45),

$$\mathrm{d}z = \frac{\partial K_D}{\partial z}\mathrm{d}t + (2K_D)^{1/2}\,\mathrm{d}W\,, \tag{7.47}$$

where $\partial K_D / \partial z$ and $(2K_D)^{1/2}$ are the corresponding drift and diffusion coefficients, respectively. For the definition of K_D in Eq. (7.45), it is discussed in detail in Section 7.5.

7.4.2. Case II

In much of the following, the procedures are parallel to those in Case I in a step-by-step manner. Thus, only those that are important will be shown. To begin with, apply $\boldsymbol{P}$ and $(\boldsymbol{1}-\boldsymbol{P})$ to Eq. (7.15), and use properties in Eq. (7.32). After some algebra, obtain

$$\begin{aligned}\boldsymbol{P}\left(\frac{\partial p}{\partial t}\right) &= \boldsymbol{P}\,(\boldsymbol{L}_1+\boldsymbol{L}_2+\boldsymbol{L}_3)(\boldsymbol{P}+(\boldsymbol{1}-\boldsymbol{P}))\,p \\ &= \boldsymbol{P}\,\boldsymbol{L}_2(\boldsymbol{1}-\boldsymbol{P})\,\boldsymbol{P}p + \boldsymbol{P}\boldsymbol{L}_3\boldsymbol{P}p\,, \quad \text{and}\end{aligned} \tag{7.48}$$

$$\begin{aligned}(\boldsymbol{1}-\boldsymbol{P})\left(\frac{\partial p}{\partial t}\right) &= (\boldsymbol{1}-\boldsymbol{P})(\boldsymbol{L}_1+\boldsymbol{L}_2+\boldsymbol{L}_3)(\boldsymbol{P}+(\boldsymbol{1}-\boldsymbol{P}))\,p \\ &= \boldsymbol{L}_1(\boldsymbol{1}-\boldsymbol{P})p + (\boldsymbol{1}-\boldsymbol{P})\,\boldsymbol{L}_2(\boldsymbol{1}-\boldsymbol{P})p + \boldsymbol{L}_2\boldsymbol{P}p + (\boldsymbol{1}-\boldsymbol{P})\,\boldsymbol{L}_3\boldsymbol{P}p + \boldsymbol{L}_3(\boldsymbol{1}-\boldsymbol{P})p\,.\end{aligned} \tag{7.49}$$

Again, use $v_1 \equiv v_1(z,w,\tau,t)$ for $\boldsymbol{P}p$ and $v_2 \equiv v_2(z,w,\tau,t)$ for $(\boldsymbol{1}-\boldsymbol{P})p$. Then,

$$\frac{\partial v_1}{\partial t} = \boldsymbol{P}\,\boldsymbol{L}_3 v_1 + \boldsymbol{P}\boldsymbol{L}_2 v_2, \quad \text{and} \tag{7.50}$$

$$\frac{\partial v_2}{\partial t} = \boldsymbol{L}_2 v_1 + (\boldsymbol{1}-\boldsymbol{P})\,\boldsymbol{L}_3 v_1 + \boldsymbol{L}_1 v_2 + (\boldsymbol{1}-\boldsymbol{P})\,\boldsymbol{L}_2 v_2 + \boldsymbol{L}_3 v_2, \tag{7.51}$$

respectively. Applying Laplace transforms to the above equations gives

$$s\tilde{v}_1 - v_1(.,0) = \boldsymbol{P}\,\boldsymbol{L}_3 \tilde{v}_1 + \boldsymbol{P}\boldsymbol{L}_2 \tilde{v}_2, \quad \text{and} \tag{7.52}$$

$$s\tilde{v}_2 - v_2(.,0) = \boldsymbol{L}_2 \tilde{v}_1 + (\boldsymbol{1}-\boldsymbol{P})\,\boldsymbol{L}_3 \tilde{v}_1 + \boldsymbol{L}_1 \tilde{v}_2 + (\boldsymbol{1}-\boldsymbol{P})\,\boldsymbol{L}_2 \tilde{v}_2 + \boldsymbol{L}_3 \tilde{v}_2. \tag{7.53}$$

Without loss of generality, $v_2(.,0)$ is assumed to equal zero. Then, obtain the expression of $\tilde{v}_2$ from Eq. (7.53), insert it into the second term on the RHS of Eq. (7.52), and rearrange all terms. After doing so,

$$s\tilde{v}_1 - v_1(.,0) = \boldsymbol{P}\boldsymbol{L}_3 \tilde{v}_1 + \boldsymbol{P}\boldsymbol{L}_2 \left[s - \boldsymbol{L}_1 - (\boldsymbol{1}-\boldsymbol{P})\,\boldsymbol{L}_2 - \boldsymbol{L}_3 \right]^{-1} (\boldsymbol{L}_2 + (\boldsymbol{1}-\boldsymbol{P})\,\boldsymbol{L}_3)\ \tilde{v}_1. \tag{7.54}$$

To a close approximation of $O(\tau_l)$, Eq. (7.54) is reduced to just

$$s\tilde{v}_1 - v_1(.,0) = \boldsymbol{P}\boldsymbol{L}_3 \tilde{v}_1 + \boldsymbol{P}\boldsymbol{L}_2\ \boldsymbol{L}_1^{-1}\ (\boldsymbol{L}_2 + (\boldsymbol{1}-\boldsymbol{P})\,\boldsymbol{L}_3)\ \tilde{v}_1. \tag{7.55}$$

Next, apply inverse Laplace transforms to both sides, resulting in

$$p_E \frac{\partial p_{z,\tau}}{\partial t} = - p_E \frac{\partial p_{z,\tau}}{\partial \tau} - p_E \frac{\partial}{\partial z}(\langle w \rangle p_{z,\tau}) + p_E \left[\begin{array}{l} \underbrace{\int \frac{\partial}{\partial z}\left[(w - \langle w \rangle) \boldsymbol{L}_1^{-1} (\boldsymbol{1} - \boldsymbol{P}) \left(\boldsymbol{L}_2 + (\boldsymbol{1} - \boldsymbol{P}) \boldsymbol{L}_3 \right) \boldsymbol{P} p \right] \mathrm{d}w}_{\text{(I)}} \\ + \underbrace{\int \frac{\partial}{\partial w} \left(\frac{\phi}{p_E} \boldsymbol{L}_1^{-1} (\boldsymbol{1} - \boldsymbol{P}) \left(\boldsymbol{L}_2 + (\boldsymbol{1} - \boldsymbol{P}) \boldsymbol{L}_3 \right) \right) \boldsymbol{P} p \, \mathrm{d}w}_{\text{(II)}} \end{array} \right]. \tag{7.56}$$

According to Appendix 7D, Term (II) is zero. By incorporating Term (I) evaluated in Eq. (7D.1) and taking out p_E on each side, the above equation becomes

$$\frac{\partial p_{z,\tau}}{\partial t} = -\frac{\partial p_{z,\tau}}{\partial \tau} - \frac{\partial}{\partial z}(\langle w \rangle p_{z,\tau}) + \frac{\partial}{\partial z}\left[\int_0^\infty \int (w - \langle w \rangle) e^{\theta \boldsymbol{L}_1} \left((w - \langle w \rangle) p_E \right) \mathrm{d}w \, \mathrm{d}\theta \, \frac{\partial p_{z,\tau}}{\partial z} \right]. \tag{7.57}$$

The last step is to convert $p_{z,\tau}$ to p_z through reversing the same procedures carried out previously in Eqs. (7.11)-(7.13). That is, the variable τ is eliminated from $p_{z,\tau}$, and any τ-dependent variables or functions automatically become t-dependent instead. By doing so, the effective FPE is

$$\frac{\partial p_z}{\partial t} + \frac{\partial}{\partial z}\left(\langle w \rangle p_z \right) = \frac{\partial}{\partial z}\left(\underbrace{\int_0^\infty \int (w - \langle w \rangle) \, e^{\theta \boldsymbol{L}_1} \left((w - \langle w \rangle) p_E \right) \mathrm{d}w \, \mathrm{d}\theta}_{\equiv K_D} \, \frac{\partial p_z}{\partial z} \right), \tag{7.58}$$

where $p_z \equiv p_z(z,t)$. As before, define the underlined term as the eddy diffusivity at the diffusion limit $K_D \equiv K_D(z,t)$. Since p_z is interchangeable with the mean concentration of a passive scalar $C \equiv C(z,t)$, the effective FPE in Eq. (7.58) is equivalent to the EDM

$$\frac{\partial C}{\partial t} + \frac{\partial}{\partial z}\left(\langle w \rangle\, C\right) = \frac{\partial}{\partial z}\left(K_D \frac{\partial C}{\partial z}\right), \tag{7.59}$$

Therefore, the corresponding SDE or RDM is

$$\mathrm{d}z = \left(\langle w \rangle + \frac{\partial K_D}{\partial z}\right)\mathrm{d}t + (2K_D)^{1/2}\,\mathrm{d}W. \tag{7.60}$$

So far, the asymptotic analysis of the general class of first-order models that meet the inertial subrange theory and the well-mixed condition has been completely performed. In the next section, the results in this section will be discussed.

7.5. Discussion

7.5.1. Analogy the eddy diffusivity at the diffusion limit

As mentioned in Section 7.1, the classical Taylor theory for stationary homogeneous turbulence states that the eddy diffusivity at large times (K_T) can be defined as the area under the curve of correlation function of velocity versus positive time lag, i.e.

$$K_T = \int_0^\infty R(\xi)\, \mathrm{d}\xi, \tag{7.61}$$

where R is the Lagrangian velocity autocovariance and ξ is the positive time lag. When turbulence is characterized by nonstationarity and/or inhomogeneity, the diffusion limit is not defined at large times but instead at local times. Nevertheless, it is still possible to interpret the eddy diffusivity at the diffusion limit in spirit of Taylor, as described below.

First, consider Case I. It is natural that the significance of K_D defined in Eq. (7.45) can be directly found by deeming the term $e^{\theta \mathbf{L}_1}(wp_E)$ as the solution to the Liouville equation (B1) (see Appendix 7B) where $f \equiv f(z,w,\theta)$ with the initial condition $f(z,w,0) = wp_E$. With this, it is straightforward to write

$$e^{\theta \mathbf{L}_1}(wp_E) = \int w'\, p_E(w')_z\, p_{1-\mathbf{L}_1}(w,\theta \mid w',0)_z\, \mathrm{d}w', \tag{7.62}$$

where $p_{1-\mathbf{L}_1}(w,\theta \mid w',0)_z$ (shortly, $p_{1-\mathbf{L}_1}$) is defined as the solution to the following Liouville equation

$$\begin{aligned} \frac{\partial p_{1-\mathbf{L}_1}}{\partial \theta} &= \mathbf{L}_1 p_{1-\mathbf{L}_1} \\ &= -\frac{\partial}{\partial w}\left(\frac{\sigma_l^2}{\tau_l} \frac{\partial \ln p_E}{\partial w} p_{1-\mathbf{L}_1} \right) + \frac{\partial^2}{\partial w^2}\left(\frac{\sigma_l^2}{\tau_l} p_{1-\mathbf{L}_1} \right), \end{aligned} \tag{7.63}$$

subject to the initial condition

$$p_{1-\boldsymbol{L}_1}(w,0 \mid w',0)_z = \delta(w-w'), \tag{7.64}$$

where $\delta(.)$ is the Dirac delta function. Note that the subscript z indicates "evaluated at z being fixed", and the subscript $\boldsymbol{L}_1$ is to emphasize that $\boldsymbol{L}_1$ is the only generator driving the evolution of w along the time coordinate θ. Using Eq. (7.62), K_D in Eq. (7.45) can be expressed as

$$K_D = \int_0^\infty \iiint w\, w'\, p_E(w')_z\; p_{1-\boldsymbol{L}_1}(w,\theta \mid w',0)_z \,\mathrm{d}w'\mathrm{d}w\,\mathrm{d}\theta. \tag{7.65}$$

The knowledge of $p_{1-\boldsymbol{L}_1}$ is required to calculate K_D above, and it depends solely on $\boldsymbol{L}_1$ and p_E, as seen in Eq. (7.65). To the authors' knowledge, there is no general analytical form of $p_{1|1-\boldsymbol{L}_1}$ available. There is however a simpler way to evaluate K_D than using Eq. (7.65) (i.e. without a need to determine $p_{1|1-\boldsymbol{L}_1}$), as will be seen in Section 7.5.2. To further the discussion, one can see without difficulty that, according to the chain rule and the fact that $\tau_l \to 0$, the product of $p_E(w')_z$ and $p_{1-\boldsymbol{L}_1}(w,\theta \mid w',0)_z$ equals the joint pdf of w at θ and w' at $\theta = 0$ (both at z being fixed) that is governed by the Liouville equation with the generator $\boldsymbol{L}_1$. Let this joint pdf be denoted by $p_{2-\boldsymbol{L}_1} \equiv p_{2-\boldsymbol{L}_1}(w,\theta;w',0)_z$. Then, $p_{2-\boldsymbol{L}_1} = p_E\, p_{1-\boldsymbol{L}_1}$. Therefore, Eq. (7.65) becomes

$$K_D = \int_0^\infty \left[\iint w\, w'\, p_{2-\boldsymbol{L}_1}(w,\theta;w',0)_z \,\mathrm{d}w'\mathrm{d}w \right] \mathrm{d}\theta. \tag{7.66}$$

Once the variable θ is thought of as a time lag variable, the main integrand (square-bracketed) can be interpreted as the Lagrangian velocity autocorrelation function of velocity. Thus, the definition of K_D is in fact the area under the curve of correlation function versus positive time lag, which is essentially analogous to K_T in Eq. (7.61). It should be noted that although θ is not the true time lag theoretically, it can be thought so given that the evolution is being fixed at z and only the *genuine* generator $\boldsymbol{L}_1$ plays a role in the evolution of w.

Likewise, for Case II, it is straightforward to write

$$e^{\theta \boldsymbol{L}_1}\left((w-\langle w\rangle)\right)p_E = \int (w'-\langle w\rangle)\, p_E(w')_{z,t}\; p_{1-\boldsymbol{L}_1}(w,\theta \mid w',0)_{z,t}\, \mathrm{d}w'. \tag{7.67}$$

Thus, K_D in Eq. (7.58) can be rewritten by

$$\begin{aligned} K_D &= \int_0^\infty \iiint (w-\langle w\rangle)(w'-\langle w\rangle)\, p_E(w')_{z,t}\; p_{1|1-\boldsymbol{L}_1}(w,\theta \mid w',0)_{z,t}\, \mathrm{d}w'\mathrm{d}w\,\mathrm{d}\theta \\ &= \int_0^\infty \left[\iint (w-\langle w\rangle)(w'-\langle w\rangle)\; p_{2-\boldsymbol{L}_1}(w,\theta;w',0)_{z,t}\, \mathrm{d}w'\mathrm{d}w\right]\mathrm{d}\theta\,, \end{aligned} \tag{7.68}$$

where the subsripts z and t indicate "evaluated at z and t being fixed". According to Eq. (7.68), K_D for this case can also be defined as the area under the curve of the correlation function for the evolution of w at both z and t being fixed and $\boldsymbol{L}_1$ being the *genuine* generator of the evolution. Also notice that only the fluctuating or turbulent component of velocity (i.e. $w-\langle w\rangle$) is taken into account, suggesting that the eddy diffusivity at the

diffusion limit implies the ability of diffusion only through the fluctuating component of velocity in one-dimensional incompressible turbulence.

It is also of importance to briefly discuss some important aspects related to the validity and accuracy of the RDM (or EDM) asymptotically reduced from a first-order model. The focus is on turbulence with significant nonstationarity and/or inhomogeneity. Using an RDM in numerical implementation often offers simplicity, resulting in an enormous decrease in computational demand. Nevertheless, one should be aware that the constraint $\tau_l << \tau_{sh}$, is necessarily required for its validity. However, a number of research works in the past have overlooked this requirement, applying RDMs directly without validating them. Thus, checking the constraint should be emphasized and encouraged so that the validity of the RDM is guaranteed for use. From the analysis here, the constraint can be seen at Eqs. (7.66) and (7.68) that the eddy diffusivity at the diffusion limit depends only on the pdf p_{2-L_1} that is locally defined in time and location, suggesting that any change in the magnitudes of any turbulence variables essential to the evolution should be small. Examples of such turbulence variables that can be considered are those that define the deterministic field of a turbulent flow, such as σ_l, τ_l, $\bar{\varepsilon}$, $\langle w^n \rangle$, etc. In practice, τ_{sh} can be defined as $\tau_{sh} = \min [T_s(\psi^{(i)}), T_h(\psi^{(i)}),$ for $i = 1, 2, 3, \ldots]$, where $T_s(\psi^{(i)})$ and $T_h(\psi^{(i)})$ are the local time scales of nonstationarty and inhomogeneity, respectively, with respect to the i^{th} turbulence variable (denoted by $\psi^{(i)}$). A stronger version for τ_{sh} can also be given by $\tau_{sh} = \min[T_s^{-1}(\psi^{(i)}) + T_h^{-1}(\psi^{(i)})]^{-1}$ for all i. Although defining T_s and T_h may not be straightforward or exact, one tentative way is resort to the time scale of the tangent of a variable, i.e. for $\psi^{(i)}$,

$$\text{(a)}\ \ T_s(\psi^{(i)}) \approx \frac{\left|\psi^{(i)}\right|}{\left|\partial\psi^{(i)}/\partial t\right|}, \quad \text{and}$$
$$\text{(b)}\ \ T_h(\psi^{(i)}) \approx \frac{\left|\psi^{(i)}\right|}{\left|\sigma\,\partial\psi^{(i)}/\partial z\right|}, \tag{7.69}$$

where $\sigma = \left\langle w^2 \right\rangle^{1/2}$. Given that the above constraint is satisfied, it is possible to say that the accuracy of the RDM in numerical simulations will simply rely on the magnitude of τ_l. That is, the smaller τ_l, the more accurate. As said in Section 7.1, given the process stays at present time t, the RDM approximates the first-order model only at $t + \Delta$ for $\tau_l << \Delta$, meaning that the first-order model needs a large separation between τ_l and Δ to relax itself to the RDM (i.e. the pdf p is allowed to be well represented by $\boldsymbol{P}p$). Therefore, implementation of the RDM at a local instant always causes an error due to the fact that the relaxation is not attained, generally giving an overestimate of the growth of local mean squared displacement.

7.5.2. Verification

To verify the results obtained from the analysis in this work, it is anticipated that the results can be consistently recast to the form given by Thomson. For conciseness, only Case II is demonstrated. To do so, reconsider the Liouville equation (B1) for $f \equiv f(z,w,t,\theta)$ with the initial condition $f(z,w,t,0) = (w - \langle w \rangle)\, p_E$. Similar to the

procedures done in Eq. (7C.1) substituting $e^{\theta \mathbf{L}_1}\left((w-\langle w\rangle)\,p_E\right)$ for f and integrating both sides of Eq. (7B.1) over θ from 0 to ∞ yield

$$0-(w-\langle w\rangle)\,p_E=\frac{\partial}{\partial w}\left\{\frac{\sigma_l^2}{\tau_l}\,p_E\,\frac{\partial}{\partial w}\left[\frac{1}{p_E}\int_0^{\infty}e^{\theta \mathbf{L}_1}\left((w-\langle w\rangle)\,p_E\right)\mathrm{d}\theta\right]\right\}, \tag{7.70}$$

with the requirement of the boundedness condition

$$\frac{\sigma_l^2}{\tau_l}\,p_E\,\frac{\partial}{\partial w}\left[\frac{1}{p_E}\int_0^{\infty}e^{\theta \mathbf{L}_1}\left((w-\langle w\rangle)\,p_E\right)\mathrm{d}\theta\right]\overset{s.f.}{\rightarrow}0\quad\text{as}\ |w|\rightarrow\infty. \tag{7.71}$$

Note that the RHS of Eq. (7.70) uses: $f=(w-\langle w\rangle)\,p_E$ at $\theta=0$ and $f=\boldsymbol{P}[(w-\langle w\rangle)\,p_E]=0$ as $\theta\rightarrow\infty$. Let $H\equiv H(z,w,t)$ denote the term $\int_0^{\infty}e^{\theta \mathbf{L}_1}\left((w-\langle w\rangle)\,p_E\right)\mathrm{d}\theta$. After some algebra on Eq. (7.70), it can be shown that

$$H=\frac{-\,p_E}{(\sigma_l^2/\tau_l)}\int_{-\infty}^{w}\left[\frac{1}{p_E}\int_{-\infty}^{w'}(w''-\langle w\rangle)\,p_E\,\mathrm{d}w''\right]\mathrm{d}w'. \tag{7.72}$$

So, K_D in Eq. (7.58) can be rearranged to give

$$
\begin{aligned}
&[1] \quad K_D = \int (w - \langle w \rangle) H \, \mathrm{d}w \\
&[2] \qquad = -\int (w - \langle w \rangle) \frac{p_E}{(\sigma_l^2 / \tau_l)} \int_{-\infty}^{w} \left[\frac{1}{p_E} \int_{-\infty}^{w'} (w'' - \langle w \rangle) p_E \, \mathrm{d}w'' \right] \mathrm{d}w' \, \mathrm{d}w \\
&[3] \qquad = \left[\frac{-q}{(\sigma_l^2 / \tau_l)} \int_{-\infty}^{w} \frac{q}{p_E} \, \mathrm{d}w' \right] \Bigg|_{w \to -\infty}^{w \to \infty} + \int \frac{q^2}{(\sigma_l^2 / \tau_l) p_E} \mathrm{d}w \\
&[4] \qquad = \int \frac{q^2}{(\sigma_l^2 / \tau_l) p_E} \mathrm{d}w \, ,
\end{aligned}
\tag{7.73}
$$

where $q \equiv q(z,w,t) = \int_{-\infty}^{w} (w' - \langle w \rangle) p_E \, \mathrm{d}w'$. As seen, the result in Line [4] provides a much more convenient way for calculating K_D. Due to the linear relationship between b^2 and τ_l^{-1} (see Eq. (7.6)), the result above can be readily rewritten as follows:

$$
\begin{aligned}
K_D &= \int \frac{q^2}{(\tfrac{1}{2} b^2 p_E)} \mathrm{d}w \\
&= \int \frac{q^2}{(\tfrac{1}{2} C_o \bar{\varepsilon} \, p_E)} \mathrm{d}w \, ,
\end{aligned}
\tag{7.74}
$$

which is the form given by Thomson. Note that the functions G and ϕ_o appeared in Section 3.5 of his work equals $-H$ and necessarily zero, respectively, in this work. As for the condition in Eq. (7.71) above, it is anticipated to hold for any p_E decreasing sufficiently fast (especially, exponentially fast) to zero as $|w| \to \infty$. Examples of such p_E's in the literature are Gaussian, Chi-type (Thomson, 1987), bi-Gaussian (Baerentsen and Berkowicz, 1984; Luhar and Britter, 1989), and Chi-type: Gram–Charlier expansion (Maurizi and Tampieri, 1999).

7.6. Supplement

According to the fact that there is no guarantee that a first-order model that asymptotically reduces to an EDM will satisfy the well-mixed condition (Thomson, 1987), Rodean (1996) which studied the asymptotic reduction of two different first-order models whose drift coefficients are of a quadratic polynomial of velocity w in his Section 6.3. Two models are Legg and Raupach (1982) and Wilson et al. (1981) that are among the pioneering models proposed for the diffusion in stationary inhomogeneous Gaussian turbulence. Note that only the latter model is valid due to its obeying the well-mixed condition. It was found that both models reduce to an EDM and share the same RDM. However, Rodean's discussion and analysis is not based on the equilibrium concept. It is thus of interest here to demonstrate how to asymptotically reduce such quadratic models within the equilibrium framework by the projection method. As will be seen later, these models have the genuine generator similar to the generator of an Orstein-Uhlenbeck (OU) process, which enables the analysis to be carried out in a simple manner using the knowledge that each eigenfunction of the OU generator takes the form of a standard Hermite polynomial.

Here, consider a stationary process governed by the first-order quadratic model whose form (regardless of the well-mixed condition) is

$$\mathrm{d}w = \left(-\frac{w}{\tau_l} + \beta_0 + \beta_1 w + \beta_2 w^2 \right) \mathrm{d}t + \left(\frac{2\sigma_l^2}{\tau_l} \right)^{1/2} \mathrm{d}W, \qquad (7.75)$$

where $\beta_0 \equiv \beta_0(z)$, $\beta_1 \equiv \beta_1(z)$, and $\beta_2 \equiv \beta_2(z)$ are functions with the dimensions of length·time^{-2}, time^{-1}, and length^{-1}, respectively, and are assumed to be independent of τ_l. For simplicity, assume that there is no mean flow (i.e. $\langle w \rangle = 0$). With Eq. (7.75), the Legg and Raupach model corresponds to $\beta_0 = \partial\sigma_l^2/\partial z$, $\beta_1 = 0$, and $\beta_2 = 0$ while the Wilson et al. model corresponds to $\beta_0 = (1/2)(\partial\sigma_l^2/\partial z)$, $\beta_1 = 0$, and $\beta_2 = (2\sigma_l^2)^{-1}(\partial\sigma_l^2/\partial z)$, where σ_l is estimated as $\langle w^2 \rangle^{1/2}$. To perform the asymptotic analysis of the model in Eq. (7.75) (coupled with the displacement equation $\mathrm{d}z = w\mathrm{d}t$), the FPE of this coupled system is

$$\frac{\partial p}{\partial t} = \boldsymbol{L}_1 p + \boldsymbol{L}_2 p, \tag{7.76}$$

where $\boldsymbol{L}_1$ and $\boldsymbol{L}_2$ are defined by

$$\begin{aligned} \boldsymbol{L}_1 &= \frac{1}{\tau_l}\frac{\partial}{\partial w} w + \frac{\sigma_l^2}{\tau_l}\frac{\partial^2}{\partial w^2}, \quad \text{and} \\ \boldsymbol{L}_2 &= -\frac{\partial}{\partial z} w - \frac{\partial}{\partial w}(\beta_0 + \beta_1 w + \beta_2 w^2). \end{aligned} \tag{7.77}$$

It is straightforward to deduce the stationary pdf of w at z being fixed (denoted by $p_s \equiv p_s(w)_z$) from (76) because the form of $\boldsymbol{L}_1$ appears similar to that of the generator of an OU process whose stationary pdf simply takes the Gaussian form

$$p_s = \frac{1}{\sqrt{2\pi}\,\sigma_l} \exp\left(-\frac{w^2}{2\sigma_l^2}\right). \tag{7.78}$$

Moreover, all eigenfunctions φ_λ's corresponding to the eigenequation $\boldsymbol{L}_1\varphi_\lambda = -\lambda\varphi_\lambda$ can be analytically determined. Without loss of generality, let a nonnegative integer-valued variable *n* be used for λ. In other words, φ_λ is replaced by φ_n. Thus, it follows that

$$\begin{aligned} &\text{(a)}\ \ \boldsymbol{L}_1\varphi_n = -\frac{n}{\tau_l}\varphi_n, \quad \text{and} \\ &\text{(b)}\ \ \varphi_n = \boldsymbol{L}_1^{-1}\boldsymbol{L}_1\varphi_n = -\frac{n}{\tau_l}\boldsymbol{L}_1^{-1}\varphi_n, \end{aligned} \tag{7.79}$$

for $n \neq 0$, where $\boldsymbol{L}_1^{-1}$ is the inverse operator of $\boldsymbol{L}_1$. As in Gardiner (1997, p. 202) and Risken (1996, p. 192-193), φ_n takes the following form

$$\varphi_n = \frac{1}{\sqrt{(2^n n!)}}\, H_n\left(\frac{w}{\sqrt{2}\,\sigma_l}\right) p_s\ , \tag{7.80}$$

where *n*! is the *n*-factorial, and $H_n(.)$ is the Hermite polynomial for $n = 0, 1, 2, 3, \ldots$, e.g.

$$
\begin{aligned}
&\text{(a)}\ \ \varphi_0 = p_s\,, \\
&\text{(b)}\ \ \varphi_1 = \frac{w}{\sigma_l}\,p_s\,, \\
&\text{(c)}\ \ \varphi_2 = \frac{1}{\sqrt{2}}\left(\frac{w^2}{\sigma_l^2}-1\right)p_s\,, \quad \text{and} \\
&\text{(d)}\ \ \varphi_3 = \frac{1}{\sqrt{6}}\left(\frac{w^3}{\sigma_l^3}-3\frac{w}{\sigma_l}\right)p_s\,.
\end{aligned}
\tag{7.81}
$$

As for the properties related to $\boldsymbol{P}$, $\boldsymbol{L}_1$, and $\boldsymbol{L}_2$ for this current case, one can find that:

$$
\begin{aligned}
&\text{(a)}\ \ \boldsymbol{P}\boldsymbol{L}_1 = 0\,, \\
&\text{(b)}\ \ \boldsymbol{L}_1\boldsymbol{P} = 0\,, \quad \text{and} \\
&\text{(c)}\ \ \boldsymbol{P}\boldsymbol{L}_2\boldsymbol{P} = 0\,.
\end{aligned}
\tag{7.82}
$$

In addition, both of the Laplace transform operator $\boldsymbol{L}_p$ and its inverse operator $\boldsymbol{L}_p^{-1}$ commute with $\boldsymbol{P}$, $(\boldsymbol{1}-\boldsymbol{P})$, $\boldsymbol{L}_1$ and $\boldsymbol{L}_2$. Also, $\boldsymbol{L}_p^{-1}$ and $\boldsymbol{L}_1^{-1}(\boldsymbol{1}-\boldsymbol{P})$ commute while $\boldsymbol{L}_1^{-1}$ and $\boldsymbol{L}_2$ do not. Now, carry out the same procedures as done in Section 7.4.1. By doing so, the effective FPE asymptotically reduced from the model in question is

$$
\frac{\partial p_z}{\partial t} = \underbrace{\int \frac{\partial}{\partial z}(w\boldsymbol{L}_1^{-1}\boldsymbol{L}_2\boldsymbol{P}p)\,\mathrm{d}w}_{\text{(I)}} \ + \ \underbrace{\int \frac{\partial}{\partial w}\left[(\beta_0+\beta_1 w+\beta_2 w^2)(\boldsymbol{L}_1^{-1}\boldsymbol{L}_2\boldsymbol{P}p)\right]\mathrm{d}w}_{\text{(II)}}\,. \tag{7.83}
$$

Using Eqs. (7.77), (7.79), and (7.81), it is found that

$$\boldsymbol{L}_1^{-1}\boldsymbol{L}_2\boldsymbol{P}p = \frac{1}{2}\tau_l\,\beta_1\,p_z p_s + \tau_l\left(\frac{\partial p_z}{\partial z} + \frac{1}{\sigma_l}\frac{\partial \sigma}{\partial z}p_z - \frac{\beta_0}{\sigma_l^2}p_z\right)(wp_s)$$
$$-\frac{1}{2}\frac{\tau_l\,\beta_1}{\sigma_l^2}p_z(w^2 p_s) + \frac{1}{3}\tau_l\left(\frac{1}{\sigma_l^3}\frac{\partial \sigma_l}{\partial z}p_z - \frac{\beta_2}{\sigma_l^2}p_z\right)p_z(w^3 p_s)\,. \tag{7.84}$$

Now, incorporate the above result in Terms (I) and (II) in Eq. (7.83). Then,

$$\text{(a) Term (I)} = \frac{\partial}{\partial z}\left[\left(\frac{\partial \sigma_l^2}{\partial z} - \beta_0 - \beta_2\,\sigma_l^2\right)\tau_l\,p_z + \sigma_l^2\tau_l\frac{\partial p_z}{\partial z}\right], \quad \text{and} \tag{7.85}$$
$$\text{(b) Term (II)} = 0.$$

Then, Eq. (7.83) is finally reduced to

$$\frac{\partial p_z}{\partial t} = -\frac{\partial}{\partial z}\left[\left(-\frac{\partial \sigma_l^2}{\partial z} + \beta_0 + \beta_2\,\sigma_l^2\right)\tau_l\,p_z + \frac{\partial}{\partial z}(\sigma_l^2\,\tau_l)\,p_z\right] + \frac{1}{2}\frac{\partial^2}{\partial z^2}(2\sigma_l^2\,\tau_l\,p_z), \tag{7.86}$$

which is equivalent to the SDE or RDM

$$\mathrm{d}z = \left[\left(-\frac{\partial \sigma^2}{\partial z} + \beta_0 + \beta_2\,\sigma_l^2\right)\tau_l + \frac{\partial}{\partial z}(\sigma_l^2\,\tau_l)\right]\mathrm{d}t + (2\sigma_l^2\,\tau_l)^{1/2}\;\mathrm{d}W. \tag{7.87}$$

So, any β_0 and β_2 that meet

$$-\frac{\partial \sigma_l^2}{\partial z} + \beta_0 + \beta_2\,\sigma_l^2 = 0 \tag{7.88}$$

will make the effective FPE equivalent to the EDM, regardless of β_1. Therefore, there are infinite combinations of β_0, β_1, and β_2 that enable the model in question to asymptotically reduce to the EDM. It is readily seen that the forms of β_0 and β_2 in the Legg and Raupach model and Wilson et al. model satisfy Eq. (7.88), yielding the same RDM.

Acknowledgements

The authors thank Dr. Brian Sawford (CSIRO, Australia) and Howard Rodean, for their useful comments and suggestions. This work is supported by the U.S. EPA under Contract No. CR827327-01.

Appendix 7A. Evaluation of $\boldsymbol{PL_2P}$ in Eq. (7.32)

Using Eqs. (7.9) and (7.25), $\boldsymbol{PL_2P}$ can be evaluated as follows:

$$
\begin{aligned}
&[1] \quad \boldsymbol{PL}_2\boldsymbol{P}f = p_E\left[-\int\frac{\partial}{\partial z}(w\,\boldsymbol{P}f)\,\mathrm{d}w-\int\frac{\partial}{\partial w}\left(\frac{\phi}{p_E}\boldsymbol{P}f\right)\mathrm{d}w\right]\\
&[2] \quad = p_E\left[-\int\frac{\partial}{\partial z}(w\,p_E\int f\,\mathrm{d}w')\,\mathrm{d}w-\int\frac{\partial}{\partial w}\left(\frac{\phi}{p_E}\,p_E\int f\,\mathrm{d}w'\right)\mathrm{d}w\right]\\
&[3] \quad = p_E\left[-\frac{\partial}{\partial z}\left(\int(w\,p_E)\,\mathrm{d}w\cdot\int f\,\mathrm{d}w\right)-\int f\,\mathrm{d}w\cdot\int\frac{\partial\phi}{\partial w}\,\mathrm{d}w\right]\\
&[4] \quad = -p_E\frac{\partial}{\partial z}\left(\langle w\rangle\int f\,\mathrm{d}w\right).
\end{aligned}
\tag{7A.1}
$$

Using the condition in Eq. (7.5), the last term in the squared-bracketed term in Line [3] is zero. Due to no mean flow in Case I (i.e. $\langle w \rangle = 0$), $\boldsymbol{P}\boldsymbol{L}_2\boldsymbol{P} = 0$.

Appendix 7B. Justification of Eq. (7.28)

In much of the following, the justification makes use of several concepts in Risken (1996, p. 103-105) and Gardiner (1997, p. 130-131). The details are given in a step-by-step but concise manner. To begin with, define $f \equiv f(w,\theta,.)$ as an arbitrary function that decreases sufficiently fast as $|w| \to \infty$, where θ is a variable with the dimension of time as usual. Then, consider the parabolic partial differential equation

$$\frac{\partial f}{\partial \theta} = \boldsymbol{L}_1 f, \tag{7B.1}$$

where $\boldsymbol{L}_1$ is the differential operator defined in Eq. (7.10). As a Liouville equation, its solution can be written as $f = e^{\theta \boldsymbol{L}_1} f(w,0,.)$ or $e^{\theta \boldsymbol{L}_1} f_o$, where $f(w,0,.)$ or f_o is the initial condition at $\theta = 0$. Often, it is advantageous to present f as a linear combination of its eigenfunctions. To do so, suppose that f_λ is a solution of Eq. (7B.1) and takes the ansatz (i.e. separable) form

$$f_\lambda = \varphi_\lambda e^{-\lambda\theta}, \tag{7B.2}$$

where $\varphi_\lambda \equiv \varphi_\lambda(w,.)$, and λ is a parameter that is independent of w and has the dimension of time^{-1}. Substitution of f_λ for f in Eq. (7B.1) gives

$$\boldsymbol{L}_1\varphi_\lambda = -\lambda\varphi_\lambda , \tag{7B.3}$$

which is the eigenequation of the operator $\boldsymbol{L}_1$ with φ_λ and λ being its eigenfunction and eigenvalue, respectively. It is simple that, for $\lambda = 0$, $\varphi_0 = p_E h$, where $h \equiv h(\theta,.)$ is a w-independent function whose value is given to be unity for simplicity. So, $\varphi_0 = p_E$. According to the Sturm-Liouville theory (O'Neil, 1995, p. 218-227], λ is real-valued, and the orthonormality of eigenfunctions holds, i.e.

$$\int q\varphi_\lambda\varphi_{\lambda'}\,\mathrm{d}w = \delta_{\lambda,\lambda'} , \tag{7B.4}$$

where $q \equiv q(w,.)$ is an appropriate weighting function, and $\delta_{\lambda,\lambda'}$ is the Kronecker function that equals unity for $\lambda = \lambda'$, otherwise zero. Hence, it is straightforward to write $q = p_E^{-1}$. Moreover, it can be shown that λ is always nonnegative. To prove this, a new variable $\Phi \equiv \Phi(z,w,t)$ is introduced and defined as follows:

$$\Phi = \ln\pi_2 - \int_{symb}\frac{\pi_1}{\pi_2}\mathrm{d}w . \tag{7B.5}$$

With this definition, the relation between $\boldsymbol{L}_1$ and Φ can be given by

$$\boldsymbol{L}_1 = \frac{\partial}{\partial w}\left(\pi_2 e^{-\Phi} \frac{\partial}{\partial w} e^{\Phi} \right). \tag{7B.6}$$

Also, introduce a Hermitian operator $\boldsymbol{L}_H$ with the following definition

$$\boldsymbol{L}_H = e^{\Phi/2} \boldsymbol{L}_1 e^{-\Phi/2}. \tag{7B.7}$$

Additionally, let $\psi_\lambda \equiv \psi_\lambda(z,w,t)$ denote $e^{\Phi/2}\varphi_\lambda$. So, f_λ in (B2) can be rewritten as

$$f_\lambda = e^{-\Phi/2} \psi_\lambda e^{-\lambda\theta}. \tag{7B.8}$$

Incorporating Eqs. (7B.7) and (7B.8) in Eq. (7B.1) results in

$$\boldsymbol{L}_H \psi_\lambda = -\lambda \psi_\lambda. \tag{7B.9}$$

It should be noted that $f_\lambda, \varphi_\lambda$, and $\psi_\lambda \overset{s.f.}{\rightarrow} 0$ as $|w| \rightarrow \infty$. As noted in passing, λ is nonnegative, which can be verified through using Eqs. (7B.7) and (7B.9) in evaluating the term $\int \psi_\lambda \boldsymbol{L}_H \psi_\lambda \, \mathrm{d}w$. After some algebra, it can be shown that

$$\int \psi_\lambda \boldsymbol{L}_H \psi_\lambda \, \mathrm{d}w = -\lambda \int \psi_\lambda^2 \, \mathrm{d}w = -\int (\pi_2 e^{-\Phi}) \left[\frac{\partial}{\partial w} (e^{\Phi} e^{-\Phi/2} \psi_\lambda) \right]^2 \mathrm{d}w \leq 0. \tag{7B.10}$$

Since $\pi_2 > 0$, comparison between the second and third terms gives $\lambda \geq 0$. Due to the fact that $\{\varphi_\lambda\}$ forms an orthogonal set, the eigenfunction expansion of f may be written by

$$f = \sum_{\lambda \geq 0} a_\lambda \varphi_\lambda \, e^{-\lambda\theta}, \tag{7B.11}$$

where a_λ is the expansion coefficient that can be expressed by $a_\lambda = = \int p_E^{-1} f \, \varphi_\lambda \, \mathrm{d}w$. Therefore, it is straightforward to write:

$$\begin{aligned}
&[1] \quad \boldsymbol{P} f_0 = \lim_{\theta \to \infty} e^{\theta \boldsymbol{L}_1} f_0 = \lim_{\theta \to \infty} f \\
&[2] \qquad = \sum_{\lambda \geq 0} \left[\lim_{\theta \to \infty} e^{-\theta\lambda} \varphi_\lambda \int \left(\frac{f_0 \varphi_\lambda}{p_E} \right) \mathrm{d}w \right] \\
&[3] \qquad = p_E \int f_0 \, \mathrm{d}w + \sum_{\lambda > 0} \left[\lim_{\theta \to \infty} e^{-\theta\lambda} \varphi_\lambda \int \left(\frac{f_0 \varphi_\lambda}{p_E} \right) \mathrm{d}w \right] \\
&[4] \qquad = p_E \int f_0 \, \mathrm{d}w .
\end{aligned} \tag{7B.12}$$

Without loss of generality, f_0 in Lines [1] and [4] can be replaced with f, and the justification is complete.

Appendix 7C. Terms (I) and (II) in Eq. (7.44)

Using Eqs. (7.10) and (7.28)-(7.30), Term (I) can be arranged to give

$$
\begin{aligned}
&[1] \quad \int \frac{\partial}{\partial z}\left(w \boldsymbol{L}_1^{-1}(\boldsymbol{1}-\boldsymbol{P}) \boldsymbol{L}_2 \boldsymbol{P} p\right) \mathrm{d}w \\
&[2] \qquad = \int \frac{\partial}{\partial z}\left\{ w \boldsymbol{L}_1^{-1}(\boldsymbol{1}-\boldsymbol{P})\left[-\frac{\partial}{\partial z}(w p_E p_z) - \frac{\partial}{\partial w}\left(\frac{\phi}{p_E} p_E\ p_z \right) \right] \right\} \mathrm{d}w \\
&[3] \qquad = \int \frac{\partial}{\partial z}\left\{ w \boldsymbol{L}_1^{-1}(\boldsymbol{1}-\boldsymbol{P})\left[-\frac{\partial}{\partial z}(w p_E p_z) - p_z \frac{\partial \phi}{\partial w} \right] \right\} \mathrm{d}w \\
&[4] \qquad = \int \frac{\partial}{\partial z}\left[w \boldsymbol{L}_1^{-1}(\boldsymbol{1}-\boldsymbol{P})\left(- w p_E \frac{\partial p_z}{\partial z} \right) \right] \mathrm{d}w \\
&[5] \qquad = \frac{\partial}{\partial z}\left[\int_0^{\infty}\!\!\int w e^{\theta \boldsymbol{L}_1}\left(w p_E \frac{\partial p_z}{\partial z} \right) \mathrm{d}\theta\ \mathrm{d}w \right] \\
&[6] \qquad = \frac{\partial}{\partial z}\left[\int_0^{\infty}\!\!\int w e^{\theta \boldsymbol{L}_1}(w p_E)\ \mathrm{d}w \mathrm{d}\theta\ \frac{\partial p_z}{\partial z} \right].
\end{aligned}
\tag{7C.1}
$$

From Lines [3] to [4], use Eq. (7.4). From Lines [4] to [5], use (3.18). Note that, in Line [5], $\partial p_z / \partial z$ can be taken out of $e^{\theta \boldsymbol{L}_1}(.)$.

Likewise, (II) can finally be written as follows:

$$
\int \frac{\partial}{\partial w}\left[\frac{\phi}{p_E} \boldsymbol{L}_1^{-1}(\boldsymbol{1}-\boldsymbol{P}) \boldsymbol{L}_2 \boldsymbol{P} p \right] \mathrm{d}w = \frac{\partial p_z}{\partial z}\left[\frac{\phi}{p_E} \int_0^{\infty} e^{\theta \boldsymbol{L}_1}(w p_E)\ \mathrm{d}\theta \right]\Bigg|_{w \to -\infty}^{w \to \infty}. \tag{7C.2}
$$

Intuitively, the term in the square brackets on the RHS is expected to be bounded over the entire range of w and to vanish sufficiently fast as $|w| \to \infty$. Despite the condition $\phi \overset{s.f.}{\to} 0$ as $|w| \to \infty$, it is still unclear about the value of this square-bracketed term at these limits. With this, it is necessary to make an additional assumption concerning its

boundedness behavior. To do so, reconsider (B1) for $f = e^{\theta \mathbf{L}_1}(wp_E)$. Integration on both sides of (B1) over θ from 0 to ∞ results in

$$\begin{aligned} 0 - wp_E &= -\frac{\partial}{\partial w}\left[\frac{\sigma_l^2}{\tau_l}\frac{\partial \ln p_E}{\partial w}\int_0^\infty e^{\theta \mathbf{L}_1}(wp_E)\,\mathrm{d}\theta \right] + \frac{\partial^2}{\partial w^2}\left[\frac{\sigma_l^2}{\tau_l}\int_0^\infty e^{\theta \mathbf{L}_1}(wp_E)\,\mathrm{d}\theta \right] \\ &= \frac{\partial}{\partial w}\left\{ \frac{\sigma_l^2}{\tau_l} p_E \frac{\partial}{\partial w}\left[\frac{1}{p_E}\int_0^\infty e^{\theta \mathbf{L}_1}(wp_E)\,\mathrm{d}\theta \right] \right\}. \end{aligned} \tag{7C.3}$$

Note that $f = wp_E$ at $\theta = 0$ while $f = \boldsymbol{P}(wp_E) = 0$ as $\theta \to \infty$. Once it is assumed that

$$\frac{\sigma_l^2}{\tau_l} p_E \frac{\partial}{\partial w}\left[\frac{1}{p_E}\int_0^\infty e^{\theta \mathbf{L}_1}(wp_E)\,\mathrm{d}\theta \right] \overset{s.f.}{\to} 0 \quad \text{as } |w| \to \infty, \tag{7C.4}$$

it is possible to write

$$\int_0^\infty e^{\theta \mathbf{L}_1}(wp_E)\,\mathrm{d}\theta = \frac{-p_E}{(\sigma_l^2/\tau_l)}\int_{symb}\left(\frac{1}{p_E}\int_{-\infty}^{w} w' p_E\,\mathrm{d}w' \right)\mathrm{d}w. \tag{7C.5}$$

For any p_E decreasing sufficiently fast as $|w| \to \infty$, the assumption of the condition in Eq. (7C.4) appears appropriate. Thus, Term (II) equals zero.

Appendix 7D. Terms (I) and (II) in Eq. (7.56)

Similar to Eq. (7C.1), Term (I) in Eq. (7.56) can be arranged to give

$$\int \frac{\partial}{\partial z}\left[(w-\langle w\rangle)\, \boldsymbol{L}_1^{-1}(\boldsymbol{1}-\boldsymbol{P})\, \underbrace{(\boldsymbol{L}_2+(\boldsymbol{1}-\boldsymbol{P})\,\boldsymbol{L}_3)\,\boldsymbol{P}p}_{\equiv Q} \right] \mathrm{d}w$$

$$\begin{aligned} Q &= -\frac{\partial}{\partial z}\left[(w-\langle w\rangle)\, p_E\, p_{z,\tau}\right] - \frac{\partial}{\partial w}(\phi\, p_{z,\tau}) - \frac{\partial}{\partial \tau}(p_E\, p_{z,\tau}) \\ &\quad - \frac{\partial}{\partial z}(\langle w\rangle\, p_E\, p_{z,\tau}) + p_E\, \frac{\partial p_{z,\tau}}{\partial \tau} + p_E\, \frac{\partial}{\partial z}(\langle w\rangle\, p_{z,\tau}) \\ &= -(w-\langle w\rangle)\, p_E\, \frac{\partial p_{z,\tau}}{\partial z} \end{aligned} \qquad (7D.1)$$

$$= \frac{\partial}{\partial z}\left[\int_0^\infty \!\!\int (w-\langle w\rangle)\, e^{\theta \boldsymbol{L}_1}\left((w-\langle w\rangle)\, p_E\right) \mathrm{d}w\, \mathrm{d}\theta \;\; \frac{\partial p_{z,\tau}}{\partial z} \right].$$

For Term (II), the arguments made for Term (II) in Appendix 7C are applied in a similar manner. However, the only differences are that p_E and ϕ are now explicit functions of τ and that $e^{\theta \boldsymbol{L}_1}(wp_E)$ is replaced by $e^{\theta \boldsymbol{L}_1}\left((w-\langle w\rangle)\, p_E\right)$ instead. By induction, for any p_E decreasing fast to zero as $|w| \to \infty$, Term (II) equals zero.

References

Akhiezer, N. I, Glazman, I. M. (1993) Theory of Linear Operators in Hilbert Space. Vol. 1, Dover Publications, New York.

Baerentsen J. H., Berkowicz, R. (1984) Monte Carlo simulation of plume dispersion in the convective boundary layer. Atmos. Environ. 18, 701-712.

Chaturvedi. S., Shibata, F. (1979) Time-convolutionless projection operator formalism for elimination of fast variables. Applications to Brownian motion. Z. Physik B 35, 297-308.

Degrazia, G., Anfossi, D. (1998) Estimation of the Kolmogorov constant (C_o) from classical statistical diffusion theory. Atmos. Environ. 32, 3611-3614.

Durbin, P. A. (1983) Stochastic Differential Equations and Turbulent Dispersion. NASA Ref. Pub.1103.

Durbin, P. A. (1984) Comments on papers by Wilson et al. (1981) and Legg and Raupach (1982). Boundary-Layer Meteor. 29, 409-411.

Gardiner, C. W. (1997) Handbook of Stochastic Methods. Springer, New York.

Grossmann, S., Thomae, S. (1982) Correlation decay of Lagrangian velocity differences in locally isotropic turbulence. Z. Phys. B 49, 253-261.

Heppe, B. M. O. (1998) Generalized Langevin equation for relative turbulent dispersion. J. Fluid Mech. 357, 167-198.

Kolmogorov, A. N. (1941) The Local Structure of turbulence in incompressible viscous fluid for very large Reynolds numbers. Dokl. Akad. Nauk. 30, 301-305.

Legg, B. J., Raupach, M. R. (1982) Markov-chain simulation of particle dispersion in inhomogeneous flows: The mean drift velocity induced by a gradient in Eulerian velocity variance. Boundary-Layer Meteor. 24, 3-13.

Luhar, A. K., Britter, R. E. (1989) A random walk model for dispersion in inhomogeneous turbulence in a convective boundary layer. Atmos. Environ. 23, 1911-1924.

Maurizi, A., Tampieri, F. (1999) Velocity probability density functions in Lagrangian dispersion models for inhomogeneous turbulence. Atmos. Environ. 33, 281-289.

Mori, H. (1965) Transport, collective motion, and Brownian motion. Prog. Theor. Phys. 33, 423-455.

Nakajima, S. (1958) On quantum theory of transport phenomena. Prog. Theor. Phys. 20, 948-959.

O'Neil, P. V. (1995) Advanced Engineering Mathematics. Brooks/Cole Publishing, Pacific Grove, California.

Risken, H. (1996) The Fokker-Planck Equation. Springer, New York.

Rodean, H. C. (1996) Stochastic Lagrangian Models of Turbulent Diffusion. Monograph No. 48, American Meteorological Society, Boston, Massachusetts.

Taylor, G. I. (1921) Diffusion by continuous movements. Proc. Lond. Math. Soc. 20, 196-211.

Thomson, D. J. (1987) Criteria for the selection of stochastic models of particle trajectories in turbulent flows. J. Fluid Mech. 180, 529-556.

Wilson, J. D, Thurtell, G. W., Kidd, G. E. (1981) Numerical simulation of particle trajectories in inhomogeneous turbulence Part II: Systems with variable turbulence velocity variance. Boundary-Layer Meteor. 21, 423-441.

Wilson, J. D., Sawford, B. L. (1996) Review of Lagrangian stochastic models for trajectories in the turbulent atmosphere. Boundary-Layer Meteor. 78, 191-210.

Zwanzig, R. (1960) Ensemble method in the theory of irreversibility. J. Chem. Phys. 33, 1338-1341.

CHAPTER 8

EVALUATION OF SOME PROPOSED FORMS OF LAGRANGIAN VELOCITY CORRELATION

(K. Manomaiphiboon and A. G. Russell, Inter. J. Heat Fluid Fl., 24 (2003), 709-712)

Abstract

This work evaluates four different forms of Lagrangian velocity correlation coefficient for stationary homogeneous turbulence at very large Reynolds numbers through consideration of simple mathematical and physical requirements. It is shown that some of them do not comply well with the requirements and may not be appropriate for use.

8.1. Introduction

One of the most fundamental statistics of a turbulent flow is the Lagrangian velocity correlation coefficient (shortly, correlation coefficient). In stationary homogeneous turbulence, its definition is given by

$$R_L(\tau) = \frac{\langle u(t)\, u(t+\tau) \rangle}{\langle u^2 \rangle}, \tag{8.1}$$

where R_L is the correlation coefficient, τ is the time lag, $u(t)$ is the Lagrangian velocity of a fluid element at time t, and $\langle\ \rangle$ denotes an ensemble average (that is equivalent to a time average for stationary turbulence) of a quantity. The objective of this work is to evaluate four different forms of R_L proposed in the literature for stationary homogeneous turbulence at very large Reynolds numbers through consideration of essential mathematical and physical requirements. The first is the classical exponential form given by Taylor (1921). This form has been discussed to a large extent in Tennekes (1979). It is included here for comparison. The others are two forms given by Frenkiel (1953) and a recent proposal of Altinsoy and Tuğrul (2002). Their expressions are given in the next section. It is important that a proper form of R_L should comply with the following requirements:

I: R_L is even around the origin $\tau = 0$ with $\left| R_L(\tau) \right| \le 1 = R_L(0)$. Also, it vanishes fast as $\left|\tau\right| \to \infty$ such that its integral over τ holds, i.e. $\lim_{|\tau| \to \infty} R_L(\tau) = 0$ and $\int_0^\infty \left| R_L(\tau) \right| \mathrm{d}\tau < \infty$.

II: R_L is smooth over τ. At the origin, $\mathrm{d}R_L / \mathrm{d}\tau = 0$ and $\mathrm{d}^2 R_L / \mathrm{d}\tau^2 < 0$.

III: As a result, the Lagrangian integral time scale T_L, defined by

$$T_L = \int_0^\infty R_L(\tau)\, \mathrm{d}\tau\ , \tag{8.2}$$

is bounded or well-defined.

IV: In addition, let E_L denote the Lagrangian turbulent energy spectrum. Mathematically, R_L and E_L can be expressed as the Fourier transform pairs:

$$R_L(\tau) = \frac{1}{\langle u^2 \rangle} \int_0^\infty E_L(\omega) \cos(\omega\tau)\, \mathrm{d}\omega\,, \quad \text{and} \tag{8.3}$$

$$E_L(\omega) = \frac{2\langle u^2 \rangle}{\pi} \int_0^\infty R_L(\tau) \cos(\omega\tau)\, \mathrm{d}\tau\,, \tag{8.4}$$

where ω is the turbulence frequency. The Fourier cosine transforms are used in the above relations due to the evenness of both R_L and E_L. According to the inertial subrange theory (K41) (Kolmogorov, 1941), E_L can be expressed by

$$E_L(\omega) = k\,\bar{\varepsilon}\,\omega^{-2} \quad (\text{or } \propto \omega^{-2}) \tag{8.5}$$

for $1 << \omega T_L << T_L / \tau_\eta$, where k is the dimensionless universal constant, $\bar{\varepsilon}$ is the mean turbulent energy dissipation rate, and τ_η is the Kolmogorov time scale that is small for large Reynolds numbers.

For convenience, the above requirements will be referred hereafter to as Reqs. I-IV, respectively. For more detailed description of these requirements, see Tennekes and Lumley (1972, Chapter 6), Hinze (1975, Chapter 1), and Pope (2000, Chapter 6). Note that Reqs. I and II are equivalent to the five conditions in Hinze (1975, p. 59-60). For this work, the underlying framework is very large-Reynolds-number turbulence, in which

K41 theory applies. Discussion of the effects of Reynolds number on R_L can be found in the rigorous work of Sawford (1991).

8.2. Forms of R_L

Four forms of R_L are considered here. The first form is given by Taylor (1921) as follows:

$$R_L(\tau) = \exp\left(\frac{-|\tau|}{T_L} \right). \tag{8.6}$$

The second and third forms are from Frenkiel (1953):

$$R_L(\tau) = \exp\left(\frac{-|\tau|}{2T_L} \right) \cos\left(\frac{\tau}{2T_L} \right), \quad \text{and} \tag{8.7}$$

$$R_L(\tau) = \exp\left(\frac{-\pi\tau^2}{4T_L^2} \right). \tag{8.8}$$

For the last form, Altinsoy and Tuğrul (2002) recently proposed

$$R_L(\tau) = \exp\left(\frac{-\pi\tau^2}{8T_L^2} \right) \cos\left(\frac{\tau^2}{2T_L^2} \right) \tag{8.9}$$

and also presented a general set for Eqs. (8.8) and (8.9) as

$$R_L(\tau) = \exp\left(\frac{-\pi \tau^2}{4(m^2+1)T_L^2} \right) \cos\left(\frac{m\tau^2}{(m^2+1)T_L^2} \right) \tag{8.10}$$

for $m > 0$, where m is called the loop parameter. Notice that Eq. (8.10) reduces to Eqs. (8.8) and (8.9) for $m = 0$ and 1, respectively. Altinsoy and Tuğrul investigated the performance of R_L in Eq. (8.10) with $m = 1$, 2, and 3 and used $m = 1$ as the proposed value. For conciseness, the forms by Eqs. (8.6)-(8.9) will be referred to as T, F1, F2, and AT, respectively. Their plots are shown in Figure 8-1.

8.3. Evaluation and Discussion

To begin with, consider Req. I. It is not difficult to see that each form is even and its magnitude equals unity at $\tau = 0$ but less than unity for $|\tau| > 0$. Furthermore, each is continuous and decreases exponentially fast to zero as $|\tau| \to \infty$. So, all forms satisfy this requirement.

For Req. II, it is straightforward that F2 and AT satisfy the requirement while T and F1 do not because their first- and second-order derivatives (with respect to τ) are not defined at the origin. In addition, it should be noted that this requirement is also directly associated with another mathematical constraint that the Lagrangian acceleration correlation coefficient (denoted by $R_{L,a}$) has no integral time (Tennekes and Lumley, 1972, p. 215-216; Hinze, 1975, p. 398), i.e.

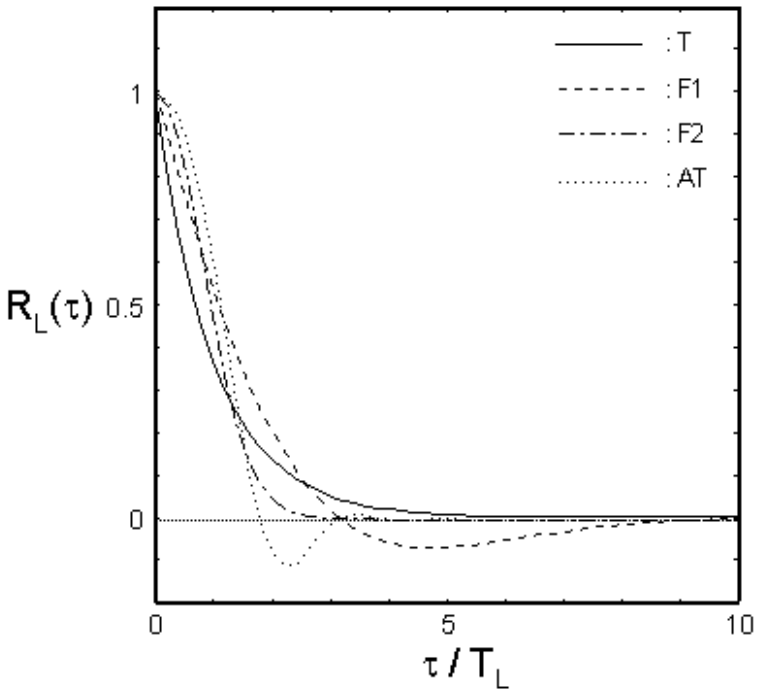

Figure 8-1. Velocity correlation coefficient versus time lag

$$\int_0^\infty R_{L,a}(\tau)\,\mathrm{d}\tau = \frac{-\left\langle u^2 \right\rangle}{\left\langle a^2 \right\rangle}\int_0^\infty \frac{\mathrm{d}^2 R_L}{\mathrm{d}\tau^2}\,\mathrm{d}\tau = \frac{-\left\langle u^2 \right\rangle}{\left\langle a^2 \right\rangle}\left.\frac{\mathrm{d}R_L}{\mathrm{d}\tau}\right|_0^\infty = 0\,, \tag{8.11}$$

where a is the Lagrangian acceleration of a fluid element. Because T and F1 fail to meet this requirement, the above constraint cannot be met. However, these drawbacks are not serious due to the fact that lack of smoothness of R_L at the origin suggests no correct viscous description for an energy spectrum. Since the viscous region only spans very high frequencies for very-large-Reynolds-number turbulence, it contains very low total energy, which is not significant in the context of turbulent diffusion (Tennekes, 1979).

Req. III is in fact nothing but the definition of T_L. Nevertheless, it is important to ensure that this definition indeed holds. By direct integration, it is straightforward to say that T, F1, and F2 meet the requirement. For AT, its integration is somewhat complicated but can be done using Eq. (8A.2) in Appendix. It is found that AT cannot produce the correct result (i.e. the integration of R_L over τ from 0 to ∞ does not yield T_L). In fact, the set given by Eq. (8.10) fails to meet the requirement for all $m > 0$, except for $m \approx 1.0056$. That is, the integral is less than T_L for $0 < m < 1.0056$ (approx.) and more than T_L for $m > 1.0056$ (approx.). For AT, the integral equals $0.9996T_L$ (approx). Thus, AT is invalid due to T_L being ill defined.

To check the compliance with Req. IV, first determine the expression of E_L corresponding to each R_L form using Eq. (8.4). After some algebra with help of the formulas in Appendix, obtain:

T:
$$\frac{E_L(\omega)}{\langle u^2 \rangle T_L} = \frac{2}{\pi(1+\omega^2 T_L^2)}, \tag{8.12}$$

F1:
$$\frac{E_L(\omega)}{\langle u^2 \rangle T_L} = \frac{2(1+2\omega^2 T_L^2)}{\pi(1-2\omega T_L+2\omega^2 T_L^2)(1+2\omega T_L+2\omega^2 T_L^2)}, \tag{8.13}$$

F2:
$$\frac{E_L(\omega)}{\langle u^2 \rangle T_L} = \frac{2}{\pi}\exp\left(\frac{-\omega^2 T_L^2}{\pi}\right), \quad \text{and} \tag{8.14}$$

AT:
$$\frac{E_L(\omega)}{\langle u^2 \rangle T_L} = \frac{1}{\sqrt{\pi}\sqrt[4]{\beta^2+A^2}} \times \exp\left[\frac{-\beta B^2}{4(\beta^2+A^2)}\right]\cos\left[\frac{1}{2}\arctan\left(\frac{A}{\beta}\right)-\frac{AB^2}{4(\beta^2+A^2)}\right], \tag{8.15}$$
with $\beta = \frac{\pi}{8}$, $A = \frac{1}{2}$, and $B = \omega T_L$.

Figure 8-2 shows E_L calculated from the above relations. Based on K41 theory, it is anticipated that E_L exhibits linear proportionality to ω^{-2} for $\omega T_L >> 1$. It is seen from Figure 8-2a that T and F1 can capture the ω^{-2} falloff. The energy spectra of AT and F2 are similar and do not have the ω^{-2} falloff, as shown in Figure 8-2b. Note that Figure 8-2b uses log-linear scale instead in plotting because the energy spectrum of AT becomes negative for some frequencies, which violates the non-negativity of the Fourier transform of an autocorrelation coefficient (Bracewell, 2000, p. 122). Hence, only T and F1 agree with K41 theory.

From the above discussion, it is fair to say that T and F1 are appropriate for use because both comply well with most of the requirements. Although they are not smooth at the origin, this problem can be considered minor in the context of turbulent diffusion.

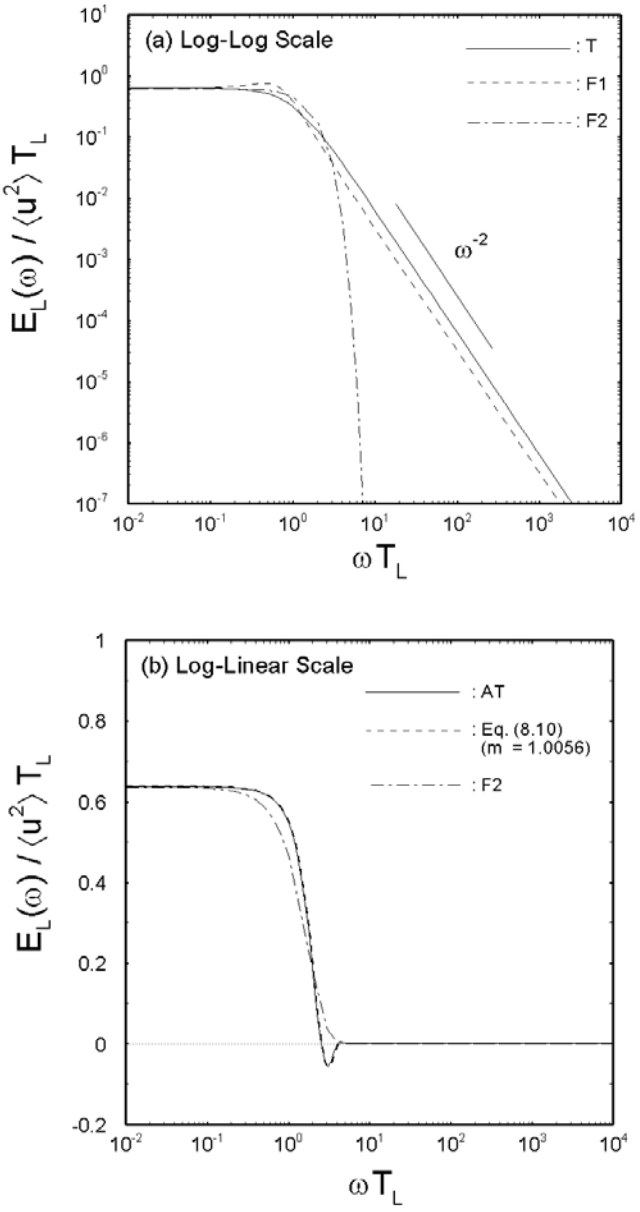

Figure 8-2. Energy spectrum versus frequency: a) T, F1, and F2 on log-log scale and b) AT, Eq. (8.10) with m = 1.0056, and F2 on log-linear scale

In addition, both have given good agreement with various numerical and experimental results. For example, Yeung and Pope (1989) obtained R_L from direct numerical simulations (DNS) of stationary homogeneous turbulence at moderate Reynolds numbers and compared the results with the data measured in grid turbulence by Sato and Yamamoto (1987), finding that the classical exponential form (or T) shows a good fit. Berlemont et al. (1990) however found better agreement when using F1 in the computer program PALAS (PArticle LAgrangian Simulation) with the experimental data from a turbulent pipe flow by Taylor and Middleman (1974). For F2, although most of the requirements are met, it does not agree with K41 theory. For AT, it suffers from lack of a well-defined T_L, disagreement with K41 theory, and its spectrum being negative for some frequencies. The first problem of AT may be remedied as follows: Let C denote the ratio of T_L to the integral of the right-hand-side term in Eq. (8.9) (i.e. $C \approx 0.9996^{-1} \approx 1.0004$). Then, AT can be rewritten by

$$R_L(\tau) = C \exp\left(\frac{-\pi \tau^2}{8 T_L^2} \right) \cos\left(\frac{\tau^2}{2 T_L^2} \right). \tag{8.16}$$

Nevertheless, this remedy still does not satisfy K41 theory and the non-negativity of the energy spectrum.

Acknowledgements

The useful comments of anonymous reviewers were appreciated. This work was supported by the U.S. EPA under Contract No. CR827327-01.

Appendix

From Gradshteyn and Ryzhik (2000, p.483 and 488),

$$\int_0^\infty \exp(-\beta x^2)\cos(Bx)\,\mathrm{d}x = \frac{1}{2}\sqrt{\frac{\pi}{\beta}}\exp\left(\frac{-B^2}{4\beta}\right) \quad (\text{for } \beta > 0), \tag{8A.1}$$

$$\int_0^\infty \exp(-\beta x^2)\cos(Ax^2)\,\mathrm{d}x = \frac{\sqrt{\pi}}{2\sqrt[4]{\beta^2 + A^2}}\cos\left[\frac{1}{2}\arctan\left(\frac{A}{\beta}\right)\right] \tag{8A.2}$$

$$= \sqrt{\frac{\pi}{8}}\sqrt{\frac{\sqrt{\beta^2 + A^2} + \beta}{\beta^2 + A^2}} \quad (\text{for } \beta,\ A > 0), \quad \text{and}$$

$$\int_0^\infty \exp(-\beta x^2)\cos(Ax^2)\cos(Bx)\,\mathrm{d}x = \frac{\sqrt{\pi}}{2\sqrt[4]{\beta^2 + A^2}}\exp\left[\frac{-\beta B^2}{4(\beta^2 + A^2)}\right] \tag{8A.3}$$

$$\times\cos\left[\frac{1}{2}\arctan\left(\frac{A}{\beta}\right) - \frac{AB^2}{4(\beta^2 + A^2)}\right] \quad (\text{for } \beta,\ A,\ B > 0).$$

References

Altinsoy, N., Tuğrul, A. B. (2002) A new proposal for Lagrangian correlation coefficient. Int. J. Heat Fluid Fl. 23, 766-768.

Berlemont, A., Desjonqueres, P., Gouesbet, G. (1990) Particle Lagrangian simulation in turbulent flows. Int. J. Multiphase Flow 16, 19-34.

Bracewell, R. N. (2000) The Fourier Transform and its Applications. McGraw-Hill, Boston.

Frenkiel, F. N. (1953) Turbulent diffusion: Mean concentration distribution in a flow field of homogeneous turbulence. Adv. Appl. Mech. 3, 61-107.

Gradshteyn, I. S., Ryzhik, I. M. (2000) Table of integrals, series, and products. Academic Press, San Diego.

Hinze, J. O. (1975) Turbulence. McGraw Hill, New York.

Kolmogorov, A. N. (1941) The local structure of turbulence in incompressible viscous fluid for very large Reynolds numbers. Dokl. Akad. Nauk. 30, 301-305.

Pope, S. B. (2000) Turbulent flows. Cambridge University Press, Cambridge, U.K.

Sato, Y., Yamamoto, K. (1987) Lagrangian measurement of fluid-particle motion in an isotropic turbulent field. J. Fluid Mech. 175, 183-199.

Sawford, B. L. (1991) Reynolds number effects in Lagrangian stochastic models of turbulent dispersion. Phys. Fluids 3, 1577-1586.

Taylor, G. I. (1921) Diffusion by continuous movements. Proc. Lond. Math. Soc. 20, 196-211.

Taylor, A. R., Middleman, S. (1974) Turbulent dispersion in drag-reducing fluids. AIChE 20, 454-461.

Tennekes, H. (1979) The exponential Lagrangian correlation function and turbulent diffusion in the inertial subrange. Atmos. Environ. 12, 1565-1567.

Tennekes, H., Lumley, J. L. (1972) A first course in turbulence. MIT Press, Cambridge.

Yeung, P. K., Pope, S. B. (1989) Lagrangian statistics from direct numerical simulations of isotropic turbulence. J. Fluid Mech. 207, 531-586.

CHAPTER 9

CONCLUSIONS AND RECOMMENDATIONS

The research described herein has applied the technique of Lagrangian particle (or stochastic) modeling to the short-range dispersion of an air pollutant. The motivation behind the research is the development and application of an advanced and accurate modeling tool in determining how an air pollutant disperses downwind from an emission source in order to estimate emission strength and mean concentrations at downwind receptors. Lagrangian particle modeling is a relatively new modeling technique that has been considerably advanced during last fifteen years. Its fundamental principle lies in the assumption that pollutant particles randomly migrate in a turbulent flow. Its major advantages are that it accounts for extensive details of a turbulent flow and that its numerical implementation is straightforward. A tradeoff is computational time that is usually large compared to other modeling approaches (e.g. Gaussian plume modeling). In practice, the applicability of a Lagrangian particle model (LPM) may be limited by lack of complete information to (i) fully parameterize turbulence quantities required by the model and (ii) suggest a valid closure to the model, resorting to some level of interpolation or approximation.

In this thesis, a single-particle, three-dimensional source-receptor LPM was developed for air pollutant dispersion in the atmospheric boundary layer (ABL) where turbulence quantities were determined by similarity-based interpolation formulas chosen from the literature. Due to the assumption of a conservative process (no gain and loss of

a pollutant's mass after release), the emission strength of a source is linearly proportional to the mean concentration at a downwind receptor. Data sets from two field studies, the Rubbertown field study and the Project Prairie Grass (PPG) experiments, were adopted for use in examining the performance of the LPM (Chapter 3). In the Rubbertown field study, large differences in the mean ground-level concentrations (shortly, concentrations) between model predictions and measurements were found but not clearly concluded from a statistical point of view for the reason that the number of available data points were limited and measurement issues (e.g. detection limit questions and measurement accuracy). This inconsistency may be alleviated by the detailed characterization of the field terrain but was not available to this work. The accuracy of basic meteorological parameters (e.g. Monin-Obukhov length and friction velocity) is also important. Errors of their estimates will impact on model results. Various measurement techniques have been proposed for estimating meteorological parameters (van Ulden and Holtslag, 1985). Most meteorological parameters were derived here based on two-height measurements. Using more heights, together with other estimation procedures, will improve the confidence level of their estimates. In the PPG experiments, the model evaluation was statistically reliable due to the availability of a large, robust, and well characterized data set. Satisfactory agreement between model predictions and field data chosen for stable conditions was achieved. The LPM parameterized for the PPG data set was then used as the platform for parametric uncertainty analysis (Chapter 4).

The effects of uncertainties in Monin-Obukhov length, friction velocity, roughness height, mixing height, and the universal constant of the LPM parameterized for the PPG data set on mean ground-level concentrations were intensively examined for

dispersion under slightly and moderately stable conditions. The spatial domain was extended to 3 km downwind from a near-ground continuous point source. The analysis was performed under a probabilistic framework using Monte Carlo simulations with Latin hypercube sampling and linear regression modeling. It has been shown that, among the meteorological parameters, friction velocity is an important input. The uncertainty contributions from Monin-Obukhov length and mixing height are generally not important for most receptors but the importance of both tend to increase when the degree of stability decreases. The universal constant is another influential input because its uncertainty contribution often dominates those from most other inputs. It has however little or no influence for some distances in the crosswind or lateral direction. The overall contribution from roughness height was found to be slight. Additional analysis of the half width of mean ground-level concentration contours downwind from the source suggested that the two largest contributors to uncertainty are the universal constant and Monin-Obukhov length whereas the other inputs do not play a significant role. Important or influential uncertainty contributors reflect the necessity of using their accurate values in the modeling.

In addition, four specific subjects related to the Lagrangian particle modeling were studied, and their conclusions are given as follows: A first study dealt with the analytical formulation of probability density functions (pdfs) of fluid velocity in a turbulent flow that are a central component of the Lagrangian particle modeling, as seen in Chapter 2. The pdf formulation for one velocity component has been quite comprehensive whereas less advance have been achieved for the formulation for more than one velocity component due to mathematical difficulties arising while incorporating

the *a priori* partial knowledge of velocity statistics (i.e. moments) into the formulation. An alternative technique in formulating an analytical form of the joint pdf of velocity has been presented in this thesis (Chapter 5) based on the technique developed by Koehler and Symanowski (1995) (shortly, KS formulation), by which a joint pdf is constructed using the knowledge of marginal distributions of velocity. How to apply the KS technique to developing a joint pdf was demonstrated and discussed. The emphasis was given to atmospheric turbulence under convective conditions where the vertical velocity is assumed to be positively skew and negatively correlated with the horizontal velocity. It has been shown that the technique facilitates a way to formulate a joint pdf using the information of marginal densities and provides high flexibility in fitting a specified correlation between two velocity components. It may be used in practice when marginal densities are well characterized or specified. Usually, the technique yields a large number of possible pdfs given the same information. Thus, selecting a practical or suitable pdf by taking into account higher product cross moments is encouraged.

A second study dealt with analyzing local increments involved in (first-order) LPMs (Chapter 6). Typically, an LPM is essentially built upon a number of assumptions, some of which are directly related to a local time scale (i.e. increment) in which the model proceeds. Several aspects of local increments in a multidimensional single-particle LPM have been analyzed and discussed. The main tools used for the analysis were the algebra of Ito integrals and the Wagner-Platen formula, giving the expanded forms of the statistics of local increments and those related to the diffusion coefficient of the model. The analysis has shown that the form of the diffusion coefficient of the model possesses an intrinsic tendency of anisotropy and velocity dependence, given that the

inertial subrange theory applies. To reduce these effects to good approximation, the magnitude of a local time increment should be (much) smaller than some specific time scales. In addition, the analysis was extended to local numerical increments and errors for the Euler (EL), Milstein (MS), and order-1.5 strong Taylor (ST) schemes, among which the ST scheme is best in terms of accuracy because of the higher level of truncating high-order terms in the scheme. Given the isotropic and velocity-independent diffusion coefficient, the EL and ML schemes become equivalent. The roles of three restriction strategies of time step sizes for the Euler scheme that have been used by some workers have also been examined. It has been shown that two strategies are to constrain time step sizes to be small such that the accuracy of the first- and second-order statistics of Δx_i is ensured. The other strategy corresponds to the restriction of the local time scale of nonstationarity and inhomogeneity of turbulence.

A third study discussed analogy between the diffusion limit of LPMs and the classical theory of turbulent diffusion of Taylor (1921) (Chapter 7). The diffusion limit refers to the asymptotic condition where the local decorrelation time scale of turbulence becomes zero, causing a first-order LPM to reduce to a zeroth-order LPM called a random displacement model (RDM) that is theoretically equivalent to an eddy diffusion model. The method used in performing the asymptotic reduction was the projection formalism. It has been shown that the eddy diffusivity may be theoretically defined as the area under the curve of correlation function versus positive time lag, given that the reduced (i.e. genuine) form of the Fokker-Planck equation defines the local evolution of a particle temporally and spatially.

A fourth study briefly discussed four proposed forms of Lagrangian velocity autocorrelation for stationary homogeneous turbulent diffusion from a classical point of view using a set of mathematical and physical requirements (Chapter 8). The deficiencies of some forms were indicated, such as an ill-defined Lagrangian time scale and the negativity of an energy spectrum for some frequencies.

Finally, as in any research, the work concluded above can be improved, extended, or investigated further beyond the scope that has been done in this thesis. Some recommendations given below suggest what could be pursued for the future work:

- Characterization of a flow field over a non-uniform terrain

  As pointed out in Chapter 3, the LPM used in this study was designed for uniform topography while the actual background terrain in the Rubbertown field study was highly non-uniform, leading to an applicability problem of the LPM in question. Improvement of the modeling process could be done using such information but it was unfortunately not available. Nevertheless, obtaining an actual flow field over a complex or non-uniform terrain is a very difficult task. Although direct measurement is straightforward and desirable, it may not be practical because an intensive measurement network (in both horizontal and vertical planes) and a detailed description of a terrain are required. Indeed, virtually no atmospheric dispersion experiments use such fine spatial instrumentation such that all essential physical processes are characterized. Laboratory-scale, modeled topography with a wind tunnel may be used as an alternative (e.g. Meroney et al., 1999). The LPM results could then be assessed using such data, and the model extended to such cases.

- Incorporation of high-order moments of velocity in the closure of a multidimensional LPM

  For a complex or non-uniform terrain, high-order moments of velocity can play a significant role in the migration of pollutant particles. The LPM considered here was based on a basic closure approach given by Thomson (1987), accounting for the first- and second-order statistics of velocity only. This closure is in fact only suitable for Gaussian turbulence. The advance of assigning a valid closure to a one-dimensional LPM (specifically speaking, the drift coefficient) for non-Gaussian turbulence is well established but this is not the case for multidimensional turbulence. Some workers have gained only slight success in using sophisticated closures for non-Gaussian turbulence and comparing model results with experimental data (Flesch and Wilson, 1992; Leuzzi and Monti, 1998), as mentioned in Chapter 3. Accordingly, this subject still needs to be developed and fulfilled in the future.

- Accuracy of estimating meteorological parameters

  The importance of using the accurate estimates of meteorological parameters was described in detail in Chapter 4. In the Rubbertown field study, most of the basic meteorological parameters used as inputs in the modeling were derived from two-height measurements (i.e. two-point profile method) at a single location, which is inadequate from a statistical point of view. To have more confidence in their estimates, measurements at multiple heights and at multiple locations are needed.

Besides the profile method, other estimation techniques, if available, can be helpful to evaluating the quality of measured data.

- Uncertainty due to using different pdfs formulated by the KS technique

  As said earlier, given specific information of marginal densities of velocity, the KS technique usually offers more than one possible pdf. This is also the case when an additional constraint (i.e. correlation between two velocity components is imposed, as seen in Chapter 5, resulting in a large set of pdfs with different third- (and higher-) order cross product moments. It may be of practical interest to examine uncertainty in particle dispersion using such pdfs.

- Issues of accuracy and computational time using different sets of restriction strategies of time step size in numeral implementation of an LPM

  Schwere et al. (2002) brought up the practical idea of how to speed up the computational time of one-dimensional LPMs based on the elimination or adjustment of some time-consuming steps during implementation by the Euler scheme. In this thesis (Chapter 6), three numerical differencing schemes and various local numerical time scales have been discussed for multidimensional LPMs. Thus, it may be of interest to extend the scope of their work to multidimensional problems, together with incorporating results found here.

- Comparison of uncertainty in mean concentrations due to two different types of Lagrangian particle modeling: zeroth-order and first-order

As said in Chapter 7, a zeroth-order LPM (or a random displacement model) is a simplified version of a first-order LPM. Its numerical implementation is less complicated and less time-consuming. Nevertheless, it has a severe limitation that the local decorrelation time scale at any point of time and space should be small. This can lead to a further investigation of how a zeroth-order LPM suitably can be applied in the context of short-range dispersion and the uncertainty in mean concentrations due to using these two different modeling approaches (i.e. zeroth- and first-order) for different conditions of the atmosphere.

References

Flesch, T. K., Wilson, J. D. (1992) A two-dimensional trajectory-simulation model for non-Gaussian, inhomogeneous turbulence within plant canopies. Boundary-Layer Meteor. 61, 349-374.

Koehler, K. J., Symanowski, J. T. (1995) Constructing multivariate distributions with specific marginal distributions. J. Multivariate Anal. 55, 261-282.

Leuzzi, G., Monti, P. (1998) Particle trajectory simulation of dispersion around a building, Atmos. Environ. 32. 203-214.

Meroney, R. N., Leitl, B. M., Rafailidis, S., Schatzmann, M. (1999) Wind-tunnel and numerical modeling of flow and dispersion about several building shape. J. Wind Eng. Ind. Aerodyn. 81, 333-345.

Monti, P., Leuzzi, G. (1996) A closure to derive a three-dimensional well-mixed trajectory-model for non-Gaussian, inhomogeneous turbulence. Boundary-Layer Meteor. 80, 311-331.

Schwere, S., Stohl, A., Rotach, M. W. (2002) Practical considerations to speed up Lagrangian stochastic particle models. Comput. Geosci. 28, 143-154.

Taylor, G. I. (1921) Diffusion by continuous movements. Proc. Lond. Math. Soc. 20, 196-211.

Thomson, D. J. (1987) Criteria for the selection of stochastic models of particle trajectories in turbulent flows. J. Fluid Mech. 180, 529-556.

van Ulden, A., Holtslag, A. (1985) Estimation of atmospheric boundary layer parameters for diffusion applications. J. Climate Appl. Meteor. 24, 1196-1207.

LITERATURE CITED

Akhiezer, N. I, Glazman, I. M. (1993) Theory of Linear Operators in Hilbert Space. Vol. 1, Dover Publications, New York.

Alcomo, J., Bartnicki, J. (1987) A framework for error analysis of a long-range transport model with emphasis on parameter uncertainty. Atmos. Environ. 21, 2121-2131.

Altinsoy, N., Tuğrul, A. B. (2002) A new proposal for Lagrangian correlation coefficient. Int. J. Heat Fluid Fl. 23, 766-768.

Anfossi, D., Ferrero, E., Sacchetti, D., Trini Castelli, S. (1997) Comparison among empirical probability density functions of the vertical velocity in the surface layer based on higher order correlations. Boundary-Layer Meteor. 82, 193-218.

Arya, S. P. S. (1984) Parametric relations for the atmospheric boundary layer. Boundary-Layer Meteor. 30, 57-73.

Baerentsen J. H., Berkowicz, R. (1984) Monte Carlo simulation of plume dispersion in the convective boundary layer. Atmos. Environ. 18, 701-712.

Barad, M. L. (Editor) (1958) Project Prairie Grass, A Field Program in Diffusion. Vol. 1. Geographical Research Paper No. 59, Air Force Cambridge Research Center, Belford, Massachusetts.

Barlow, R. E., Proschan, F. (1975) Statistical Theory of Reliability and Life Testing. Holt, Rinehart and Winston, New York.

Benkley, C. W., Schulman, L. L. (1979) Estimation hourly mixing depth from historical meteorological data. J. Appl. Meteor. 18, 772-780.

Bergin, M. S., Noblet,, G. S., Petrini, K., Dhieux, J. R. , Milford, J. B., Harley, R. A. (1999) Formal uncertainty analysis of a Lagrangian photochemical air pollution model. Environ. Sci. Tech. 33, 1116-1126.

Berlemont, A., Desjonqueres, P., Gouesbet, G. (1990) Particle Lagrangian simulation in turbulent flows. Int. J. Multiphase Flow 16, 19-34.

Borgas, M. S., Sawford, B. L. (1991) The small-scale structure of acceleration correlations and its role in the statistical theory of turbulent dispersion. J. Fluid Mech. 228, 295-320.

Bracewell, R. N. (2000) The Fourier Transform and its Applications. McGraw-Hill, Boston.

Briggs, G. A. (1972) Diffusion Estimation for Small Emissions. In ERL, ARL USAEC Report ATDL-106, U.S. Atomic Energy Commission, Oak Ridge, Tennessee.

Briggs, G. A. (1982) Similarity forms for ground-source surface-layer diffusion. Boundary-Layer Meteor. 23, 489-502.

Brost, R. A., Wyngaard, J. C. (1978) A model study of the stably stratified planetary boundary layer. J. Atmos. Sci. 35, 1427-1440.

Caputo, A. (1998) Some properties of the family of Koehler-Symanowski distributions. The Collaborative Research Center (SFB) 386, Discussion Paper No. 103, University of Munich.

Chaturvedi. S., Shibata, F. (1979) Time-convolutionless projection operator formalism for elimination of fast variables. Applications to Brownian motion. Z. Physik B 35, 297-308.

Dabberdt, W. F., Miller, E. (2000) Uncertainty, ensembles and air quality dispersion modeling: Applications and challenges. Atmos. Environ. 34, 4667-4673.

Dall'Aglio, G. (1972) Fréchet classes and compatibility of distribution functions. Symp. Math. 9, 131-150.

Degrazia, G., Anfossi, D. (1998) Estimation of the Kolmogorov constant C_o from classical statistical diffusion theory. Atmos. Environ. 32, 3611-3614.

Derwent, R. G. (1987) Treating uncertainty in models of the atmospheric chemistry of nitrogen compounds. Atmos. Environ. 21, 1445-1454.

Dias, N. L., Brutsaert, W., Wesely, M. L. (1995) Z-less stratification under stable conditions. Boundary-Layer Meteor. 75, 175-187.

Dreeben, T. D., Pope, S. B. (1998) Probability density function/Monte Carlo simulation of near-wall turbulent flows. J. Fluid Mech. 357, 141-166.

Du, S., Sawford, B. L., Wilson, J. D., Wilson, D. J. (1995) Estimation of the Kolmogorov constant (C_o) for the Lagrangian structure function, using a second-order Lagrangian model of grid turbulence. Phys. Fluids 7, 3083-3090.

Du, S., Wilson, J. D., Yee, E. (1994) Probability density functions for velocity in the convective boundary layer and implied trajectory models. Atmos. Environ. 28, 1211-1217.

Durbin, P. A. (1983) Stochastic Differential Equations and Turbulent Dispersion. NASA Ref. Pub.1103.

Durbin, P. A. (1984) Comments on papers by Wilson et al. (1981) and Legg and Raupach (1982). Boundary-Layer Meteor. 29, 409-411.

Einstein, A. (1905) Uber die von der molekularkinetischen Theorie der Warme geforderte Bewegung von in ruhenden Flussigkeiten suspendierten Teilchen. Ann. der Physik, 17, 549-560.

Flesch, T. K., Wilson, J. D. (1992) A two-dimensional trajectory-simulation model for non-Gaussian, inhomogeneous turbulence within plant canopies. Boundary-Layer Meteor. 61, 349-374.

Flesch, T. K., Wilson, J. D., Yee, E. (1995) Backward-time Lagrangian stochastic dispersion models and their application to estimate gaseous emissions. J. Appl. Meteor. 34, 1320-1332.

Fréchet, M. (1951) Sur les tableaux de corrélation dont les marges sont données. Ann. Univ. Lyon., Sci. 14, 53-77.

Freeman, D. L., Egami, R. T., Robinson, N. F., Watson, J. G. (1986) A method for propagating measurement uncertainties through dispersion models. JAPCA 36, 246-253.

Frenkiel, F. N. (1953) Turbulent diffusion: Mean concentration distribution in a flow field of homogeneous turbulence. Adv. Appl. Mech. 3, 61-107.

Gaines, J. G., Lyons, T. J. (1994) Random generation of stochastic area integrals. SIAM J. Appl. Math. 54, 1132-1146.

Gardiner, C. W. (1997) Handbook of Stochastic Methods. Springer, New York.

Gradshteyn, I. S., Ryzhik, I. M. (2000) Table of integrals, series, and products. Academic Press, San Diego.

Grossmann, S., Thomae, S. (1982) Correlation decay of Lagrangian velocity differences in locally isotropic turbulence. Z. Phys. B 49, 253-261.

GTRI (2001) Remote Sensing Technology to Support the Toxics Release Inventory. Technical Report, Georgia Tech Research Institute, Atlanta.

Hanna, S. R. (1982) Applications in air pollution modeling. in Atmospheric Turbulence and Air Pollution Modelling, edited by Nieuwstadt, F. T. M. and van Dop, H., D. Reidel Publishing, 37-68.

Hanna, S. R., Chang, J. C., Fernau, M. E. (1998) Monte Carlo estimates of uncertainties in predictions by a photochemical grid model (UAM-IV) due to uncertainties in input variables. Atmos. Environ. 32, 3619-3628.

Hanna, S. R., Paine, R. J. (1989) Hybrid plume dispersion model (HPDM) development and evaluation. J. Appl. Meteor. 21, 206-224.

Helton, J. C. and Davis, F. J. (2002) Illustration of sampling-based methods for uncertainty and sensitivity analysis. Risk Analysis 22, 591-622.

Heppe, B. M. O. (1998) Generalized Langevin equation for relative turbulent dispersion. J. Fluid Mech. 357, 167-198.

Hinze, J. O. (1975) Turbulence. McGraw Hill, New York.

Holtslag, A. A. M., Nieuwstadt, F. T. M. (1986) Scaling the atmospheric boundary layer. Boundary-Layer Meteor. 36, 201-209.

Iman, R. L., Shortencarier, M. J. (1984) A FORTRAN 77 Program and User's Guide for the Generation of Latin Hypercube and Random Samples for Use with Computer Models. NUREG/CR-3624 (SAND83-2365), Sandia National Laboratories, Albuquerque, New Mexico.

Irwin, J. S., Rao, S. T., Petersen, W. B., Turner, D. B. (1987) Relating error bounds for maximum concentration estimates to diffusion meteorology uncertainty. Atmos. Environ. 21, 1927-1937.

Isukapalli S. S., Roy, A., Georgopoulos, P. G. (1998) Stochastic response surface methods (SRSMs) for uncertainty characterization and propagation: application to environmental and biological systems. Risk Analysis 18, 351-363.

Johnson, M. E. (1987) Multivariate Statistical Simulation. Wiley, New York.

Kemp, J. F. (1963) Advanced problem No. 5894. Am. Math. Mon. 80, 73. (Solution by Blyth. C. R., Am. Math. Mon. 80, 413).

Kloeden, P. E., Platen, E. (1989) A survey of numerical methods for stochastic differential equations. Stoch. Hydrol. Hydraul. 3, 155-178.

Kloeden, P. E., Platen, E. (1991) Relations between multiple Ito and Strotonovich integrals. Stochastic Anal. Appl. 9, 311-321.

Kloeden, P. E., Platen, E., Wright, I. W. (1992) The approximation of multiple stochastic integrals. Stochastic Anal. Appl. 10, 431-441.

Koehler, K. J. and Symanowski, J. T. (1995) Constructing multivariate distributions with specific marginal distributions. J. Multivariate Anal. 55, 261-282.

Kolmogorov, A. N. (1941) The local structure of turbulence in incompressible viscous fluid for very large Reynolds numbers. Dokl. Akad. Nauk. 30, 301-305.

Kotz, S., Balakrishnan, N., Johnson, N. L. (2000) Continuous Multivariate Distributions. Vol. 1: Models and Applications. Wiley, New York.

Langevin, P. (1908) Sur la th'eorie du mouvement brownien. Comptes. Rendues, 146, 530-533.

Law, A. M., Kelton, W. D. (2000) Simulation Modeling and Analysis. McGraw-Hill, Boston, Massachusetts.

Legg, B. J., Raupach, M. R. (1982) Markov-chain simulation of particle dispersion in inhomogeneous flows: The mean drift velocity induced by a gradient in Eulerian velocity variance. Boundary-Layer Meteor. 24, 3-13.

Lena, F., Desiato, F. (1999) Intercomparison of nocturnal mixing height estimate methods for urban air pollution modeling. Atmos. Environ. 33, 2385-2393.

Lenschow, D. H., Li, X. S., Zhu, C. J., Stankov, B. B. (1988) The stably stratified boundary layer over the Great Plains. I. Mean and turbulence structure. Boundary-Layer Meteor. 42, 95-121.

Leuzzi, G., Monti, P. (1998) Particle trajectory simulation of dispersion around a building, Atmos. Environ. 32. 203-214.

Lewellen, W. S., Sykes, R. I. (1989) Meteorological data needs for modeling air quality uncertainties. J. Atmos. Ocean. Tech. 6, 759-768.

Li, C. W., Liu, X. Q. (1997) Approximation of multiple stochastic integrals and its application to stochastic differential equations. Nonlinear Anal.-Theor. 30, 697-708.

Luhar, A. K., Britter, R. E. (1989) A random walk model for dispersion in inhomogeneous turbulence in a convective boundary layer. Atmos. Environ. 23, 1911-1924.

Luhar, A. K., Hibberd, M. F., Hurley, P. J. (1996) Comparison of closure schemes used to specify the velocity PDF in Lagrangian stochastic dispersion models for convective conditions. Atmos. Environ. 30, 1407-1418.

Marshall, A. W., Olkin, I. (1988) Families of multivariate distributions. J. Amer. Statist. Assoc. 83, 834-841.

Maurizi, A., Tampieri, F. (1999) Velocity probability density functions in Lagrangian dispersion models for inhomogeneous turbulence. Atmos. Environ. 33, 281-289.

McKay, M. D., Beckman, R. J., Conover, W. J. (1979) A comparison of three methods for selecting values of input variables in the analysis of output from a computer code. Technometrics 21, 239-245.

McRae, G. J., Tilden, J. W., Seinfeld, J. H. (1981) Global sensitivity analysis - A computational implementation of the Fourier amplitude sensitivity test (FAST). Comput. Chem. Eng. 6, 15-25.

Meroney, R. N., Leitl, B. M., Rafailidis, S., Schatzmann, M. (1999) Wind-tunnel and numerical modeling of flow and dispersion about several building shape. J. Wind Eng. Ind. Aerodyn. 81, 333-345.

Monin, A. S., Yaglom, A. M. (1975) Statistical Fluid Mechanics. Vol. 2, MIT Press, Cambridge, Massachusetts.

Monti, P., Leuzzi, G. (1996) A closure to derive a three-dimensional well-mixed trajectory-model for non-Gaussian, inhomogeneous turbulence. Boundary-Layer Meteor. 80, 311-331.

Morgan, M., Henrion M. (1990) Uncertainty: A Guide to Dealing with Uncertainty in Quantitative Risk and Policy Analysis. Cambridge University Press, Cambridge.

Mori, H. (1965) Transport, collective motion, and Brownian motion. Prog. Theor. Phys. 33, 423-455.

Nakajima, S. (1958) On quantum theory of transport phenomena. Prog. Theor. Phys. 20, 948-959.

Naslund, E., Rodean, H. C., Nasstrom, J. S. (1994) A comparison between two stochastic diffusion models. Boundary-Layer Meteor. 67, 369-384.

NCRP (1996) A Guide for Uncertainty Analysis in Dose and Risk Assessments Related to Environmental Contamination. NCRP Commentary No. 14, Edited by Hoffman, E. A., National Council on Radiation Protection and Measurements, Bethesda, Maryland.

Neter, J., Wasserman, W.. Kutner, M. H., Nachtschiem, C. J. (1996) Applied Linear Statistical Models. McGraw-Hill, Boston, Massachusetts

Nieuwstadt, F. T. M. (1984) The turbulent structure of the stable, nocturnal boundary layer. J. Atmos. Sci. 41, 2202-2216.

O'Neil, P. V. (1995) Advanced Engineering Mathematics. Brooks/Cole Publishing, Pacific Grove, California.

Obukhov, A. M. (1959) Description of turbulence in terms of Lagrangian variables. Adv. Geophys., 6, 113-116.

Øksendal, B. (2000) Stochastic Differential Equations. Springer, New York.

Panofsky, H. A., Dutton, J. A. (1984) Atmospheric Turbulence: Models and Methods for Engineering Applications. Wiley, New York.

Pasquill, F., Smith, F. B. (1983) Atmospheric Diffusion. John Wiley & Sons, New York.

Platen, E., Wagner, W. (1982) On a Taylor formula for a class of Ito processes. Prob. Math. Statist. 3, 37-51.

Pope, S. B. (1985) PDF methods of turbulent reactive flows. Prog. Energy Combust. Sci., 11, 119-192.

Pope, S. B. (1987) Consistency conditions for random-walk models of turbulent dispersion. Phys. Fluids, 30, 2374-2379.

Pope, S. B. (1994) Lagrangian PDF methods for turbulent flows. Annu. Rev. Fluid Mech. 26, 23-63.

Pope, S. B. (2000) Turbulent Flows. Cambridge University Press, Cambridge.

Pope, S. B. (2002) Stochastic Lagrangian models for velocity in homogeneous turbulent shear flow. Phys. Fluids 14, 1696-1702.

Press, W. H., Teukolsky, S. A., Vetterling, W. T., Flannery, B. P. (1992) Numerical Recipes in FORTRAN. Cambridge University Press, Cambridge.

Rao, K. S. (1999) Lagrangian stochastic modeling of dispersion in the stable boundary layer. Boundary-Layer Meteor. 90, 541-549.

Richardson, L. F. (1926) Atmospheric diffusion shown on a distance-neighbor graph. Proc. Roy. Soc. Lond. A, 110, 709-737.

Risken, H. (1996) The Fokker-Planck Equation. Springer, New York.

Rodean, H. C. (1991) The universal constant for the Lagrangian structure function. Phys. Fluids. 3, 1479-14780.

Rodean, H. C. (1996) Stochastic Lagrangian Models of Turbulent Diffusion. Monograph No. 48, American Meteorological Society, Boston, Massachusetts.

Rotach, M. W., Gryning, S. E., Tassone, C. (1996) A two-dimensional Lagrangian stochastic dispersion model for daytime conditions. Q. J. R. Meteorol. Soc. 122, 367-389.

Russell, A. G., Dennis, R. L. (2000) NARSTO critical review of photochemical models and modeling. Atmos. Environ. 34, 2283-2324.

Sato, Y., Yamamoto, K. (1987) Lagrangian measurement of fluid-particle motion in an isotropic turbulent field. J. Fluid Mech. 175, 183-199.

Sawford, B. L. (1985) Lagrangian statistical simulation of concentration mean and fluctuation fields. J. Appl. Meteor., 24, 1152-1166.

Sawford, B. L. (1991) Reynolds number effects in Lagrangian stochastic models of turbulent dispersion. Phys. Fluids 3, 1577-1586.

Sawford, B. L. (1993) Recent developments in the Lagrangian stochastic theory of turbulent dispersion. Boundary-Layer Meteor., 62, 197-215.

Schnelle, K. B., Dey, P. R. (2000) Atmospheric Dispersion Modeling Compliance Guide. McGraw-Hill, New York.

Schwere, S., Stohl, A., Rotach, M. W. (2002) Practical considerations to speed up Lagrangian stochastic particle models. Comput. Geosci. 28, 143-154.

Smoluchowski, M. von (1906) Zur kinetischen Theorie der Brownschen Molekularbewegung und der Suspensionen. Ann. Phys., 21, 756-780.

Sorbjan, Z. (1986) On similarity in the atmospheric boundary layer. Boundary-Layer Meteor. 34, 377-397.

Sykes, R. I., Lewellen, W. S., Parker, S. F. (1984) A turbulent transport model for concentration fluctuations and fluxes, J. Fluid Mech. 139, 193-218.

Tatang, M. A., Pan, W., Prinn, R. G., McRae, G. J. (1997) An efficient method for parametric uncertainty analysis of numerical geophysical models. J. Geophysic. Res. 102, 21,925-21,932.

Taylor, A. R., Middleman, S. (1974) Turbulent dispersion in drag-reducing fluids. AIChE 20, 454-461.

Taylor, G. I. (1921) Diffusion by continuous movements. Proc. Lond. Math. Soc. 20, 196-211.

Tennekes, H. (1979) The exponential Lagrangian correlation function and turbulent diffusion in the inertial subrange. Atmos. Environ. 12, 1565-1567.

Tennekes, H., Lumley, J. L. (1972) A first course in turbulence. MIT Press, Cambridge.

Thomson, D. J. (1987) Criteria for the selection of stochastic models of particle trajectories in turbulent flows. J. Fluid Mech. 180, 529-556.

Thomson, D. J., Montgomery, M. R. (1994) Reflection boundary conditions for random walk models of dispersion in non-Gaussian turbulence. Atmos. Environ. 12, 1981-1987.

Thomson, D. J. (1990) A Stochastic model for the motion of particle pairs in isotropic high-Reynolds-number turbulence, and its application to the problem of concentration variance. J. Fluid Mech., 210, 113-153.

Turner, D. B. (1970) Workbook of Atmospheric Dispersion Estimates. U. S. EPA, Office of Air Programs, Research Triangle Park, North Carolina.

U. S. EPA (2004) Support center for regulatory air models (SCRAM). http://www.epa.gov/ttn/scram.

van Ulden, A. P. (1978) Simple estimates for vertical diffusion from sources near the ground. Atmos. Environ. 12, 2125-2129.

van Ulden, A., Holtslag, A. (1985) Estimation of atmospheric boundary layer parameters for diffusion applications. J. Climate Appl. Meteor. 24, 1196-1207.

Venkatram, A., Du, S. (1997) An analysis of the asymptotic behavior of cross-wind-integrated ground-level concentrations using Lagrangian stochastic simulation. Atmos. Environ. 31, 1467-1476.

Wagner, W., Platen, E. (1978) Approximation of Ito integral equations. Preprint ZIMM, Akad. Wissenschaften, DDR, Berlin.

Weil, J. C. (1990), A diagnosis of the asymmetry in top-down bottom-up diffusion using a Lagrangian stochastic model, J. Atmos. Sci., 47, 501-515.

Wilczak, J. M., Phillips, M. S. (1984) An indirect estimation of convective boundary layer structure for use in routine dispersion models. EPA-600/3-84-091, U.S. EPA, Research Triangle Park, North Carolina.

Wilson, J. D, Thurtell, G. W., Kidd, G. E. (1981) Numerical simulation of particle trajectories in inhomogeneous turbulence Part II: Systems with variable turbulence velocity variance. Boundary-Layer Meteor. 21, 423-441.

Wilson, J. D., Flesch, T. K. (1993) Flow boundaries in random-flight dispersion models: enforcing the well-mixed condition. J. Appl. Meteor. 32, 1695-1707.

Wilson, J. D., Sawford, B. L. (1996) Review of Lagrangian stochastic models for trajectories in the turbulent atmosphere. Boundary-Layer Meteor. 78, 191-210.

Wilson, J. D., Zhuang, Y. (1989) Restriction on the timestep to be used in stochastic Lagrangian models of turbulent dispersion. Boundary-Layer Meteor. 49, 309-316.

Yang, Y.-J., Milford, J. B. (1996) Quantification of uncertainty in reactivity adjustment factors from reformulated gasolines and methanol fuels. Environ. Sci. Technol. 30, 196-203.

Yegnan, A., Williamson, D. G. and Graettinger, A. J. (2002) Uncertainty analysis in air dispersion modeling. Env. Model. Software 17, 639-649.

Yeung, P. K., Pope, S. B. (1989) Lagrangian statistics from direct numerical simulations of isotropic turbulence. J. Fluid Mech. 207, 531-586.

Zilitinkevich, S. S. (1972) On the determination of the height of the Ekman boundary layer. Boundary-Layer Meteor. 3, 141-145.

Zwanzig, R. (1960) Ensemble method in the theory of irreversibility. J. Chem. Phys. 33, 1338-1341.

APPENDIX A

TIMES SERIES OF DATA FROM THE RUBBERTOWN FIELD STUDY

The time series of wind, temperature, and heat flux data collected at the Chickasaw Park and processed by the GTRI team during the afternoon of June 23, 2000 are provided below. In the figures, *u*, *v*, and *w* are the velocity components in along-wind, crosswind, and vertical directions, respectively, while *z*, *T* and $\langle w'T' \rangle$ are the measurement height, the temperature, and the heat flux, respectively. Extreme values (i.e. outliers) were removed from the original datasets. Missing data points appear in some time series and are not used in calculation.

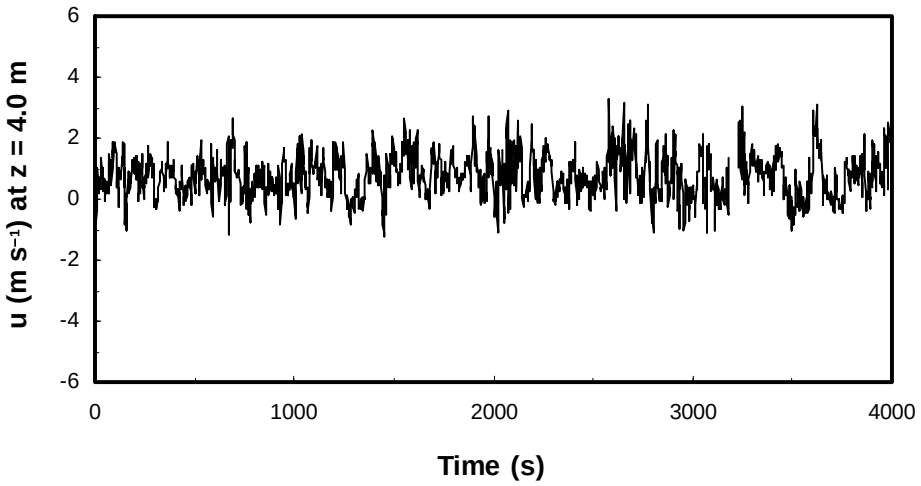

Figure A-1. Time series of *u* by the ultrasonic anemometer at $z = 4.0$ m

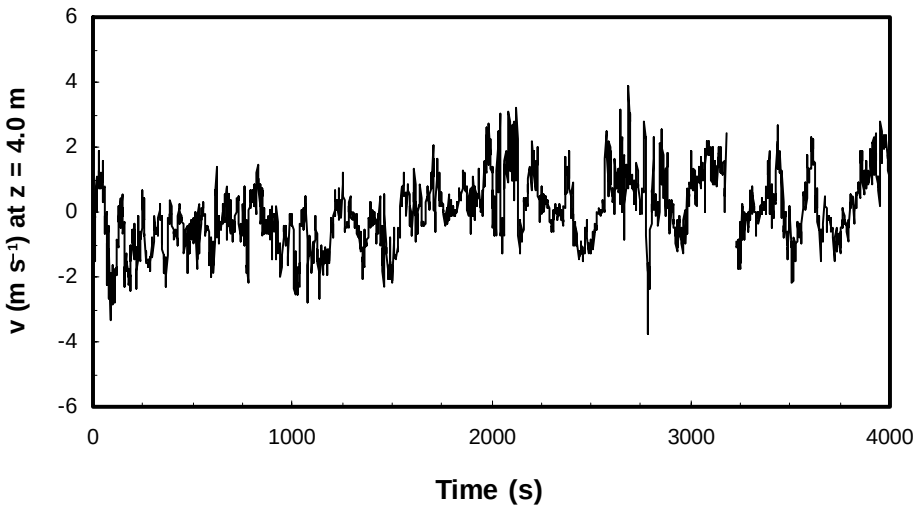

Figure A-2. Time series of *v* by the ultrasonic anemometer at $z = 4.0$ m

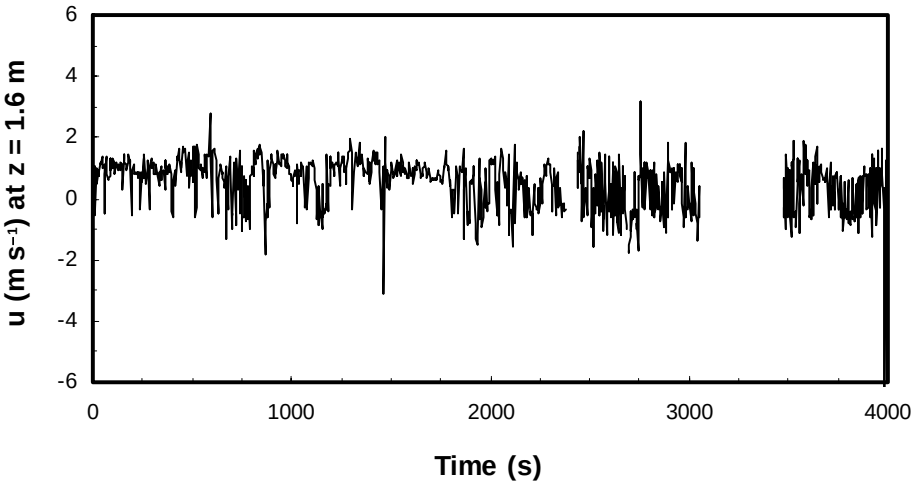

Figure A-3. Time series of *u* by the laser wind sensor at $z = 1.6$ m

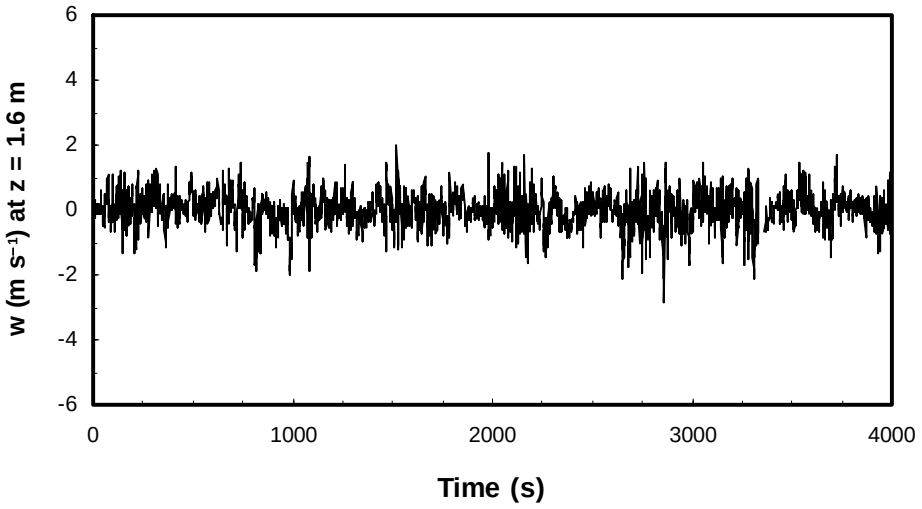

Figure A-4. Time series of *w* by the ultrasonic anemometer at $z = 1.6$ m

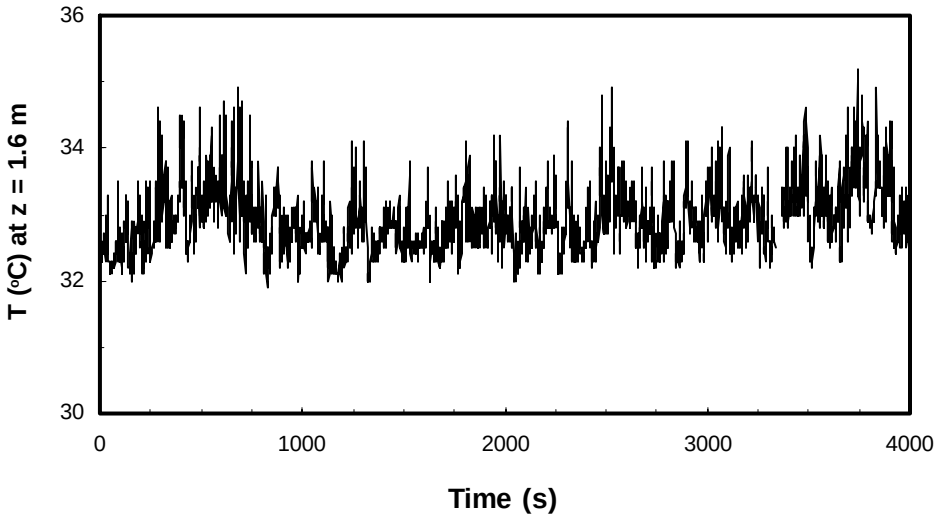

Figure A-5. Time series of *T* by the ultrasonic anemometer at $z = 1.6$ m

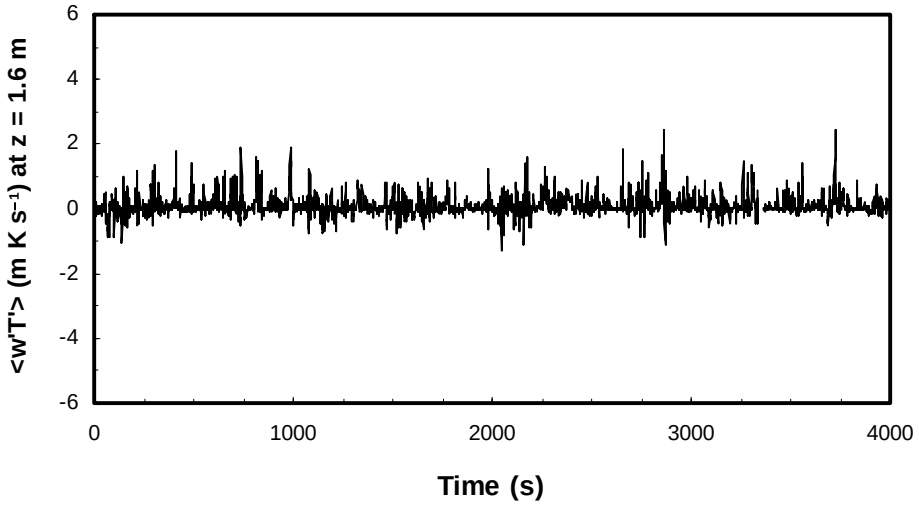

Figure A-6. Time series of $\langle w'T' \rangle$ by the ultrasonic anemometer at z = 1.6 m

APPENDIX B

DATA FROM THE PROJECT PRAIRIE GRASS EXPERIMENTS

The concentration and meteorological data preprocessed for 25 runs chosen from the Project Prairie Grass (PPG) experiments for model evaluation are given below. The former data are from the PPG report of Barad (1958), and the latter data are from van Ulden (1978).

Notations:
Q: Emission Rate
L: Monin-Obukhov Length
u_*: Friction Velocity
z_o: Roughness Height
θ: MeanWind Direction
(= 180 deg. at Pole 45 for arcs 50-400 m and at Pole 90 for arc 800 m)

Source Type	Continuous, Point
Terrian	Flat, Smooth
Source Height (m)	0.46
z_o (m)	0.008
Concentration Unit	mg m^{-3}

No	1	Average θ (deg.)	183.0	L (m)	48	
PPG Run No.	17	Q (g s^{-1})	56.5	u_* (m s^{-1})	0.21	
Pole	Arc at 50 m	Arc at 100 m	Arc at 200 m	Arc at 400 m	Pole	Arc at 800 m
37	0.160				82	0.085
38	1.40	0.030			83	0.435
39	20.1	0.345			84	1.86
40	54.3	2.96	0.110	0.025	85	4.94
41	159	20.1	1.84	0.150	86	8.09
42	302	76.2	13.4	2.03	87	9.74
43	518	177	46.8	13.1	88	9.04
44	633	269	83.2	26.9	89	6.28
45	645	254	86.2	25.7	90	2.98
46	561	164	46.0	8.63	91	0.755
47	330	90.6	14.4	1.11	92	0.285
48	195	33.2	2.70		93	0.035
49	106	8.93	0.245			
50	29.4	1.00				
51	8.72	0.090				
52	1.19					
53	0.235					

No	2	Average θ (deg.)	188.0	L (m)	25	
PPG Run No.	18	Q (g s^{-1})	57.6	u_* (m s^{-1})	0.20	
Pole	Arc at 50 m	Arc at 100 m	Arc at 200 m	Arc at 400 m	Pole	Arc at 800 m
39	0.095				89	0.040
40	0.645				90	0.665
41	5.57	0.095			91	5.04
42	29.6	1.59	0.025		92	11.6
43	106	17.1	0.730		93	14.0
44	218	69.6	14.3	0.640	94	11.3
45	368	158	50.9	11.7	95	8.49
46	584	257	95.0	32.3	96	8.34
47	620	242	82.4	29.5	97	9.35
48	615	177	51.4	17.9	98	6.86
49	467	152	52.0	16.8	99	2.38
50	321	118	31.6	8.56	100	0.435
51	206	42.2	6.64	0.695	101	0.080
52	72.6	6.66	0.545	0.055	102	0.075
53	17.4	0.783	0.065		103	0.035
54	3.15	0.085				
55	1.49					
55	0.025					

No	3	Average θ (deg.)	180.0	L (m)	172	
PPG Run No.	21	Q (g s^{-1})	50.9	u_* (m s^{-1})	0.38	
Pole	Arc at 50 m	Arc at 100 m	Arc at 200 m	Arc at 400 m	Pole	Arc at 800 m
34	0.230				78	0.020
35	0.925				79	0.215
36	2.55	0.025			80	0.595
37	6.63	0.380			81	0.915
38	15.6	2.39	0.040		82	1.26
39	39.3	8.70	0.975	0.095	83	1.11
40	66.5	22.5	5.29	1.11	84	1.46
41	131	41.0	11.6	3.22	85	2.31
42	210	65.9	19.1	4.72	86	3.03
43	267	91.7	27.1	8.37	87	3.26
44	275	96.6	29.6	9.03	88	2.95
45	255	91.5	27.6	8.43	89	1.99
46	201	66.3	17.1	2.18	90	0.955
47	129	34.7	4.98	0.485	91	0.280
48	76.2	12.0	1.51	0.035	92	0.075
49	35.6	1.83	0.140			
50	10.6	0.415				
51	1.36	0.085				
52	0.110					
53	0.025					
54	0.045					

No	4	Average θ (deg.)	176.0	L (m)	204	
PPG Run No.	22	Q (g s^{-1})	48.4	u_* (m s^{-1})	0.46	
Pole	Arc at 50 m	Arc at 100 m	Arc at 200 m	Arc at 400 m	Pole	Arc at 800 m
33	0.235				78	0.015
34	1.56				79	0.040
35	4.65	0.035			80	0.305
36	11.7	0.865			81	0.685
37	27.0	4.22	0.060		82	2.13
38	59.0	11.4	1.04		83	2.51
39	117	30.8	5.92	0.230	84	2.31
40	170	55.8	14.4	2.37	85	1.74
41	213	78.5	25.5	7.11	86	0.865
42	224	81.8	27.7	8.64	87	0.450
43	200	60.3	16.3	4.75	88	0.205
44	143	33.8	7.45	1.71	89	0.075
45	84.6	16.7	3.75	0.695	90	0.020
46	37.4	6.78	0.895	0.065		
47	18.5	2.24	0.265			
48	7.08	0.480	0.070			
49	2.60	0.080	0.020			
50	0.750					
51	0.185					
52	0.030					

No	5	Average θ (deg.)	128.0	L (m)	193	
PPG Run No.	23	Q (g s^{-1})	40.9	u_* (m s^{-1})	0.39	
Pole	Arc at 50 m	Arc at 100 m	Arc at 200 m	Arc at 400 m	Pole	Arc at 800 m
10	0.060				31	0.035
11	0.670				32	0.165
12	3.42	0.045			33	0.260
13	9.87	1.18			34	0.595
14	33.6	5.04	0.120		35	1.24
15	69.6	15.6	1.66	0.050	36	1.87
16	95.0	32.9	7.95	0.740	37	2.09
17	124	43.7	13.7	1.51	38	1.66
18	145	52.8	18.1	4.81	39	1.34
19	170	61.7	19.5	6.36	40	1.15
20	176	55.2	16.8	3.94	41	0.875
21	136	40.4	10.6	2.71	42	0.485
22	94.7	23.7	5.82	1.77	43	0.345
23	54.9	14.3	4.49	0.810	44	0.125
24	24.5	8.39	2.20	0.245		
25	16.4	3.84	0.555	0.049		
26	7.53	1.42	0.080			
27	3.60	0.360	0.025			
28	1.48	0.080	0.025			
29	0.300					
30	0.185					
31	0.045					

No	6	Average θ (deg.)	141.0	L (m)	248	
PPG Run No.	24	Q (g s^{-1})	41.2	u_* (m s^{-1})	0.38	
Pole	Arc at 50 m	Arc at 100 m	Arc at 200 m	Arc at 400 m	Pole	Arc at 800 m
15	0.040				46	0.110
16	0.130				47	0.345
17	0.510	0.020			48	0.795
18	0.830	0.120			49	1.23
19	3.62	0.310			50	1.60
20	10.0	0.800	0.050		51	1.81
21	31.1	2.25	0.245		52	1.92
22	53.4	9.21	1.07	0.050	53	1.68
23	79.7	21.9	4.30	0.755	54	1.19
24	101	34.8	10.9	2.60	55	0.645
25	124	45.3	14.9	5.00	56	0.435
26	158	50.4	17.0	5.58	57	0.185
27	152	50.7	16.0	5.43	58	0.110
28	144	46.5	14.9	4.24	59	0.035
29	125	39.2	9.56	1.68		
30	86.4	22.4	4.05	0.420		
31	51.5	10.0	1.73	0.055		
32	29.6	4.32	0.215			
33	13.3	0.990				
34	4.37	0.155				
35	1.44					
36	0.250					
37	0.025					

No	7	Average θ (deg.)	174.0	L (m)	24	
PPG Run No.	28	Q (g s^{-1})	41.7	u_* (m s^{-1})	0.16	
Pole	Arc at 50 m	Arc at 100 m	Arc at 200 m	Arc at 400 m	Pole	Arc at 800 m
33	0.070				78	0.055
34	0.180				79	0.370
35	12.0	0.370			80	2.35
36	42.5	5.81	0.065		81	6.79
37	100	20.4	1.03		82	10.1
38	152	45.6	8.24	0.12	83	8.65
39	218	79.8	22.4	2.28	84	6.87
40	299	115	33.9	10.4	85	4.72
41	378	156	42.8	18.2	86	2.57
42	488	192.0	57.9	21.1	87	0.925
43	450	179	59.5	19.0	88	0.250
44	408	144	46.9	13.5	89	0.065
45	326	98.3	24.3	4.93	90	0.030
46	209	52.2	13.9	0.755		
47	107	17.4	4.82	0.020		
48	50.7	5.75	0.490			
49	21.3	1.10	0.030			
50	5.91	0.115				
51	0.610					

No	8	Average θ (deg.)	220.0	L (m)	36	
PPG Run No.	29	Q (g s^{-1})	41.5	u_* (m s^{-1})	0.23	
Pole	Arc at 50 m	Arc at 100 m	Arc at 200 m	Arc at 400 m	Pole	Arc at 800 m
48	0.025				114	0.025
49	0.020				115	0.085
50	0.070				116	0.230
51	0.170				117	0.745
52	0.790				118	1.40
53	2.43	0.025			119	2.18
54	6.93	0.205			120	2.60
55	16.7	1.23	0.015		121	2.48
56	44.6	6.32	0.370		122	1.78
57	91.5	16.5	1.94	0.180	123	1.54
58	127	35.7	8.63	1.27	124	1.24
59	167	63.0	19.9	5.45	125	1.56
60	234	79.5	27.6	9.18	126	1.82
61	234	87.8	24.2	7.37	127	1.78
62	248	74.9	21.8	5.66	128	1.60
63	191	71.1	21.9	7.62	129	1.10
64	186	51.5	13.3	4.48	130	0.905
65	152	41.7	12.6	2.9	131	0.795
66	146	45.6	12.6	3.24	132	0.625
67	128	40.5	11.2	3.55	133	0.795
68	112	35.6	10.6	2.65	134	0.835
69	115	43.5	15.4	4.18	135	0.835
70	101	46.8	16.7	5.97	136	1.06
71	81.0	30.8	8.31	3.09	137	0.970
72	38.1	11.1	2.93	0.715	138	1.41
73	15.6	3.47	0.735	0.125	139	1.80
74	4.13	0.845	0.180	0.055	140	1.44
75	0.920	0.305	0.115	0.025	141	1.23
76	0.380	0.135	0.055		142	0.880
77	0.185	0.055	0.015		143	0.435
78	0.100				144	0.150
79	0.040				145	0.035
					146	0.010

No	9	Average θ (deg.)	170.5	L (m)	8.3	
PPG Run No.	32	Q (g s^{-1})	41.4	u_* (m s^{-1})	0.13	
Pole	Arc at 50 m	Arc at 100 m	Arc at 200 m	Arc at 400 m	Pole	Arc at 800 m
32	0.085				78	0.015
33	0.090				79	0.115
34	0.565				80	1.66
35	3.12	0.075			81	6.18
36	7.22	0.660			82	19.7
37	32.1	6.39			83	41.1
38	78.5	31.5	0.750		84	58.6
39	207	57.3	14.5	0.395	85	31.3
40	356	162	53.1	7.17	86	5.20
41	615	434	129	7.17	87	0.270
42	729	624	285	46.8	88	0.030
43	707	518	205	121	89	0.010
44	608	240	45.2	60.3	90	0.015
45	369	58.8	1.83	0.045		
46	132	6.35	0.015			
47	44.9	0.435	0.010			
48	8.55	0.050	0.010			
49	0.850					
50	0.080					

No	10	Average θ (deg.)	131.5	L (m)	6.8	
PPG Run No.	35	Q (g s^{-1})	38.8	u_* (m s^{-1})	0.11	
Pole	Arc at 50 m	Arc at 100 m	Arc at 200 m	Arc at 400 m	Pole	Arc at 800 m
12	0.225				25	0.065
13	2.15	0.105			26	3.23
14	14.30	2.07	1.59	0.435	27	13.8
15	59.3	16.4	14.7	13.0	28	10.2
16	168	61.4	45.8	32.8	29	10.2
17	359	180	75.6	37.4	30	6.74
18	312	228	145	41.9	31	5.77
19	591	575	253	76.2	32	7.41
20	641	575	200	50.5	33	5.91
21	660	405	81.1	8.45	34	4.75
22	552	198	14.8	0.420	35	3.52
23	366	54.6	0.755		36	3.21
24	182	6.81			37	2.47
25	87.0	0.49			38	1.03
26	24.2				39	0.225
27	3.78				40	0.130
28	0.440				41	0.080

No	11	Average θ (deg.)	159.0	L (m)	7.8	
PPG Run No.	36	Q (g s^{-1})	40.0	u_* (m s^{-1})	0.10	
Pole	Arc at 50 m	Arc at 100 m	Arc at 200 m	Arc at 400 m	Pole	Arc at 800 m
23	0.075				70	0.045
24	0.090				71	0.160
25	0.095				72	0.760
26	0.105	0.035			73	2.63
27	0.140	0.045			74	6.85
28	0.135	0.085			75	15.5
29	0.185	0.075			76	29.8
30	2.95	0.130	0.040		77	38.6
31	12.0	0.140	0.040		78	21.9
32	83.5	2.19	0.025		79	2.34
33	251	24.3	0.220			
34	492	161	6.51	0.055		
35	747	405	71.4	0.445		
36	830	540	203	17.9		
37	794	431	152	64.6		
38	660	266	79.2	38.9		
39	423	130	59.2	31.3		
40	210	53.3	26.0	20.7		
41	76.2	10.3	3.25	1.08		
42	21.9	0.580	0.054			
43	5.45					
44	1.74					

No	12	Average θ (deg.)	186.5	L (m)	95	
PPG Run No.	37	Q (g s^{-1})	40.3	u_* (m s^{-1})	0.29	
Pole	Arc at 50 m	Arc at 100 m	Arc at 200 m	Arc at 400 m	Pole	Arc at 800 m
39	0.055				87	0.050
40	0.795	0.025			88	0.230
41	3.09	0.325			89	0.795
42	11.8	1.53	0.040		90	1.41
43	27.8	6.53	0.780	0.045	91	1.94
44	53.0	17.6	4.53	0.860	92	1.98
45	99.3	37.1	10.3	3.06	93	1.55
46	173	56	16.4	5.54	94	1.44
47	176	60.9	18.5	4.29	95	1.34
48	224	78.0	18.9	5.40	96	1.46
49	224	74.1	22.9	7.39	97	2.08
50	170	57.6	18.5	4.61	98	2.02
51	128	36.6	8.01	2.03	99	1.62
52	68.9	15.5	3.31	0.520	100	0.975
53	28.4	6.42	0.905	0.100	101	0.480
54	15.5	1.56	0.085		102	0.150
55	7.86	0.490	0.080		103	0.025
56	3.53	0.130				
57	1.39	0.055				
58	0.055					
59	0.020					

No	13	Average θ (deg.)	170.0	L (m)	99	
PPG Run No.	38	Q (g s^{-1})	45.4	u_* (m s^{-1})	0.28	
Pole	Arc at 50 m	Arc at 100 m	Arc at 200 m	Arc at 400 m	Pole	Arc at 800 m
31	0.020				75	0.075
32	0.350				76	0.520
33	1.74				77	1.660
34	5.48	0.210			78	3.85
35	19.4	1.08	0.020		79	6.01
36	54.6	5.00	0.270		80	6.44
37	126	19.8	1.85	0.055	81	4.63
38	219	57.6	11.5	1.36	82	1.91
39	333	118	33.0	7.90	83	0.580
40	380	153	51.4	18.7	84	0.085
41	360	134	46.9	13.7		
42	273	87.3	17.4	3.44		
43	170	31.5	4.61	0.430		
44	84.3	7.55	0.980	0.050		
45	30.3	1.97	0.140	0.025		
46	2.64	0.300				
47	1.38	0.050				
48	0.210					
49	0.030					

No	14	Average θ (deg.)	139.5	L (m)	9.8	
PPG Run No.	39	Q (g s^{-1})	40.7	u_* (m s^{-1})	0.14	
Pole	Arc at 50 m	Arc at 100 m	Arc at 200 m	Arc at 400 m	Pole	Arc at 800 m
17	0.225	0.040			40	M
18	1.22	0.110			41	M
19	7.83	0.340	0.050		42	M
20	30.3	1.86	0.210	0.060	43	M
21	91.8	11.1	0.350	0.075	44	M
22	182	39.6	4.62	0.045	45	M
23	276	98.4	23.8	1.38	46	M
24	302	117	36.8	8.24	47	M
25	470	140	42.7	17.0	48	M
26	425	161	54.2	20.1	49	M
27	378	130	49.6	10.7	50	3.70
28	249	79.7	20.6	3.43	51	2.16
29	155	37.5	4.42	0.540	52	1.56
30	92.2	13.1	1.95	0.080	53	1.83
31	38.6	2.13	0.180		54	1.36
32	11.6	0.310			55	0.835
33	2.62	0.015			56	M
34	0.445				57	M
35	0.005				58	M

No	15	Average θ (deg.)	179.5	L (m)	8.0	
PPG Run No.	40	Q (g s^{-1})	40.5	u_* (m s^{-1})	0.11	
Pole	Arc at 50 m	Arc at 100 m	Arc at 200 m	Arc at 400 m	Pole	Arc at 800 m
35	0.295				80	0.035
36	0.640				81	0.260
37	2.85	0.080			82	0.735
38	11.6	0.455	0.025		83	1.38
39	24.9	2.97	0.180	M	84	1.64
40	64.8	14.2	2.33	M	85	1.72
41	156	42.2	11.5	M	86	1.57
42	227	76.4	25.8	M	87	1.55
43	318	105	27.9	M	88	1.49
44	312	99.9	26.8	M	89	1.56
45	281	77.1	24.3	M	90	1.38
46	215	75.6	18.5	4.95	91	1.34
47	201	53.7	17.7	3.73	92	1.28
48	204	52.7	16.6	5.05	93	1.36
49	168	55.8	14.5	4.80	94	1.15
50	180	74.1	23.7	5.85	95	0.900
51	185	76.4	32.7	14.6	96	1.22
52	125	49.1	14.5	5.85	97	1.36
53	68.3	16.1	2.15	0.375	98	1.62
54	33.0	2.19	0.085		99	1.79
55	10.7	0.195			100	2.21
56	1.35				101	3.33
57	0.150				102	5.99
58	0.025				103	6.48
					104	2.80
					105	0.465
					106	0.045

No	16	Average θ (deg.)	198.0	L (m)	35	
PPG Run No.	41	Q (g s^{-1})	39.9	u_* (m s^{-1})	0.23	
Pole	Arc at 50 m	Arc at 100 m	Arc at 200 m	Arc at 400 m	Pole	Arc at 800 m
48	0.260				102	0.010
49	2.60	0.185			103	0.240
50	22.7	1.92	0.125		104	1.34
51	74.7	18.6	2.27	0.235	105	4.33
52	198	59.7	17.6	4.32	106	8.57
53	378	142	48.8	16.7	107	9.92
54	450	189	67.8	25.0	108	6.43
55	362	144	39.0	9.00	109	1.72
56	236	64.7	9.81	0.675	110	0.400
57	106	15.0	0.765		111	0.055
58	33.6	2.10	0.035			
59	4.97	0.295				
60	0.270					

No	17	Average θ (deg.)	212.0	L (m)	120	
PPG Run No.	42	Q (g s^{-1})	56.4	u_* (m s^{-1})	0.37	
Pole	Arc at 50 m	Arc at 100 m	Arc at 200 m	Arc at 400 m	Pole	Arc at 800 m
51	0.580				113	0.070
52	0.945				114	0.280
53	2.61				115	0.725
54	9.68	0.440			116	1.31
55	21.0	2.88	0.075	0.005	117	1.70
56	50.3	5.87	1.07	0.045	118	2.13
57	106	25.2	5.24	1.07	119	1.98
58	183	53.6	15.6	3.49	120	1.95
59	242	83.9	25.3	7.12	121	2.11
60	276	100	31.5	7.77	122	2.11
61	254	84.8	23.4	5.59	123	1.94
62	204	56.1	15.5	5.16	124	1.76
63	127	41.3	12.6	4.17	125	1.36
64	103	32.3	8.56	1.94	126	0.815
65	76.2	17.1	2.76	0.455	127	0.310
66	48.6	4.52	0.595	0.060	128	0.070
67	19.7	1.23	0.090		129	0.020
68	5.18	0.225				
69	1.05	0.055				
70	0.075					

No	18	Average θ (deg.)	134.0	L (m)	114	
PPG Run No.	46	Q (g s^{-1})	99.7	u_* (m s^{-1})	0.34	
Pole	Arc at 50 m	Arc at 100 m	Arc at 200 m	Arc at 400 m	Pole	Arc at 800 m
14	0.065	0.110	0.055		35	0.095
15	0.535	0.125	0.055		36	0.445
16	4.59	0.325	0.085		37	1.10
17	16.4	2.09	0.420	0.050	38	3.22
18	59.3	13.5	3.530	0.715	39	6.08
19	177	58.8	17.6	3.95	40	6.33
20	384	131	53.1	15.0	41	3.63
21	512	198	60.8	20.9	42	3.11
22	564	188	47.8	12.6	43	4.01
23	546	142	33.3	9.79	44	3.06
24	434	114	27.8	4.84	45	1.86
25	363	111	32.8	8.48	46	1.01
26	267	92.1	32.0	11.0	47	1.12
27	206	72.5	22.1	6.63	48	1.81
28	147	41.0	11.8	1.44	49	2.62
29	99.0	28.4	4.29	0.233	50	3.08
30	54.5	17.1	0.480		51	2.83
31	37.1	4.79			52	1.74
32	18.9	0.265			53	0.895
33	11.4	0.130			54	0.445
34	1.88	0.040			55	0.110
35	0.370	0.140			56	0.060
36	0.160	0.155			57	0.015

No	19	Average θ (deg.)	132.5	L (m)	10	
PPG Run No.	53	Q (g s^{-1})	45.2	u_* (m s^{-1})	0.17	
Pole	Arc at 50 m	Arc at 100 m	Arc at 200 m	Arc at 400 m	Pole	Arc at 800 m
14	0.110				36	0.150
15	2.60				37	4.41
16	23.1	0.710	0.050		38	24.7
17	109	16.7	0.775	0.035	39	34.2
18	218	102	21.0	0.925	40	25.6
19	608	305	115	31.7	41	12.8
20	786	534	233	86.2	42	2.52
21	923	488	162	50.3	43	0.210
22	755	258	28.4	3.48	44	0.025
23	410	47.1	0.955			
24	155	4.53				
25	37.8	0.115				
26	2.76					
27	0.035					

No	20	Average θ (deg.)	140.0	L (m)	40	
PPG Run No.	54	Q (g s^{-1})	43.4	u_* (m s^{-1})	0.24	
Pole	Arc at 50 m	Arc at 100 m	Arc at 200 m	Arc at 400 m	Pole	Arc at 800 m
17	0.240				43	0.040
18	0.780				44	0.155
19	6.81	0.190	0.135		45	1.04
20	29.1	2.04	0.180		46	3.60
21	80.1	13.8	1.11	0.050	47	7.92
22	152	44.4	8.01	0.88	48	9.51
23	261	99.3	32.2	7.12	49	6.62
24	374	156	62	22.3	50	2.64
25	422	171	55.8	19.3	51	0.800
26	356	105	25.0	4.82	52	0.050
27	215	43.4	6.38	0.670	53	0.065
28	105	13.2	1.11	0.555	54	0.080
29	40.1	2.31	0.205		55	0.085
30	5.87	0.350			56	0.015
31	1.37				57	0.070
32	0.070					

No	21	Average θ (deg.)	155.5	L (m)	124	
PPG Run No.	55	Q (g s^{-1})	45.3	u_* (m s^{-1})	0.37	
Pole	Arc at 50 m	Arc at 100 m	Arc at 200 m	Arc at 400 m	Pole	Arc at 800 m
23	0.330				59	0.025
24	0.485	0.010			60	0.115
25	0.635	0.020			61	0.365
26	2.45	0.030			62	0.885
27	8.16	0.190			63	1.85
28	20.6	1.01	0.035		64	2.49
29	44.7	5.49	0.430		65	2.83
30	86.9	18.5	2.53	0.345	66	2.39
31	145	44.7	13.4	2.10	67	1.81
32	192	66.8	22.4	5.54	68	1.19
33	219	84.2	27.2	7.83	69	0.615
34	218	82.7	26.3	7.35	70	0.275
35	192	65.6	18.7	3.45	71	0.085
36	156	38.0	6.09	0.860	72	0.020
37	97.2	14.9	1.36	0.045		
38	50.1	4.04	0.335			
39	14.3	0.805	0.090			
40	1.61	0.300				
41	0.580	0.080				
42	0.160					
43	0.050					

No	22	Average θ (deg.)	152.5	L (m)	76	
PPG Run No.	56	Q (g s^{-1})	45.9	u_* (m s^{-1})	0.29	
Pole	Arc at 50 m	Arc at 100 m	Arc at 200 m	Arc at 400 m	Pole	Arc at 800 m
21	0.085				57	0.050
22	0.115	0.070			58	0.195
23	0.200	0.120			59	0.745
24	0.34	0.130			60	2.08
25	2.90	0.155	0.020		61	3.76
26	8.55	0.405	0.035		62	4.50
27	33.0	3.50	0.245		63	4.74
28	77.9	14.1	2.13	0.055	64	4.20
29	156	40.5	9.01	1.18	65	2.48
30	216	74.0	22.7	4.90	66	0.905
31	284	110	33.0	11.3	67	0.230
32	308	110	36.3	12.6	68	0.075
33	279	91.7	28.7	8.46	69	0.025
34	218	70.2	16.7	2.89		
35	147	36.9	5.58	0.510		
36	92.7	13.0	0.915	0.030		
37	41.3	2.81	0.095	0.010		
38	10.8	0.370				
39	2.40					
40	0.310					

No	23	Average θ (deg.)	178.5	L (m)	6.4	
PPG Run No.	58	Q (g s^{-1})	40.5	u_* (m s^{-1})	0.11	
Pole	Arc at 50 m	Arc at 100 m	Arc at 200 m	Arc at 400 m	Pole	Arc at 800 m
40	0.020				86	0.040
41	0.560				87	3.10
42	6.68				88	24.5
43	60.2	2.96	0.035		89	59.4
44	279	48.9	4.34	0.800	90	48.2
45	557	293	80.9	43.8	91	12.0
46	1000	660	311	140	92	0.215
47	794	575	221	27.1		
48	633	318	37.9	0.090		
49	410	52.1	0.550			
50	150	2.93	0.020			
51	21.6					
52	1.10					
53	0.090					

No	24	Average θ (deg.)	173.5	L (m)	11	
PPG Run No.	59	Q (g s^{-1})	40.2	u_* (m s^{-1})	0.14	
Pole	Arc at 50 m	Arc at 100 m	Arc at 200 m	Arc at 400 m	Pole	Arc at 800 m
35	0.110				82	0.165
36	0.165				83	3.43
37	0.330				84	20.3
38	1.36				85	39.4
39	14.3	0.300			86	22.3
40	100	7.01	0.090		87	3.55
41	332	77.0	7.43	0.325	88	0.295
42	567	303	88.8	22.1	89	0.030
43	723	524	239	101.0		
44	707	419	134	26.4		
45	552	174	22.1	0.835		
46	239	23.6	0.870	0.870		
47	67.2	2.51				
48	11.8	0.305				
49	4.43	0.055				
50	0.265					

No	25	Average θ (deg.)	198.5	L (m)	58	
PPG Run No.	60	Q (g s^{-1})	38.5	u_* (m s^{-1})	0.28	
Pole	Arc at 50 m	Arc at 100 m	Arc at 200 m	Arc at 400 m	Pole	Arc at 800 m
44	0.015	0.010			104	0.085
45	0.045	0.070			105	0.545
46	0.125	0.515			106	1.79
47	0.210	0.480			107	4.15
48	0.870	0.375	0.070		108	6.07
49	4.07	0.470	0.120		109	4.75
50	22.5	1.73	0.275		110	2.440
51	65.0	8.12	0.795	0.030	111	0.815
52	130	33.2	6.40	0.540	112	0.135
53	237	83.1	26.4	5.18	113	0.050
54	302	118	43.6	15.1		
55	281	114	40.2	10.8		
56	212	53.4	13.3	3.20		
57	110	27.2	2.98	0.270		
58	44.7	4.94	0.330			
59	10.6	0.415				
60	1.76	0.060				
61	0.220	0.045				
62	0.140					
63	0.110					

References

Barad, M. L. (Editor) (1958) Project Prairie Grass, A Field Program in Diffusion. Vol. 1. Geographical Research Paper No. 59, Air Force Cambridge Research Center, Belford, Massachusetts.

van Ulden, A. P. (1978) Simple estimates for vertical diffusion from sources near the ground. Atmos. Environ. 12, 2125-2129.

VITA

Kasemsan Manomaiphiboon was born in Bangkok, Thailand, on March 22, 1971. He is a son of Banyong and Aree Manomaiphiboon. He spent 12 years at St. Gabriel's College, Bangkok, for his elementary, junior-school, and high-school education, and then received his bachelor's degree from the Faculty of Engineering, Chulalongkorn University, Bangkok. He worked as an engineer in some consultant companies for 3 years and won an award granted by the governments of Japan and Thailand for postgraduate study in the U.S. He earned his Master's degree in Environmental Engineering (Air Quality Program) from the University of Cincinnati, Ohio, and pursued his doctoral degree at the Georgia Institute of Technology, Georgia. He married Supinda Salatan in 1999.